USING LOW-DOSE RADIATION THERAPY TO PROPAGATE SYSTEMIC RESPONSE TO *IN SITU* VACCINES: A STUDY OF METHODOLOGY, TECHNIQUE, AND EFFICACY

By

Peter Michael Carlson

A dissertation submitted in partial fulfilment of

the requirements for the degree of

Doctor of Philosophy

(Cellular and Molecular Biology)

At the

University of Wisconsin-Madison

2020

Date of final oral examination: August 25th 2020

The dissertation is approved by the following members of the Final Oral Committee:

Paul M. Sondel, Professor, Pediatrics and Human Oncology
Zachary S. Morris, Assistant Professor, Human Oncology
Anna Huttenlocher, Professor, Pediatrics
Douglas G. McNeel, Professor, Medicine
Jamey P. Weichert, Professor, Radiology

Acknowledgements

This thesis represents the sum total of four years of work that absolutely could not have been accomplished on my own. I want to take this first opportunity to thank each and every individual who took the time to help me throughout this process, in whatever capacity you helped. This would not have been possible without you. I want to thank my advisor, Dr. Paul Sondel, for his steadfast and sound guidance throughout these years. For teaching me not only *how* to ask the right scientific questions, but to never forget *why* I am asking them; to help patients through improving our understanding of cancer immunotherapy. Your mentorship and advice have proven invaluable, and I cannot truly thank you enough for your support.

I would also like to thank my co-mentor Dr. Zachary Morris, whom I had the honor of working with as he set up his lab from his very early days consisting of just a PI, half a graduate student, and a couple of undergrads all the way through now establishing himself as a fully funded, thriving laboratory. Zach's door was always open, and he always was willing to talk through my most recent data, findings, and experimental designs with me. I am truly lucky to benefit from the life experiences and advice of not one, but two fantastic physician-scientist mentors.

The other members of my thesis committee, Drs. Anna Huttenlocher, Jamey Weichert, and Doug McNeel have also been instrumental during my time in graduate school. Both in thesis committee meetings and individually, I have benefited greatly from the collective advice and wisdom of these scientists, for which I will always be grateful.

Research is a team effort, and to that end the members of the Sondel and Morris labs have been invaluable in helping to progress this work to where it is today. Dr. Alexander Rakhmilevich taught me proper handling of mice, design of experiments, and most importantly to be critical of results presented by others in the literature. He can also always be counted on for a perfectly timed pun in any situation. Dr. Jacquelyn Hank taught me much of the early benchwork and cell culture analysis techniques that I use today, in addition to lending a sharp

and insightful assessment of my data that almost always forced me to consider an alternate explanation. Dr. Amy Erbe taught me about molecular analyses, experimental design, and was always willing to help in the mouse room. She provided insightful scientific discussion, critical review of my ideas, and most importantly helped me to keep the larger perspective when experiments gave me frustrating results. Dr. Ravi Patel was fantastic mentor and friend throughout my time in graduate school, and we worked on several projects together. He provided valuable guidance both scientifically and professionally as I developed (and continue to develop) my long-term career goals. Other graduate students including Alexander Pieper and Anna Hoefges, as well as post-doctoral researchers Alexa Heaton, Taylor Aiken, and statistician Jen Birstler provided fantastic and engaging discussion of our work, and always were able to come up with exciting new ideas.

I want to specifically thank those students that worked with me during their undergraduate years as well as their post-baccalaureate time in helping me with my projects. These include Matthew Rodriguez and Claire Sun, both of whom have been critical in collecting the data in this work, as well as Manasi Mohan and Clinton Heinze, who helped me in earlier years to generate my initial data, and have since continued their training in graduate school. In addition, thank you to Arika Feils, Mackenzie Heck, and Sabrina Vandenheuvel for your assistance with my mouse work and analyzing samples for flow cytometry. I appreciate each of you for the opportunity to mentor you in some small capacity, and for helping me to discover a passion for teaching and mentorship.

I also wish to share my gratitude for the other research teams and laboratories that have assisted in my training and data collection. Reinier Hernandez and Joseph Grudzinski, working in the lab or Dr. Jamey Weichert, generously provided their time and expertise in synthesizing the targeted radionuclide therapy agents used in this work. Justin Jeffery and the Small Animal Imaging and Radiotherapy Facility assisted in scanning mice and performing biodistribution experiments. Ian Marsh, working in the lab of Dr. Bryan Bednarz, assisted in analyzing PET/CT

images and estimating dosimetry. Lastly, to the three fearless leaders of the Flow Cytometry Core; Dagna Sheerar, Lauren Nettenstrom, and Kathryn Fox – thank you all for indulging my endless barrage of questions, for taking the time to teach me how to properly design a staining panel, and for ensuring that only the highest quality work would come from someone trained by your hands.

As part of the Medical Scientist Training Program as well as the Cell and Molecular Biology graduate program, this PhD is part of a larger path of training that I have been walking for the past seven years. I am truly fortunate to have been given the opportunity to train both as a scientist and as a physician, and I owe that entirely to the MSTP. Thank you to the directors of the program Drs. Anna Huttenlocher, Mark Burkard, JP Yu, Caitlin Pepperell, and Scott Reeder for their encouragement, wisdom, and engagement with the class throughout the years. I also wish to thank my fellow MSTP classmates, especially those in my year; Laura Swanson, Nick Vogt, Mazdak Bradberry, Amelia Haj, Yang Hu, Jack Hunt, Richard Merkhofer, and Jorge Rodriguez-Gil. We have become a family over the course of our time together, and I cannot thank you all enough for your support and friendship.

Lastly, I wish to thank my family, who have supported me throughout my graduate training, medical training, and long, long before either. My mother, Linda, never once doubted me and has never failed to lend an ear, a hug, or to just simply be there when I need her. Her profession as a dental hygienist has been my inspiration for becoming a physician myself. My father, Michael, has been a steadfast source of strength and support for as long as I have known him. He taught us to work hard by his example, yet somehow always reminds me not to worry, and to keep an eye on both the bigger picture, and simple joys in life. My Physical Therapist sister, Stephanie, and my Rocket Scientist brother, Tim, have each inspired and driven me more than they know simply by example, even though I am the oldest and (somehow) still in school. I love you all, I am so proud of each of you, and I cannot thank you enough for being such an awesome family.

Abstract

USING LOW-DOSE RADIATION THERAPY TO PROPAGATE SYSTEMIC RESPONSE TO *IN SITU* VACCINES: A STUDY OF METHODOLOGY, TECHNIQUE, AND EFFICACY

By
Peter Michael Carlson

Under the supervision of Professor Paul M. Sondel, M.D., Ph.D.
At the University of Wisconsin-Madison

Despite substantial improvement in clinical cancer care, disease progression still occurs. In particular, disease recurrence at distant sites apart from the primary treated tumor remains high, and is the most common cause of cancer-related mortality. *In situ* vaccination is an immunotherapeutic approach designed to use local treatments directed at a single disease site and drive increased antigen processing with subsequent antigen-specific adaptive responses, ideally capable of spreading to distant sites of disease. The Sondel lab has developed a combination *in situ* vaccine approach consisting of 12Gy local external beam radiation (RT) and intratumoral injections of the hu14.18-IL2 immunocytokine (IC, a fusion of a monoclonal antibody and IL-2), which is directed against disialoganglioside GD2 (expressed in neuroectodermally derived tumors including neuroblastoma, osteosarcoma, and melanoma). This *in situ* vaccine approach can render up to 70% of mice bearing a single B78 melanoma flank tumor disease-free, with tumor-specific systemic memory. However, this *in situ* vaccine is insufficient to control distant, untreated tumors in models of multiple B78 implanted tumors. The goal of this thesis was to characterize the efficacy of using low-dose radiation delivered to all sites of disease in enabling a systemic antitumor response following RT/IC *in situ* vaccination.

To deliver radiation to all disease sites, both external beam RT and an injectable molecular targeted radionuclide therapy (TRT) were investigated. The TRT agent, NM600, can be conjugated to ^{90}Y for therapeutic delivery of radiation dose to all disease sites. One powerful

method of assessing immune changes following combination RT/IC and TRT is flow cytometry However, many shared resource cytometry facilities do not permit analysis of radioactive tissue for safety and radioactive waste disposal concerns. Thus in order to proceed, a novel method, permitting reliable and accurate analysis of radioactive tissue by flow cytometry, was required. By evaluating a cryopreservation step at each of three separate points in the flow cytometry workflow, I demonstrated that cryopreservation of dissociated tumor and spleen cells after surface staining, fixation/permeabilization, and internal staining produces flow cytometry results most concordant with non-cryopreserved samples. This technique was used to safely stain and store radioactive dissociated tumor cells from mice treated with ^{90}Y-NM600, and demonstrated time- and dose- dependent alterations to the immune tumor microenvironment following administration of TRT.

Multiple studies conducted by different scientists in our research group demonstrated a high degree of variance in response among B78 tumors implanted into the flank and then treated with RT/IC *in situ* vaccine. In the interest of improving reproducibility in our animal model, characterization of this discrepancy in treatment outcome was required. By directly comparing tumor-bearing mice implanted by different experimenters, I determined that tumors implanted subcutaneously are localized deep to the panniculus carnosus muscle in the murine skin, remain ‘fixed’ to the underlying tissue when the overlying skin is moved, and most importantly do not respond well to RT/IC *in situ* vaccination. Conversely, tumors implanted intradermally are localized superficial to the panniculus carnosus, are ‘mobile’ in phenotype upon movement of the skin, and respond well to RT/IC *in situ* vaccination. Importantly, this ‘mobile’ vs ‘fixed’ phenotype could be used to predict treatment response without prior knowledge of implantation technique, which demonstrates its use as a potential inclusion criterion in future syngeneic implanted tumor experiments.

After controlling for implantation depth, I determined that RT/IC *in situ* vaccine delivered to a primary B78 melanoma combined with 12Gy additional RT delivered to a secondary

melanoma tumor resulted in greater control at both tumor locations compared to either RT/IC alone or radiation alone. This improved response was demonstrated as greater overall survival, greater proportion of mice clearing both tumors, and a slower rate of tumor growth. Combining RT/IC *in situ* vaccine with ^{90}Y-NM60 TRT also improved overall survival compared to RT/IC or TRT alone. These data suggest that additional radiation to all disease sites is indeed capable of improving response to RT/IC *in situ* vaccination at distant sites. Ongoing studies are using flow cytometry and cytokine quantification to characterize the nature of the immune response to *in situ* vaccination at distant tumors, with and without additional radiation.

Table of Contents

List of Tables

List of Figures

Chapter 1

Introduction and Background

1.1 Overview

This thesis represents the collective work of four years focused on studying the immune effects of tumor-directed radiation, particularly in combination with an *in situ* vaccine in a syngeneic $GD2^+$ melanoma model. It is based mainly on the observation that some tumors, both clinically and preclinically, have a predominantly immunosuppressive microenvironment that may limit the systemic effects of a local *in situ* vaccine. This thesis investigates the use of low-dose radiation delivered to all such immunosuppressive tumor sites concurrent with immunotherapy to facilitate a stronger antitumor immune response. This introduction chapter covers a brief conceptual summary of how the immune system influences cancer development, and how *in situ* vaccines can be used to re-direct effector immune responses against the tumor. It next discusses the immunologic effects of radiation on the tumor microenvironment, and introduces the concept of targeted radionuclide therapy as a vehicle for delivering immunomodulatory doses of radiation. This chapter closes with a discussion of several conceptual challenges in conducting immunophenotyping studies with radioactive tissues, briefly outlines the syngeneic mouse model used in this work, and summarizes the hypotheses and experimental approach used in the remaining chapters.

1.2 Cancer immunotherapy and *in situ* vaccines

1.2.1 *The cancer immunoediting hypothesis*

One of the most profound breakthroughs in our understanding of cancer biology has been the illumination of the complex interplay between cancer and the immune system. It is clear now that the immune system plays a role in surveilling almost all tissues and eliminates the vast majority of neoplastic or aberrantly functioning cells long before they become clinically identifiable [1]. Yet there is substantial clinical and preclinical evidence that the regulatory and immunosuppressive capabilities of the immune system can at times favor tumor growth, angiogenesis, and even metastatic spread [2,3]. One popular hypothesis for this seemingly

dichotomous role of the immune system posited by Schreiber and colleagues is the cancer immunoediting hypothesis, which consists of the “three E’s”: Elimination, Equilibrium, and Escape [4]. In the ‘Elimination’ phase, the immune system surveils all normal cells and can identify and eliminate any neoplastic or dysregulated cells. As some of these cells continue to accumulate genetic ‘hits’ and mutations, they eventually reach an ‘Equilibrium’ between neoplastic uncontrolled cell division and immune-mediated elimination [4]. Eventually resistant clones and subclones persist, and the tumor progresses into the ‘Escape’ phase, where the immune system is largely unable to affect the tumor, and clinically identifiable cancer arises [4]. Almost all cancer that we consider in a clinical context (meaning it is either symptomatic, grossly identifiable, or detected by various cancer screening methods) has already reached the ‘Escape’ phase. In this sense, the immune system has “edited” the tumor to be specifically immune suppressive and/or evasive.

One of the goals of cancer immunotherapy is to reengage the immune system through supraphysiologic intervention and tip the balance back in favor of immune-mediated cancer ‘Elimination’. Upon further investigation it has become clear that the three E’s are not a sequence, but instead a continuum that may exist in different states in different regions of a tumor, different locations in the body, and at different times throughout the disease course [5]. Some tumors have a high degree of lymphocytic infiltration upon biopsy (termed immunologically “hot” tumors), while others appear mostly devoid of immune cells (termed “cold” tumors) [6]. Though both hot and cold tumors clearly represent a failure of the endogenous immune system to adequately control the tumor, it may be that the mechanism of tumor escape is different in these two situations. In a “hot” tumor, there may be a predominance of immunosuppressive mechanisms in the tumor microenvironment (TME) that prevents tumor-specific effector CD4 and CD8 T cells from attacking the tumor. In contrast, the “cold” tumors seem to have a lack of recognition by the effector T cell compartment to the tumor at all, possibly due to a lack of antigen processing and recognition by professional antigen presenting

cells (APCs) or a deficiency in tumor antigens that can be readily recognized by endogenous T cells [6,7]. This critical difference may explain why patients with “hot” tumors are more likely to respond to checkpoint blockade immunotherapy compared to “cold” tumors [7].

1.2.2 In Situ *vaccines as a means of engaging the immune system against an “escaped” tumor*

An ideal cancer immunotherapy should be capable of overcoming a suppressive tumor microenvironment and stimulating activation and recruitment of antitumor effector immune cells. One technique being studied to this end is *in situ* vaccination [8]. This technique involves treatments directed at a tumor *in vivo* such that the tumor antigens expressed by that tumor are released, identified, processed by antigen presenting cells (APCs), and presented to naïve T cells, to sensitize them and enable them to then recognize and destroy other antigenically-similar cancer cells. The approach capitalizes on the natural biological processes involved in antigen recognition and presentation without the explicit characterization of the exact antigen or antigens being targeted, even if those antigens are *different* between patients. In essence, a particular tumor is then *converted* into a vaccine, where enhanced recognition and presentation of antigenic targets stimulates and diversifies an anti-tumor T-cell response [8]. Ultimately an *in situ* vaccine should be able to activate a systemic immune response capable of attacking not only the treated, vaccine-converted tumor, but other distant sites of metastatic disease as well. Thus a local, targeted, treatment drives a systemic antitumor response.

Several agents and approaches have been investigated as tools to drive *in situ* vaccination, both clinically and preclinically. One of the first agents injected intratumorally for the purpose of driving antitumor immunity was Bacillus Calmette-Guerin (BCG), a bacterial pathogen that drives an inflammatory response at the injection site [9]. As the immune system reacts against the BCG via activation of toll-like receptors (TLRs), some tumor cells are killed simply as “bystanders,” yet their tumor-specific antigens are processed by APCs in the inflammatory BCG-containing tumor microenvironment, and can potentially drive production of

antitumor responses as well as anti-BCG responses. This process is still used in the clinic for treatment of superficial bladder cancer [10]. Other live bacterial strains, including *Clostridium novyi*, have also been shown effective in generating CD8+ T cell responses in preclinical models of renal, colon, and anaplastic squamous cell carcinoma models [11]. Similar to live bacterial injections, viral strains including variants of the herpes simplex virus have been engineered to target moieties on tumor cells. These have the dual effect of activating "bystander" immune destruction of tumor cells while also directly lysing tumors and releasing tumor associated antigens [12]. This has lead to the FDA approval in 2017 for the oncolytic virus Talimogene laherparepvec (T-VEC) for the treatment of advanced melanoma [13].

The chief means of immune activation by intratumoral injection of live bacteria or bacterial components is through recognition of pathogen associated molecular patterns (PAMPS) by toll-like receptors (TLRs). Further study has identified specific molecular patterns for several TLRs that lead to downstream immune activation. Imiquimod, a TLR 7 and 8 agonist, has been used clinically against cutaneous cancers and warts to great effect [14]. TLR9 recognizes hypomethylated CG-enriched oligonucleotides (CpG) in prokaryotic DNA, and can drive activation of macrophages and dendritic cells [15]. Intratumoral CpG has been shown effective in combination with checkpoint blockade antibodies preclinically against lymphoma [16], and in combination with radiation, tumor-targeted antibodies, and IL-2 in melanoma [17]. Other TLR agonist agents under active investigation include Poly-inosinic:polycytidylic acid (poly-IC, a TLR3 agonist) and bacterial lipopolysaccharide (LPS, a TLR4 agonist) [18,19].

While pathogen-derived and TLR-targeted agents aim to drive *in situ* vaccination through innate inflammatory processes leading to enhanced phagocytosis and antigen presentation, these are often combined with agents directed at propagating an adaptive antitumor immune response. Interleukin-12 (IL-12) is a potent cytokine released by APCs and other monocyte-derived cells, which has a strong stimulatory effect on type 1 helper T cells. These T cells are the chief source of interferon gamma (IFNγ), which can drive proliferation and sustained

activation of cytotoxic T lymphocytes among others [20]. Systemic administration of IL-12 has demonstrated substantial preclinical antitumor activity [21], but has been associated with substantial toxicity in patients when used systemically [22]. Interleukin 2 (IL-2) has also been explored, as it is required for T cell proliferation and activation, and is FDA-approved for treatment of renal cell carcinoma and melanoma, though it is also associated with substantial toxicity when given systemically [23]. Intratumoral administration of these potent yet toxic cytokines (and others) present an opportunity to preserve antitumor effect while avoiding toxic side effects. To that effect, intratumoral administration of IL-12, both by direct injection of cytokine and by local transfection of cytokine-producing plasmid, has been shown to have modest clinical effect [24]. Much more promising results have been obtained using intratumoral injections of IL-2, with melanoma patients showing near universal response rates at injected tumors, and some modest response at distant, untreated tumors [25].

The above examples demonstrate the wide variety of approaches under investigation, targeting different and multiple steps in the immune response, to achieve antitumor effect. As our understanding of cancer biology and immunology grow, so do the novel and hypothesis-driven means of using that understanding to achieve greater antitumor efficacy. There are many other approaches being investigated that show both clinical and preclinical promise, including systemic immunotherapies such as immune checkpoint blockade, autologous Chimeric Antigen Receptor (CAR) T cells, engineered plasmid-based vaccines, and many others [1]. There has also been substantial progress made in combination immunotherapies, both local and systemic, as well as combination with other cancer treatment modalities including radiation therapy, chemotherapy, and surgical resection [26].

1.3 Rationale for Combining Radiation and Immunotherapy

Another means of driving *in situ* vaccination in some tumors is the use of tumor-directed radiation. The interaction between radiation therapy and the immune response has been

described for nearly 100 years. In 1921, Murphy and colleagues demonstrated that radiated mouse skin had an increased degree of lymphoid infiltration, and that attempting to engraft a tumor into radiated skin was less successful compared to unirradiated skin [27]. In the 1970s, Helen Stone and colleagues showed in murine models that the dose of radiation required to eradicate an implanted flank tumor was twice as high in immune-deficient mice compared to immune-competent mice [28]. These researchers and many others demonstrated that an intact immune system contributes to the local killing of tumor cells following radiation.

The abscopal effect is a rare, but well documented, phenomenon in radiation oncology whereby patients with metastatic disease may experience partial or complete responses at distant, unirradiated tumor sites following radiation of a separate tumor location [29]. This phenomenon is mediated by systemic activation of an anti-tumor immune response [30]. Thus, the immune system has always been a critical component of radiation therapy, and radiation has the potential to drive antitumor immunity.

Radiation elicits both immune stimulatory and immune suppressive effects, which can be heterogenous and dynamic within both the tumor and the body. These can be categorized as: 1) direct effects on tumor cells; and 2) effects on the tumor microenvironment including fibroblasts, endothelial cells, and tumor-infiltrating immune cells. As a cumulative result of these influences, focal external beam radiation can elicit an *in situ* tumor vaccination effect – converting a patient's own tumor into a nidus for presentation of tumor-specific antigens in a way that stimulates and diversifies the patient's anti-tumor T cell response [31,32].

1.3.1 *Immunomodulatory Effects of Radiation on Tumor Cells*

The tumor-killing effect of radiation is traditionally thought to result from the accumulation of DNA damage in malignant cells leading to tumor cell death by mitotic catastrophe [33]. While this process does occur, recent studies have also demonstrated that at least some tumor cells undergo a form of controlled cell death termed Immunogenic Cell Death. While apoptosis,

autophagy, and necrosis exert limited inflammation in surrounding normal tissues, immunogenic cell death involves strong inflammatory mechanisms [34–36]. In cells undergoing immunogenic cell death following radiation therapy, calreticulin is translocated to the cell surface. Calreticulin is a well-known endoplasmic reticulum chaperone protein that is upregulated during times of stress, and is a potent activator of dendritic cell (DC) phagocytosis [37]. High Mobility Box Group 1 (HMGB1) protein is also released from the nuclear compartment of cells dying following radiation and is released to the extracellular tumor microenvironment [38]. HMGB1 is classified as a Damage Associated Molecular Pattern (DAMP) and can activate innate immune cell inflammatory response by binding Toll-Like Receptor (TLR) family members, including TLR2 and TLR4 [39,40]. Immunogenic cell death following radiation is also associated with the extracellular release of ATP, which has been shown to activate the P2XR7 purinergic receptor pathway and the DC inflammasome [41]. This leads to increased secretion of inflammatory cytokines including IL-1B, TNF-α, and IL-12 [42], culminating in DC activation, enhanced antigen processing and presentation, and $CD8^+$ T cell recruitment and activation [35].

Radiation is also known to have broad effects on those tumor cells receiving a sublethal dose. For instance, doses of external beam radiation as low as 2-4 Gy have been shown to increase expression of major histocompatibility complex class I (MHC-I) on the surface of cancer cells both *in vitro* and *in vivo*. Formenti and colleagues demonstrated that 4 Gy of radiation caused an increase in MHC-I expression through increased synthesis of the beta-2 microglobulin subunit in GL621 glioma cells [43]. Increased tumor cell MHC-I expression renders these tumor cells more recognizable by tumor-specific $CD8^+$ T cells recruited and activated as sequalae of immunogenic cell death. This effect has been observed in numerous cancer cell lines including human lung adenocarcinoma, hepatocellular carcinoma, prostate adenocarcinoma, melanoma, and others [44]. Interestingly, the dose of radiation required to optimally induce MHC-I upregulation is different for different tumor cell lines, which emphasizes the heterogeneity in tumor radiobiology and radiosensitivity. This radiation-induced effect on

MHC-I is also observed following treatment with alpha-emitting ^{223}Ra [45]. This has important implications for targeted radionuclide-based platforms.

Tumor cells surviving radiation are also modified in their susceptibility to immune response by increased expression of cell death pathway proteins including FAS [46], which is a target of T cell killing. Radiation can also activate a type I interferon (IFN) response in surviving cells. cGAS is a cytosolic sensor of DNA that, upon detection of cytosolic DNA (as during viral infection), activates the Stimulator of Interferon Genes (STING) pathway, leading to phosphorylation of IRF3/7, production of type I IFN, and upregulated expression of IFN-stimulated genes (e.g. *MX1*, *OAS2*, *OAS3*) [47,48]. Ionizing radiation elicits double-strand DNA breaks that may result in chromosome fragments lacking a centromere, leading to formation of micronuclei when such cells progress through mitosis [49,50]. The compromised nuclear envelope of these micronuclei enables detection by cGAS and activation of a type I IFN response that increases with radiation dose up to 8-12 Gy.

1.3.2 *Immunomodulatory Effects of Radiation on the Tumor Microenvironment*

Radiation also directly affects components of the tumor microenvironment, which has both positive and negative influences on anti-tumor immunity. Radiation increases expression of vascular and matrix adhesion proteins including VCAM1, ICAM1, and CD31, which facilitate immune cell diapedesis and infiltration into the tumor [46]. Radiation further stimulates tumor infiltration by and activation of immune cells through an immediate local release of inflammatory cytokines. This includes reported effects on the production of IL-10, IL-12, IL-15, IL-17, IL-18, Ifn-α, Ifn-γ, Ifn-β and Tgf-β [51]. Radiation also modifies the tumor microenvironment at low doses (1-4 Gy) through a rapid and direct cytotoxic effect on radiation-sensitive tumor-infiltrating lymphocytic lineages. Doses of 0.5, 2, and 3 Gy trigger apoptosis in 10%, 50%, and 90% of naïve T lymphocytes within 2-8 hours of radiation therapy exposure, respectively [52]. Activated T effector cells and immunosuppressive regulatory T cells (T_{regs}) may be slightly less sensitive to

radiation therapy compared to naïve T cells [53,54]. Nevertheless, both T effector cells and T_{regs} are highly radiosensitive relative to most tumor cells [52,54]. Notably, compared to most other cell types, which commonly exhibit reduced response to low dose rate radiation, lymphocytes show little change in radiation therapy sensitivity with reduced dose rate[55]. This implies that low dose, low dose-rate radiation delivered by a low dose-rate radionuclide could also modify the lymphocytic infiltrate in the tumor microenvironment.

Conversely, radiation also triggers immunosuppressive effects in the tumor microenvironment including delayed recruitment of suppressive immune lineages including T_{regs}, M2-polarized macrophages, and myeloid-derived suppressor cells (MDSCs) [56,57]. Moreover, negative feedback pathways may also be activated after radiation therapy with increased expression of immunosuppressive ligands, including PD-L1 on tumor cells, and T cell exhaustion markers including PD1, TIM3, and LAG-3 on tumor infiltrating lymphocytes (TILs)[58]. Finally, large volume external beam radiation may irradiate a significant portion of the blood pool and bone marrow, leading to radiation-induced systemic lymphopenia, which is associated with reduced survival in cancer patients [59,60].

1.4 Combination RT and Immunocytokine synergize to create an *in situ* vaccine when treating a single tumor

The Sondel and Morris labs have developed a combination immunotherapeutic approach that capitalizes on the immunomodulation of local external beam radiation and the tumor-targeting capacity of a tumor-specific immunocytokine (IC). This IC is a fusion protein consisting of a tumor-specific monoclonal antibody genetically linked to two human IL2 molecules. Antitumor antibodies have been used as systemic monotherapy and in combination with other treatments for a number of cancers [61]. Some mAbs can bind to and inhibit specific targets such as growth factor receptors, thereby directly altering the function of the tumor cell

[61]. However antibodies themselves are immune effector molecules, and a number of immune cells have specific Fcγ receptors that can bind the Fc portion of a tumor-bound antibody thereby inducing antibody dependent cellular cytotoxicity (ADCC) [62]. The particular combination approach pursued in this thesis utilizes a mAb against a disialoganglioside, GD2, which is expressed on neuroblastoma, melanoma, and other neuroectodermally-derived tissues [62]. Sondel and others used a combination of anti-GD2 mAb, IL2, granulocyte-macrophage colony stimulating factor (GMCSF), and cis-retinoic acid in children with neuroblastoma and demonstrated improved event free survival and overall survival with the immunotherapy arm compared to standard treatment [63]. This mAb is the backbone for the fusion protein hu14.18-IL2, which has been shown to have greater effect against GD2+ tumors when given systemically than the combination of hu14.18 and soluble IL2 [64]. At least part of the benefit of such a fusion molecule-based approach is: 1) the close proximity of IL2 cytokines to effector molecules interacting with the Fc region of the antibody; and 2) binding of IL2 to the IL2 receptor on effector T and NK cells effectively brings the cell into contact with the tumor cell target bound by the immunocytokine, thus expanding the population of immune cells capable of “recognizing” the tumor target.

Morris and colleagues demonstrated that 12Gy of external beam RT synergized with intratumoral injections of the hu14.18-IL2 immunocytokine (IC) to generate an *in situ* vaccine in murine models of $GD2^+$ syngeneic melanoma [65]. After a series of optimization experiments, they identified that delivering RT on treatment day 0 and intratumoral IC daily on treatment days 5 through 9 resulted in optimal antitumor effect. Whereas each treatment alone was unable to cure mice, the combination of RT + IC resulted in complete responses in 70% of treated mice under these conditions [65]. It was demonstrated using depletion studies that this vaccine effect was dependent on T cells and NK cells, and resulted in a tumor-specific memory that prevented engraftment of subsequent additional tumor of the same or antigenically related type [65]. This

approach, referred as “RT+IC” or “RT/IC”, forms the foundation for the *in situ* vaccine effect that is used throughout chapters 2, 3, and 4 of this thesis.

In this work, we explore the mechanisms by which some of the response induced with this RT/IC *in situ* vaccine can still fail to generate an adequate anti-tumor immune response. In a follow up study, the Morris group found that although systemic memory is generated following this *in situ* vaccine, the response failed to clear large (~500mm^3), established tumors [65]. In addition, this *in situ* vaccine was substantially less effective when treating mice bearing two similar tumors in distinct locations [66]. Radiation and immunotherapy to a single tumor resulted in tumor clearance, but the presence of a distant, *untreated* tumor prevented the generation of an immune response at *either* tumor. This phenomenon was only observed when the two tumors were of the same type: a treated B78 melanoma was cleared if the secondary tumor was Panc02 pancreatic adenocarcinoma, but not if it was another B78 tumor. Likewise, a Panc02 primary was cleared if the secondary was B78, but not if it was Panc02 [66]. This suggests that this tolerizing effect of a distant, untreated tumor is specific to the antigens of that tumor, meaning it is likely an immune-mediated phenomenon. This concomitant immune tolerance (CIT) is not fully understood, and appears to fluctuate in the magnitude of antagonism at the treated primary tumor depending on size of tumor and treatment type. Though the mechanism of CIT is not fully elucidated, T_{regs} seem to play a substantial role. Using the DEREG mouse model which can induce depletion of T_{reg} cells that transgenically express a diptheria toxin receptor that is driven by the Treg-selective foxp3 promoter, it was demonstrated that eliminating T_{regs} eliminates CIT and restores response to the RT+IC *in situ* vaccine [66]. Regardless of the anti-tumor effect at the primary tumor, no use of RT+IC *in situ* vaccine to the primary tumor was able to clear a distant, untreated secondary B78 tumor [66]. See Appendix B for more details on this work describing CIT.

1.5 Rationale for using Targeted Radionuclide Therapy (TRT) in combination with Immunotherapy

While focal external beam radiation consistently induces a local inflammatory response, this alone rarely leads to a sustained and systemic anti-tumor immune response [29]. This may reflect a negative impact of distant tumor sites on the priming and propagation of systemic anti-tumor immunity from a focal *in situ* vaccine site, as we have observed in the case of CIT. While focal external beam radiotherapy can dramatically alter the immune landscape in a targeted tumor, it does not alter the landscape within *all* tumors. Immune suppressive cells and pathways in these unaltered non-radiated tumors may quench the activation of effector immune cells emerging from the *in situ* vaccination site or may circulate between tumor sites and reconstitute a suppressive tumor microenvironment at the radiated site. Consequently, to engage radiation in effectively priming and propagating anti-tumor immunity, it may be necessary to deliver immunomodulatory radiation to the *collective* tumor microenvironment at *all* tumor sites. This question forms the basis of this thesis work and will be tested in a mouse model of two implanted tumors in Chapter 4.

In metastatic settings of multiple sites of disease, radiation therapy has historically been reserved for palliative indications targeting symptomatic lesions. In patients with limited or oligometastatic disease, recent studies demonstrate feasibility and a survival benefit from delivering radiation to all tumor sites [67]. This supports a notion that metastatic disease may be managed by delivering some form of radiation in combination with other therapies to all sites of disease. Radiating all tumor sites using external beam radiation is often not possible in settings of widely metastatic disease due to 1) normal tissue toxicity, and 2) radiating radiographically occult tumor sites in this context would require whole body radiation resulting in systemic bone marrow and immune suppression.

Targeted Radionuclide Therapy (TRT) is a systemic form of radiation therapy that combines a tumor-selective vector or mechanism with a therapeutic radioisotope. These vectors can include antibodies, antibody fragments, peptides, lipids, and small molecules [68]. These vectors, though they circulate systemically, selectively bind to a target structure while being cleared from other non-specific targets. The end result is selective binding and retention of these radioactive molecules in the target tissue (in this instance, the tumor), where the radionuclides undergo radioactive decay, delivering ionizing radiation to the surrounding environment while sparing other tissues. TRT has been used for nearly a century [69] and a growing number of TRT agents are approved for the treatment of cancers [70,71]. As a monotherapy TRTs generally have shown limited efficacy in most solid tumors [70]. In part, this reflects difficulty in delivering high dose radiation to an entire tumor using TRT while sparing other tissues in the body. Heterogeneity in targeting moiety expression, tumor vascular supply, and cell radiosensitivity also contribute to a lack of effective response to TRT monotherapy in clinical settings for many common solid tumors [72]. Combining TRT with immunotherapies may overcome these limitations and, in turn, the delivery of radiation to all tumor microenvironments may prime and propagate a more effective response to immunotherapies. This is largely due to the previously discussed immunogenic alterations to the tumor microenvironment that derive from sublethal doses of radiation; the combination of TRT and immunotherapy may require much lower doses of TRT, which could avoid systemic toxicity issues previously encountered with TRT monotherapy.

1.6 Translational development and testing of TRT in combination with immunotherapies

1.6.1 TRT in combination with immune checkpoint inhibitors

Immune checkpoint inhibitors are a class of therapeutic antibodies that modulate tumor tolerance by recognizing and blocking specific inhibitory receptors on the surface of immune cells and thereby enhancing T cell activation. Antibodies targeting checkpoint receptors have

shown therapeutic benefit for a variety of tumor types. These include antibodies targeting cytotoxic T-lymphocyte antigen-4 (CTLA-4) as well as programmed cell death-1 (PD-1) and its ligand PD-L1 [73]. In the context of strong or prolonged TCR signaling, CTLA-4 expression is up-regulated on T cells and competes with CD28 for binding of B7-1/2, resulting in inhibition of further T cell activation [74]. By blocking the interaction of CTLA-4 and B7-1/2, anti-CTLA-4 antibodies can promote continued T cell activation. PD-1 is expressed on activated T cells as well as B cells, NK cells, and monocytes. Its ligands, PD-L1 and PD-L2, are expressed on antigen presenting cells, tumor cells, placenta, and cells in an inflammatory microenvironment. Binding of PD-1 by its ligands results in inhibition of T cell activation. Importantly, tumor cell expression of PD-L1 is correlated with diminished tumor-infiltrating lymphocytes and poor clinical outcome for multiple cancer types [74]. Antibodies targeting PD-1 or PD-L1 have been approved in the treatment of many different types of cancer.

Preclinical studies demonstrated the potential for TRT to augment response to immune checkpoint inhibitors. The alkylphosphocholine analog NM600, which can chelate radiometals and preferentially accumulates in malignant cells [75], has been used to deliver ^{90}Y to the tumor microenvironment in a variety of syngeneic murine tumor models and consistently augments response to anti-PD-1 and anti-CTLA-4 [76]. This agent will be studied in further detail in Chapter 4 and Appendices A and B. In other preclinical studies, a peptide-based TRT, ^{177}Lu-Arg-Gly-Asp (^{177}Lu-RGD), which targets $\alpha_v\beta_3$ integrin on activated angiogenic endothelial cells, was found to be cooperative with anti-PD-L1 in controlling the growth and extending survival of mice bearing syngeneic MC38 tumors [77]. A separate preclinical study demonstrated that a small molecule TRT (^{177}Lu-LLP2A) targeting $\alpha_4\beta_1$ integrin (also called Very Late Antigen-4, VLA-4), enhanced tumor response in B16-F10 melanoma tumors when combined with anti-PD-1, anti-PD-L1, and anti-CTLA-4 antibodies [78]. Collectively, these preclinical studies demonstrate the potential for TRT to enhance response to immune checkpoint inhibition.

Several clinical trials are now testing the safety and efficacy of combining TRT and immune checkpoint inhibition. Among these is a promising ongoing study evaluating the combination of ^{131}I-metaiodobenzylguanidine (MIBG), nivolumab (anti-PD-1 antibody), and dinutuximab (anti GD-2 antibody) in pediatric patients with neuroblastoma [79]. For men with metastatic castrate-resistant prostate cancer (mCRPC), ^{223}Ra (Xofigo), is approved for treatment as monotherapy [80]. Radium is a calcium mimetic that naturally accumulates in the bony metastatic tumor sites that typify mCRPC. At least two studies are now evaluating the addition of an anti-PD-1 antibody to ^{223}Ra in mCRPC [81,82]. Also in mCRPC, a small molecule TRT targeting prostate-specific membrane antigen (^{177}Lu-PSMA) is being tested in combination with anti-PD-1 antibody in a phase Ib/II study evaluating safety and efficacy [83].

1.6.2 *TRT in combination with in situ vaccines*

In immunologically “cold” tumors that are poorly recognized by the immune system, simply “taking the brakes off” of the immune response with immune checkpoint inhibitors is generally ineffective. As discussed above, external beam radiation can elicit an *in situ* vaccine in some tumors and may prime immune recognition of tumor antigens not recognized prior to radiation [84,85]. In immunologically “cold” tumors, it may be advantageous to combine external beam radiation and TRT to prime and propagate anti-tumor immunity, respectively. Combination Internal and External RadioTherapy (CIERT) has been hypothesized as a strategy for enhancing dose to tumors and improving treatment of patients with metastatic disease [86]. The combination of TRT and external beam radiation therapy delivers radiation dose to a target volume while affecting two different sets of off-target organs. External beam radiation therapy tends to demonstrate toxicity in tissues neighboring the irradiated tissue, while TRT typically affects distant organs that have off-target TRT uptake. These radiation modalities have been studied in the context of maximizing dose to a target tumor, but have not been thoroughly

explored as a combinatorial approach at much lower doses for enhancing response to immunotherapy [87].

Oncolytic viruses are a class of immunotherapy with the capacity to deliver genetic payloads to targeted tumor cells while also triggering apoptosis and lytic release of additional virus particles [88]. By priming immune recognition of tumor antigens from lysed tumor cells, oncolytic viruses may elicit an *in situ* vaccine effect. Preclinical studies have begun to evaluate combinations of TRT and oncolytic virus. Sorensen and colleagues have engineered an oncolytic herpesvirus to deliver the noradrenaline transporter (NAT), which selectively transports MIBG into infected cells [89]. This oncolytic virus renders infected tumors susceptible to MIBG while also stimulating an antitumor immune response. This combination has been shown effective in controlling the growth of UWV and SK-MEL-3 xenograft tumor models [89]. Similarly, Peerlinck and colleagues have engineered an adenoviral vector that delivers the Na/I importer gene to colorectal carcinoma cells [90]. This importer promotes ^{131}I uptake into infected cancer cells, and a combination of the Na/I adenovirus and a single dose of ^{131}I is capable of shrinking HCT116 tumor xenografts [90].

1.6.3 *TRT in combination with other immunotherapies*

DNA vaccines for cancer are designed to be taken up by antigen presenting cells, affect synthesis of a tumor antigen encoded in the DNA, and present those protein fragments through MHC-I-mediated pathways to T cells in the immune system [91]. In preclinical studies of prostate cancer, Olsen and colleagues demonstrate that a DNA vaccine encoding the androgen receptor ligand binding domain increases tumor infiltration by tumor-specific $CD8^+$ T cells and controls growth of syngeneic prostate cancer in mice [92,93]. In a MyC-CaP murine prostate tumor model, these investigators observed that TRT using ^{90}Y-NM600 increased T cell infiltrate and that TRT combined with DNA vaccination controlled tumor growth to a greater degree than either agent alone [94].

Sipuleucel-T is an autologous cellular therapy for the treatment of mCRPC. This therapy uses leukopheresis to isolate antigen presenting cells, which are incubated with GM-CSF and a prostate cancer-specific antigen prostatic acid phosphatase (PAP). These cells are then reinfused back into the patient with the goal of stimulating the patient's T cells to target prostate cancer cells [95]. In 2010 the FDA approved sipuleucel-T, after a phase III randomized trial demonstrated a 4 month survival increase in patients with mCRPC [96]. A phase II study is now testing the combination of ^{223}Ra with sipuleucel-T. That study recently completed accrual of 36 patients, half of whom received 6 courses of ^{223}Ra during treatment with sipuleucel-T [97]. The primary endpoint for this study is degree of antitumor T cell proliferation and results are pending as of this writing.

1.7 Challenges to consider during translational testing and development of combination RT, TRT, and immunotherapeutic approaches

1.7.1 *Performing advanced immunologic assays of radioactive tissues – challenges facing flow-cytometry based approaches*

Part of a rigorous and thorough evaluation of a novel cancer immunotherapy treatment requires evaluation of the immune system itself. Though *in vivo* evidence of tumor regression and survival benefit is the most effective gauge of treatment efficacy, understanding the mechanisms of action is important to confirming cellular and molecular hypotheses, as well as for hypothesis generation for adjustments to treatment regimens. Commonly used approaches in the clinic include enumeration of immune cell subsets (lymphocytes, monocytes, neutrophils, and others) in the blood through the use of flow cytometry [98]. Briefly, flow cytometry assays take a population of single cells and draw them into a narrow stream of running fluid, such that cells "flow" in a single-file line past a series of excitation lasers. Cells are often labeled prior to running on the instrument using fluorophore-conjugated antibodies to specific targets. The fluorescence intensity of that target/antibody/fluorophore complex is recorded for all cells in the

population as they move past the detector, recording up to millions of cells in a single sample. Depending on instrument configuration and capacity, these instruments can record anywhere from four to 32 different colors, meaning multispectral/multidimensional analysis can then be performed [99,100]. This is the basis for determining differences in populations of T cells, B cells, NK cells, macrophages, dendritic cells, and many others in response to treatment. Further, expression of markers of activation or exhaustion such as PD-1, CD69, CD25, and others can be measured within populations of interest such as CD8+ T cells [101]. Applied on a population level, flow cytometry has been established as a powerful tool for the interrogation of different immune cell types, markers of activation, signaling pathway phosphorylation states, transcription factors, cytokines, and others in complex populations of cells.

In considering preclinical and clinical studies with TRT, it is important to consider the novel difficulties that are presented by the radioactive agent itself. As most TRT agents bind to or are taken up by their target cancer cells, single cell suspensions derived from this tissue would also contain the radioactive agent. This presents several safety and waste disposal concerns for use in flow cytometric applications. First, after the cells pass through the detector apparatus, they are flushed into a “waste” container, along with the sheathe or running buffer that was used while running the cells single file. This results in a fairly large volume of liquid biohazard waste, on the scale of liters per day in some shared resource flow cytometry facilities. Waste containers containing radioactive cells would additionally need to be stored in shielded areas until they decay to background levels before being disposed of. Combined with the risk of damage to instrument electronics from high dose rate isotopes, surface contamination risk, and danger to other researchers, almost all shared resource flow cytometry facilities in large academic institutions ban the analysis of radioactive materials by policy.

Analysis of radioactive tissue for immune monitoring is typically limited to *in vivo* imaging or histology-based approaches. In this approach, the radioactive tissue is harvested, formalin-fixed or flash frozen, and stored under proper shielding until the samples have decayed to

background levels. Then the samples are retrieved, and the histology processing workflow is resumed. While this approach is helpful, and can provide valuable geographic and proximity-based information, it does not provide population-level descriptions of the entire immune system within the TME. Ideally a similar approach as used in histology could be applied to the single cell suspension used for flow cytometry, namely introducing a storage step that could allow the radioactive cells to decay to background levels before proceeding with the flow cytometry staining and analysis workflow. However as the cells retrieved from a disaggregated tumor are alive and metabolically active, one simply cannot wait until the radioactivity had decayed, as the cells would no longer be viable, processes including autophagy and necrosis would destroy many molecular targets of interest. Chapter 2 of this thesis explores alternate means of addressing this problem, including introducing both fixation and cryopreservation steps into the preparation workflow, and how these impact the resulting flow cytometry data.

1.7.2 *Maximizing rigor and reproducibility in murine models of cancer and in situ vaccines*

The continued development of preclinical models for studying the complex interaction between the immune system and cancer is of paramount importance in maintaining translatability of findings into clinical benefit. The laboratory mouse has been the mainstay of cancer research both before and throughout the rise of cancer immunotherapy. Although previous mouse studies of cytotoxic chemotherapies used human xenograft models in immunocompromised mice, effective studies of cancer immunotherapy require an intact immune system, and therefore cannot use this gold-standard approach [102]. To address this limitation, several different approaches have been used to develop tumor models in immunocompetent mice for studies of preclinical immunotherapy. Syngeneic models are the most commonly used, and consist of a mouse-derived tumor (either spontaneously arising or carcinogen-driven) being harvested and cultured as a tumor cell line that can then be injected to the same inbred

laboratory strain such as C57BL/6 [102]. This approach carries the advantage of being relatively easy to use and expand into large cohort sizes for robust statistical analyses. These tumors are also species and strain-compatible with their host strain, meaning any resulting immune response is attributed largely to its tumor-associated antigens. These tumor cell lines can also be manipulated to express reporter genes, candidate antigen targets such as ovalbumin (OVA), and other factors prior to implantation. The line does not however mimic the natural developmental process of a tumor from its cancer stem cells; the injected inoculum is already fairly undifferentiated and grows at a relatively fast rate compared to spontaneously arising tumors [102].

To address the limitations of syngeneic approaches, genetically engineered mouse models have been developed that use tissue-specific expression of oncogenes or enzymes designed to eliminate tumor suppressor genes. These mouse lines undergo tissue-specific, neoplastic transformation and have a more physiologically faithful tumor immune microenvironment that develops alongside the tumor [103]. However these lines typically require crossing of breeder pairs, and require noninvasive imaging modalities such as ultrasound or MRI to monitor for tumor growth and treatment response. Together, these limitations result in small sample sizes, with increased variability between subjects. A more novel class of murine tumor models involve patient-derived xenografts transplanted in immunocompromised mice along with human lymphoid tissue, to develop human tumors in mice that have components of human immune systems. While this may be the most “faithful” recreation of the human TME and modeling of human immune responses, these mice require access to patient tumor samples, are resource- and labor- intensive to generate, and may result in substantial variability in immunotherapeutic effect depending on variability in the donor tissues [102].

This thesis focuses on the use of the B78 syngeneic murine melanoma cell line. This line was derived from the commonly studied B16-F10 melanoma line, and was transfected to

express the human GD2 antigenic target of the hu14.18-IL2 immunocytokine. This work uses a syngeneic approach to allow for adequate sample sizes in experiments, ease of use, and for comparison to previously understood controls. Though there are models that may more faithfully recreate the genomic instability and heterogeneity of human cancers, the relatively uniform nature of the syngeneic approach, combined with the larger sample sizes, greatly increases our ability to detect differences in effect between treatments. One important consideration in syngeneic, implantable, tumor models is the surrounding tissue in which the tumor develops; whenever possible an orthotopic implantation is preferred to more faithfully replicate the tissue stromal architecture of the original tumor. For cutaneous melanoma models, implantation into the skin, typically the flank, is preferred. The epidermal and dermal layers of skin contain unique subsets of dendritic cells (DCs) including Langerhans cells, tissue resident T cells, and macrophages [104,105]. By contrast the deeper tissue layers, which are often referred to as the "subcutaneous" plane, have fewer resident DCs and macrophages, with different subtypes and functions. Studies of human vaccines against pathogens have suggested that immunogenic material injected in the intradermal space (ID, within the dermis between the epidermis and the dermal adipose tissue) generate stronger immune responses compared to the same material injected in the subcutaneous space (SC, the space between the dermal adipose tissue and underlying muscular fascia) [106]. Studies involving more immunogenic syngeneic tumor lines, like OVA-expressing variants of B16-F10, have demonstrated differences in engraftment rates depending on the depth of tumor implantation [107]. Chapter 3 of this thesis further explores the difference in growth rate and response to *in situ* vaccination of B78 tumors implanted at slightly different depths, and highlight a critical need to control for this confounding factor.

1.8 Thesis Structure and Hypotheses

By engaging a patient's immune system to attack cancer cells, immunotherapies have the potential to cure even advanced or metastatic cancers. However, the response rate to

immunotherapies remains low in most treated patients with solid tumors. Radiation not only triggers an immunogenic form of tumor cell death but tumor cells surviving radiation commonly exhibit phenotypic changes that increase susceptibility to immune detection and elimination. By delivering radiation to all tumor sites while limiting dose to immune organs, including lymph nodes, blood, spleen, and bone marrow, TRTs have the potential to increase the response rates to immunotherapies and in this way may have a beneficial impact on the survival of cancer patients. To that end, the core hypothesis of this body of work is that delivering an immunomodulatory dose of radiation to all tumor sites can drive improved systemic antitumor responses to *in situ* vaccination.

To adequately address this question, a novel approach to flow cytometric analysis had to be developed. In **Chapter 2**, the impact of a fixation and cryopreservation step in the flow cytometry sample preparation workflow on resulting outcomes is explored. This chapter demonstrates a technique modification that permits safe, reliable storage of radioactive samples for flow cytometry up to 30 days after tissue harvest, and that technique is used to describe several immune modulations to the TME following treatment with the TRT agent ^{90}Y-NM600. **Chapter 3** addresses an inconsistency in results following treatment of a single tumor with RT+IC *in situ* vaccination and identifies a key difference in response based on the depth of implantation of the syngeneic B78 tumor inoculum. Using these techniques, **Chapter 4** explores the use of both external beam radiation and ^{90}Y-NM600 TRT in a model of two implanted B78 tumors given concurrently with RT+IC *in situ* vaccination and demonstrate clear *in vivo* benefit. **Chapter 5** summarizes these findings and their possible implications, discusses additional questions raised by this work, and proposes further studies to characterize this promising *in vivo* benefit of combining radiation with *in situ* vaccine immunotherapy.

Acknowledgement:

This introductory chapter for my thesis expands on a Review Chapter, that I wrote together with my PhD co-mentor, Dr. Zach Morris. That manuscript has been submitted and is in revision*. I am grateful to Dr. Morris for his help in organizing the outline of that submitted manuscript, and for editing and revising with me the submitted version. I have expanded its content here, to enable it to serve as an overview and introduction to this thesis.

*****Peter M. Carlson, Zachary S. Morris. Translational development and testing of theranostics in combination with immunotherapies. Chapter in *Nuclear Medicine and Immunology*. Springer Publishing, 2020, in Revision.

Chapter 2

Optimizing flow cytometric analysis of immune cells in samples requiring cryopreservation from tumor-bearing mice

Preface

This chapter pertains to a series of experiments that was conducted over a two year period focused on developing a flow cytometry technique for analyzing radioactive tissue. In combining molecular targeted radionuclide therapy (MTRT) with immunotherapy, we needed to develop a technique that allows us to probe the immune system within these radioactive tumors. Since shared resource flow cytometry facilities typically do not allow radioactive material in their research spaces, I tackled the issue of developing an alternate means of storing these samples until they decayed to background. These observations and techniques were implemented into the research workflow for several other researchers in our group, which have been utilized in several publications (see appendix B for manuscripts using this technique). The work described in this chapter has been submitted for publication as a novel immunologic method and is under review at the time of this writing.

2.1 Abstract

Most shared resource flow cytometry facilities do not permit analysis of radioactive samples. We are investigating low dose molecular targeted radionuclide therapy (MTRT) as an immunomodulator in combination with *in situ* tumor vaccines (ISV), and need to analyze samples from MTRT-treated mice using flow cytometry to characterize immunologic changes within the tumor. Further, the sudden shutdown of core facilities in response to the COVID-19 pandemic in March of 2020 has created an unprecedented work stoppage. In these and other research settings, a robust and reliable means of cryopreservation of immune samples is required. We evaluated different fixation and cryopreservation protocols of disaggregated tumor cells with the aim of identifying a protocol for subsequent flow cytometry of the thawed sample which most accurately reflects the flow cytometric analysis of the tumor immune microenvironment (TME) of a freshly disaggregated and analyzed sample. Cohorts of C57BL/6 mice bearing B78 melanoma tumors were evaluated using dual lymphoid and myeloid immunophenotyping panels involving fixation and cryopreservation at three distinct points during the workflow. Results demonstrate that freezing samples after all staining and fixation are completed most accurately matches the results from non-cryopreserved equivalent samples. We observed that cryopreservation of living, unfixed cells introduces a nonuniform alteration to PD1 expression. We confirm the utility of our cryopreservation protocol by comparing tumors treated with ISV, analyzing both freshly obtained and cryopreserved tumor samples, demonstrating similar results. Lastly, we use this cryopreservation protocol with radioactive specimens to demonstrate potentially beneficial effector cell changes to the TME following administration of a novel MTRT in a dose- and time-dependent manner.

2.2 Introduction

Continued preclinical and clinical progress in the field of tumor immunology hinges on the ability to analyze accurately and reliably the immune tumor microenvironment (TME) before and after treatment. Flow cytometry is a powerful tool for the interrogation of different immune cell types, markers of activation, signaling pathway phosphorylation states, transcription factors, cytokines, and others in complex populations of cells [99]. Effective, rigorous flow cytometric analyses can be hindered by several barriers that disrupt experiment workflow. Unexpected instrument breakdown, maintenance, or overcrowding of shared resource facilities can delay analysis of samples after harvest, or delay planned harvest days, which may have detrimental effects on time-sensitive experiments. An extreme example our working group encountered beginning in March of 2020 is the sudden shutdown of our shared resource flow cytometry core due to the global COVID-19 pandemic. There are also some instances where rapid (same-day) acquisition of samples by flow cytometry is not logistically possible, for instance if samples are collected at multiple sites and need to be transported to other buildings, institutions, or countries for analysis in a central lab. Another critical example is that most shared resource facilities prohibit analysis of radioactive samples for safety and radioactive-contamination reasons. Dedicated cytometers for analysis of radioactive material are expensive and difficult to maintain, and may not benefit from the expertise and efficiencies afforded by the shared resource facility structure. In these instances, the ability to cryopreserve harvested samples for flow cytometric analysis at a later time would be of great benefit.

While cryopreservation is a commonplace laboratory procedure with many different applications and protocol variations, it is generally not recommended to cryopreserve samples for analysis by flow cytometry [100,108–111]. It is known that cells undergoing cryopreservation exhibit a stress response to the freezing process, which is one reason why many prefer flow cytometry analyses be performed on freshly obtained cells [112]. One could consider avoiding

the biological stress of cryopreservation by staining and fixing samples prior to freezing. However fluorophore-conjugated antibodies, especially those using tandem-dye fluorophores, are generally not considered stable through freeze/thaw cycles due to risk of degradation [113–115]. Furthermore, fixed cells may have a substantial degree of crosslinked structural rigidity [116]. While it has not been clearly demonstrated, and likely depends on the fixative used, there is a risk that crystals formed during the cryopreservation process may damage these rigid cells and reduce recovery of intact cells following cryopreservation. Several studies have described the changes that can occur to detected frequencies of various immune populations in human peripheral blood mononuclear cells (PBMCs) following cryopreservation, and concluded that while possible, it is preferable to stain and analyze fresh cells without cryopreservation [100,110,117,118]. Pinto and colleagues have demonstrated it is feasible to surface-stain and fix human PBMCs prior to subsequent cryopreservation, and observed comparable immune cell frequencies to those of freshly analyzed samples [119]. However, it is unclear how this translates to immunophenotyping in the murine TME, and how the cryopreservation methodology might influence detection of markers such as transcription factors that require cell membrane permeabilization.

External beam radiation therapy (RT) is known to have direct tumor cell-killing effects and is used in clinic to treat cancer patients [120]. Recently, much interest has arisen in the effect of radiation on the immune system and the TME. Low to moderate doses of radiation (8-12Gy) have been shown to elicit a type I interferon response through activation of the Stimulator of Interferon Genes (STING) pathway [50,121]. Studies have also demonstrated a rise in MHC-I concurrent with infiltrating CD4+ and CD8+ T cells, as well as increased proinflammatory cytokines in the TME following 2-5 Gy doses of radiation [43,122,123]. Radiation can also have a direct cytotoxic effect on certain immune cell lineages, especially lymphocytes, with almost 90% of lymphocytes driven to apoptosis within 8 hours of a 3Gy dose in one study [52]. This may have the beneficial effect of temporarily clearing the tumor of suppressive lineages like

CD4+ FOXP3+ T regulatory cells (T_{regs}) [53,124]. Taken together, low to moderate doses of radiation have the potential to temporarily immunomodulate a suppressive TME into a more favorable effector environment capable of responding to subsequent immunotherapy. This principle was proven effective in demonstrating a synergy between 12Gy local RT and intratumorally injected hu14.18-IL2 immunocytokine ([IC], an anti-disialoganglioside [GD2] antibody fused to IL2) in treating GD2+ murine tumors [65]. This form of immunotherapy is one of several strategies that aim to induce the generation of an *in situ* vaccine using the tumor's own antigens. This is driven by triggering targeted immunogenic cell death, antigen processing and presentation; these can then induce recruitment and sensitization of antitumor effector cells capable of recognizing multiple different antigens selectively expressed by the tumor [125].

In preclinical studies, we have begun to test treatment approaches using systemically administered, molecular targeted radionuclide therapy (MTRT) to deliver low to moderate doses of immunomodulatory RT to all tumor sites. This approach holds promise, at least in part, because the efficacy of *in situ* vaccines may be suppressed in the setting of distant, non-radiated metastases [66]. In this sense, systemic low dose MTRT may modulate the immune susceptibility of the *collective* TME for all tumor sites in an individual with metastatic disease and thereby facilitate greater systemic propagation of an *in situ* vaccine delivered at a single tumor site [126]. Alkylphosphocholine (APCh) analogs can be used to deliver MTRT and have been shown to be preferentially retained in over 50 different mammalian tumor types regardless of anatomic location [75]. ^{90}Y-NM600 is an APCh analog that has been characterized in murine and canine models, and can be used to safely deliver 2-5Gy to all tumor sites without causing bone marrow suppression or systemic lymphopenia [127]. Though preclinical anti-tumor efficacy has been demonstrated for the combination of MTRT and checkpoint blockade immunotherapy [126], the mechanisms by which this form of low dose MTRT alters the TME to provide this immunotherapeutic synergy has not been clearly described. Addressing these issues requires careful flow cytometry analyses of serially obtained tumor samples from mice undergoing

curative combination therapy with MTRT and immunotherapy. However, this form of flow cytometry requires either a dedicated flow cytometer able to analyze radioactive samples, or the ability to cryopreserve these samples long enough to allow radiation to decay to background levels prior to analysis.

Here we address this methodological challenge by evaluating the impact of introducing a cryopreservation step to our flow cytometry workflow for dissociated murine tumor and spleen samples. Our goal was to determine what strategy/workflow for cryopreservation would give flow cytometry results that most closely match those for freshly obtained and analyzed replicate samples that were never cryopreserved. We demonstrate that timing of cryopreservation, relative to surface staining, fixation, permeabilization, and internal target staining, has a strong effect on immunophenotyping results. Our data show that freezing after all staining and fixation is completed, rather than before or during these sequential steps, enables flow cytometry results that are most concordant with the flow cytometric results obtained with freshly analyzed, non-cryopreserved aliquots of these samples. We demonstrate that this protocol of freezing cells after all staining is completed can be used to evaluate the impact of an *in situ* vaccine, and describe the changes to the TME as a function of time and dose of radioactive ^{90}Y-NM600.

2.3 Materials and Methods:

2.3.1 *Syngeneic tumor cell line*

B78-D14 (B78) murine melanoma is a cell line derived from B16-F10 melanoma, as previously described [128]. This cell line was generously provided by Ralph Reisfeld at the Scripps Research Institute (La Jolla, CA). Cells were cultured in RPMI 1640 (Mediatech, Inc, Manassas, VA) supplemented with 10% fetal bovine serum, 100U/mL penicillin, 100µg/mL streptomycin, and 2mM L-glutamine. As previously described, B78 cells have been engineered to express GD2- and GD3-synthase under the control of 400µg/mL G418 and 50µg/mL hygromycin and were selected over three days in selection media prior to being frozen down as

lab stock [129,130]. Cells were kept below 90% confluence and were used within 7 passages of thaw from the common bank. Cells were confirmed mycoplasma negative by PCR within 6 months of use.

2.3.2 Animal studies and tumor models

Animals used in this study were housed and cared for using an approved protocol reviewed by the University of Wisconsin-Madison Institutional Animal Care and Use Committee (IACUC). Female, 6-8 week old C57BL/6 mice were ordered from Taconic Biosciences (Rensselaer, NY) and allowed to acclimate in our animal facility for at least one week following arrival. Tumors were engrafted by injecting $2x10^6$ B78 cells in 100µL of sterile PBS intradermally in the right flank using a 26g needle. Of note, the flank was shaved 24-48h prior to implantation to ensure consistency of injection, and to ensure resolution of any irritation and inflammation resulting from shaving. Tumors were monitored twice weekly and developed over 6 weeks. Tumor volume was measured using calipers and approximated as ($width^2$ x length)/2. Mice receiving MTRT or immunotherapy were randomized to begin treatment when tumor volumes reached 90 – 180mm^3.

2.3.3 *External beam radiation, molecularly targeted radionuclide preparation and administration*

External beam RT was delivered using an X-RAD 320 system (Precision X-Ray Inc, North Branford, CT). Mice were immobilized using custom lead jigs and surgical tape such that only the dorsal right flank was exposed, with the rest of the mouse (including the contralateral flank and spleen) shielded. Irradiation settings were beam strength 320Kv/12.5mA, beam conditioning filter 2, platform height 36 cm, treatment duration 331 seconds, which has been measured to reliably deliver 11 +/- 1 Gy to the tumor by thermoluminescent dosimetry (data not shown). $^{90}YCl_3$ was purchased from Perkin Elmer (Waltham, MA). The vehicle used for

molecular targeted radionuclide therapy, 2-(trimethylammonio)ethyl(18-(4-(2-(4,7,10-tris(carboxymethyl)-1,4,7,10-tetraazacyclododecan-1-yl)acetamido)phenyl)octadecyl) phosphate (NM600), was kindly provided by Archeus Technologies (Madison, WI). The radiolabeling and characterization of ^{90}Y-NM600 and its PET-detectible counterpart ^{86}Y-NM600 has been described elsewhere [127,131]. Briefly, 5-10mCi of $^{90}YCl_3$ was buffered in 0.1 M NaOAc (pH = 5.5.) and 10-15 nmol/mCi of NM600 was added to the mixture. The reaction was placed at 90°C for 30 minutes under constant shaking at 500rpm. The reaction mixture was loaded into a hydrophilic-lipophilic balance solid phase extraction cartridge (Waters), washed with 5 mL of H_2O, and ^{90}Y-NM600 was eluted in 2 mL of absolute ethanol. Nitrogen steam was used to evaporate the eluate, and ^{90}Y-NM600 was reconstituted in normal saline containing 0.4% v/v Tween 20 and sodium ascorbate (0.5% w/v). Mice receiving RT were radiated on treatment day 1, and mice receiving MTRT were injected with 50μCi or 250μCi of ^{90}Y-NM600 preparation by tail vein injection on treatment day 1.

2.3.4 *Immunotherapy preparation and administration*

Immunocytokine (IC, hu14.18-IL2) was provided in lyophilized form (4mg/vial) by Apeiron Biologics (Vienna, Austria). It was reconstituted by adding 8mL of sterile PBS for a working concentration of 0.5mg/mL. For mice being treated with RT+IC, 100μL of the 0.5mg/mL IC solution was injected intratumorally (IT) daily on treatment days 6 through 10, for a total dose of 250μg per mouse in five doses. Injections were through a 30G needle, and care was taken to inject slowly when administering IC via IT injection. In addition, drug was not drawn up into the syringe from the vial through the 30G needle when preparing IC, as to avoid shear-induced denaturation of the immunocytokine.

2.3.5 Tumor and spleen tissue harvest

At the time of harvest, mice were euthanized by CO_2 asphyxiation, and the tumor was dissected out. The tumor was cut into ~5mm fragments, and added to gentleMACS C tubes (Miltenyi Biotec, Bergish Gladbach, Germany) containing 2.5 mL of RPMI 1640 + 10% fetal bovine serum, 100U/mL penicillin, 100µg/mL streptomycin, and 2mM L-glutamine. 100µL of DNAse I solution in RPMI 1640 (2.5mg/mL, Sigma-Aldrich, St. Louis, MO) and 100µL collagenase IV solution in RPMI 1640 (25mg/mL, Gibco, Life Technologies, Grand Island, NY) were then added, and the samples were disaggregated using a GentleMACS octodissocator (Miltenyi Biotec, Bergish Gladbach, Germany) using the preset dissociation protocol "37C_m_TDK1" for mouse tumor dissociations. Sample dissociate was filtered through a 70µm cell strainer, washed with 10mL of cold PBS, and kept on ice until aliquoted into flow cytometry tubes. Tumors analyzed for changes in immune microenvironment were dissociated individually. For comparing different cryopreservation protocols, n=5 tumor bearing mice were harvested, individually dissociated, strained, and pooled into one common reference population. When required, spleens were dissected out and transferred into a sterile petri dish with 1 mL of ice-cold sterile PBS. Spleens were physically ground on the plate into the PBS and transferred into a 5 mL Eppendorf tube. Red blood cells in the spleen dissociate were lysed by adding 3mL of 1X RBC lysis buffer for 10min per the manufacturer's instructions (Biolegend, San Diego, CA). They were then filtered through a 70µm cell strainer, and single cell suspensions from 5 separate spleens were combined to create a common reference population.

2.3.6 Flow Cytometry Antibodies

We optimized two antibody panels for analysis of myeloid and lymphoid immune cells. See Table 2.1 for the complete list of antibodies, including fluorophore, clone, company, and optimized volume of stock added per sample, and Table 2.2 for the two full immunophenotypes used in separate panels, and Figure 2.1 for the corresponding gating strategy. These complete

antibody panels were used in the comparisons of cryopreservation techniques as seen in Figure 2.2 and 2.3. In Figures 2.4 and 2.5, single staining panels consisting of a combination of targets from the lymphoid and myeloid panels were used for efficiency. See Tables 2.4 and 2.5 for these antibody panels.

2.3.7 *Sample preparation, staining, and cryopreservation*

Single cell suspensions from either tumor or spleen were counted and $3x10^6$ cells were aliquoted to labeled flow tubes. Aliquoted samples were stained with 0.5µL GhostRed780 stock (Tonbo Biosciences, San Diego, CA) in 50µL of PBS per sample, light protected at 4°C for 30 minutes. Samples were washed with flow buffer (PBS +2% FBS), then Fc blocked by adding 0.25µL of stock TruStain FcX™ Plus anti mouse CD16/32 antibody (BioLegend San Diego, CA) in 50µL flow buffer per sample at room temperature, light protected, for 10 minutes. Samples were then stained using 50µL of an antibody master mix (prepared up to 24h before) for the corresponding surface markers, light protected at 4°C for 30 minutes. Master mix volumes were calculated given a 50µL target addition volume, with optimal volumes of stock antibody (in Table 2.1, Table 2.4, and Table 2.5) added for each 50µL test. Total number of samples for calculations was increased by 10% to account for loss during pipetting. After surface staining, samples were again washed with flow buffer, then fixed and permeabilized using the eBioscience FOXP3 fix/perm kit at room temperature, light protected for 30 minutes according to manufacturer's instructions (Thermo Fisher, Waltham, MA). Of note, samples were vortexed immediately prior to and following addition of fixative to prevent formation of large cell aggregates. After washing with 1x perm buffer from the fix/perm kit, samples were stained for intracellular targets (e.g. FOXP3) by adding 50µL of perm buffer containing the optimal antibody volume per sample and incubated (with light protection) at room temperature for 30 minutes. For

consistency of staining and sample reproducibility, all samples were fixed, even if no intracellular targets were in the antibody staining panel.

Modified preparation techniques were conducted according to the schematic outlined in Figure 2.2 and discussed in the Results section. When cryopreservation was performed, samples were washed and resuspended in 0.5mL FBS, then transferred to cryotubes containing 0.5mL of FBS + 20% DMSO (final concentration 1mL of FBS+10% DMSO) and frozen in isopropyl alcohol bath containers in a -80°C freezer in a custom wooden box with lead and plexiglass lining. Radioactive samples were stored until 30 days post injection of activity, when radioactivity is at background (approximately 11.25 half-lives for ^{90}Y). Proper shielding was confirmed via survey with Geiger counters calibrated by the University of Wisconsin Department of Environment, Health, and Safety. Samples were thawed at 37°C and transferred into flow cytometry tubes containing 3mL of flow buffer. Tubes were then pelleted and resuspended in 200µL of flow buffer.

2.3.8 *Flow Cytometry*

Previously radioactive samples were confirmed to be at background levels via survey with a calibrated Geiger counter. Samples were acquired on an Attune™ NxT flow cytometer (Thermo Fischer, Waltham, MA) with manufacturer provided acquisition software. This instrument was maintained by the University of Wisconsin Carbone Cancer Center Flow Cytometry Laboratory, which performs daily quality control checks and instrument calibration using Attune™ Performance Tracking Beads (Thermo Fischer, cat 4449754). This cytometer was equipped with the following excitation lasers: 488nm (BL), 561nm (YL), 405m (VL), and 633nm (RL). The cytometer was equipped with the following channel/bandpass filter combinations: BL1 (530/30), BL2 (590/40), BL3 (695/40), YL1 (585/16), YL2 (620/15), YL3 (695/40), YL4 (780/60), VL1 (440/50), VL2 (512/25), VL3 (603/48), VL4 (710/50), RL1 (670/14),

RL2 (720/30), and RL3 (780/60). Of note, staining panels that used BV711 used the 710/50 filter on VL4, and staining panels that used BV785 required substituting the 710/50 filter on VL4 with a 780/60 filter. To ensure validity of comparisons made on different days, Rainbow Fluorescent beads (Spherotech, Inc. Lake Forest, IL) were acquired after the first day of sample acquisition, and used to align voltages to calibrate equivalent fluorescence intensities on later analysis dates. All flow cytometry experiments included Fluorescence Minus One controls used for setting gates. Data were analyzed using the FCS Express 7 software (De Novo Software, Pasadena, CA) platform.

2.3.9 *Statistical Analysis*

All data presenting results for analyses of identical replicate samples include the individual sample values as well as mean +/- standard error of the mean (SEM), except where otherwise noted. All significance tests were determined by p-values at the $\alpha=0.05$ level. Comparisons between the 'Control' staining technique to each cryopreservation technique were done using two-sided two-sample t-tests. Each method was compared to the 'Control' staining technique based on the mean difference from the 'Control' mean. Comparisons in Figure 2.5 were made using linear models assessing outcome association with cryopreservation method, treatment, or preparation-treatment interaction. Comparisons in Figure 2.6 were made using linear models to assess the effect of time, dose of treatment, and time-dose interaction on the measured immune parameters. For both analyses, F-tests were conducted to evaluate covariate significance. If the interaction term was determined insignificant, it was removed from the model. If significance was found in treatment effect by F-tests, then pairwise differences between treatment categories were reported. P-values were not corrected for multiple comparisons. Statistical analyses were done using R and Prism (Graphpad Software, San Diego, CA).

2.4 Results

2.4.1 Optimization of antibody staining panels and gating strategy

After gating out debris and doublets using both forward scatter and side scatter area vs. height, viable cells are identified in all staining panels by their low expression of fixable viability dye, ghostRed780 (Figure 2.1A). In the live cell gate, tumor cells (GD2+) are distinguished from hematopoietic derived (CD45+) cells. In the Lymphoid staining panel, live CD45+ cells are then divided by expression of CD3 (Figure 2.1A). Within the CD3+ population, the identification of NKT cells, CD4+ T cells, and CD8+ T cell subpopulations can be made. The CD3- population then contains the NK cell and CD19+ B cell populations. In our hands, NK cells were best identified by plotting NK1.1 against side scatter, though the population can be identified using other parameters such as NK1.1 vs CD45 or CD3. Among CD4+ T cells, co-expression of CD25 and the transcription factor FOXP3 clearly identifies the T (T_{reg}) cell subset [132,133]. An exclusion gate then distinguishes the T_{reg} from the non-T_{reg} CD4+ T cells, which can include both naïve and effector helper T cells. Programmed Cell Death receptor 1 (PD1) was included in the adaptive panel to quantify activation/exhaustion status of PD1-expressing immune cells including T, B, and NK cells (Figure 2.1A, Figure 2.4) [134]. Similarly, CD103 was included in this panel to identify tissue-resident lymphocytes, specifically CD8+ and CD4+ memory cell populations [135,136].

In a separate panel focused on myeloid cells (Figure 2.1B), tumor and splenic tissues were again gated to remove debris, isolate single cells, and isolate live CD45+ cells. Neutrophils and/or myeloid-derived suppressor cells (MDSCs) are first identified by their co-expression of CD11b and Ly-6G. Second, macrophages were identified from the Ly-6G negative population based on co-expression of F4/80 and CD64 [137]. The use of a second macrophage identifier like CD64 is critical for downstream differentiation of cDC2s, as some of these dendritic cells also express F4/80, and removal of the more autofluorescent macrophage population helps to eliminate contamination in other gates [138,139]. MHCII can then be used to further

subcategorize the macrophages into the more active, MHCII^{hi} , M1-like macrophages and more anti-inflammatory, MHCII^{lo}, M2-like macrophages. While this panel is certainly not enough to fully delineate the phenotypes of these macrophage lineages, the panel can easily be adjusted, by including markers such as CD206 and CD80/86, to more completely phenotype the macrophage population [140] if desired. The neutrophil-negative, macrophage-negative population is then subdivided based on expression of CD11b and Ly6C, and separates into four distinct populations. Within the CD11b-Ly6C- population, the CD11c+MHCII+ double positive cells are likely to be type 1 classical dendritic cells (cDC1s) based on their confirmatory co-expression of CD103 and XCR1 [138,141]. Conversely, within the CD11b+Ly6C+ population, the CD11c+MHCII+ double positive cells are likely to be type 2 classical dendritic cells (cDC2s) based on their CD103- and XCR1-double negative status. The CD11b+ Ly6C- population that expresses both CD11c and MHCII are largely monocyte-derived DCs (moDCs) based on their confirmatory expression of F4/80 and absence of CD103 [142,143]. The CD11b-Ly6C+ population may consist of granulocyte precursors or could represent Ly6C+ T cells in the tumor [144]. Further delineation of these populations could be achieved using a pooled lineage marker for CD3, CD19, and NK1.1 and confirming populations to be lineage negative [138], although this was not done here. Exact immunophenotypes for these above described populations are outlined in Table 2.2.

2.4.2 *Cryopreservation following staining and fixation is most concordant with freshly stained samples.*

After optimizing our comprehensive immunophenotyping panels, we sought to determine how cryopreservation affects immunophenotyping outcome based on when in the staining process cryopreservation is performed. Based on the literature [119,145–148], we identified three points in the process of sample preparation and staining to test introduction of a cryopreservation step (Figure 2.2A). The first point, labeled ‘Before’ in Figure 2.2A, freezes the

cells after dissociation but before any staining. This minimizes handling time following harvest and cryopreserves the cells in the ‘freshest’ possible state. Since freeze/thaw cycles are not recommended for either fixed samples or for the integrity of fluorophore-labeled antibodies [113–115] the ‘Before’ method may minimize the impact of cryopreservation on the quality of fixation and staining. The potential downside is that living cells experiencing a freeze/thaw cycle may alter their metabolism, surface expression of various markers, and viability and therefore become a confounding factor in subsequent analyses [119]. The second point, labeled ‘During’ in Figure 2.2A, freezes the cells after surface staining but prior to fixation and permeabilization. Thus, any change in surface marker expression due to cryopreservation would not be reflected in these samples. The cells are also still alive, meaning they are known to be able to survive cryopreservation without substantial damage or rupture of the cells. The ‘During’ method does freeze the fluorophore-labeled antibodies bound to the cells, which is a potential risk for signal degradation especially in tandem dyes [113–115]. The third point, labeled ‘After’ in Figure 2.2A, freezes the cells after all surface staining, fixation/permeabilization, and internal staining. This method most accurately captures the ‘fresh’ state of the TME at the time of harvest for the entire staining process, and avoids any expression changes that may be due to prolonged processing time and the stress of the cryopreservation process. It does however carry the risk of damaging the more rigid fixed cells as well as destroying the fluorophore labels through both fixation and freezing in the process.

To compare these four staining techniques (termed ‘Control’, ‘Before’, ‘During’, and ‘After’ throughout this manuscript) across both lymphoid and myeloid panels common pools of dissociated tumors and RBC-lysed spleens were made. We measured 27 distinct parameters for both tumor (Figure 2.2B and Figure 2.4A-D) and spleen (Figure 2.3 and Figure 2.4E-H) cell preparations and compared the performance of the 3 different cryopreservation protocols to the “fresh” control and to each other. In order to test whether the different cryopreservation methods had different effects on flow cytometry results, we compared the ‘Before’, ‘During’, and ‘After’

conditions to each other using Kruskal-Wallis tests for differences in all 27 immune parameters for both tumor and spleen cell preparations (Table 2.3). Significant ($p<0.05$) differences were observed for all 27 parameters in the spleen samples, and in 25 out of 27 parameters in the tumor samples, indicating that the cryopreservation protocol did impact most immunophenotyping results.

To determine which of the three cryopreservation protocols most closely resembled the non-cryopreserved control, we used a difference of means approach to determine the cryopreservation method that was closest to the reference 'Control' method for all parameters. Our results demonstrate that cryopreservation after all staining and fixation (the 'After' condition) had the smallest difference of means compared to the 'Control' in 18 out of 27 parameters for tumors and 17 out of 26 parameters for spleen. The 'Before' condition had the smallest difference compared to the 'Control' in 6 out of 27 parameters for tumor and 2 out of 26 parameters for spleen, and the 'During' condition had the smallest difference compared to the 'Control' in 3 out of 27 parameters in the tumor and 7 out of 26 parameters in the spleen. In addition, Student's t-tests could not reject the null hypothesis of equivalence ($p > 0.05$) when directly comparing the 'After' and 'Control' groups in 13 out of 27 parameters in the tumor and 5 out of 26 parameters in the spleen; in other words, for these parameters, these data could not prove the 'After' and 'Control' groups were different, even though this does not prove they were equivalent. While unable to statistically establish noninferiority or equivalence, these results do support the conclusion that the 'After' cryopreservation protocol yielded results very similar to the 'Control' method for these nonsignificant comparisons. Finally, the total number of cells analyzed (recovered events) were similar among the cryopreservation protocols, however the degree of live cell recovery was substantially lower in the 'Before' staining group compared to the 'Control', 'During' or 'After' groups. Taken together, these results suggest that cryopreservation after staining and fixation yields immunophenotyping results most concordant with freshly stained and analyzed samples.

It is known that PD1 is expressed on several immune cells, in particular T cells in response to T cell receptor stimulation [101]. Thus it is used as a gauge of both T cell activation and exhaustion, which is commonly evaluated in the context of the immune TME. In comparing the degree of PD1 expression measured on CD8+ T cells and CD4+ non-T_{reg} cells, a substantial difference was observed based on staining method (Figure 2.4). Median Fluorescence Intensity of PD1 on CD4+ non T_{reg} cells was almost double in the 'Before' staining condition in both tumor and spleen compared to the freshly stained control (Figure 2.4B and F). CD8+ T cells in the spleen exhibited the same doubling effect using the 'Before' staining condition (Figure 2.4E). However in the tumor, where resident T cells are known to be exhausted and have high expression of PD1 [149], no such difference in PD1 expression was detected (Figure 2.4A). In both CD19+ B cells (Figure 2.4D & H) and NK1.1+ NK cells (Figure 2.4C & C), the 'Before' staining condition resulted in increased PD1 expression in both the tumor and the spleen, again by an almost twofold difference. These results suggest that the process of cryopreservation and thawing can increase expression of PD1 on cells that are not already highly expressing PD1, and that the 'After' cryopreservation method results in the least change to detected PD1 levels compared to 'Control'.

2.4.3 *The 'After' cryopreservation technique yields similar conclusions as non-cryopreserved samples when analyzing the immune effects of an* in-situ *tumor vaccine*

It is known that immune cells can have different physical and biological properties depending on their activation state. For example, activated lymphocytes are more resistant to ionizing radiation and genotoxic anticancer drugs than naïve lymphocytes [150]. To study the potential for a differential impact on immunophenotyping results based on the activation state of the immune TME, we compared the 'Control' and 'After' cryopreservation techniques (as depicted in Figure 2.2A) by flow cytometry analyses for tumor samples from mice receiving a

previously published *in situ* vaccine tumor immunotherapy regimen [65]. C57BL/6 mice bearing ~5wk syngeneic B78 flank melanoma tumors were treated with either PBS sham, 12Gy RT only, or with 12Gy RT + intratumoral hu14.18-IL2 immunocytokine as previously described [65]. Tumors were harvested, dissociated, and processed according to either the 'Control' (fresh) or 'After' (cryopreserved) staining protocols (from Figure 2.2A) using a hybrid lymphoid/myeloid flow cytometry staining panel (Table 2.4). Eight immune parameters were assessed using linear regression models for association with treatment (PBS, RT, or RT+IC), preparation condition ('After' or 'Control' protocol), or treatment-preparation interaction (Figure 2.5). No interaction between treatment and preparation technique was detected for any of the immune parameters, suggesting that the preparation technique used did not affect the impact of treatment. In addition, no significant effect of preparation was detected in the model other than for NK cells, which had a borderline p value of 0.046 (Figure 2.5D). This suggests that NK cell content is slightly different in the cryopreserved preparation compared to fresh, but this difference does not change with treatment. Our analyses, based on modeling of treatment effect, identified significantly greater percentages for all seven distinct immune populations (CD45+ cells, CD4+ T cells, NK1.1+ NK cells, CD8+ T cells, CD4+CD25+ T_{reg} cells, CD19+ B cells, and CD11b+ myeloid cells), expressed as a percentage of live cells, in the RT+IC immunotherapy group compared to PBS control (Figure 2.5A,C,D,E,F,G,H). Though immunosuppressive T_{reg} cells were higher in the RT+IC group, the CD8/T_{reg} ratio was also substantially greater in the RT+IC group as well (Figure 2.5B). Taken together, these data suggest that the 'After' cryopreservation technique largely reflects the same flow cytometry results in the immunotherapy-treated TME as obtained using the 'Control' technique, and allow for similar conclusions to be drawn about the effect of an *in situ* vaccine.

2.4.4 Use of the 'After' cryopreservation preparation technique enables demonstration of alterations to the TME following ^{90}Y-NM600 MTRT.

To demonstrate the use of the 'After' cryopreservation protocol in analyzing radioactive tissue and to explore the time- and dose-dependent effects of ^{90}Y-NM600 MTRT on the immune TME, we conducted a time course study in C57BL/6 mice bearing ~5 week syngeneic B78 flank tumors (Figure 2.6). On treatment day 0, mice were given a tail vein injection of either PBS control, 50μCi of ^{90}Y-NM600, or 250μCi of ^{90}Y-NM600. Tumors were harvested weekly on treatment days 1, 7, 14, and 21 following injection, dissociated, and stained for analysis according to the 'After' cryopreservation protocol using a hybrid innate/adaptive staining panel (Table 2.5). Immune parameters were assessed using linear regression models for association with time following injection, dose of treatment (PBS, 50μCi, or 250μCi), or time-dose interaction. Results demonstrate significant ($p<0.05$) effect of time for all parameters, and significant time-dose interaction for all parameters except for NK cell content (Figure 2.6B), the fraction of NK cells expressing CD11b (Figure 2.6C), and Neutrophil/MDSC content (Figure 2.6E). This demonstrates that MTRT had a time-and dose-dependent effect on most immune populations.

The 50μCi dose resulted in increased infiltration of CD11b^{hi} myeloid cells on Days 1 and 7 (Figure 2.6D), and a mildly decreased infiltration of CD19^{+} B cells on Day 7 compared to PBS (Figure 2.6F). The 50μCi dose also briefly increased the CD8+ T cell:T_{reg} cell ratio on day 1 (Figure 2.6G) due to a decrease in T_{reg} content (Figure 2.6I). The larger 250μCi dose resulted in a sustained decreased in CD45^{+} cells (Figure 2.6A), NK cells (Figure 2.6B), CD19 B cells (Figure 2.6F), and T_{reg} cells (Figure 2.6I) compared to both the PBS control and the 50μCi dose on days 7, 14, and 21. The higher dose also resulted in a relative increase in CD11b^{hi} myeloid cells on day 1, but a relative decrease on Day 14 compared to PBS control (Figure 2.6D). In addition to substantially decreased T_{reg} cells, the higher MTRT dose also resulted in a decrease

in CD8+ T cells on days 7 and 21 compared to control (Figure 2.6H), however the CD8 T cell:T_{reg} ratio was significantly greater on days 7, 14, and 21 in the higher dose group compared to either PBS control or the lower 50μCi dose group (Figure 2.6G). Lastly, although total NK cells were decreased in the higher dose group on days 7, 14 and 21 (Figure 2.6B), the fraction of NK cells expressing CD11b was higher in the 250μCi dose group compared to PBS control for days 1, 7, and 14 (Figure 2.6C). Together, these data demonstrate the changes in the immune TME following systemic administration of ^{90}Y-NM600 as a function of both MTRT dose and time, with prominent, MTRT dose dependent, long-lasting decreases of several immune populations, that are now able to be analyzed using the 'After' cryopreservation protocol.

2.5 Discussion

In this study we describe a cryopreservation and immunophenotyping approach for analyzing dissociated cell preparations from murine spleens and tumors that must be cryopreserved prior to flow cytometry analyses. We used two panels of phenotyping mAbs to evaluate the impact of three separate cryopreservation strategies that differed by when the cryopreservation step is performed in the staining/processing sequence. We compared cryopreservation done 'Before,' 'During,' and 'After' staining/processing (Figure 2.2A). Our data show that cryopreserving samples after all surface staining, fixation/permeabilization, and internal staining has been performed (the 'After' protocol) resulted in the least impact of cryopreservation on immunophenotyping results, when compared in parallel to analyses of freshly obtained (non-cryopreserved) spleen and tumor cell preparations. This cryopreservation approach was then compared head-to-head with a no-cryopreservation protocol for tumors in mice receiving combination immunotherapy; analyses of the fresh and the cryopreserved tumor samples demonstrated the same TME phenotype changes in response to an *in situ* vaccine. Lastly, this flow cytometry approach was used to characterize time- and dose-dependent

changes to the TME following ^{90}Y-NM600 injection in radioactive tissues requiring cryopreservation (in order to allow the radioactivity to decay to baseline levels to enable analysis using our core facility's flow cytometer).

Cryopreservation of PBMCs is a common practice for multicenter studies to reduce variability and delays in processing and has been used heavily in the clinical study of HIV treatments [151]. One study found that cryopreservation of PBMCs prior to staining did not substantially change the frequency of detected CD4 and CD8 T cell subsets, but did notice changes in markers of activation including CD62L and CCR5 [110]. Another study concluded that cryopreservation of human PBMCs had a relatively small impact on detected frequencies of terminally differentiated CD4+ and CD8+ T cells [152]. However other more recent studies have described a drop in detected T and NK subsets following cryopreservation and staining [153,154]. This is consistent with our study, which shows that the frequency of NK1.1+, CD3+, CD4+, and CD8+ T cells are substantially reduced with the 'Before' and 'During' cryopreservation methods; but these decreased frequencies are substantially less (or not) evident with the 'After' cryopreservation method (Figure 2.2B and Figure 2.3). We also observed a significant decrease in CD19+ B cell frequency in both tumor and spleen, particularly following the 'Before' method, which is consistent with published observations with cryopreserved PBMCs in humans [118]. This decrease in B cells was substantially less evident when using the 'After' cryopreservation method (Figure 2.2B and Figure 2.3).

Studies of human T_{reg} cells, defined by surface marker expression of CD4, CD25, and lack of CD127, suggest a decrease in the frequency of detectable T_{reg} cells following cryopreservation of PBMCs [146,155]. However van Pul and colleagues detected a relative increase in the number of CD4+ CD25+ cells in cryopreserved breast sentinel lymph node dissociate [117]. This latter result is consistent with our observation that the relative number of CD4+CD25+ FOXP3+ cells is substantially higher in the 'Before' and 'During' cryopreservation

methods for both spleen and tumor, but not for the ‘After’ cryopreservation method (Figure 2.2B and Figure 2.3). One possible explanation for the differences reported for human PBMC and solid tissue T_{regs} [100,117,146] may be that PBMCs from liquid tissue and splenocytes extracted from solid tissue may react to cryopreservation differently. It is also important to note that our method for defining T_{regs} includes the intracellular transcription factor FOXP3 in addition to surface markers. Nevertheless, van Pul and colleagues speculate that the cryopreservation process may stress these populations such that regulatory immunosuppressive processes are activated. Indeed, we observed that lymphocytes (CD4, CD8, NK and B cells) analyzed with the ‘Before’ method had higher expression of PD1 compared to control (Figure 2.4). This pattern is observed in tumor and splenic CD4+ T cells, B cells, and NK cells, and also in splenic (but not tumor) CD8+ T cells. However in the tumor, which has high baseline expression of PD1 on tumor infiltrating CD8+ T cells, no further increase over control was seen for PD1 levels using the ‘Before’ cryopreservation method. This suggests that cryopreservation prior to staining may nonuniformly alter PD1 expression depending on its baseline expression and may bias resulting conclusions. As most multicenter clinical trials use a version of the ‘Before’ cryopreservation method, studying the potential magnitude of this bias on other markers of activation and exhaustion may prove to be helpful.

The above described changes in T cell, NK cell, B cell frequencies and PD1 expression following cryopreservation highlight the significant stress that cells can be subjected to during the cryopreservation and thawing process. Though there are multiple published protocols which propose methods of mitigating the impact of cryopreservation on surface marker expression, including resting the cells in culture conditions prior to staining [133], it is likely that any protocol that subjects live, metabolically active cells to cryopreservation prior to staining risks nonuniformly altering an immune population and biasing conclusions. In particular, cryopreserving live cells and then thawing those cells that remained viable through the

cryopreservation process, might cause an increase in stress related markers (like PD1) that would be apparent when the anti-PD1 staining is done after both the freezing and thawing. Our study demonstrates that, contrary to some of our initial assumptions, staining and fixing an immune cell population prior to cryopreservation reliably produces flow cytometry results most concordant with the flow cytometry analyses of non-cryopreserved samples, which avoids the risk of such nonuniform biases. This principle has been demonstrated in *ex vivo* stimulated splenocytes by Alice, Zebertavage and colleagues, in which splenocytes were surface stained, fixed, frozen for 4 hours, then stained for internal markers in a study of IFNγ production [156,157]. We hypothesize that the "stress" of cryopreservation would be less likely to change the amount of stress molecules on the cells detected by fluorescent mAbs when the antibodies have been applied and the cells have been fixed prior to the cryopreservation, as is the case for the 'After' method used here.

Our data re-demonstrate evidence of enhanced immune cell activation following combination RT+IC. In a previous study by Morris and colleagues, immunohistochemical analysis was used to demonstrate increased concentration of both CD8+ T cells and NK cells in B78 melanoma tumors treated with combined RT+IC compared to either alone [65]. Our results confirm these prior findings of increased infiltrates of CD8+ T cells and NK cells. With these observations we extend the characterization of the immune infiltrate following RT+IC *in situ* vaccine by demonstrating increased CD45+ cells, CD4+ T cells, CD19+ B cells, CD11b+ myeloid cells, and an increased CD8/T_{reg} ratio. We also observe an increase in CD4+CD25+ FOXP3+ T_{reg} cells, which could limit the efficacy of treatment, although the enhanced CD8/T_{reg} ratio supports a predominantly antitumor effector response. Importantly, comparing the effect of the cryopreservation technique ('Control' vs 'After') in the linear models demonstrated no difference in outcome based on technique, save for a borderline significant effect in NK cells. However, as there was insignificant interaction between treatment effect and preparation effect,

it is likely that this difference would not affect comparisons between a treatment group and control group. Importantly, the lack of significant treatment-preparation interaction in most parameters implies that cryopreservation does not affect activated immune cells differently than inactive ones. Thus, our ‘After’ cryopreservation technique can be used to interrogate changes to the immune TME following immunotherapy.

Our cryopreservation protocol was also used to evaluate samples from mice treated with ^{90}Y-NM600 MTRT, that required 25+ days of lead-shielded storage to enable sufficient half-lives of the ^{90}Y to expire to allow the radioactivity of the mouse tissues to decay to background levels. This allowed us to do the flow cytometry analyses of these samples, which were no longer radioactive, using our cancer center’s shared core service flow cytometry equipment (which does not allow analyses of any radioactive samples). This analysis successfully demonstrated phenotypic changes to the cells in the TME in a time- and dose-dependent manner following administration of ^{90}Y-NM600. The analysis did detect a time-dependent effect in most cell populations for all treatment groups, including the PBS untreated control (data in Figure 2.6, statistical analysis not shown). These time-dependent alterations in the immune TME of these untreated tumors may be explained by the constantly changing size of the tumors over time. Tumor size at the time of treatment is known to have an impact on efficacy of immunotherapies in similar preclinical settings [64]. Thus it is reasonable to expect some variation in immune populations in the control PBS tumors that are growing over time. However, the model results additionally demonstrated that the effect of dose changes with time for almost all of the measured parameters (as indicated by significant treatment-time interaction by F-tests), which confirms that, in addition to baseline time-dependent changes without treatment, the MTRT agent does cause alterations to the immune TME in a dose-dependent manner.

The use of the ‘After’ cryopreservation protocol has allowed for more detailed analysis of dose effect in the immune TME than has been previously described. Compared to untreated

controls on the same day post-treatment, the 50μCi dose did not alter most immune populations substantially, save for $CD11b^{hi}$ myeloid cells and T_{regs} on post injection day 1 (Figure 2.6). This caused a small but statistically significant increase in the CD8/Treg ratio relative to the untreated control tumor. More substantial phenotypic changes were demonstrated with the higher 250 μCi dose, including a decrease in the number of $CD45^{+}$ immune cells, NK cells, B cells, and T_{reg} cells on days 7, 14, and 21 following injection compared to control. In addition to these decreases in cell numbers for some parameters, there is evidence that the proportions of certain immune populations were also altered following the higher dose. For instance, the fraction of NK cells expressing CD11b, which are considered "mature" NK cells, rose in the 250μCi group following treatment [158]. In addition, although CD8+ T cells were decreased on days 7 and 21, T_{reg} cells were more substantially decreased on all post-treatment days, resulting in greater $CD8/T_{reg}$ ratios in the 250μCi group on days 7, 14, and 21. These observations may indicate different radiosensitivities in different immune populations (for example T_{regs} vs. CD8+ T cells). Importantly, these changes observed at 250μCi were generally not observed at 50μCi, which emphasizes the dose-dependent nature of MTRT. Additionally, changes following a 50μCi injection were not detected after Day 7, but the changes from the 250μCi injection lasted longer, in some cases through Day 21. This timing effect may be important in future studies when considering combining MTRT with other immunotherapies. Further investigation of the kinetic changes, dose response, and sensitivity of tumor type to MTRT are warranted to follow up on these findings. Clearly, there is a complex dynamic in the tumor in response to MTRT, and our 'After' cryopreservation technique provides opportunity to study these effects in detail.

This cryopreservation strategy may also be helpful in the several other situations where flow cytometric analyses need to be performed at a delayed time, requiring cryopreservation of samples. Many immune flow cytometric analyses in animal models receiving cancer immunotherapy require analyses on samples from randomized groups of mice collected over

several weeks; time is needed implant tumors, allow them to grow to treatment size, administer treatment, and then wait until the predetermined time points post-treatment to harvest and analyze the tissues. During this window when mice are “committed” to the experiment, a loss in access to flow cytometers would result in a lost experiment. The ability to stain and cryopreserve the tumor samples for prolonged periods is a critical reserve option to preserve the experiment. In our institution’s case, the University of Wisconsin Carbone Cancer Center Flow Cytometry lab was abruptly shut down for a 14 day quarantine following a positive contact with a COVID-19 patient. Using this cryopreservation method, experiments requiring flow cytometry were able to be stained and cryopreserved until the lab was properly disinfected, institutional policies could be drafted and followed, and adequate PPE was available to use safely, enabling completion of the planned flow cytometry analyses.

2.6 Acknowledgements and clarification of collaborative efforts from others in this work

As science is best conducted in a team setting, I would be remiss not to acknowledge the contributions of those that assisted me in this chapter. Manasi Mohan, Matthew Rodriguez, and Ravi Patel assisted in the acquisition of tumor and spleen tissue, as well as assisted in flow cytometry staining. Lauren Nettenstrom, Dagna Sheerar, Kathryn Fox, and Anna Hoefges are each themselves experts in flow cytometry and provided valuable discussion and feedback during the experimental design and analysis phases of this project. Reinier Hernandez and thesis committee member Jamey Weichert provided the radiolabeled MTRT agent ^{90}Y-NM600 for use in this and in many other studies. Jen Birstler assisted in statistically analyzing these results and in figure generation. Chris Zahm, working with thesis committee member Doug McNeel, has previous experience in fixing cells prior to freezing them for flow analysis, and helped in the original design of the first set of experiments. Finally, Thesis committee members and co-mentors Zach Morris and Paul Sondel provided the guidance, funding, discussion, and

editing support for the final version of this chapter. This chapter has been edited slightly from a complete manuscript that has recently been submitted for publication*. All of these above individuals are listed as co-authors on that submitted manuscript, and read and/or edited as well as approved of that submission. Special thanks to Drs. Alexander L. Rakhmilevich, Amy K. Erbe, and Jacquelyn A. Hank for thoughtful discussion of experimental design and results. We would like to thank Steve Kovo for the design and creation of the artwork in Figure 2.2A (website at www.stevekovo.com).

* Carlson PM, Mohan M, Patel R, Birstler J, Nettenstrom l, Sheerar D, Fox K, Rodriguez M, Hoefges A, Hernandez R, Zahm C, Kim KM, McNeel DG, Weichert J, Morris ZS, Sondel PM. Optimizing flow cytometric analysis of immune cells in samples requiring cryopreservation from tumor-bearing mice. Submitted 2020.

Table 2.1: Flow Cytometry Panels used to evaluate different cryopreservation protocols.

	Target	Fluorophore	Company (Cat.)	Clone	Volume per Test (µL)
Lymphoid Panel	CD25	BB515	BD Biosciences (564424)	PC61	1.5
	CD103	PE	BioLegend (121406)	2E7	1.5
	NK1.1	PE-CF594	BD Biosciences (562864)	PK136	1.2
	CD19	PE-Cy5	BioLegend (115510)	6D5	0.5
	FOXP3	PE-Cy7	Invitrogen (25-5773-82)	FJK-16s	1.4
	PD-1	V450	Tonbo (75-9981-U100)	RMP1-30	1.2
	CD45	BV510	BioLegend (103137)	30-F11	1
	CD3	BV605	BioLegend (100351)	145-2C11	1.2
	CD4	BV785	BioLegend (100453)	GK1.5	1
	GD2	APC	BioLegend (357306)	14G2a	1
	CD8	APC-R700	BD Biosciences (564983)	53-6.7	1
	Live/Dead	GhostRed 780	Tonbo (13-0865-T100)	-	0.5µL
Myeloid Panel	CD45	FITC	Tonbo (35-0451-U500)	30-F11	1
	CD103	PE	BioLegend (121406)	2E7	1.5
	MHCII	PE-Dazzle594	BioLegend (107648)	M5/114.15.2	1.2
	F4/80	PE-Cy5	Invitrogen (15-4801-82)	BM8	1
	CD64	PE-Cy7	BioLegend (139314)	X54-5/7.1	1.2
	CD11b	V450	BD Biosciences (560455)	M1/70	1.5
	XCR1	BV510	BioLegend (148218)	ZET	3
	Ly6C	BV605	BD Biosciences (563011)	AL-21	2
	CD24	BV711	BD Biosciences (563450)	M1/69	1.2
	CD11c	APC	BioLegend (117310)	N418	1.2
	Ly6G	AF700	BD Biosciences (561236)	1A8	1.2
	Live/Dead	GhostRed 780	Tonbo (13-0865-T100)	-	0.5µL

Table 2.2: Gating Immunophenotypes used in comparing staining protocols. All samples were gated on all cells, followed by single cells identified by both forward and side scatter area vs height, and live cells by viability dye exclusion.

	Population	Gating Phenotype (after Cells/Single/Live)
Lymphoid Panel	CD45+	CD45+
	Tumor Cells	CD45- /GD2+
	NKT Cells	CD45+/CD3+/NK1.1+
	CD8+ T Cells	CD45+/CD3+/NK1.1-/CD8+
	CD4+ T Cells	CD45+/CD3+/NK1.1-/CD4+
	Treg Cells	CD45+/CD3+/NK1.1-/CD4+/CD25+/foxp3+
	B Cells	CD45+/CD3-/CD19+
	NK Cells	CD45+/CD3-/NK1.1+
Myeloid Panel	Neutrophils	CD45+/CD11b+/Ly6G+
	Macrophages	CD45+/Ly6G-/F4/80+CD64+
	M1-Like Macrophages	CD45+/Ly6G-/F4/80+CD64+/MHCII^{hi}
	M2-Like Macrophages	CD45+/Ly6G-/F4/80+CD64+/MHCII^{lo}
	Classical type 1 DCs	CD45+/Ly6G-/F4/80-CD64-/CD11b-/Ly6C-/CD11c+/MHCII+/CD103+/XCR1+
	Classical type 2 DCs	CD45+/Ly6G-/F4/80-CD64-/CD11b+/Ly6C+/CD11c+/MHCII+/CD103-/XCR1-
	Monocyte-derived DCs	CD45+/Ly6G-/F4/80-CD64-/CD11b+/Ly6C-/CD11c+/MHCII+/F4/80+/CD103-

Table 2.3: Statistical differences between staining methods are detected in almost all parameters. The performance of both lymphoid and myeloid staining panels in tumor and spleen were compared to each other by testing for differences within the 3 cryopreservation protocols (excluding the non-cryopreserved 'Control' group) using Kruskal-Wallis tests. Note that GD2 was not tested for in splenic tissue, as it is a tumor-specific marker. Significant differences were detected within the three cryopreservation protocols for all parameters except for cDC1 percent of Live cells in the tumor, and cDC2 percent of live cells in the tumor.

Parameter	Spleen	Tumor
Total Events	<0.001	0.018
Total Live Events	<0.001	<0.001
GD2 (% of Live)	-	<0.001
CD45 (% of Live)	<0.001	<0.001
CD19 (% of Live)	<0.001	<0.001
NK1.1 (% of Live)	<0.001	<0.001
CD3 (% of Live)	<0.001	<0.001
NKT (% of Live)	<0.001	0.002
CD8 (% of Live)	<0.001	<0.001
CD4 (% of Live)	<0.001	<0.001
Tregs (% of CD4)	<0.001	<0.001
Non-Tregs (% of CD4)	<0.001	<0.001
CD4+PD1+ (% of non-Tregs)	<0.001	<0.001
CD4+CD103+ (% of non-Tregs)	<0.001	0.010
CD8+PD1+ (% of CD8)	<0.001	<0.001
CD8+CD103+ (% of CD8)	<0.001	<0.001
Neutrophils/MDSCs (% of Live)	0.011	<0.001
Macrophages (% of Live)	0.006	0.002
M1-like (% of Macrophages)	0.004	<0.001
M2-like (% of Macrophages)	0.005	<0.001
cDC1 (% of Live)	0.001	0.363
cDC2 (% of Live)	<0.001	0.558
Monocyte-Derived DCs (% of Live)	<0.001	0.007
CD4+ non-Tregs PD1 MFI	<0.001	<0.001
CD8+ PD1 MFI	<0.001	0.003
NK1.1 + PD1 MFI	<0.001	<0.001
CD19+ PD1 MFI	<0.001	<0.001

Table 2.4: Staining panel used in the comparison of 'Control' vs. 'After' protocols on tumors treated with EBRT+IC immunotherapy (Figure 2.5). Note that although Ly6G and Helios are included in the staining panel, comparison to Fluorescence Minus One controls demonstrated failure to stain for these markers.

Target	Fluorophore	Company (Cat.)	Clone	Volume per Test (µL)
CD25	BB515	BD Biosciences (564424)	PC61	1.5
Ly6G	PE	BioLegend (127608)	1A8	1
NK1.1	PE-CF594	BD Biosciences (562864)	PK136	1.2
CD19	PE-Cy5	BioLegend (115510)	6D5	0.5
FOXP3	PE-Cy7	Invitrogen (25-5773-82)	FJK-16s	1.4
CD11b	V450	BD Biosciences (560455)	M1/70	1.5
CD45	BV510	BioLegend (103137)	30-F11	1
CD4	BV785	BioLegend (100453)	GK1.5	1
Helios	APC	BioLegend (137221)	22F6	1
CD8	APC-R700	BD Biosciences (564983)	53-6.7	1
Live/Dead	GhostRed 780	Tonbo (13-0865-T100)	-	0.5µL

Table 2.5: Staining panel for time course evaluation of the impact of ^{90}Y-NM600 on tumor immune infiltrates (Figure 2.6).

Target	Fluorophore	Company (Cat.)	Clone	Volume per Test (µL)
CD25	BB515	BD Biosciences (564424)	PC61	1.5
MHCI	PE	BioLegend (114608)	28-8-6	1.5
NK1.1	PE-CF594	BD Biosciences (562864)	PK136	1.2
CD19	PE-Cy5	BioLegend (115510)	6D5	0.5
FOXP3	PE-Cy7	Invitrogen (25-5773-82)	FJK-16s	1.4
PD-1	V450	Tonbo (75-9981-U100)	RMP1-30	1.2
CD11b	V450	BD Biosciences (560455)	M1/70	1.5
Ly6G	BV605	BD Biosciences (563005)	1A8	1
CD4	BV785	BioLegend (100453)	GK1.5	1
GD2	APC	BioLegend (357306)	14G2a	1
CD8	APC-R700	BD Biosciences (564983)	53-6.7	1
Live/Dead	GhostRed 780	Tonbo (13-0865-T100)	-	0.5µL

Figure 2.1: Representative gating strategy for evaluation of 25 immune parameters in dissociated tumor or splenic tissue. Tumors or spleens from C57BL/6 mice were harvested and dissociated as outlined in materials and methods. The gating strategy outlined in **(A)** shows the lymphoid immune panel used to identify the following populations from a sample after excluding debris and gating on single cells: total live cells; GD2+ tumor cells; CD45+; CD3+; CD4+; T_{reg} Cells; T helper cells; CD8+; CD19+; NK; and NKT cell populations. Populations of T, B, and NK cells were also evaluated for expression of the CD103 memory marker and PD1 activation/exhaustion marker [the representative gating strategy presented here shows PD1 and CD103 evaluation for the T cell subsets (CD8+, CD4+ T_{reg}, CD4+ non-T_{reg}) only]. The gating strategy outlined in **(B)** shows the myeloid immune panel used to identify the following populations in a sample (after excluding debris and gating on single cells as in A): total live cells; CD45+; Neutrophils/MDSCs; Macrophages; type 1 classical dendritic cells (cDC1); type 2 classical dendritic cells (cDC2); and monocyte-derived dendritic cells (Mo-DCs). Macrophages were also subcategorized into M1-like and M2-like based on high or low expression of MHCII, respectively. Gates were set using corresponding Fluorescence Minus One controls. All assay replicates were pooled for this representative gating strategy for visualization of rare populations.

Figure 2.1

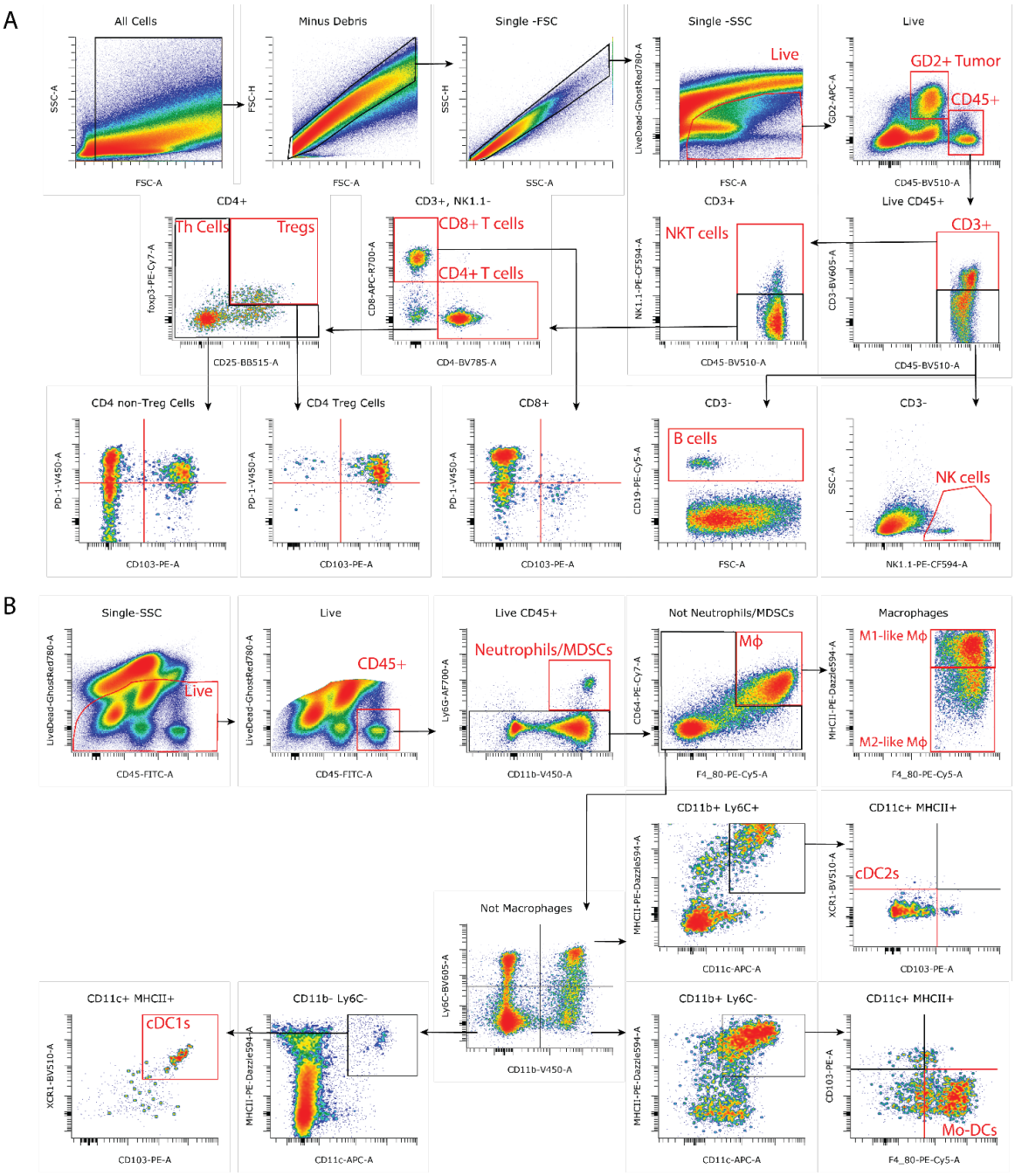
A
All Cells
Minus Debris
Single -FSC
Single -SSC
Live
GD2+ Tumor
CD45+
CD4+
Th Cells
Tregs
CD3+, NK1.1-
CD8+ T cells
CD4+ T cells
CD3+
NKT cells
Live CD45+
CD3+
CD4 non-Treg Cells
CD4 Treg Cells
CD8+
CD3-
B cells
CD3-
NK cells
B
Single-SSC
Live
Live
CD45+
Live CD45+
Neutrophils/MDSCs
Not Neutrophils/MDSCs
Mϕ
Macrophages
M1-like Mϕ
M2-like Mϕ
CD11b+ Ly6C+
CD11c+ MHCII+
cDC2s
Not Macrophages
CD11c+ MHCII+
cDC1s
CD11b- Ly6C-
CD11b+ Ly6C-
CD11c+ MHCII+
Mo-DCs

Figure 2.2: Comparison of sample staining and cryopreservation techniques across comprehensive immunophenotyping panels. **A)** As described in the text, tumor and spleen samples were dissociated and resuspended. These single-cell suspensions are stained with fixable viability dye, Fc Blocked, surface target stained, fixed and permeabilized, internal target stained, and analyzed, with a wash and pelleting step in between each. Results of these analyses on freshly obtained, never cryopreserved samples are shown in black ('Control'). For replicate samples, 3 separate times in this workflow of staining-fixation-permeabilization-staining were tested for cryopreservation. These included cryopreservation prior to all staining ('Before', red); after surface staining but before fixation ('During', green); or after all fixation and staining ('After, blue). **B)** Five C57BL/6 mice bearing B78 syngeneic melanoma tumors had tumors (shown here) and spleens (shown in Figure 2.3) harvested as described in materials and methods and pooled to create a homogenous starting population of tumor or spleen dissociates. Each population was analyzed using the lymphoid and myeloid phenotyping panels described in Figure 2.1 and Tables 2.1 and 2.2, using each of the four cryopreservation protocols: 'Control '(not cryopreserved), or cryopreserved 'Before', 'During' or 'After'. The 23 separate graphs show the mean and 95% confidence interval of n=7 assay replicates in each parameter listed above each graph for each cryopreservation protocol in the dissociated tumor cell preparations. Filled red, green or blue symbols indicate a significant ($p < 0.05$) difference on a t test when compared to the 'Control'(black) protocol, and open red, green or blue symbols indicate nonsignificant ($p > 0.05$) differences when compared to the 'Control' protocol.

Figure 2.2

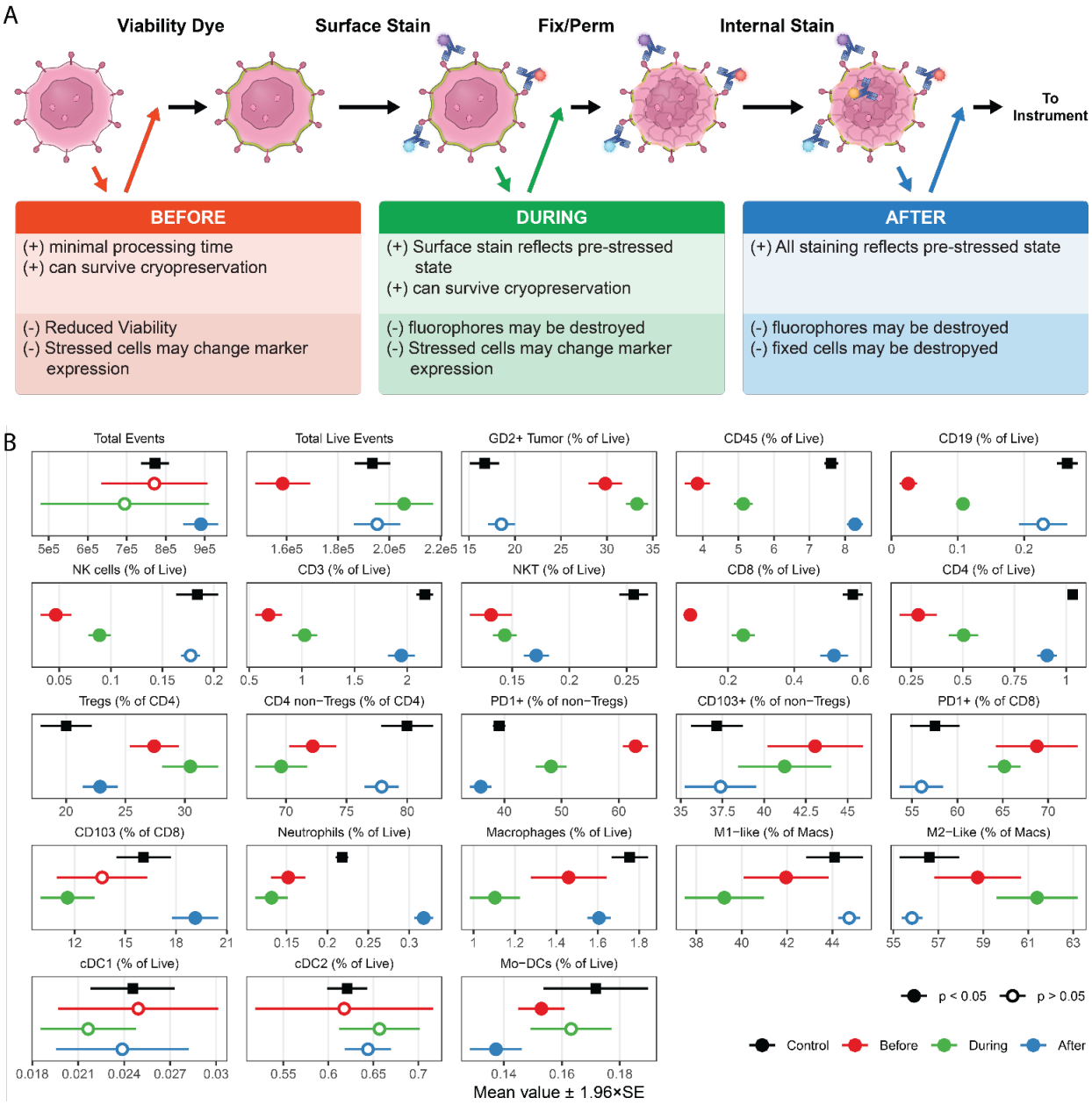
A
Viability Dye
Surface Stain
Fix/Perm
Internal Stain
To Instrument
BEFORE
(+) minimal processing time
(+) can survive cryopreservation
(-) Reduced Viability
(-) Stressed cells may change marker expression
DURING
(+) Surface stain reflects pre-stressed state
(+) can survive cryopreservation
(-) fluorophores may be destroyed
(-) Stressed cells may change marker expression
AFTER
(+) All staining reflects pre-stressed state
(-) fluorophores may be destroyed
(-) fixed cells may be destropyed
B
Total Events
Total Live Events
GD2+ Tumor (% of Live)
CD45 (% of Live)
CD19 (% of Live)
NK cells (% of Live)
CD3 (% of Live)
NKT (% of Live)
CD8 (% of Live)
CD4 (% of Live)
Tregs (% of CD4)
CD4 non−Tregs (% of CD4)
PD1+ (% of non−Tregs)
CD103+ (% of non−Tregs)
PD1+ (% of CD8)
CD103 (% of CD8)
Neutrophils (% of Live)
Macrophages (% of Live)
M1−like (% of Macs)
M2−Like (% of Macs)
cDC1 (% of Live)
cDC2 (% of Live)
Mo−DCs (% of Live)
p < 0.05
p > 0.05
Control
Before
During
After
Mean value ± 1.96×SE

Figure 2.3: Comparison of 24 immune parameters across myeloid and lymphoid panels in pooled spleen samples. B) Five C57BL/6 mice bearing B78 syngeneic melanoma tumors had spleens harvested and RBC lysed as described in materials and methods and pooled to create a homogenous starting population of splenic samples. Each population was analyzed using the lymphoid and myeloid phenotyping panels described in Figure 3.1 and Tables 2.1 and 2.2, using each of the four cryopreservation protocols (Control, Before, During, After) described in Figure 3.2. The analyses of the tumor cell preparations are shown in Figure 3.2B and the spleen cell preparations are shown here. The 24 graphs show the mean and 95% confidence interval of n=7 assay replicates in each parameter, listed above each graph, for each cryopreservation protocol in spleen samples. Note that GD2 was not tested for in splenic tissue, as it is a tumor-specific marker. Filled red, green or blue symbols indicate a significant ($p < 0.05$) difference on a t test when compared to the 'Control' (black) protocol, and open red, green or blue symbols indicate nonsignificant ($p > 0.05$) differences compared to the control.

Figure 2.3

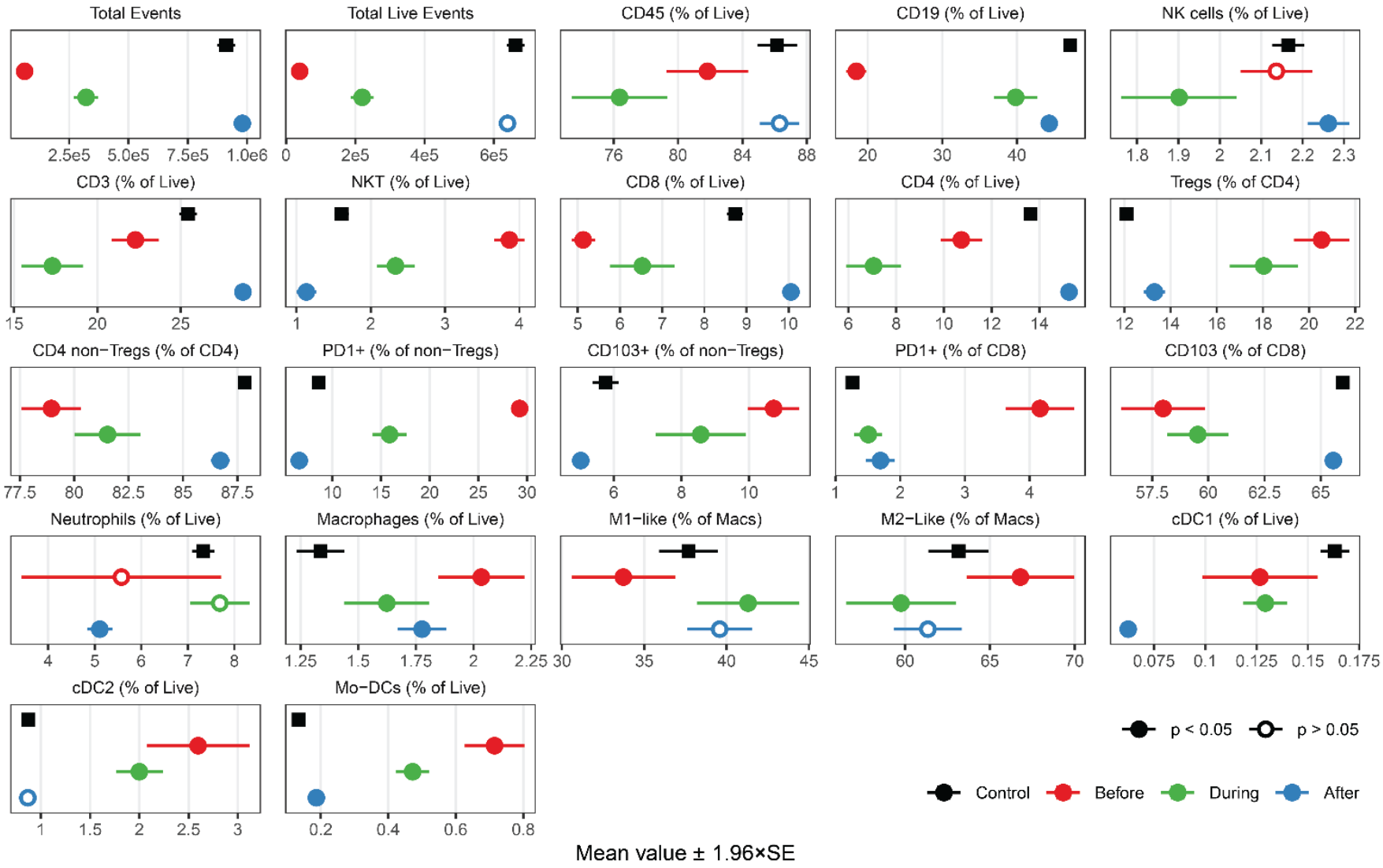

Mean value ± 1.96×SE

Figure 2.4: Sequence of cryopreservation nonuniformly alters PD1 expression in T cells, B cells, and NK cells. Five C57BL/6 mice bearing B78 syngeneic melanoma tumors had tumors and spleens harvested as described in materials and methods and pooled to create a homogenous starting population of both tumor and spleen dissociated cells. Each population was analyzed using the lymphoid and myeloid phenotyping panels described in Figure 2.1 and Tables 2.1 and 2.2, using each of the four cryopreservation protocols (Control, Before, During, After). Median Fluorescence Intensity (MFI) of PD1 staining was measured for CD8+ T cells (A and E), CD4+ helper (gated as CD4+, non-T_{reg}) T cells (B and F), NK1.1+ NK cells (C and G) , and CD19+ B cells (D and H) in both tumor (A through D) and spleen (E through H) samples. Statistical Comparisons were made using two-sample t-tests, comparing each staining condition to the non-frozen control method. * = $p<0.05$, ** = $p<0.01$, *** = $p<0.001$, **** = $p<0.0001$, ns = not significant.

Figure 2.4

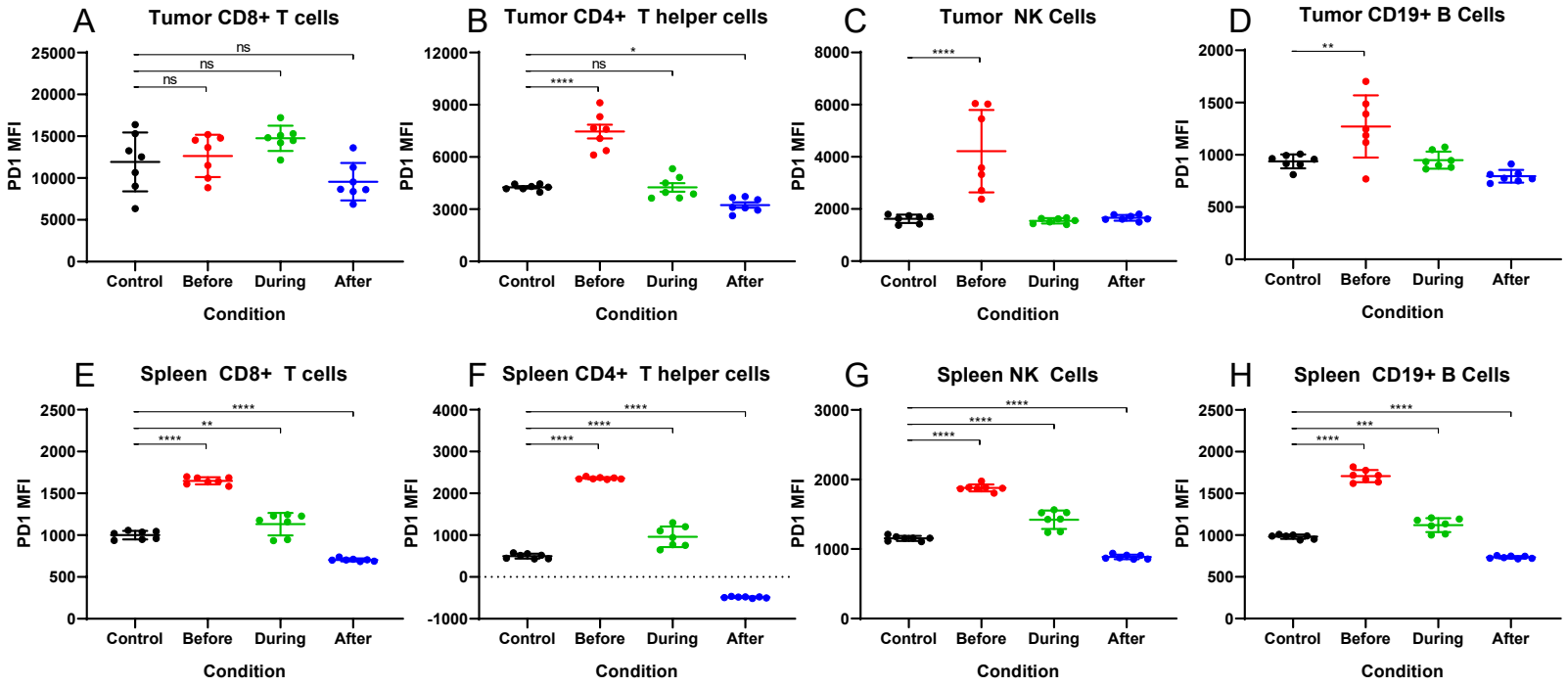
A
Tumor CD8+ T cells
B
Tumor CD4+ T helper cells
C
Tumor NK Cells
D
Tumor CD19+ B Cells
E
Spleen CD8+ T cells
F
Spleen CD4+ T helper cells
G
Spleen NK Cells
H
Spleen CD19+ B Cells
PD1 MFI
Control
Before
During
After
Condition
ns
*
**
***
****

Figure 2.5: Comparison of 'Control' and 'After' preparation methods for flow cytometric analyses of immune cells in the TME following immunotherapy with RT and IT-IC. C57BL/6 mice bearing ~5wk syngeneic B78 melanoma flank tumors were treated using a previously published *in situ* vaccine consisting of 12Gy external beam radiation (RT) on treatment day 1, followed by 5 daily intratumoral injections of 50μg hu14.18-IL2 immunocytokine (IC) on treatment days 6-10. Staining method is indicated by the 'Cryopreservation' row with (-) for 'Control', and (+) for the 'After' protocol. Staining was done using a hybrid lymphoid/myeloid panel of antibodies. Immune populations are expressed as a percentage relative to all single, live cells in the sample, save for panel B, which depicts the CD8+ T cell : T_{reg} cell ratio. Data are presented with individual mouse tumors as data points, with bars representing mean +/- SEM for each treatment and staining condition combination. Statistical comparisons were made using linear models assessing preparation protocol, treatment effect, and interaction. All parameters were determined to have an insignificant interaction on F-test. P-values corresponding to 'Control' vs. 'After' preparation protocol differences are presented in the bottom left of each corresponding graph. Pairwise differences between PBS, RT and RT+IC treatment groups derived from the linear model are indicated as * = $p<0.05$, ** = $p<0.01$, *** = $p<0.001$, **** = $p<0.0001$. Data are representative of two independent biological replicates.

Figure 2.5

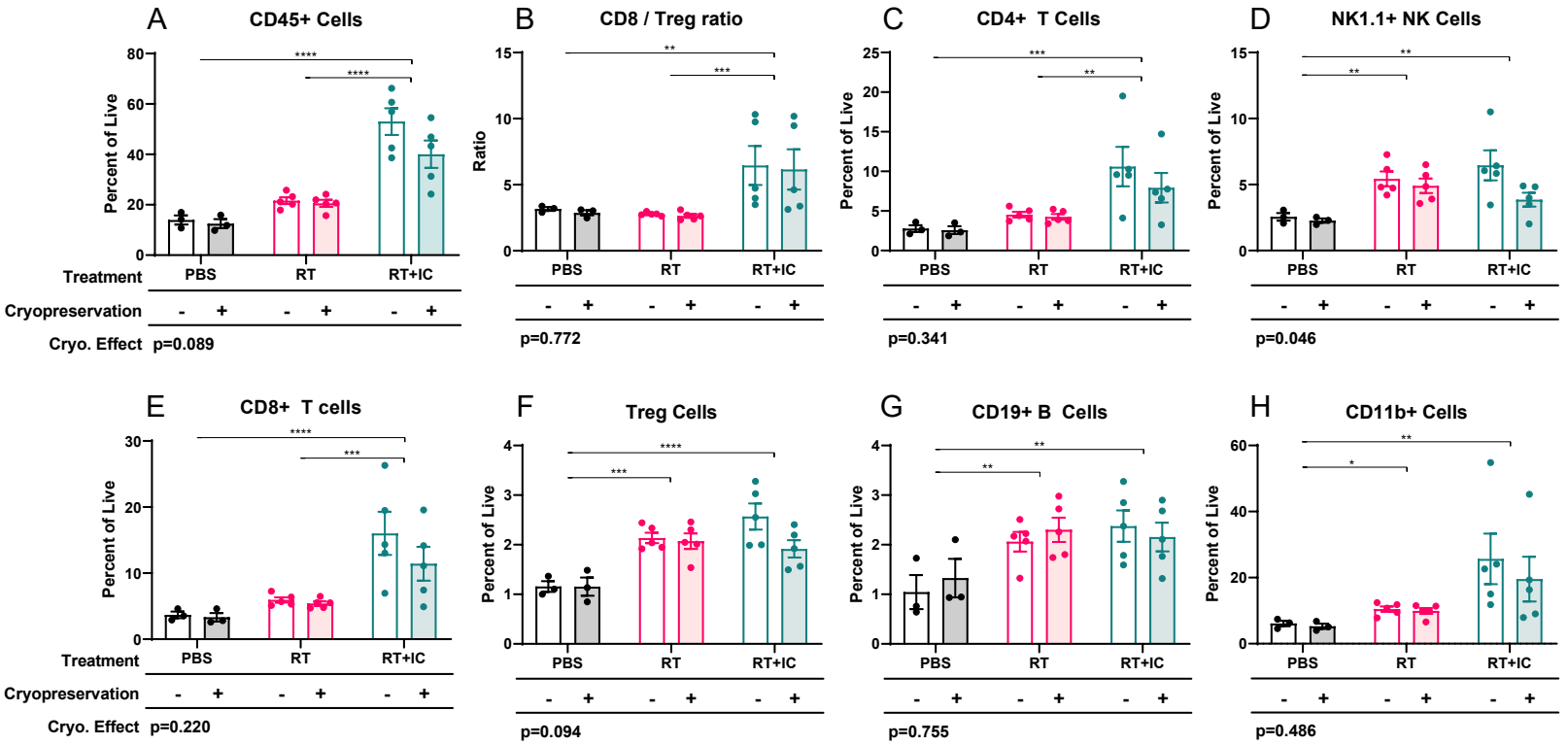
A
CD45+ Cells
Percent of Live
Treatment
PBS
RT
RT+IC
Cryopreservation
Cryo. Effect p=0.089
B
CD8 / Treg ratio
Ratio
p=0.772
C
CD4+ T Cells
Percent of Live
p=0.341
D
NK1.1+ NK Cells
Percent of Live
p=0.046
E
CD8+ T cells
Percent of Live
Cryo. Effect p=0.220
F
Treg Cells
Percent of Live
p=0.094
G
CD19+ B Cells
Percent of Live
p=0.755
H
CD11b+ Cells
Percent of Live
p=0.486

Figure 2.6: Use of the 'After' cryopreservation method to analyze radioactive tumor samples over time following MTRT. Mice bearing ~5-week B78 syngeneic melanoma tumors were treated with tail vein injections of either PBS control, 50μCi, or 250μCi of ^{90}Y-NM600 MTRT. N=4 tumors per group were harvested on days 1,7,14, and 21 post injection, dissociated, and stained using a hybrid lymphoid/myeloid panel using the 'After' cryopreservation protocol described in Figure 3.2. After 30 days stored behind lead shielding at -80C, samples were confirmed to be at background radioactivity, thawed and analyzed by flow cytometry. The above immune parameters were calculated and presented as a percentage of cells of interest relative to all single, live cells save for panel C, which depicts the percentage of NK cells that are CD11b+, and panel G, which depicts the CD8 T cell:T_{reg} cell ratio. Due to the very low frequency of CD19+ B cells, panel F presents data as natural log transformed. These data shown here are representative of two independent experiments. Data were analyzed using linear models to assess effects of time, treatment condition, and time-treatment interaction on the above immune parameters. F-statistics for time-dose interaction are presented as p values in the bottom left corner of each graph. Pairwise analyses from the models were conducted within each time point only, and are depicted as * = $p<0.05$, ** = $p<0.01$, *** = $p<0.001$, **** = $p<0.0001$, ns = not significant. No corrections for multiple comparisons were conducted.

Figure 2.6

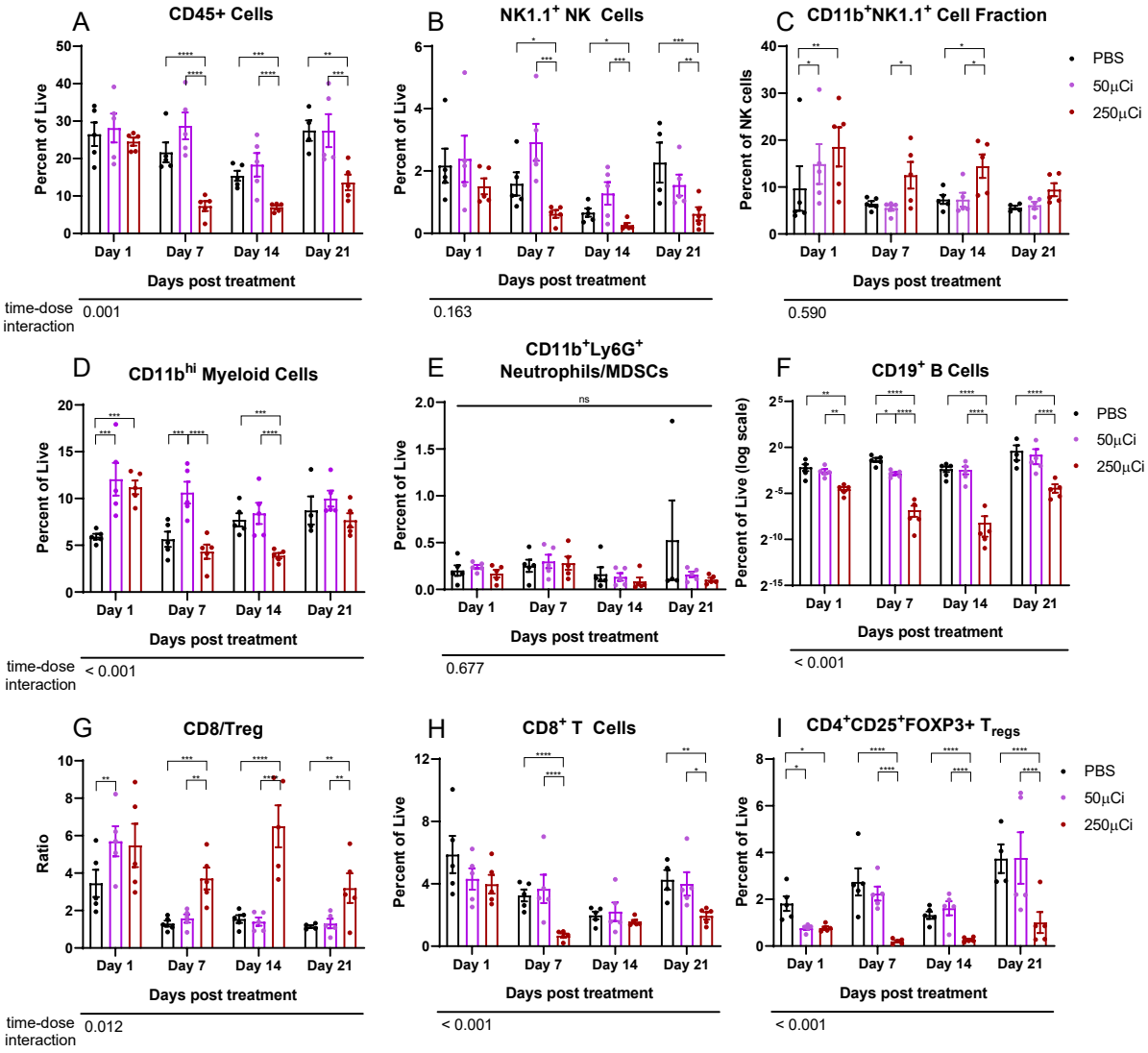
A
CD45+ Cells
Percent of Live
Day 1
Day 7
Day 14
Day 21
Days post treatment
time-dose interaction 0.001
B
NK1.1+ NK Cells
Percent of Live
Days post treatment
0.163
C
CD11b+NK1.1+ Cell Fraction
Percent of NK cells
Days post treatment
0.590
PBS
50μCi
250μCi
D
CD11bhi Myeloid Cells
Percent of Live
Days post treatment
time-dose interaction < 0.001
E
CD11b+Ly6G+ Neutrophils/MDSCs
ns
Percent of Live
Days post treatment
0.677
F
CD19+ B Cells
Percent of Live (log scale)
Days post treatment
< 0.001
PBS
50μCi
250μCi
G
CD8/Treg
Ratio
Days post treatment
time-dose interaction 0.012
H
CD8+ T Cells
Percent of Live
Days post treatment
< 0.001
I
CD4+CD25+FOXP3+ Tregs
Percent of Live
Days post treatment
< 0.001
PBS
50μCi
250μCi

Chapter 3

Depth of tumor implantation affects response to *in situ* vaccination in a syngeneic murine melanoma model

Preface

This chapter presents work conducted over the past three years directed at troubleshooting inconsistencies in our animal model for *in situ* vaccines. Most researchers developing a new technique or learning a technique in a lab tend to face a “learning curve” in replicating data and gaining the skills necessary to conduct the intended research. I initially faced substantial difficulty in replicating the response rates to the RT+IC *in situ* vaccine in our B78 melanoma model, and eventually worked with other researchers in the lab to clearly demonstrate that something about my implantation technique was resulting in drastically different results. While I did correct my technique and substantially improved my response rates, I also further characterized the impact of this difference in implantation depth on the response to *in situ* vaccination and identified a simple, effective, physical exam finding to incorporate as an “inclusion criteria” before starting experiments that improves experimental consistency. I encountered the initial troubleshooting issue within my experiments and designed and conducted all of the experiments contained in this chapter. I created these figures and drafted the body of this text. These data were recently submitted as a manuscript for publication.

3.1 Abstract

An important component of all research using animal models is ensuring rigor and reproducibility. This study was prompted after two experimenters performing virtually identical studies were noted to obtain different results when syngeneic B78 murine melanoma cells were implanted into the skin overlying the flank and treated with an *in situ* vaccine (ISV). Although both experimenters thought they were using identical technique, we determined that one was implanting the tumors intradermally (ID) and the other was implanting them subcutaneously (SC). Though the baseline *in vivo* immunogenicity of tumors can depend on depth of their implantation, the response to ISV as a function of tumor location, particularly in immunologically "cold" tumors, has not been thoroughly investigated. The goal of this study was to evaluate the difference in growth kinetics and response to ISV between identically sized melanoma tumors following ID vs. SC implantation. We injected C57BL/6 mice with syngeneic B78 melanoma cells in the flank region. Half these mice were injected ID, and half were injected SC. When tumors reached 190-230mm^3, they were grouped into a 'wave' and treated with our previously published ISV regimen (12Gy local external beam radiation and intratumoral injections of hu14.18-IL2 immunocytokine). Physical examination demonstrated that ID-implanted tumors were mobile upon palpation, while SC-implanted tumors became fixed to the underlying fascia. Histologic examination identified a critical fascial layer, the panniculus carnosus, which separated ID and SC tumors. SC tumors reached the target tumor volume significantly faster compared to ID tumors. The majority of ID tumors exhibited either partial or complete response to our ISV protocol, whereas the majority of SC tumors did not. Further, the 'mobile' or 'fixed' phenotype of tumors predicted response to ISV, regardless of intended implantation depth. We demonstrate that the physical 'fixed' vs. 'mobile' characterization of the tumors may be one method of ensuring implanted tumors are in the same tissue plane prior to initiation of treatment. Moreover, after controlling for strain of mouse, type, size, and growth rate of tumor, we

demonstrate that small differences in the depth of tumor implantation still have a dramatic effect on response to immunotherapy.

3.2 Introduction

Cancer immunotherapy has been widely accepted as a powerful tool for treating cancer. Translational research investigations, largely conducted using animal models, have been instrumental in the progression and development of successful immunotherapies. Despite many such studies identifying successful pre-clinical results in animal models, many of these promising immunotherapies fail during translation to clinical use [159]. This pattern is not limited to cancer immunotherapies, but has been observed in cancer research as a whole; strong animal model preclinical data often does not translate to comparable results when evaluated in humans, and as such has been implicated in what many have termed the ‘reproducibility crisis’ in cancer research [160].

Scientific investigations conducted in an effective and reproducible manner are the mainstay of basic, translational, and clinical biomedical research. The National Institutes of Health (NIH) continues to implement new guidelines in an effort to improve rigor and reproducibility in scientific research, with the goal of enhancing scientific integrity and transparency in reported results [161]. In syngeneic implantable models for tumor immunotherapy, great care is taken to control confounding factors. Subtle variances within these systems can lead to aberrant and differing responses, despite holding constant as many factors as possible. Variations in diet, animal housing temperature, and even vendor source can affect the response to immunotherapy [162–164]. Sivan and colleagues recently showed that C57Bl/6 mice respond differently to anti-PD1 immunotherapy if purchased from Jackson Laboratories vs. Taconic Farms due to differences in the gut microbiome [162]. Other stressors, such as the frequency of handling the mice, can affect treatment outcome [165,166]. These

factors, and other potentially unknown factors, can result in key differences in the tumor-immune microenvironment (TME), and thus can influence response to immunotherapy. It is also known that murine tumor immunology experiments can be plagued by high variability, which can make statistical evaluation difficult and hamper the ability to extend and build upon the published results of other investigators [103,167].

Previous work in vaccine development has demonstrated that different cutaneous tissue planes can influence the degree of immunogenicity and immune response [168,169]. The epidermal and dermal layers play a role in pathogen surveillance and elimination, with unique subsets of dendritic cells (DCs), tissue resident T cells, macrophages and others [104,105]. By contrast, the deeper tissue layers have fewer resident DCs and macrophages. In studying the immunogenic EL4-OVA transfected tumor line, Joncker and colleagues demonstrated that a tumor cell inoculum injected intradermally (ID) failed to develop into a tumor, while the same tumor inoculum injected subcutaneously (SC) grew into a progressive and lethal tumor [170]. The difference in response was due to a difference in the kinetics of DC migration and tumor-specific T cell activation, which occurred in both tumor instances, but only controlled the tumor in the ID space. Since tumor-reactive effectors are present in tumors implanted in both planes, a tumor-directed immunotherapy regimen may be sufficient to drive antitumor effector response regardless of tumor implantation depth. Yet the effects of depth of tumor implantation in the skin on response to immunotherapy have not been thoroughly investigated in syngeneic murine models, which are commonly used for preclinical and translational cancer research.

We have previously demonstrated that external beam radiation (RT) strongly synergizes with intratumoral injections of hu14.18-IL2 immunocytokine ([IC], an anti-disialoganglioside [GD2] antibody fused to IL2) to achieve tumor control in the implantable GD2-positive B78 syngeneic melanoma model [65]. Mice rendered disease-free are capable of rejecting challenges with the antigenically related, GD2-negative B16 melanoma line, which

demonstrates the ability of RT+IC immunotherapy to act as an *in situ* vaccine. (ISV). Yet our group noted substantial inter-experimenter variability in tumor response rates to ISV. This study investigates the influence of tumor implantation depth on response to this ISV immunotherapy.

3.3 Materials and Methods

3.3.1 *Syngeneic tumor cell line*

B78-D14 (B78) murine melanoma is a cell line derived from B16-F10 melanoma, as previously described [128]. This cell line was generously provided by Ralph Reisfeld at the Scripps Research Institute (La Jolla, CA). Cells were cultured in RPMI 1640 (Mediatech, Inc, Manassas, VA) supplemented with 10% fetal bovine serum, 100U/mL penicillin, 100µg/mL streptomycin, 2mM L-glutamine, 400µg/mL G418 and 50µg/mL hygromycin [129,130].

3.3.2 *Animals and tumor models*

Animals were housed and cared for using a protocol approved by the University of Wisconsin-Madison Institutional Animal Care and Use Committee. Female, 6-8 week old C57BL/6 mice from Taconic Biosciences (Rensselaer, NY) were allowed to acclimate in our facility for at least one week prior to innoculation with $2x10^6$ B78 cells in 100µL PBS. All tumors were injected in a suspension of sterile PBS in a 1mL disposable syringe loaded with a sterile polystyrene bead and tipped with a 30G needle. For tumors intentionally implanted ID, the beveled tip of the needle was inserted face up at a <10 degree angle, and advanced no more than 2-3mm into the tissue parallel to the skin while lifting the needle to create a tenting effect. This resulted in a well-demarcated wheal (or bubble) and could be felt as pressure-resistance during injection. For tumors intentionally implanted SC, the needle was inserted at a ~20 degree angle, and advanced 5-7mm into the tissue while remaining superficial to the flank musculature. This created a less clearly observable wheal, and did not have strong resistance or pressure

during suspension administration. Tumor volume [(width^2 x length)/2] was measured twice weekly using calipers. Mice were randomized into treatment groups when tumors reached 190-230mm^3 and assigned to a 'wave.' Mice with tumors that grew larger than 230mm^3 were not included in the study. One to two mice per wave were randomly assigned to receive PBS control treatment.

3.3.3 *Tumor Treatments*

External beam radiation therapy (RT) was delivered using an X-RAD 320 system (Precision X-Ray Inc, North Branford, CT). Mice were immobilized using custom lead jigs and surgical tape such that only the dorsal right flank was exposed, with the rest of the mouse (including the contralateral flank and spleen) shielded. Irradiation settings were beam strength 320Kv/12.5mA, beam conditioning filter 2, platform height 36 cm, treatment duration 331 seconds, which has been measured to reliably deliver 11 +/- 1 Gy to the tumor by thermoluminescent dosimetry (data not shown).

Immunocytokine (IC, hu14.18-IL2) was provided in lyophilized form (4mg/vial) by Apeiron Biologics (Vienna, Austria). It was reconstituted by adding 8mL of sterile PBS for a working concentration of 0.5mg/mL. For mice being treated with RT+IC, 100μL of the 0.5mg/mL IC solution was injected intratumorally (IT) daily on treatment days 6 through 10, for a total dose of 250μg per mouse in five doses. Injections were through a 30G needle, and care was taken to inject slowly and not draw drug up into the syringe through the needle, as to avoid shear-induced denaturation of the immunocytokine (Figure 3.1A).

3.3.4 *Tissue harvest, preparation, and histological analysis*

Tumors were dissected *en bloc* to preserve anatomical relation to surrounding tissues. Specimens were fixed in 10% Neutral Buffered Formalin for 48 hours. Samples were were paraffin processed, sectioned into 5μm slices, and stained with hematoxylin and eosin. Sections were visualized under a SCOPE.A1 microscope (Zeiss), and images were captured using an AxioCam HR camera (Zeiss).

3.3.5 Statistical Analysis

The data are presented as mean +/- standard error of the mean (SEM), except where noted. Time to treatment size and overall survival analyses was performed using either the Kaplan-Meier method with comparisons using a log-rank test or by Cox proportional hazards modeling. Comparisons of tumor volume at treatment day 33 were done using a one-way ANOVA with multiple comparisons conducted by the Sidak method. Comparison of growth rates between ID and SC tumors treated with ISV was done using linear mixed effects models of log-transformed data to estimate slopes. Statistical analyses were conducted using R and Graphpad Prism Software (San Diego, CA).

3.4 Results

3.4.1 *Experimenters conducting the same experiment obtained disparate results associated with different tumor implantation depths*

We noticed that the efficacy of ISV varied in some experiments, especially when comparing the efficacy obtained by different experimenters. To test the difference in implantation technique as a possible reasons for this variability, two cohorts of five C57BL/6 mice were implanted with B78 tumor cells, one by experimenter-A and another by experimenter-

B. Both experimenters injected tumors consistent with their understanding of a “subcutaneous” injection. Once each cohort reached ~150mm^3 average, they were treated by experimenter-A using our ISV regimen [65]. Four out of five tumors implanted by experimenter-B became tumor-free, while only 1 out of 5 mice implanted by experimenter-A became tumor-free (Figure 3.1B).

Tumors implanted by experimenter-B also took ~1 week longer to reach ~150mm^3. Examination of untreated tumors implanted by both experimenters revealed that tumors implanted by experimenter-A had a ‘fixed’ phenotype, where lateral displacement of the skin over the tumor did not result in tumor displacement. There was no apparent tumor connection to the skin, as it would move over the tumor (Figures 3.1C, 3.1D). In contrast, tumors implanted by experimenter-B had a ‘mobile’ phenotype, where lateral displacement of the skin resulted in displacement of the tumor as well. These tumors appeared connected to, and moved freely with, the skin (Figures 3.1I,3.1J).

Histologic analysis confirmed that these ‘fixed’ and ‘mobile’ tumors occupied different tissue planes within the skin compartment. ‘Fixed’ tumors were deep to the thin layer of dermal striated muscle called the Panniculus Carnosus (PC), which is present in most mammals and separates the true skin compartment from underlying fascial layers (Figure 3.1E, 3.1F)[171,172]. In contrast, ‘mobile’ tumors were either completely superficial to or invading/involved with the PC; they could be seen invading true skin compartment structures including the dermal white adipose tissue, dermis, and lymphatics (Figure 3.1K, 3.1L). Several smaller, mononuclear cells (possibly infiltrating lymphocytes) could be observed in the periphery of the ‘mobile’ tumor, but not in the ‘fixed’ tumor (Figure 3.1N). Together, these observations demonstrate that despite a desire to implant tumors similarly, different experimenters with substantial mouse-handling experience can implant tumors at different depths in the skin, which may impact treatment outcome and contribute to increased variability.

3.4.2 *Response rates to ISV are higher in ID vs. SC tumors*

It is known that the starting size of a tumor has an impact on treatment response to *in situ* vaccination, with larger tumors less likely to respond [64]. Indeed, mice implanted by experimenter B (which were largely ID) took one week longer to reach treatment size than those implanted by experimenter A. By extension, one may also consider that faster growing tumors may be less likely to respond to treatment than slow growing tumors. To explore the effect of tumor implantation depth on response to ISV while controlling for tumor size, a staggered-treatment approach was used. A cohort of mice was injected with B78 cells to intentionally be ID/mobile, while a second cohort was injected with the same number of cells to be intentionally SC/fixed. When tumors reached 210 +/- 20mm^3, they were grouped into a 'treatment wave' and treated with the same ISV (Figure 3.1A), with 1-2 untreated control mice per wave.

In total, there were ten distinct treatment 'waves', which started treatment between 15 and 47 days following implantation (Figure 3.2). Tumors intentionally implanted SC grew faster, reaching treatment size in a median of 22 days post implantation, while those intentionally implanted ID took a median of 36 days to reach treatment size (Figure 3.2A). Consistent with Figure 3.1B, ID-implanted tumors responded to ISV better than SC-implanted tumors (Figure 3.2B, Table 3.1). Median survival for treated ID-implanted tumors was significantly longer than the median survival for treated SC-implanted tumors (Figure 3.2B and Table 3.1). Both SC- and ID-implanted tumors had a prolonged survival following treatment compared to untreated controls (Figure 3.2B, Table 3.1). Eleven out of 22 (50%) ID-implanted mice demonstrated a complete response to ISV and stayed disease-free, compared to 0/24 SC-implanted mice (Figure 3.2C, 3.2D). Direct comparison of tumor volumes on post-treatment day 33 demonstrated significant differences between all treated and untreated groups, with significantly lower average tumor volume in the ID-treated compared to the SC-treated groups (Figure 3.2E). In addition, linear mixed effects modeling predicted a growth factor of 0.42 [0.37 to 0.48] every

30 days for ID implanted treated tumors, while SC implanted treated tumors grew by a factor of 3.07 [2.64 to 3.53] every 30 days ($p<0.0001$ on difference in growth rates). This means that while ID implanted tumors on average shrank over time in response to treatment, SC implanted tumors on average grew over time. Lastly, response to ISV as measured by overall survival did not depend on the rate of tumor growth before treatment for both ID ($p=0.877$) and SC ($p=0.340$) implanted tumors. (Figure 3.2F, Figure 3.3, and Figure 3.4).

3.4.3 *'Mobile' vs. 'Fixed' tumor status is associated with treatment outcome*

As a means of noninvasively confirming tumor implantation depth, the 'fixed' or 'mobile' status of each tumor was evaluated in a blind fashion. At each time point, tumors were designated as entirely 'fixed', entirely 'mobile', or 'intermediate' if they had qualities of both, such as a bilobed or partially mobile phenotype (Figure 3.5). Results were largely consistent with the intended injection depth; all but four ID-implanted mice developed predominantly 'mobile' tumors (two were 'fixed' and two were 'intermediate'), and all but three SC-implanted mice developed 'fixed' tumors (three were 'intermediate'). A heat map was generated to track physical-exam status of the tumors over time. After ranking all mice based on the tumor volume at treatment day 60, a clear clustering phenomenon was observed (Figure 3.5). All mice rendered disease free had a predominantly 'mobile' phenotype; all mice that died from tumor burden had predominantly 'fixed' or 'intermediate' phenotype. In general, mice with the smallest day 60 tumor volumes were 'mobile,' those with the largest tumor volumes were 'fixed,' and most 'intermediate' phenotypes had an intermediate day 60 tumor volume. In addition, those tumors intended to be ID, but with 'fixed' phenotypes, behaved similarly to the other 'fixed' tumors. This implies a strong association between the response to ISV and depth of tumor implantation; the physical 'fixed' or 'mobile' status appeared more closely associated with treatment outcome than the original 'intended' treatment group.

3.5 Discussion

Our findings highlight the need for detailed documentation of experimental methods and procedures, and expand published studies indicating that tumor depth can influence antitumor immune response[169,170]. Not only did B78 tumors grow at different rates in the ID vs. SC space, they also had significant differences in response to RT+IC *in situ* vaccination (Figure 3.2). As reported by Joncker et al, OVA-antigen-laden dermal dendritic cells (DDCs) were detected in the draining lymph node of EL4-OVA tumors as early as two days post-inoculation for ID-implanted tumors, but took 8 days for detection in SC-implanted tumors [170]. Nevertheless, tumor antigen-specific T cells were detected for both ID and SC tumors, suggesting that the endogenous response in the SC space, while present, was insufficient to control the tumor before it developed a suppressive microenvironment [170]. Our results here expand on this past work by including ISV therapy and the more immunologically “cold” B78 melanoma model, which grows readily, escaping immune destruction even in the ID space. In this model system, potent RT+IC ISV can cure some mice of ID tumors, but can only slow the progressive growth of SC tumors (Figures 3.2B, 3.2D).

There are several possible explanations for why the same tumor, capable of recognition by the immune system, yielded different responses to RT+IC *in situ* vaccination. We identified that the mobile, ID-implanted tumors were either associated with or above the PC, while deeper, fixed, SC-implanted tumors were entirely below the PC plane. The ID space is known to contain a higher density of antigen-presenting cells (APC), specifically DDCs, with specialized blind-ended lymphatics connected to a superficial lymphatic plexus, whereas the SC space contains mostly monocytes and macrophages, with lymphatic vessels connecting to a deep lymphatic plexus [105,173]. It is also possible that the PC itself may form a physical barrier that can prevent communication between these two spaces [171]. This difference in lymphatic architecture, combined with differences in APC populations, likely explains why Joncker and

colleagues observed differential kinetics of DC mobilization upon tumor challenge in these two spaces [170]. Further, SC tumors may be able to capitalize on different vascular architecture to more readily drive angiogenesis from vessels feeding the underlying musculature, which could explain the faster growth rate of SC tumors. Lastly, the PC itself has been hypothesized to play a role in wound healing and inflammation [171]. As ID-implanted tumors are invading ('wounding') the PC in some fashion, factors released from the PC may enhance immune recognition of the tumor. Clinically, tumors that have greater immune infiltrates at diagnosis seem to have a higher rate of response to immunotherapy [174]. This is likely consistent with both our and Joncker's observations, given the greater potential tumor immune cell infiltrate in some ID vs. SC tumors (Figure 3.2N), though further characterization to define exact differences in tumor immune cell infiltrate, both before and after immunotherapy, will be required [170].

Though the PC is a integral organ structure in many mammals including rodents, dogs, cats, horses, and pigs, [171] it is largely absent in humans. Vestigial remnants of this superficial cutaneous musculature in humans are phylogenetically described to include the occipitofrontalis muscles of the scalp, the platysma in the anterior part of the neck, the palmaris brevis muscle of the hand, and Langer's axillary arch in the axilla [171]. As such, distinguishing between the dermal and subcutaneous layers in humans is more difficult, but still critically important. In a phase 2 study of 51 patients with metastatic melanoma, Weide and colleagues injected all palpable lesions with intratumoral IL-2 three times weekly and evaluated clinical response [175]. The authors noted that the depth of the injected tumor affected the outcome of treatment. In patients with stage III disease, 97.9% of dermally located lesions experienced a complete local response, whereas 90.3% of subcutaneous lesions experienced a complete local response. In the more advanced stage IV patients, that difference widened even further, with 56.7% of intradermal lesions responding to treatment compared to 34.4% of subcutaneous lesions. The authors noted that the size of subcutaneous lesions were slightly larger than the intradermal

lesions, which mirrors our preclinical findings here as well. This observation provides a clinical correlate for our preclinical observations that the tissue plane harbors a different baseline immune activity, and that the intradermal space may provide a better immune environment for responding to tumor-targeted immunotherapy.

We identified that slight differences in depth of tumor implantation (~300 μm, Figure 3.1E, 3.1K) can create substantial differences in response to immunotherapy. This phenomenon may be relevant not only for immunotherapy, but for other therapies known to have immunologically active components such as RT or chemotherapy [123]. Detailed and rigorous documentation of experimental procedures is essential. The NIH has asked researchers to be more transparent and explicit with their methodologic descriptions [176]. Based on our experience, it is likely that in mouse experiments “subcutaneous” is sometimes used as a common term to describe either SC or ID implantation. Subtle differences in experimental methodology, such as tumor implantation depth, can substantially affect the reproducibility of published studies. Researchers rely heavily on published work to generate new hypotheses for testing. This study documents the importance of accurately and rigorously describing the method and location of tumor implantation. Using histologic and physical observations, we delineate between deeper, ‘fixed’ tumors and more superficial, ‘mobile’ tumors, and propose incorporating this physical exam finding as additional criterion for conducting consistent, reproducible implantable tumor immunotherapy experiments. Grouping tumors in this fashion controls for yet another confounding factor, and reduces variability of subsequent experiments, allowing for improved comparisons between different immunotherapy approaches.

3.6 Acknowledgements and clarification of collaborative efforts from others in this work

I would like to thank those researchers and scientists that assisted in the design and collection of the data for this chapter. Manasi Mohan, Matthew Rodriguez, and Claire Sun all

assisted in the mouse handling and data collection. Vladimir Subbotin volunteered his substantial histopathologic expertise in the harvest, sectioning, and staining of tumor tissues. Jen Birstler assisted in statistical analysis of data. Ravi Patel, Amy Erbe and Alexander Rakhmilevich contributed substantially to experimental design, and discussion of data and results. Jackie Hank provided insight regarding the issue of scientific rigor and provided helpful editing. Thesis committee members and co-mentors Zach Morris and Paul Sondel provided the guidance, funding, discussion, and editing support for this chapter. This chapter is modified from a complete manuscript of this work that has recently been submitted for publication.* All of these above individuals are listed as co-authors on our submitted manuscript and provided edits and/or approval for its submission. I would also like to thank Anna Hoefges, Alex Pieper, Alexa Barres, and Taylor Aiken for thoughtful discussion throughout this project.

*Carlson PC, Mohan M, Rodriquez M, Subbotin V, Sun C, Patel RB, Birstler J, Hank JA, Rakhmilevich AL, Morris ZS, Erbe AK, Sondel PM. Depth of tumor implantation affects response to *in situ* vaccination in a syngeneic murine melanoma model. Submitted 2020.

Table 3.1: Time-to-Event comparisons corresponding to figure 3.2.

Comparator A	Parameter	Comparator B	Corresponding Figure	A median (days)	B median (days)	P-value
ID (all)	time to treatment	SC (all)	Figure 2A	36	22	<0.0001
ID (treated)	Time to death/sacrifice	SC (treated)	Figure 2B	100.5	61	<0.0001
ID (treated)	Time to death/sacrifice	ID (untreated)	Figure 2B	100.5	38	<0.0001
SC (treated)	Time to death/sacrifice	SC (untreated)	Figure 2B	61	25	<0.0001
ID (untreated)	Time to death/sacrifice	SC (untreated)	Figure 2B	38	25	0.0104

Figure 3.1: Different results obtained from two different researchers conducting the same experiment. A) Schema of *in situ* vaccine treatment approach, as described in the Methods section. **B)** Average +/- SEM tumor volume of n=5 mice implanted with tumors by either experimenter-A (blue) or experimenter-B (red), and treated using the *in situ* vaccine described in **A**. Both groups were treated and measured identically by experimenter-B. Vertical dotted lines represent the day that treatment began (when tumors reached 190-230 mm^3) for the mice implanted by experimenter-A (blue) or by experimenter-B (red). **C&D)** Physical examination of tumors implanted by experimenter-A reveals a distinct 'Fixed' phenotype of the tumors in response to lateral displacement of the overlying skin. Note in **C** the short distance (blue bar) between the experimenters finger and the left margin of the tumor; in contrast note in **D** how the lateral leftward movement (white arrow) of the overlying skin increases the distance from the finger to the left margin of the tumor (blue bar), indicating that the tumor is not attached to the skin. **E-H**) Histologic examination by H&E staining of 'Fixed' tumors demonstrates the tumors reside deep to the cutaneous proper, which is delineated by the panniculus carnosus. **I&J)** Physical examination of tumors implanted by experimenter-B reveals a distinct 'Mobile' phenotype of the tumors in response to lateral displacement of the overlying skin. Note in **I** the short distance (red bar) between the experimenters finger and the left margin of the tumor does not increase in **J** with lateral leftward movement (white arrow shown in **J**) of the skin that is attached to the 'Mobile' tumor. **K-N)** Histologic examination shows that 'Mobile' tumors are either superficial to or invading the PC (seen in **K**), and reside in the true skin compartment. Further, qualitative assessment identifies distinct monoculear cells, likely infiltrating lymphocytes, invading the 'Mobile' tumor (**N**, marked by arrows). PC = panniculus carnosus, Ep = Epidermis, De = Dermis, SA = Subcutaneous Adipose.

Figure 3.1

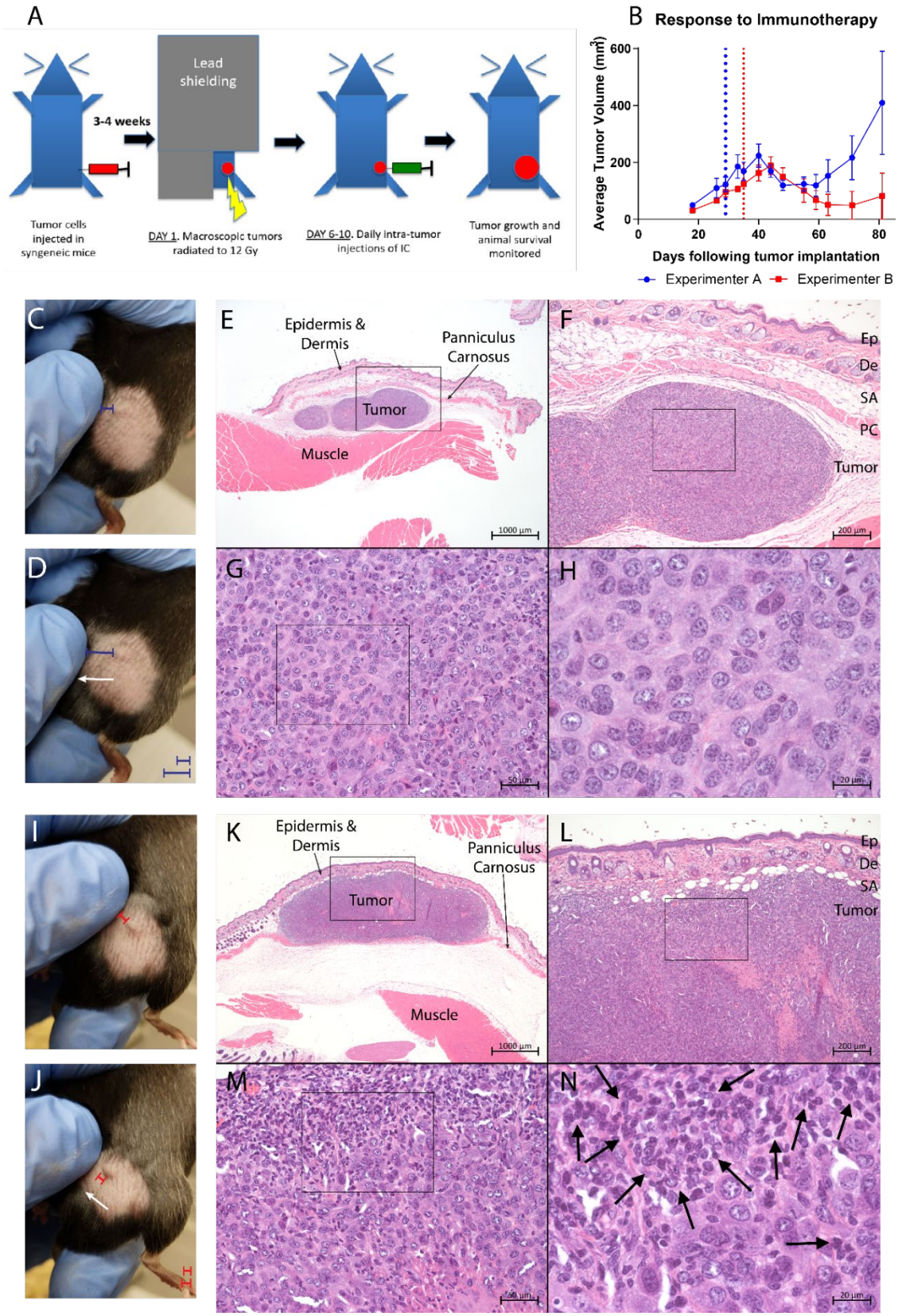
A
Lead shielding
3-4 weeks
Tumor cells injected in syngeneic mice
DAY 1. Macroscopic tumors radiated to 12 Gy
DAY 6-10. Daily intra-tumor injections of IC
Tumor growth and animal survival monitored
B Response to Immunotherapy
Average Tumor Volume (mm³)
Days following tumor implantation
Experimenter A
Experimenter B
C
D
E
Epidermis & Dermis
Panniculus Carnosus
Tumor
Muscle
F
Ep
De
SA
PC
Tumor
G
H
I
J
K
Epidermis & Dermis
Panniculus Carnosus
Tumor
Muscle
L
Ep
De
SA
Tumor
M
N

Figure 3.2: Intradermal tumors are more likely to respond to immunotherapy than subcutaneous tumors. Female, C57BL/6 mice were injected on the same day in the right flank intentionally aiming for either intradermal (ID, red) or subcutaneous (SC, blue) placement of the tumor. Mice were monitored weekly, and when tumors reached treatment size (190-230mm^3), they were collected into a treatment group and treated with either PBS control, or our previously published *in situ* vaccine as described in the Methods. **A)** Time to event analysis representing the time from tumor implantation to reaching treatment size. **B)** Survival analysis representing the time from initiation of treatment (either PBS control or RT+IC ISV) to death or tumor meeting size criteria for sacrifice. Statistical comparisons for **A** and **B** were conducted using log-rank comparisons, with resulting p-values presented in **Table 1**. **C)** Tumor volumes (mm^3) were measured twice weekly for all untreated tumors. **D)** Tumor measurements for all treated tumors were also measured weekly. **E)** Tumor volume at day 33 following treatment initiation for both treated and control mice. Data are presented as points representing individual values, and horizontal bars representing the mean +/- SEM tumor volume for each treatment group. Black dots represent tumors on mice that died before treatment day 33, with their last value carried forward and shown here. Statistical analysis was conducted by one-way ANOVA with multiple comparisons using the Sidak method. **F)** Tumor volume at day 33 of treatment for mice bearing ID or SC tumors, divided into treatment waves (defined by the day post tumor-implant of treatment initiation). Ten different waves are included:waves at D15, 19 and 22 for the SC tumors, a wave at D 27 for both SC and ID tumors, and waves at D 31, 33, 36, 40, 43 and 47 for the ID tumors. Shown here are only those waves that have 2 or more mice. A single additional wave (not shown here but included in Supplemental Figures 1 and 2) included a single ID mouse starting treatment on D 22. Data are presented as points representing individual tumor volumes, with horizontal bars representing the mean +/- SEM tumor volume for each treatment group. * = $p<0.05$, ** = $p<0.01$, *** = $p<0.001$, **** = $p<0.0001$, ns = not significant.

Figure 3.2

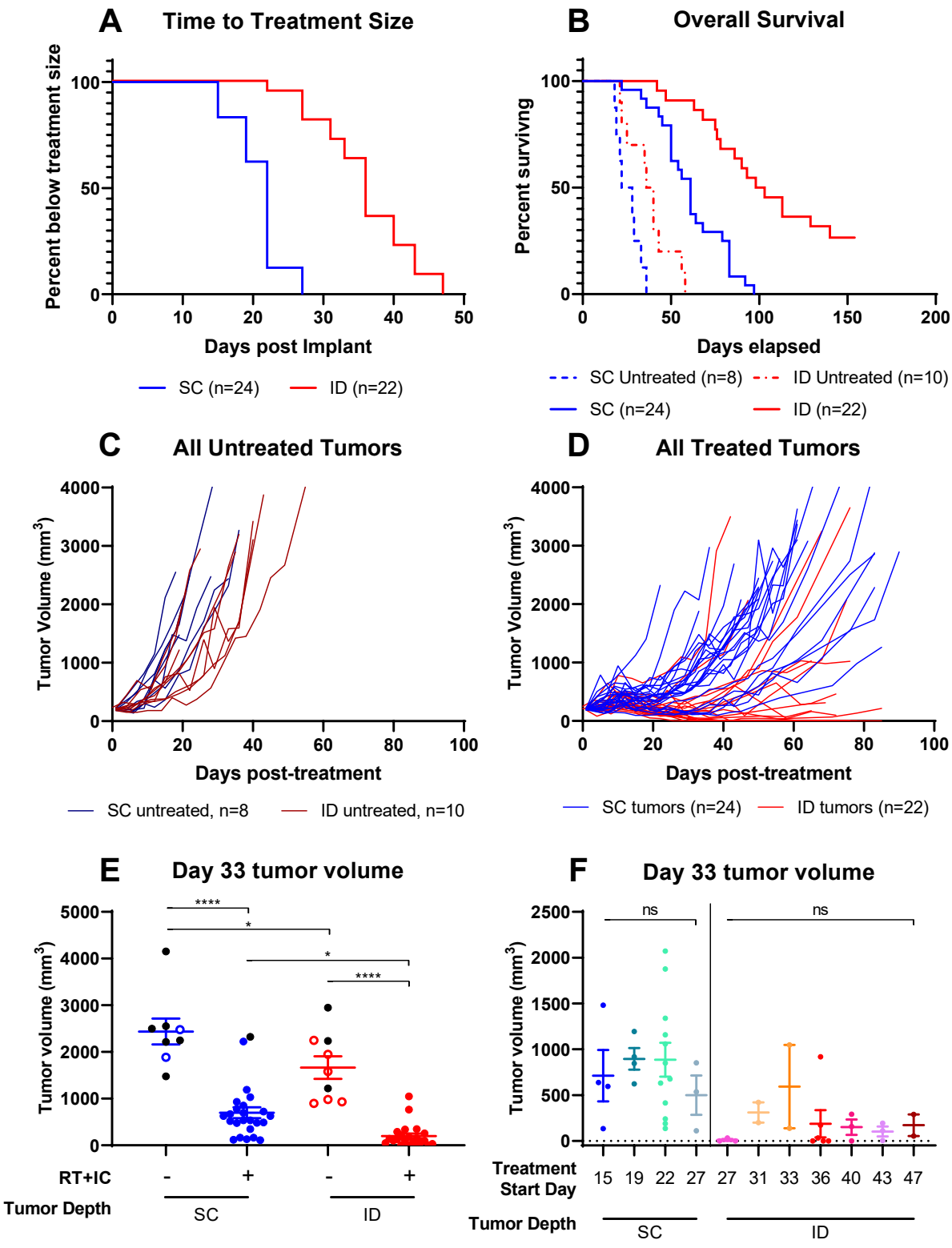
A
Time to Treatment Size
Percent below treatment size
Days post Implant
SC (n=24)
ID (n=22)
B
Overall Survival
Percent survivng
Days elapsed
SC Untreated (n=8)
ID Untreated (n=10)
SC (n=24)
ID (n=22)
C
All Untreated Tumors
Tumor Volume (mm3)
Days post-treatment
SC untreated, n=8
ID untreated, n=10
D
All Treated Tumors
Tumor Volume (mm3)
Days post-treatment
SC tumors (n=24)
ID tumors (n=22)
E
Day 33 tumor volume
Tumor volume (mm3)
RT+IC
Tumor Depth
SC
ID
F
Day 33 tumor volume
Tumor volume (mm3)
ns
Treatment Start Day
Tumor Depth
SC
ID

Figure 3.3: Controlling for growth rate, identically sized ID tumors are more likely to respond to RT + IC *in situ* vaccination. Female, C57BL/6 mice were injected on the same day intentionally aiming for either Intradermal (ID) or Subcutaneous (SC) placement of the tumor. Mice were monitored weekly, and whenever tumors reached treatment size (190-230mm^3), they were collected into a treatment group and treated with either PBS control, or our previously published *in situ* vaccine (12Gy external beam radiation on treatment day 1 followed by intratumoral hu14.18-IL2 immunocytokine on treatment days 6-10). **A)** Frequency histogram of the number of mice reaching treatment size for each of the 'treatment waves' reached during the course of the experiment. Blue-green bars correspond to the SC waves and red-purple-brown bars correspond to ID waves. **B)** Overlap in time to treatment size between ID and SC implanted tumors occurred for multiple SC and ID mice only on post-implant day 27, in which n=3 mice of both ID-implanted (pink) and SC-implanted (green) groups reached the 190-230mm^3 treatment window. Shown is the average +/- SEM tumor volume following ISV treatment starting on post-implant day 27, to enable comparison of treatment outcome for ID and SC tumors when all treated tumors have the same tumor size and growth rate at the time treatment is initiated.

Figure 3.3

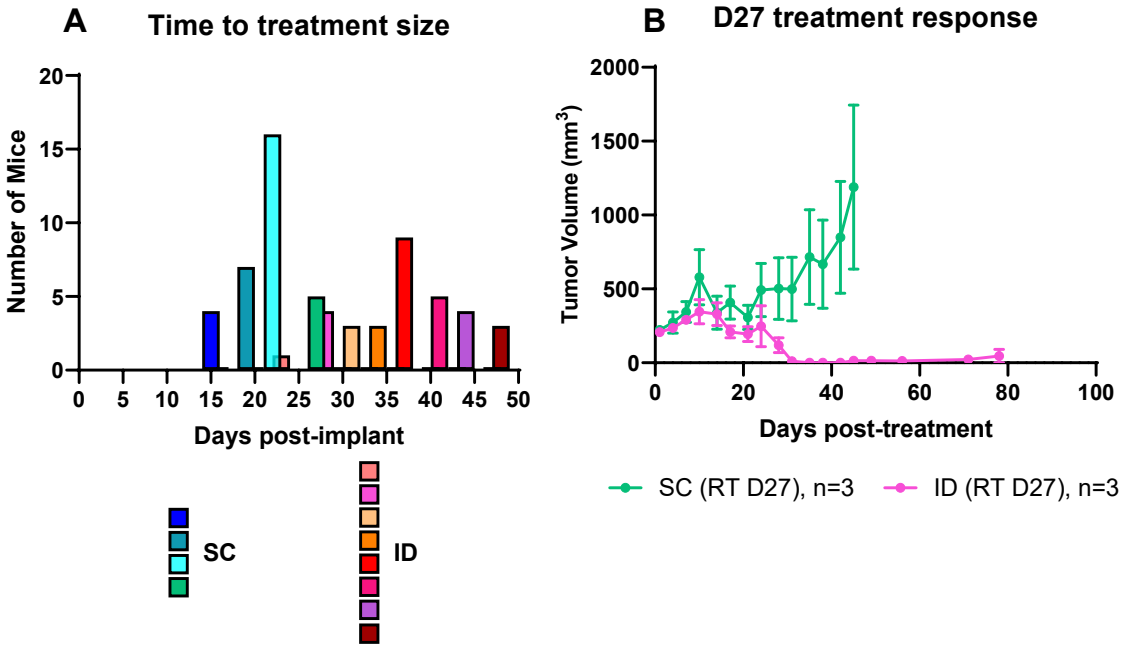
A
Time to treatment size
Number of Mice
Days post-implant
SC
ID
B
D27 treatment response
Tumor Volume (mm3)
Days post-treatment
SC (RT D27), n=3
ID (RT D27), n=3

Figure 3.4: Controlling for starting size, ID tumors are more likely to respond to RT + IC *in situ* vaccination. Female, C57BL/6 mice were injected on the same day intentionally aiming for either Intradermal (ID) or Subcutaneous (SC) placement of the tumor. Mice were monitored weekly, and whenever tumors reached treatment size (190-230mm^3), they were collected into a treatment group and treated with either PBS control or our previously published *in situ* vaccine (12Gy external beam radiation on treatment day 1 followed by intratumoral hu14.18-IL2 immunocytokine on treatment days 6-10). For **A** and **B**, the Average +/- SEM tumor volume is plotted for each individual wave, for the SC tumors (in **A,** shades of blue) and the ID tumors (in **B,** shades of red) to enable comparison of treatment outcome for 190-230mm^3 tumors. Although numbers are small, there are no significant differences between the 4 waves shown in **A**, and there are no significant differences between any of the 8 waves plotted in **B** as determined by Cox proportional hazards modeling, for both ID (p=0.877) and SC (p=0.340) implanted tumors. This indicates that in this setting, the initial growth rate of the tumor is not influencing response to treatment. **C)** Tumor volumes for each individual mouse in the 4 waves of treatment for SQ mice. **D)** Tumor volumes for each individual mouse in the 8 waves of treatment for ID mice.

Figure 3.4

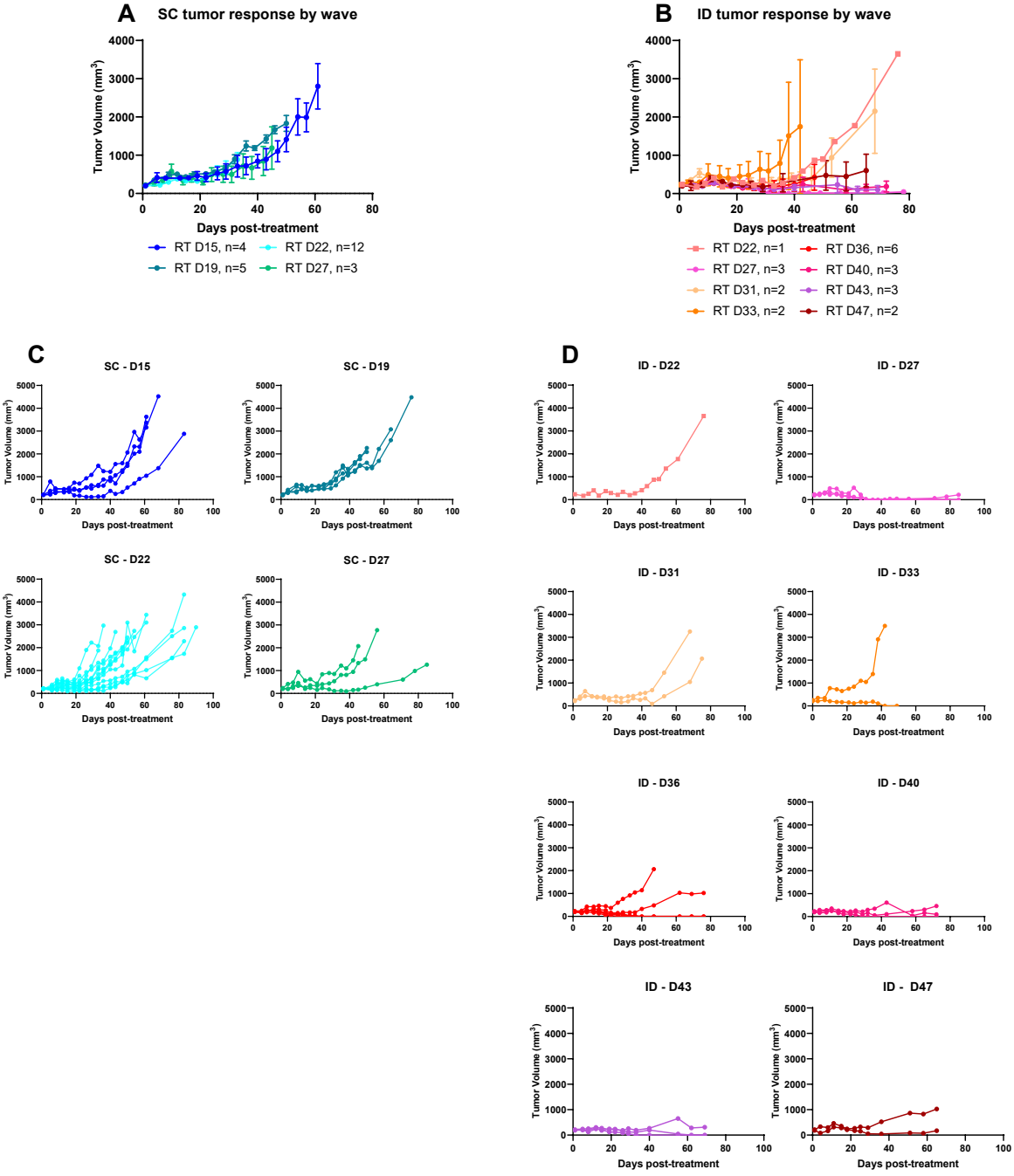
A
SC tumor response by wave
Tumor Volume (mm3)
Days post-treatment
RT D15, n=4
RT D19, n=5
RT D22, n=12
RT D27, n=3
B
ID tumor response by wave
Tumor Volume (mm3)
Days post-treatment
RT D22, n=1
RT D27, n=3
RT D31, n=2
RT D33, n=2
RT D36, n=6
RT D40, n=3
RT D43, n=3
RT D47, n=2
C
SC - D15
SC - D19
SC - D22
SC - D27
D
ID - D22
ID - D27
ID - D31
ID - D33
ID - D36
ID - D40
ID - D43
ID - D47

Figure 3.5: Mobile/Fixed status predicts response to RT+IC *in situ* vaccine. Female C57BL/6 mice used in the experiment described in Figure 2 were evaluated by physical exam at each measurement time point. Each row in the figure above represents an individual mouse, and each column represents the measurement time point in days post tumor implantation. Mice with mobile tumors (as described in Figure 1 and in the results section) were coded Red, and mice with fixed tumors (Figure 1 and the results section) were coded Blue. Mice with mixed or intermediate physical exam findings (as described in the results section) were coded Purple. Mice that were sacrificed due to tumor burden have an 'X' in their cells starting at the time of sacrifice, and mice that were rendered Disease Free by treatment have a 'DF' in their cell, starting at the time tumor was no longer detected. Mice were then ranked in the far-right column based on their tumor volume at treatment-day 60, and listed as dead if they had died or been sacrificed prior to day 60. The "intended injection" column on the left indicates which depth of tumor was intended upon implantation (light gray for ID, dark gray for SC).

Figure 3.5

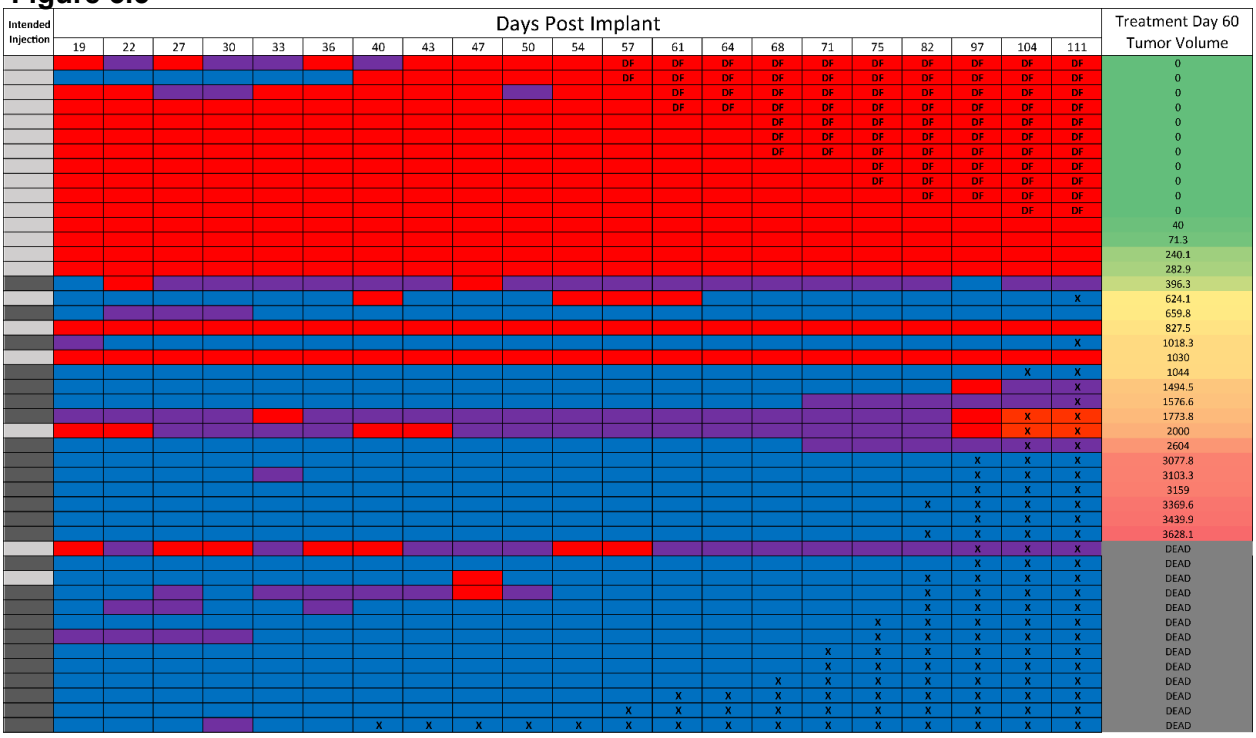
Intended Injection
Days Post Implant
19 22 27 30 33 36 40 43 47 50 54 57 61 64 68 71 75 82 97 104 111
Treatment Day 60 Tumor Volume
= Mobile
= Intermediate
= Fixed
= intended ID
= intended SC

Chapter 4

Radiation to all sites of tumor permits greater systemic antitumor response to *in situ* vaccination

Preface

This work is the culmination of a series of related studies I have been working on over the four year course of my PhD work. Exploring the ability of radiation to further propagate, or improve the impact of, local immunotherapy was the overall objective of my PhD since joining the lab of Dr. Sondel, under the co-mentorship of Dr. Morris. In generating and replicating the various findings and mouse models for this project, I encountered difficulty in replicating previously identified results, which led to the finding concerning tumor implantation depth and mobility, presented in Chapter 3. After optimizing this approach and model generation technique, I was able to confidently generate the models and findings discussed here in this chapter. This work demonstrates that radiating both sites of disease in a mouse with two tumors, but delivering immunotherapy to only one, improves responses at both sites. I also lay the groundwork in this chapter for using an alternate means of delivering this radiation in molecular targeted radionuclide therapy. This work, combined with the immunologic mechanism studies contained in Appendix A of this thesis, will form the basis for a manuscript in preparation for submission by early 2021.

4.1 Abstract

Effective antitumor effects of external beam radiation therapy RT is known to require intact immune responses. Our group has previously reported that a low dose (12Gy) single fraction of RT combined with intratumoral injections of the anti-GD2 hu14.18-IL2 immunocytokine (IC) synergize to generate an effective *in situ* vaccine (ISV) against syngeneic GD2-positive murine tumors. While this ISV is effective in eradicating single tumors, it fails to generate an abscopal response against (and in some cases is even inhibited by) established distant, untreated tumors. Given the immune-stimulatory capacity of radiation, we hypothesized that additional, low-dose radiation to *all* sites of disease would augment systemic antitumor response to ISV and result in abscopal effects following local *in situ* vaccination. In a murine model consisting of a larger right 'primary' flank tumor and a smaller left 'secondary' flank tumor, we conducted a titration of external beam RT dose to the secondary tumor in the setting of RT+IC *in situ* vaccine to the primary tumor. Our results demonstrate that abscopal effects of local ISV can be achieved using as little as 2-6Gy of external beam radiation, with maximal abscopal effects with a 12Gy dose. Confirmatory studies demonstrated improved overall survival and a greater proportion of mice rendered disease-free in mice treated with RT+IC +12Gy RT to the secondary compared to either RT+IC ISV alone or 12Gy radiation only to both tumors. In addition, linear mixed effects modeling estimated a slower average growth rate for both the primary and secondary tumors in mice treated with ISV and 12Gy to the secondary compared to either ISV alone, or 12Gy radiation alone. As means of potentially delivering radiation to all sites of disease, both known and occult, we used a novel alkylphosphocholine analog, NM600, as a theranostic targeted radionuclide therapy (TRT) by conjugating either ^{86}Y or ^{90}Y. We demonstrate that injected activities of this TRT agent as high as 100μCi do not interfere with the antitumor effect of RT+IC *in situ* vaccination. Similar to the case with external beam, combination TRT with RT+IC ISV resulted in improved overall survival compared to either ISV alone or TRT alone, and trended to demonstrate reduced growth rates as well. This

work demonstrates a novel use for low dose external beam radiation, and possibly for TRT – not as a direct antitumor killing agent, but as an immune adjuvant capable of improving the efficacy of cancer immunotherapy in the metastatic or occult disease setting.

4.2 Introduction

Immunotherapy has been recently recognized as an effective means of treating many different types of cancer, both clinically and preclinically. The use of checkpoint blockade, tumor-targeting antibodies, activating cytokines including IL-2, and autologous cell therapies including Chimeric Antigen Receptor (CAR)-T cells have been demonstrated to be effective and are FDA approved for several different cancers [1,4,32,177]. These breakthroughs have been direct results of advances in our understanding of cancer biology, immune biology, and the complex regulatory interplay between them. One means of immunotherapy under active study is *in situ* vaccination. This is an immunotherapeutic technique that aims to utilize the unique antigenic targets in a tumor as the source of immune recognition and activation [32,178]. In essence, *in situ* vaccines are *local* treatments that garner a *systemic* immune response. This is ideal in the setting of metastatic and micrometastatic disease, as the immune system is capable of surveilling and identifying such microscopic disease following activation.

It is now understood that the immune system is intimately associated with the development of almost all cancerous lesions [179]. The immunoediting hypothesis posits that immune cells are capable of recognizing tumor-specific antigens and directing cytotoxic effectors towards such targets. Thereby creating a selective pressure within a neoplastic population and ‘editing’ the tumor to be resistant to immune-mediated destruction. The result of these processes is tumor ‘escape,’ whereby clinically identifiable tumors develop and spread relatively unhindered by the immune system [4]. The specific mechanism of escape can vary and is likely a unique mixture of modalities for each patient, depending on a multitude of factors.

Extensive study of clinical tumor biopsies at diagnosis has suggested that tumors can present with a variable amount of immune infiltration [7]. Those patients with extensive lymphocytic infiltrate at diagnosis are referred to as immunologically “hot,” and may represent a fully intact antigen presentation and activation pathway, which is hindered in the tumor by immunosuppressive processes including T regulatory cells (T_{regs}), M2 macrophages, and myeloid-derived suppressor cells [3,122]. By contrast, those tumors with little to no immune infiltrate at diagnosis are referred to immunologically “cold” tumors. These tumors may be the result of very little immune activation, interruption of the normal antigen recognition and presentation cycle, or failure of activated T cells to identify tumor targets [6]. This dynamic between “cold” and “hot” tumors is fluid, and can change within a single tumor, between tumors in the same patient, and over time.

Our group has developed an *in situ* vaccine approach consisting of local external beam radiation therapy (RT) combined with an intratumoral (IT) injection of the hu14.18-IL2 immunocytokine (IC) [65]. This IC is an anti-disialoganslioside (GD2, expressed on neuoectodermally-derived tumors such as melanoma) monoclonal antibody fused to two IL-2 cytokines. The combination of 12Gy RT followed by IT-IC has been shown to improve survival in mice bearing B78 syngeneic melanoma tumors, and can render up to 70% of mice bearing a single small B78 melanoma disease-free [65]. Further, mice rendered disease-free by this combination approach reject further challenges from implanted B78s, as well as related GD2-negative melanoma lines. We thus demonstrated that this response requires T cells and results in antigen-specific memory, consistent with an *in situ* vaccine.

Though there have been numerous clinical studies combining RT with immunotherapy, few have resulted in strong clinical outcomes [180]. Though the explanation is likely complex, one possible contributing factor may be the overall tumor immune environment. Many preclinical models are tested on a single tumor which is typically immunologically “hot” such as a tumor transfected to express the strong OVA target antigen , the CT-26 colon cancer, the EL4

lymphoma, or other functionally immunogenic mouse tumors [169]. Though promising, these do not necessarily replicate clinical cancer presentation, which often includes multiple sites of disease, both known (metastases) and occult (microscopic disease) and can present with either "hot" or "cold" tumors. As most immune cells can circulate between secondary lymphoid structures and sites of inflammation, these multiple sites of disease may fundamentally affect the entire tumor immune landscape. Indeed, our group has previously published that this same RT+IC *in situ* vaccine, capable of clearing ~70% of tumors in mice with a single localized tumor (a one-tumor model), is only capable of clearing ~10% or fewer treated tumors in a mouse with two distinct, anatomically separate, sites of the same cancer (two-tumor model) [66]. The presence of a distant, untreated tumor provides a tumor-specific antagonism of the vaccine effect, a phenomenon we have termed Concomitant Immune Tolerance (CIT) [66]. In addition, the RT/IC immunotherapy given to the first tumor had little effect at the secondary tumor. Clinically, some locally targeted treatments including surgical resection and high-dose RT have been highly effective in controlling a primary tumor. Most recurrences of cancer occur at distant sites away from the primary tumor, and development of resistant and recurring clones are the main cause of death among cancer patients. Understanding how *in situ* vaccines may be able to drive *systemic* antitumor effects is important in translating such treatments into the clinic.

Growing evidence suggests that RT used at low to moderate doses can affect the immune tumor microenvironment (TME). RT is known to trigger immunogenic cell death in some tumor cells, characterized by translocation of calreticulin to the cell surface and subsequent DC activation [34,35,181]. Doses as low as 4Gy have also been shown to increase the tumor cell expression of both MHCI and interferon [43]. Lastly, low dose RT may also have a direct cytotoxic effect on immune cells within the tumor, including tumor-resident suppressive lineages such as T_{regs} [35]. Together, these changes have been shown to drive the tumor into a more immune active state, making a "cold" TME more "hot." In some models, RT itself can also drive increased antigen presentation and T cell diversification in what is very likely an *in situ* vaccine

effect. Clinically this can present in rare cases as immune-mediated attack of distant tumors outside of the radiation field, termed the “abscopal effect” [182–184]. Yet, in the setting of multiple “cold” tumors, it is not known how conversion of a single tumor to “hot” status, via locally delivered *in situ* vaccination, may affect the systemic anti-tumor response at distant tumors, which may remain largely “cold”. We hypothesized that systemic response to RT+IC delivered to a single site, measured at a distant tumor not receiving *in situ* vaccination, would be augmented by delivering RT to all sites of disease.

There is growing interest in using RT to treat multiple sites of disease, particularly in the oligometastatic setting [185,186]. However it is nearly impossible to use external beam RT to deliver a potentially immunomodulatory dose of radiation to all sites of disease, especially in the setting of micrometastases. To do so would require radiating large potions of the body, which would be associated with substantial toxicity and marrow/immune-system suppression, which may interfere with subsequent immunotherapy. Our lab has therefore been exploring the use of molecularly targeted radionuclide therapy (TRT) as an alternate means of delivering low dose radiation to all disease sites. This class of radiation treatment uses a molecular vector conjugated to a radionuclide injected systemically, but trafficked or targeted selectively to tumors [187]. Once in the tumor, the energy deposited by radioactive decay delivers the therapeutic dose to the tumor microenvironment, while sparing the surrounding tissue. Our group has been exploring the use of alkylphosphocholine analogs as a vector for delivering the beta-emitter ^{90}Y. Alkylphosphocholines are known to be abundant in nearly every type of tumor, and we have previously published a high degree of uptake and retention of these conjugated agents [75,188]. The particular ^{90}Y labelled alkylphosphocholine molecule we have studied, termed ^{90}Y-NM600, is capable of delivering 2-5Gy of radiation to all sites of disease in murine models of multiple tumors, and has been shown to have immune modulating effects on the TME [76,127,131]. We hypothesized that systemic ^{90}Y-NM600, delivered prior to RT+IC *in situ*

vaccination, would permit greater systemic control of distant tumors compared to RT+IC immunotherapy alone.

In this chapter, we explore using additional radiation to distant tumor sites in order to further expand a systemic immune response to RT+IC *in situ* vaccination given to a single site. In order to harness the *in situ* vaccine capabilities of RT+IC to enable attack of distant, metastatic disease, we explored the use of engaging further immune-stimulation via the use of "distant" radiation, both with external beam RT or molecular TRT in combination with RT+IC. We present the results of our analyses of tumor growth rates in models of mice bearing multiple tumors, that demonstrate improved survival in mice receiving additional RT or TRT prior to immunotherapy.

4.3 Materials and methods

4.3.1 Syngeneic tumor cell lines

B78-D14 (B78) murine melanoma is a cell line derived from B16-F10 melanoma, as previously described[128]. This cell line was generously provided by Ralph Reisfeld at the Scripps Research Institute. Panc02 murine pancreatic adenocarcinoma cells were obtained from ATCC. B78 and Panc02 Cells were cultured in RPMI 1640 (Mediatech, Inc, Manassas, VA) supplemented with 10% fetal bovine serum, 100U/mL penicillin, 100µg/mL streptomycin, and 2mM L-glutamine. As previously described, B78 cells are engineered to express GD2- and GD3-synthase under the control of 400µg/mL G418 and 50µg/mL hygromycin and were selected over three days in selection media prior to being frozen down as lab stock. Cells were kept below 90% confluence and were used within 7 passages of thaw from the common bank. Cells were confirmed mycoplasma negative by PCR within 6 months of use.

4.3.2 Animal studies and tumor models

Animals used in this study were housed and cared for using an approved protocol reviewed by the University of Wisconsin-Madison Institutional Animal Care and Use Committee (IACUC). Female, 6-8 week old C57BL/6 mice were ordered from Taconic Biosciences (Rensselaer, NY) and allowed to acclimate in our animal facility for at least one week following arrival. Tumors were engrafted by injecting $2x10^6$ cells (either B78 or Panc02) in 100μL intradermally in the right flank using a 26g needle. Secondary tumors were injected similarly, with $2x10^6$ B78 cells, 10-14 days after the primary tumor in the contralateral (left) flank, again intradermally. Of note, the flank was shaved with electronic clippers 24-48 hours prior to tumor implantation to ensure consistency of injection, and to limit potential impact from any irritation and inflammation resulting from shaving. Tumors were monitored twice weekly and were allowed to develop over 4-6 weeks. For all mouse studies, mice that did not have a palpable secondary tumor were excluded.Tumor volume for all experiments was measured using calipers and approximated as $(width^2 \times length)/2$. Some of the experiments were performed prior to the findings presented in Chapter 3 regarding the difference between ID and SC implantation effects on the efficacy of RT + IT-IC. In those studies, our retrospective assessment is that the tumors were implanted SC rather than ID.

4.3.3 External beam radiation and molecularly targeted radiation preparation and administration

External beam radiation was delivered using an X-RAD 320 system (Precision X-Ray Inc, North Branford, CT). Mice were immobilized using custom lead jigs and surgical tape such that only the dorsal right flank is exposed, with the rest of the mouse (including the contralateral flank and spleen) shielded. Irradiation settings were beam strength 320Kv/12.5mA, beam conditioning filter 2, platform height 36 cm, treatment duration 331 seconds, which has been measured to reliably deliver 11 +/- 1 Gy to the tumor by thermoluminescent dosimetry (data not

shown). To deliver external beam radiation dose to the secondary tumor on the left flank, at the same time that the primary (right flank) tumor is irradiated, lead shields were left off of the mouse's left flank during the radiation of the right flank. Once the scheduled dose (2, 6 or 12 Gy) was delivered to the secondary tumor, it was re-shielded, so that the remaining dose (if any was scheduled, up to 12Gy) could be delivered to the primary tumor.

$^{90}YCl_3$ was purchased from Perkin Elmer (Waltham, MA). The alkylphosphocholine molecule used for molecular targeted radionuclide therapy, 2-(trimethylammonio)ethyl(18-(4-(2-(4,7,10-tris(carboxymethyl)-1,4,7,10-tetraazacyclododecan-1-yl)acetamido)phenyl)octadecyl) phosphate (NM600), was kindly provided by Archeus Technologies (Madison, WI). The radiolabeling and characterization of ^{90}Y-NM600, and its PET-detectible counterpart ^{86}Y-NM600, has been described elsewhere [127,131]. Briefly, 5-10mCi of $^{90}YCl_3$ was buffered in 0.1 M NaOAc (pH = 5.5.) and 10-15 nmol/mCi of NM600 was added to the mixture. The reaction was placed at 90°C for 30 minutes under constant shaking at 500rpm. The reaction mixture was loaded into an HLB (hydrophilic lipophilic balance) solid phase extraction (Waters) cartridge, washed with 5 mL of H_2O, and ^{90}Y-NM600 was eluted in 2 mL of absolute ethanol. Nitrogen stream was used to evaporate the eluate, and ^{90}Y-NM600 was reconstituted in normal saline containing 0.4% v/v Tween 20 and sodium ascorbate (0.5% w/v). Mice receiving EBRT were radiated on treatment day 1, and mice receiving TRT were injected with 100μCi of ^{90}Y-NM600 preparation by tail vein injection on treatment day 1. An injected activity of 100μCi, which corresponds to a dose of approximately 4Gy at the secondary tumor, was chosen as it was the highest activity previously demonstrated not to limit (via immunosuppression) efficacy of RT+IC in situ vaccination in a one-tumor B78 model (data not shown).

4.3.4 Immunotherapy preparation and administration

Immunocytokine (IC, hu14.18-IL2) was provided in lyophilized form (4mg/vial) by Apeiron Biologics (Vienna, Austria). It was reconstituted by adding 8mL of sterile PBS for a

working concentration of 0.5mg/mL. For mice being treated with EBRT+IC, 100μL of the 0.5mg/mL IC solution was injected intratumorally (IT) daily on treatment days 6 through 10, for a total dose of 250μg per mouse. Injections were through a 30G needle, and care was taken to inject slowly and not draw drug up through the needle, to avoid shear-induced denaturation of the immunocytokine.

4.3.5 *Cause of death and immune memory analyses*

Mice were evaluated twice weekly, using calipers, to measure both primary and secondary tumors. If the mouse required euthanization due to tumor dimensions exceeding our predetermined threshold (measuring $\geq$ 20mm in any dimension), the tumor location (either primary or secondary) was recorded. Furthermore, if the mouse was still alive at the completion of the study, the larger tumor of the two tumors (presumably the tumor that would be responsible for killing the mouse) was also recorded. In addition mice that required euthanization due to ulcer formation or extensive dermatitis, as determined by veterinary recommendation, were recorded, as well as mice that were disease-free at the time of experiment completion. Disease free mice were rechallenged by injecting an inoculum of $2x10^6$ B78 cells intradermally above the right shoulder 30 days after confirmation of disease-free status. After 30 days post-rechallenge, any palpable tumor at the injection site was assigned a "rejection failure" and recorded. Following B78 rechallenge, $2x10^6$ Panc02 murine pancreatic adenocarcinoma cells were injected ID above the left shoulder and monitored for another 30 days, with rechallenge success or failure noted accordingly.

4.3.6 *Statistical Analysis*

All data presenting replicates include the individual values as well as mean +/- standard error of the mean (SEM) except where otherwise noted. Differences in tumor growth rates were assessed using linear mixed effects models. Growth rates were estimated from the model as a

ratio of change every 21 days. Models predicted tumor volume based on treatment group, days since treatment started, an interaction between treatment and time, and a random intercept per mouse. The statistics of interest were the interaction between treatment and time, which represented the ratio between one treatment's estimated 21-day growth rate (expressed as an estimated average fold change in volume every 21 days, applied across the entire growth curve) and the average rate of another treatment. These estimates along with 95% confidence intervals and Kenward-Rogers p-values were calculated and are presented in Tables 4.1, 4.2, 4.4, and 4.5. Tumor volumes for some analyses were transformed with the natural log function to correct patterns in residuals and to account for the exponential growth of tumors. Zero-valued measurements were imputed as 4 mm^3 (the smallest recordable tumor volume using calipers) in order to be defined under the transformation. Statistical analysis was conducted using R version 4.0.2; the lme4 package was used for fitting mixed models and Kenward-Rogers p-values were estimated from the lmerTest package. Significance was assessed at the alpha = 0.05 level and no corrections were made to account for inflated type 1 error rate of multiple hypotheses. Note that although tumors grow exponentially in the early phases of their growth (before they are limited by outgrowing their vascular supply [189], the impact of treatment can cause tumors to either fully or temporarily deviate from exponential growth. This is often observed in treated primary tumors, which experience a period of "response" during treatment days 10-30, and a period of "growth" after treatment day 30. Linear mixed effects modeling can handle this deviation effect in its estimation of growth rates, but does not truly describe the growth rate of the tumor **in its entirety**. As such, the estimated growth rate of all tumors within a treatment group is somewhat arbitrary, and does not describe the "true" degree of response to treatment. These systems for more accurately modeling tumor growth kinetics, particularly once kinetics are altered in response to treatment, are an area of active research and debate within the field of biostatics, and is beyond the scope of this thesis [190–192]. However the **ratio** of growth rates between treatment groups is a valid means of comparing these relative, yet arbitrary,

growth rates between groups, and is the basis for the use of this modeling approach to describe the impact of treatment.

Simple comparison between tumor volumes on a particular day post-treatment were conducted using a two-tailed t test. Treatment days chosen to analyze in Figures 1, 2, and 5 were based on the latest recorded treatment day for which all members of a treatment cohort are alive (excluding the PBS no treatment control groups). Mice that died in the PBS group prior to the chosen day for analysis were included as last value carried forward, and are represented by an 'X' in the figures. Comparisons of proportions of mice dying from primary tumor burden or proportions of mice rendered disease free were made using chi-square tests.

4.4 Results

4.4.1 *External beam radiation to a distant tumor can improve control following in situ vaccination to primary tumor*

To determine the effect of additional radiation delivered to a secondary tumor in the setting of RT+IC immunotherapy, and to determine the impact of dose in this respect, a titration of RT dose to a secondary tumor alongside RT+IC *in situ* vaccination to a primary tumor was conducted (Figure 4.1). Mice were implanted intradermally with B78 murine melanoma cells in the right flank, followed by a second injection in the left flank two weeks later. After approximately 2 more weeks, these mice then had a right flank "primary" tumor ~150mm^3 in size, and a smaller left flank "secondary" tumor ~50mm^3 in size. These references to "primary" as the right flank tumor and "secondary" as the left flank tumor will remain throughout this chapter. Mice were then randomized to receive either PBS (no treatment control), 12Gy of RT to both tumors (12Gy/12Gy radiation control), or *in situ* vaccine (12Gy of RT+IC) at the primary tumor combined with either 0, 2, 6, or 12Gy RT to the secondary tumor (Figure 4.1). Results demonstrated that while 12Gy radiation to both tumors did slow tumor growth at both primary and secondary sites, the combination of radiation to the second tumor together with RT/IC to the

primary was more effective at slowing tumor growth. Primary tumors treated with RT/IC immunotherapy all grew at a reduced rate compared to either the PBS control or the 12Gy/12Gy radiation only control (Figure 4.1A-G, Table 4.1) and had smaller average tumor volume on treatment day 60, compared to last-value-carried forward PBS controls (Figure 4.1H).

At the secondary tumor, RT/IC immunotherapy delivered to the primary was able to slow growth of the secondary tumor, compared to the PBS control (Figure 4.1, Table 4.2), which does suggest that RT/IC immunotherapy itself has some degree of systemic effect. The addition of RT to the secondary tumor concurrent with RT/IC to the primary did improve control of the secondary tumor, in what trended to be a dose-dependent manner. Average secondary tumor volume measured at treatment day 60 (Figure 1H) in the RT/IC + 12Gy group was lower than the 12Gy+12Gy radiation alone group ($p = 0.0214$), and trended lower when compared to the RT/IC alone group ($p=0.0625$). No difference was detected in comparing the RT/IC + 2Gy groups and RT/IC + 6Gy groups at the secondary tumor to that of RT/IC alone. When evaluating estimated growth rates of the secondary tumor from mixed effects modeling of log-transformed data, all three RT doses at the secondary tumor added to the RT/IC at the primary caused a significantly slower growth rate than RT/IC alone, with a difference in growth rates that tended to increase with RT dose (Table 4.2). These data suggest that radiation in the form of external beam RT delivered to a secondary tumor combines with an *in situ* vaccine to slow the growth of the secondary tumor.

4.4.2 *External beam radiation delivered to a secondary tumor, concurrent with in situ vaccination to primary tumor, improves overall survival, reduces tumor growth rates, and induces immune memory*

To test the effect of RT combined with *in situ* vaccine on overall survival and to more robustly characterize its impact on tumor growth rates, a series of larger studies were conducted. C57BL/6 mice were implanted in both flanks with B78 tumor cells, with a 14-day

delay in implanting the secondary flank tumor, as described for Figure 4.1. Only mice with a palpable secondary tumor were included in randomization and treatment. Mice were treated with either PBS (no treatment control), 12Gy of RT to both tumors (radiation only control), RT+IC to the primary tumor only, or RT+IC to the primary with 12Gy RT concurrently delivered to the secondary (Figure 4.2). All RT was delivered on treatment day 0, and all IC was injected intratumorally on treatment days 5-10 (Figure 4.2A). A RT dose of 12Gy to the secondary tumor was selected due to its greater potential impact on overall survival as determined by the radiation dose titration effects on tumor growth in the previous experiment (Figure 4.1). This experiment was repeated independently three times. Results demonstrated that all three treatment interventions extended overall survival compared to the no treatment PBS control (comparison p values of <0.0001 each for log rank test comparing PBS to 12Gy+12Gy, RT/IC, and RT/IC+12Gy individually, Table 4.3). In addition, survival was improved for RT/IC +12Gy compared to RT/IC alone (median survival 125 vs.85 days, p = 0.0025), as well as RT/IC + 12Gy compared to 12Gy+12Gy RT only (median survival 125 vs. 97 days, p = 0.0052) (Figure 4.2B, Table 4.3).

For all three experimental replicates, the cause of death or likely cause of death was evaluated for each mouse at the completion of the experiment (Figure 4.2C). Eleven out of 16 mice (68.8%) in the PBS control group died from their primary tumor, as did 12/16 mice (75%) of mice treated with 12Gy RT only to both tumors. This proportion shifted in the RT/IC treated group, where only 5/26 (19.2%, p = 0.001 compared to PBS) mice died from their primary tumor, and 17/26 (65.4%) died from secondary tumor burden. Four out of 26 mice (15.4%) treated with RT/IC *in situ* vaccine were disease-free. In the group treated with both RT/IC + 12Gy, 8/26 (30.8%) mice were disease-free, 9/26 (34.6%) mice died from primary tumor burden, and 6/26 (23.1%) mice died from secondary tumor burden. In addition, 3/26 (11.5%) RT/IC + 12Gy mice were recommended for euthanasia by veterinary staff due to ulceration/inflammation at the tumor site, which was thought to be self-inflicted by the mice. Though the degree of

ulcerataion led to to a recommendation for euthanasia prior to assessment of disease-free status, there was no detectable tumor burden at either the primary or secondary flank at the time of euthanasia. This means that in total 11/26 (42.3%) mice treated with RT/IC+12Gy were cleared of their tumors as a result of treatment, which is significantly more than the 4/26 (15.4%) mice that cleared their tumors following RT/IC only ($p = 0.032$).

To test for tumor antigen-specific memory, mice rendered disease-free by treatment were rechallenged with a second inoculum of B78 tumor cells in the upper shoulder region at least 30 days after being declared disease free. Of the eight disease-free mice in the RT/IC +12Gy group, all 8 (100%) failed to develop a tumor at the rechallenge injection site. Three out of four (75%) disease free mice in the RT/IC group rejected a rechallenge tumor, and zero out of 1 (0%) disease free mice in the 12Gy + 12Gy group rejected the rechallenge tumor. To confirm that this rejection of the rechallenge with a B78 tumor is tumor-specific, these same 13 disease-free mice were also challenged with an unrelated panc02 syngeneic pancreatic cancer cell line in the contralateral shoulder. All 13 disease free mice, across all 3 treatment groups, failed to reject the challenge and developed palpable tumors at the site of injection. Taken together, these data suggest that the combination of *in situ* vaccination and 12Gy radiation to distant tumors may result in a greater proportion of disease-free mice than *in situ* vaccine alone, and that any mice rendered disease-free by *in situ* vaccination retain a tumor-reactive immune memory after clearance of their disease burden, that appears tumor-specific.

To further characterize the effect of radiation and *in situ* vaccine combination on the growth rate of both primary and secondary tumors, tumor volume and growth rates were analyzed (Figure 4.2E). Average treatment day 54 primary tumor volume in the RT/IC + 12Gy group was smaller than the 12Gy + 12Gy group ($p < 0.0001$), and trended smaller compared to the RT/IC group ($p = 0.062$). Average treatment day 54 secondary tumor volume in the RT/IC + 12Gy group was smaller than in the 12Gy + 12Gy group ($p=0.0005$), and was smaller than in the RT/IC group ($p < 0.0001$). Individual tumor volumes for mice in one representative

experiment is presented in Figure 4.3 A-D. In addition, linear mixed effects modeling was conducted on log-transformed individual tumor growth curves over the lifetime of the experiment (Figure 4.3E, Tables 4.4 and 4.5). By comparing growth rates of the modeled data, it was estimated that primary tumors in the RT/IC group grew 1.344 (1.186 to 1.53) times faster than the RT/IC + 12Gy group (Table 4.4). This result is consistent with our prior demonstration of CIT, where an un-irradiated distant tumor can hinder the effect of RT/IC on the primary tumor [66]. For secondary tumors, those in the RT/IC group grew 1.605 (1.453 to 1.776) times faster than the RT/IC + 12Gy group. Further, comparing the RT/IC +12Gy group to the 12Gy + 12Gy radiation only group yielded similar results; both primary and secondary tumors in the RT/IC + 12Gy group grew at a slower rate than the radiation only control group (Tables 4.4 and 4.5). In total these data suggest that external beam radiation delivered to all sites of disease improves response to locally delivered *in situ* vaccine, at both primary and distant tumors.

4.4.3 *Molecular Targeted Radionuclide Therapy (TRT) combined with in situ vaccine improves overall survival*

In order to be able to deliver radiation dose to all sites of disease, both known and occult, a different modality beyond external beam RT is required. A systemically administered molecular targeted radionuclide therapy (TRT), that selectively binds to cancer cells on a molecular level, can circulate to all tissues of the body, and theoretically deliver RT dose to all sites of disease. In order to determine if we could apply the same findings from combination external beam RT and *in situ* vaccine to combination TRT and *in situ* vaccine, we used the beta particle-emitting TRT agent ^{90}Y-NM600. One key difference between radiation dose delivered by external beam RT and dose delivered by targeted radionuclide therapy is the dose rate; external beam delivers energy at a very high rate, while the TRT agent delivers the energy over a prolonged period of time as the radionuclide decays. In addition, the external beam RT delivers a similar dose to all tissue in the radiation field, and extremely lower doses of radiation to distant

areas outside of the radiation field. In contrast, TRT delivers radiation systemically to all tissues of the body, where it is retained selectively by tumor and cleared more rapidly by non-tumor tissue; thereby resulting in radiation delivery to all tumor sites, with lower-dose radiation to non-tumor tissue. Because antitumor immune effector cells themselves are sensitive to radiation, and would be exposed to some low dose radiation with the systemically administered TRT, we conducted a dose-titration of TRT combined with RT+IC *in situ* vaccine in a one-tumor mouse model to determine the dose of TRT that may be sufficiently immunosuppressive to interfere with generation of an antitumor immune response. C57BL/6 mice bearing a single ~150mm^3 flank tumor were randomized to receive RT+IC *in situ* vaccine plus 0, 25, 50, or 100μCi of ^{90}Y-NM600 (Figure 4.4). If there were no immunologic effect of the RT+IC component of this therapy on tumor growth, we would expect the tumors to be affected purely by the radiation dose delivered by the RT and the TRT, so the negative control group (no immunotherapeutic effect) for this experiment was 12Gy RT plus 100μCi of ^{90}Y-NM600. Results of two independent experiments pooled together demonstrate a significantly reduced tumor volume in all groups treated with combined RT+IC and TRT at 0, 25 and 50 μCi of ^{90}Y-NM600 injected activity, and a trend towards reduced tumor volume in the group treated with RT+ IC and 100μCi of ^{90}Y-NM600 compared to the radiation-only control. No side effects of radiation toxicity including weightl loss, hair loss, or ulceration were observed at any of the TRT injected activities. These data suggest that there is still an immune effect being generated in response to *in situ* vaccination capable of further controlling tumor growth beyond the effect of radiation alone, up to an injected activity as high as 100μCi.

To determine if systemically administered ^{90}Y-NM600 can provide benefit in controlling multiple tumors when combined with *in situ* vaccination, C57BL/6 mice were implanted ID with a primary B78 tumor, and a B78 secondary tumor 14 days after the primary, as described in the materials and methods section (Figure 4.5A). Mice were randomized to either PBS control, 100μCi of TRT only, RT/IC *in situ* vaccine to the primary tumor, or RT/IC + 100μCi TRT. The

PBS and RT/IC groups were shared with the previous set of experiments described in Figures 4.2 and 4.3, which were conducted concurrently with the TRT studies shown in Figures 4.5 and 4.6. Mice receiving TRT were injected with 100μCi of ^{90}Y-NM600 by tail vein injection on treatment day 0, the same day they were treated with 12Gy external beam RT to the primary tumor. Immunocytokine was delivered intratumorally on treatment days 5-9 (Figure 4.5A). Results demonstrate that the combination of RT/IC + TRT resulted in significantly increased overall survival compared to RT/IC immunotherapy alone (median 112 vs 85 days, $p = 0.025$) (Figure 5B, Table 4.6). Mice treated with TRT alone did not have improved survival compared to PBS (median 56 vs 60 days, $p = 0.1839$). Analysis of the cause of death revealed that 14/16 (87.5%) mice in the TRT only group died from primary tumor burden, while only 6/25 (24%, $p<0.0001$ compared to TRT only) mice in the RT/IC + TRT group died from primary tumor burden. Four out of 25 (16%) mice in the RT/IC + TRT group became disease free. Of these four disease free mice, all of them rejected subsequent rechallenge with an additional B78 tumor inoculum, but developed tumors in response to the unrelated panc02 challenge (data not shown), which suggests a tumor-specific memory response.

Analysis of tumor volumes on treatment day 34 (Figure 4.5E) indicate that primary tumors treated with RT/IC + TRT were smaller than those treated with TRT only ($p<0.0001$). No difference was detected between primary tumors treated with RT/IC + TRT compared to those treated with RT/IC only. Secondary tumors in mice treated with RT/IC+TRT had a lower day 34 treatment volume than those in mice treated with TRT alone ($p=0.0043$) and those treated with RT/IC alone ($p=0.0106$). Individual tumor volumes for mice in one representative experiment is presented in Figure 4.6 A-D. Linear mixed effects-based modeling of average tumor growth rate was conducted on log-transformed tumor volumes and used to compare growth rates between treated groups (Figure 4.6E, Tables 4.7 and 4.8). Primary tumors treated with RT/IC grew 1.352 (1.191 to 1.562) times faster than those treated with RT/IC + TRT (Table 4.7). Secondary tumors treated with RT/IC grew at the same average rate as those treated with RT/IC+TRT

(0.907 to 1.111, Table 4.8). Tumors treated with TRT alone showed substantially faster growth than RT/IC + TRT at both the primary (3.329, 2.299 to 4.763) and secondary (1.706, 1.316 to 2.188) tumors (Tables 4.7 and 4.8).

4.5 Discussion

In this chapter we demonstrate the utility of radiation to both sites of disease prior to *in situ* vaccination with RT + IC in controlling the growth of both tumors in mice with 2 distinct sites of B78 melanoma. We demonstrate that a range of external beam doses to a secondary tumor, shows a trend towards a dose-dependent effect in improving response following RT+IC *in situ* vaccination; the greatest effect identified appeared to be with a 12Gy dose, which was the highest dose tested (Figure 4.1). Further characterizing the *in vivo* effect of this regimen, we demonstrate improved survival with combination RT+IC to the primary and 12Gy RT to the secondary tumor compared to either RT+IC alone, or 12Gy RT only to both tumors (Figure 4.2B). We also explored delivering this radiation to both sites of disease using a systemically injected molecular targeted radionuclide therapy, ^{90}Y-NM600. We demonstrate that an injected activity as high as 100μCi given five days prior does not interfere with the antitumor effect of RT+IC *in situ* vaccination, and is safe to use in our regimen (Figure 4.4). Lastly, we demonstrate *in vivo* effect of combining 100μCi ^{90}Y-NM600 with *in situ* vaccine, with increased overall survival compared to RT+IC *in situ* vaccine alone (Figure 4.5B).

Cancer care has made significant progress in the last several decades in terms of surgical, medical, and radiologic treatment of disease. Surgical resection followed by radiation to the resection margin has reduced the rate of local recurrence in many cancer types dramatically [1]. It is now our understanding that the majority of fatal cancer cases are a result of disease at a location other than the primary tumor, typically what is termed either

oligometastatic (few numbers of additional lesions) or metastatic disease [193]. Though chemotherapy has made substantial contribution to controlling microscopic disease, resistance often develops [194]. Immunotherapy holds great promise in treating these distant lesions; this has been particularly evident with the recent use of immune checkpoint blockade in the setting of inflamed, immunogenically “hot” cancers. Despite the success of such treatments, a clear dichotomy in response between “hot” and “cold” cancer patients has developed when checkpoint blockade is used as the sole immunotherapeutic strategy [195]. While supraphysiologic activation of immune effectors can be sufficient to achieve strong antitumor response in “hot” tumors, these effectors either may fail to be generated, or fail to find adequately hospitable environments in “cold” tumors [ref]. Our effort now is directed towards converting “cold” tumors to “hot” tumors, which may in turn make them more responsive to immunotherapy.

There is growing evidence now that radiation can have immunologic effects that can prime the TME to be more responsive to immunotherapy. In cells undergoing immunogenic cell death following radiation therapy, calreticulin is translocated to the cell surface. Calreticulin is a chaperone protein that is upregulated during times of stress, and is a potent activator of dendritic cell (DC) phagocytosis [37]. Also released during immunogenic cell death is High Mobility Box Group 1 (HMGB1), is classified as a Damage Associated Molecular Pattern (DAMP) and can activate innate immune cell inflammatory response by binding Toll-Like Receptor (TLR) family members, including TLR2 and TLR4 [39,40]. These processes can culminate in DC activation and migration, enhanced antigen processing, and increased presentation/activation of antigen-specific effector T cells [35]. Some studies have also demonstrated an increase in expression of MHCI on tumor cells surviving low doses (1-4Gy) of external beam radiation , as well as increased expression of inflammatory adhesion proteins including VCAM1, ICAM1, and CD31 [43], [46]. Demaria and colleagues have also

demonstrated that double stranded DNA breaks induced by radiation can be detected in the cytosol and activate expression of type 1 interferon in the tumor cells themselves, which have potent inflammatory effects [50]. Lastly, radiation can have a direct cytotoxic effect on immune cells in the radiation field, including T_{regs}, which can serve to eliminate any long-standing immunosuppressive or regulatory populations in the “cold” tumor microenvironment [35]. Taken together, radiation may be “resetting” the immune tumor microenvironment to a state before it had escaped from the immune system. Though in traditionally “cold” tumors this is likely not enough to drive sustained immune activation before becoming suppressed again, RT may be able to create a window of opportunity for which an *in situ* vaccine or other systemically activating immunotherapy can drive effective infiltration into this temporarily “hot” TME.

Our results with local *in situ* vaccination in the setting of multiple “cold” B78 tumors highlight the challenge faced by an activated immune system to overcome a suppressive tumor microenvironment. Our studies demonstrate that the addition of RT at the secondary tumor improves the disease course with a reduction in secondary tumor growth at day 60 in comparison to RT+IC at the primary site alone (Figure 4.1). In our follow up confirmatory experiments, the RT+IC plus 12Gy group demonstrated significantly reduced average tumor volume on treatment day 54, as well as a significantly reduced estimated average growth rate at the secondary tumor compared to either *in situ* vaccination or radiation only (Table 4.2, last two rows). This suggests that although RT+IC *in situ* vaccination does slow the growth of the secondary tumor compared to the no treatment control, a substantially greater degree of control is achieved when adding 12Gy RT to the secondary. Importantly, secondary tumors in mice that received 12Gy to the secondary and *in situ* vaccination also had lower average day 54 tumor volume than mice receiving only radiation. This suggests that the systemic effect of RT+IC immunotherapy (on the distant tumor) is at least additive in achieving antitumor effect and slowing/reversing tumor growth. This is supported by our clear demonstration of improved

overall survival, with significant extension of lifespan in mice receiving RT+IC plus 12Gy of RT at the secondary in comparison to either RT+IC only at the primary site, or 12Gy radiation to both tumors alone (Figure 4.2B).

Looking into the cause of death amongst these groups provided some insight into potential mechanisms through which this lifespan extension was conferred. While the majority of mice that died in the RT+IC only group died due to secondary tumor burden, those mice that died in the RT+IC + 12Gy to the secondary group died equally between primary tumor, secondary tumor, or inflammation/dermatitis (Figure 4.2C). This suggests that while there is likely a similar effect of RT+IC alone versus RT+IC plus 12Gy to the secondary tumor on primary tumor growth, the addition of the 12Gy to the secondary site provided a benefit to at least some of the mice that would have died as a result of uncontrolled growth of the secondary tumor. Thus in this chapter we have demonstrated that there is likely an in vivo benefit to radiation at both sites of disease in conjunction with *in situ* vaccination of this B78 melanoma. Further testing is needed to see if this may apply preclinically in other settings. The clinical implication is that provision of radiation at an immunomodulatory dose (like 12 Gy or potentially lower) to all sites of disease, if feasible, may help immunotherapies that work (in part) through an *in situ* vaccine effect, to better control local and distant disease. If provision of radiation to all disease sites is proven to be clinically beneficial when combined with immunotherapy, an important challenge will be how RT can be delivered to all sites of disease without causing substantial radiation-toxicity or functionally meaningful systemic immune suppresion. While external beam radiation would not be used to treat all disease sites in widely metastatic cases for fear of this widespread local toxicity and systemic immunesuppression, there is growing interest in aggressively treating all known lesions in cases of oligometastatic cancer (cancer limited to 5 or fewer metastases). The results of a randomized phase II trial of stereotactic ablative radiotherapy to all disease sites vs standard of care in 99 oligometastatic patients in

Europe demonstrated improvement in median survival (41 months vs 28 months) in the group receiving treatment to all tumors [196]. In this setting, one could consider adding local *in situ* vaccination to one of these sites in order to further drive antitumor effect. Though prone to off target effects, it is technically and financially easier to radiate all sites of disease as opposed to intratumorally injecting all sites of disease; by this logic the combination of RT to all sites and *in situ* vaccine to a single site holds immediate translatable clinical potential.We have presented *in vivo* evidence that radiating additional sites of disease can turn “cold” tumors “hot,” and permit a stronger systemic antitumor immune response. Though external beam radiation may be useful combined with immunotherapy in the setting of multiple macroscopic lesions, it is not feasible to radiate every micrometastatic site using such an approach in patients with a large number of measureable tumor sites or with disseminated metastases. Systemically administered, molecularly targeted radionuclide therapy presents an alternative approach to deliver radiation to all sites of disease and therefore create an immune-susceptible TME. This principle has been demonstrated with ^{90}Y-NM600 in combination with dual anti-PD1 and anti-CTLA4 checkpoint blockade [197], but not with a locally administered *in situ* vaccine. The use of a modular molecular compound like NM600 is that the agent can be chelated to a number of radiometals, which can have varying half-lives, decay particle types, path lengths, and positron emissions [198,199]. In the setting of NM600, conjugation of ^{86}Y instead of ^{90}Y results in a PET-detectable compound that has the exact chemical and pharmacokinetic properties of the ^{90}Y agent. This allows for PET/CT based imaging of a patient over time to predict, in a patient-specific manner, the uptake, distribution, and dose delivered to target and off-target tissues for ^{90}Y-NM600. Thus this agent is a theranostic, possessing both diagnostic and therapeutic properties [75,200]. This approach has been used effectively as a single-agent therapy against the more radiosensitive EL4 lymphoma line where it is capable of tumor eradiation and facilitates generation of immune memory [131].

Similar to external beam RT, in this chapter, the use of TRT combined with immunotherapy improved overall survival compared to immunotherapy alone (Figure 4.5).The impact of this TRT dose was somewhat less than that of 12Gy external beam RT, however. Though a difference in treatment day 36 volume was detected, the linear mixed effects model was unable to detect a statistically different growth rate in secondary tumors in mice treated with RT+IC alone or RT+IC and TRT combined, and there was no difference in the number of disease-free mice resulting between these two groups. This may be due to a difference in overall dose delivered to the tumor; while the external beam delivered 12Gy, the TRT only delivered 3-5Gy, as it was the highest dose we knew we could administer without interfering (via immune-suppression) with the *in situ* vaccine (Figure 4.4). Interestingly, the rate of growth was significantly lower at the primary tumor in mice treated with RT/IC + 100μCi of ^{90}Y-NM600 TRT compared to mice treated with RT/IC alone. This is consistent with the equivalent effect observed in the case of 12Gy external beam delivered to the secondary tumor, though it should be noted that more sophisticated means of statistically modeling tumor growth will likely be required to confirm this added effect on the growth rate of the primary tumor. Any added effect may be due to the extra accumulation of dose in the primary tumor resulting from greater tumor cell kill prior to immunotherapy. A second possibility for the improved primary tumor response could be that radiation of the secondary TME is able to have a distant immunologic effect at the primary TME. Elimination of T_{regs}, increased activation of cytokine-producing effector cells, increased migration both to and from the tumor bed may result in a stronger circulating antitumor immune response, that in turn is able to positively impact the primary tumor as well. This would be consistent with overcoming a CIT-like response at the primary by delivering radiation to the secondary, and could support the use of radiation to prime all sites of disease prior to immunotherapy [66].

One of the major questions that still remains are the mechanisms by which immune-activating treatment at one tumor site can have additional impact on other sites of disease. In the RT+IC alone group, treatment of the primary tumor did result in slower secondary tumor growth compared to mice that received no treatment, which suggests some degree of a systemic response in mice treated with immunotherapy; immune cells generated by the *in situ* vaccine do slow the growth of this otherwise "untreated" tumor. This was further supported by our findings that treatment of the secondary site with 12Gy trended towards improvement in response at the primary tumor evidenced by reduced growth rate at both sites of disease (Figure 2). However, this improvement in response was inadequate to control the established "cold" B78 secondary tumor in most mice. The addition of 12Gy RT to the secondary tumor may have allowed for the systemic immune response generated by the *in situ* vaccine to eliminate a greater proportion of tumor cells, thus slowing growth or even curing some mice.

To help address these mechanistic questions, we have begun to characterize changes in immune cell populations in the TME of mice with 2 B78 tumors receiving the regimens shown in this chapter through flow cytometry analyses/ We are using the novel staining and preparation technique outlined in chapter 2 of this thesis. Through this technique and development of reliable and robust staining panels, we have developed means of querying both the adaptive and innate arms of the immune system, as well as markers of immune activation, in both primary and secondary tumors as well as in the tumor-draining lymph nodes. To supplement these data, we are also conducting direct measurement of cytokine production in tumor lysates and correlating them with our flow cytometric data. A detailed presentation and analysis of these preliminary flow-cytometry and cytokine-production data is included in Appendix A of this thesis. Ongoing and future studies will also assess the role of these immune populations through *in vivo* depletion analyses aimed at CD8 T cells, CD4 T cells, NK cells, and others. Future analyses may also include evaluation of the degree of activation / functional role

of these populations using qPCR to amplify effector molecules such as interferon gamma, IL-2, perforin, and Granzyme B.

4.6 Acknowledgements and clarification of collaborative efforts from others in this work

I would like to acknowledge the contributions of those that assisted me in the work presented in this chapter. Manasi Mohan, Matthew Rodriguez, and Claire Sun assisted in managing mice, tumor measurements, and survival analysis. Joeseph Grudzinski, Reinier Hernandez, and thesis committee member Jamey Weichert provided the ^{90}Y-NM600 TRT agent. Jen Birstler assisted in statistically analyzing these results and in figure generation. Amy Erbe and Ravi Patel provided assistance in mouse measurement, experimental design, discussion of analysis, and editing of this chapter. Special thanks to Drs. Alexander L. Rakhmilevich and Jacquelyn A. Hank for thoughtful discussion of experimental design and results. Thesis committee members and co-mentors Zach Morris and Paul Sondel provided the guidance, funding, discussion, and editing support for this chapter. All of these individuals will be included as co-authors on the manuscript presenting these findings, which is currently in preparation.

Table 4.1: Primary tumor growth rates for mice and treatments depicted in Figure 1. Tumor volumes were log-transformed, and linear mixed-effects modeling was conducted to estimate a proportional growth rate every 21 days, integrated over all time points for each tumor. The average (designated "Estimate") and 95% confidence interval (CI) of these growth rates are presented here. By comparing the average growth rates to each other, inferences (supported by Kenward-Rogers p values) can be made about the rate of growth on average of one treatment group compared to another. Estimates for these ratios represent the proportion of change from one group compared to the other over a 21 day period. The Kenward-Rogers p value is presented as a comparison to a null hypothesis of zero tumor volume change over time or no proportional difference between two groups compared as a ratio (both of which would correspond to an Estimate value of 1).

Parameter	Estimate	95% CI	p-value	Conclusion
Growth rate of PBS	3.786	2.751 to 5.460	<0.001	Tumors on average grew over time
Growth rate of 12Gy+12Gy	2.306	1.894 to 2.798	<0.001	Tumors on average grew over time
Growth rate RT/IC	0.648	0.538 to 0.789	< 0.001	Tumors on average shrank over time
Growth rate RT/IC+2Gy	0.842	0.698 to 1.014	0.068	No change detected, but trending to shrink slightly on average
Growth rate RT/IC+6Gy	0.777	0.637 to 0.958	0.017	Tumors on average shrank over time
Growth rate RT/IC+12Gy	0.848	0.698 to 1.017	0.080	No change detected, but trending to shrink on average
Ratio of (PBS) to (RT/IC)	5.840	3.722 to 8.780	<0.001	PBS tumors grew **faster** than RT/IC tumors
Ratio of (RT/IC) to (12Gy+12Gy)	0.281	0.216 to 0.371	<0.001	RT/IC tumors grew **slower** than 12Gy+12Gy tumors
Ratio of (RT/IC) to (RT/IC+12Gy)	0.765	0.581 to 0.996	0.051	**No statistical difference** in growth rate but RT/IC + 12Gy shows a trend towards slower growth

Table 4.2: Secondary tumor growth rates, for mice and treatments depicted in Figure 4.1. Tumor volumes were log-transformed, and linear mixed-effects modeling was conducted to estimate a proportional growth rate every 21 days, integrated over all time points for each tumor. The average and 95% confidence interval of these growth rates are then reported. By comparing the average growth rates to each other, inferences (supported by Kenward-Rogers p values) can be made about the rate of growth on average of one treatment group compared to another. Estimates for these ratios represent the proportion of change from one group compared to the other over a 21 day period. The Kenward-Rogers p value is presented as a comparison to a null hypothesis of zero tumor volume change over time or no proportional difference between two groups compared as a ratio (both of which would correspond to an estimate of 1).

Parameter	Estimate	95% CI	p-value	Conclusion
Growth rate PBS	5.437	4.110 to 7.270	< 0.001	Tumors on average grew over time
Growth rate 12Gy+12Gy	2.431	2.114 to2.843	< 0.001	Tumors on average grew over time
Growth rate RT/IC	2.706	2.344 to 3.133	< 0.001	Tumors on average grew over time
Growth rate RT/IC+2Gy	2.031	1.796 to 2.332	< 0.001	Tumors on average grew over time
Growth rate RT/IC+6Gy	1.871	1.626 to 2.211	< 0.001	Tumors on average grew over time
Growth rate RT/IC+12Gy	1.230	1.074 to 1.429	0.003	Tumors on average grew over time
Ratio of (PBS) to (RT/IC)	2.009	1.493 to 2.721	0.008	RT/IC tumors grew **slower** than PBS tumors
Ratio of (RT/IC) to (RT/IC+2Gy)	1.332	1.081 to 1.593	0.008	RT/IC + 2Gy tumors grew **slower** than RT/IC tumors
Ratio of (RT/IC) to (RT/IC+6Gy)	1.446	1.173 to 1.761	0.001	RT/IC + 6Gy tumors grew **slower** than RT/IC tumors
Ratio of (RT/IC) to (RT/IC+12Gy)	2.200	1.809 to 2.677	<0.001	RT/IC +12 Gytumors grew **slower** than RT/IC tumors
Ratio of (RT/IC + 12Gy) to (12Gy + 12Gy)	0.506	0.411 to 0.619	<0.001	RT/IC +12Gy tumors grew **slower** than 12Gy + 12Gy tumors

Table 4.3: survival analyses for mice treated with PBS, radiation only, *in situ* vaccine only, or combination radiation and *in situ* vaccine. These analyses correspond to the survival curve depicted in Figure 2B. Groups were compared using the Log-Rank test, with corresponding P-values reported here.

Comparator A	Parameter	Comparator B	A median (days)	B median (days)	P-value
RT/IC	Time to death/sacrifice	PBS	85	56	<0.0001
12Gy + 12Gy	Time to death/sacrifice	PBS	97	56	<0.0001
RT/IC + 12Gy	Time to death/sacrifice	PBS	125	56	<0.0001
RT/IC + 12Gy	Time to death/sacrifice	RT/IC	125	85	0.0025
RT/IC + 12Gy	Time to death/sacrifice	12Gy + 12Gy	125	97	0.0052

Table 4.4: Primary tumor growth rates corresponding to Figure 4.3. Tumor volumes were log-transformed, and linear mixed-effects modeling was conducted to estimate a proportional growth rate every 21 days, integrated over all time points for each tumor. The estimated mean growth rates, 95% confidence intervals, and Kenward-Rogers p-values are then reported. Growth rate p-values are calculated under the null hypothesis that the growth rate is 1 or 100%, that the tumor does not change over time. Treatments are compared by estimating the ratio of growth rates between two treatments. Treatment difference p-values are calculated under the null hypothesis that this ratio is 1, that the growth rates of the two treatments are the same.

Parameter	Estimate	95% CI	p-value	Conclusion
Growth rate PBS	3.527	2.478 to 5.022	<0.001	Tumors on average grew over time
Growth rate 12Gy+12Gy	1.548	1.211 to 1.988	<0.001	Tumors on average grew over time
Growth rate RT/IC	1.407	1.283 to 1.571	<0.001	Tumors on average grew over time
Growth rate RT/IC+12Gy	1.047	0.960 to 1.127	0.263	Tumors on average did not change over time
Ratio of (RT/IC) to (RT/IC + 12Gy)	1.344	1.186 to 1.523	<0.001	RT/IC + 12Gy grew **slower** than RT/IC
Ratio of (12Gy+12Gy) to (RT/IC+12Gy)	1.479	1.147 to 1.868	0.002	RT/IC + 12Gy grew **slower** than 12Gy+12Gy

Table 4.5: Secondary tumor growth rates corresponding to Figure 4.3. Tumor volumes were log-transformed, and linear mixed-effects modeling was conducted to estimate a proportional growth rate every 21 days, integrated over all time points for each tumor. The estimated mean growth rates, 95% confidence intervals, and Kenward-Rogers p-values are then reported. Growth rate p-values are calculated under the null hypothesis that the growth rate is 1 or 100%, that the tumor does not change over time. Treatments are compared by estimating the ratio of growth rates between two treatments. Treatment difference p-values are calculated under the null hypothesis that this ratio is 1, that the growth rates of the two treatments are the same.

Parameter	Estimate	95% CI	p-value	Conclusion
Growth rate PBS	5.200	4.184 to 6.776	<0.001	Tumors on average grew over time
Growth rate 12Gy+12Gy	1.927	1.597 to 2.306	<0.001	Tumors on average grew over time
Growth rate RT/IC	2.428	2.253 to 2.642	<0.001	Tumors on average grew over time
Growth rate RT/IC+12Gy	1.513	1.423 to 1.610	<0.001	Tumors on average grew over time
Ratio of (RT/IC) to (RT/IC + 12Gy)	1.605	1.453 to 1.776	<0.001	RT/IC + 12Gy tumors grew **slower** than RT/IC
Ratio of (12Gy+12Gy) to (RT/IC+12Gy)	1.274	1.052 to 1.515	0.008	RT/IC + 12Gy tumors grew **slower** than 12Gy + 12Gy

Table 4.6: survival analyses for mice treated with PBS, TRT only, *in situ* vaccine only, or combination TRT and *in situ* vaccine. These analyses correspond to the survival curve depicted in Figure 5B. Note that thes experiments were conducted concurrently with the experiments depicted in Figure 2, and the PBs and RT/IC groups are re-presented here for comparison. Groups were compared using the Log-Rank test, with corresponding P-values reported here.

Comparator A	Parameter	Comparator B	A median (days)	B median (days)	P-value
RT/IC	Time to death/sacrifice	PBS	85	56	<0.0001
TRT (100μCi)	Time to death/sacrifice	PBS	60	56	0.1839
RT/IC + TRT	Time to death/sacrifice	PBS	112	56	<0.0001
RT/IC + TRT	Time to death/sacrifice	RT/IC	112	85	0.0458
RT/IC + TRT	Time to death/sacrifice	TRT (100μCi)	112	60	<0.0001

Table 4.7: Primary tumor growth rates corresponding to Figure 4.6. Tumor volumes were log-transformed, and linear mixed-effects modeling was conducted to estimate growth rates for each treatment using the data presented in Figure 4.6. The model estimates a proportional growth rate every 21 days, integrated over all time points for each tumor. The estimated mean growth rates, 95% confidence intervals, and Kenward-Rogers p-values are then reported. Growth rate p-values are calculated under the null hypothesis that the growth rate is 1 or 100%, that the tumor does not change over time. Treatments are compared by estimating the ratio of growth rates between two treatments. Treatment difference p-values are calculated under the null hypothesis that this ratio is 1, that the growth rates of the two treatments are the same.

Parameter	Estimate	95% CI	p-value	Conclusion
Growth rate PBS	3.527	2.478 to 5.022	<0.001	Tumors on average grew over time
Growth rate TRT	3.463	2.497 to 4.970	<0.001	Tumors on average grew over time
Growth rate RT/IC	1.407	1.283 to 1.571	<0.001	Tumors on average grew over time
Growth rate RT/IC+TRT	1.040	0.954 to 1.138	0.363	Tumors on average did not change over time
Ratio of (RT/IC) to (RT/IC + TRT)	1.352	1.191 to 1.562	<0.001	RT/IC tumors grew **faster** than RT/IC + TRT
Ratio of (TRT) to (RT/IC + TRT)	3.329	2.299 to 4.763	<0.001	TRT tumors grew **faster** than RT/IC + TRT

Table 4.8: Secondary tumor growth rates corresponding to Figure 4.6. Tumor volumes were log-transformed, and linear mixed-effects modeling was conducted to estimate growth rates for each treatment using the data presented in Figure 4.6. The model estimates a proportional growth rate every 21 days, integrated over all time points for each tumor. The estimated mean growth rates, 95% confidence intervals, and Kenward-Rogers p-values are then reported. Growth rate p-values are calculated under the null hypothesis that the growth rate is 1 or 100%, that the tumor does not change over time. Treatments are compared by estimating the ratio of growth rates between two treatments. Treatment difference p-values are calculated under the null hypothesis that this ratio is 1, that the growth rates of the two treatments are the same.

Parameter	Estimate	95% CI	p-value	Conclusion
Growth rate PBS	5.200	4.184 to 6.776	<0.001	Tumors on average grew over time
Growth rate TRT	4.116	3.347 to 5.216	<0.001	Tumors on average grew over time
Growth rate RT/IC	2.428	2.253 to 2.642	<0.001	Tumors on average grew over time
Growth rate RT/IC+TRT	2.412	2.268 to 2.574	<0.001	Tumors on average grew over time
Ratio of (RT/IC) to (RT/IC + TRT)	1.007	0.907 to 1.111	0.895	**No difference** in growth rates between groups
Ratio of (TRT) to (RT/IC + TRT)	1.706	1.316 to 2.188	<0.001	TRT tumors grew **faster** than RT/IC + TRT

Figure 4.1: Titration of external beam dose to secondary tumor combined with RT/IC immunotherapy. Female C57BL/6 mice were implanted with B78 syngeneic melanoma in the ID space in the R flank, with a secondary B78 tumor implanted in the L flank 2 weeks later. Primary tumors were on average ~100mm^3 while secondary tumors were on average ~50mm^3. On day 0 (when radiation was given). Mice were treated with PBS control (orange), 12Gy RT to both primary and secondary (black), and 12Gy RT+IC to the primary with either 0Gy (blue), 2Gy (green), 6Gy (red), or 12Gy (purple) of RT to the secondary tumor. Treatment group nomenclature is indicated as (12Gy RT dose to primary + IC to primary /RT dose to secondary). Tumor volumes were measured twice weekly. Mice with no palpable secondary tumor on treatment day 0 were excluded from analysis. A) Average +/- SEM tumor volume for both primary (right side) and secondary (left side) tumors. B-G) Individual tumor growth curves for each of the mice in the treatment groups as described. H) Primary (right) and Secondary (left) tumor volume on day 60 post-treatment. Data points represent individual mice, and the bars depict the average +/- SEM. Statistical comparisons were conducted as two student's t tests comparing 12/0 + IC to 12/12 + IC, and 12/12 RT only and 12/12 + IC. P-values for other comparisons are not shown. Data presented here are representative of two independently conducted experiments. * = $p<0.05$; **= $p<0.01$; ns = not significant.

Figure 4.1

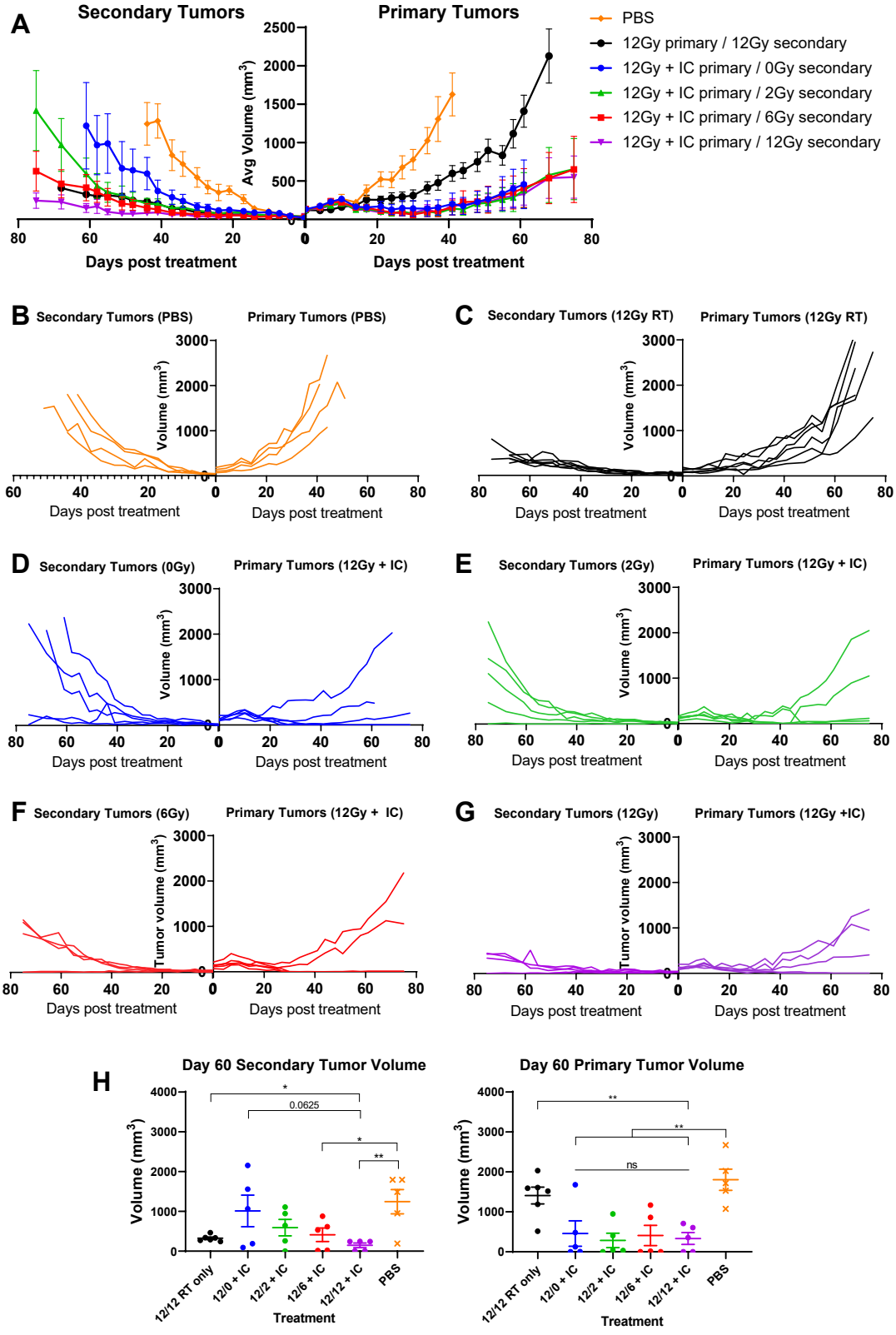
A
Secondary Tumors
Primary Tumors
Avg Volume (mm3)
Days post treatment
PBS
12Gy primary / 12Gy secondary
12Gy + IC primary / 0Gy secondary
12Gy + IC primary / 2Gy secondary
12Gy + IC primary / 6Gy secondary
12Gy + IC primary / 12Gy secondary
B Secondary Tumors (PBS)
Primary Tumors (PBS)
C Secondary Tumors (12Gy RT)
Primary Tumors (12Gy RT)
D Secondary Tumors (0Gy)
Primary Tumors (12Gy + IC)
E Secondary Tumors (2Gy)
Primary Tumors (12Gy + IC)
F Secondary Tumors (6Gy)
Primary Tumors (12Gy + IC)
G Secondary Tumors (12Gy)
Primary Tumors (12Gy +IC)
Volume (mm3)
Tumor volume (mm3)
H
Day 60 Secondary Tumor Volume
Day 60 Primary Tumor Volume
0.0625
ns
12/12 RT only
12/0 + IC
12/2 + IC
12/6 + IC
12/12 + IC
PBS
Treatment

Figure 4.2: 12Gy RT to both primary and secondary tumor allows for better control induced by subsequent IT-IC immunotherapy. A) schema of mouse multiple tumor model setup and subsequent in situ vaccination approach. C57BL/6 mice were implanted intradermally with B78 melanoma approximately 4 weeks prior to treatment at the right flank, and approximately 2 weeks prior to treatment on the left flank. Mice were then treated with radiation to either the primary only or the primary and secondary tumors on treatment day 0, and given IT-IC immunotherapy on treatment days 5-9. B) overall survival of animals pooled over three separate experiments following treatment. Animals either died from their tumor burden or reached a predetermined size of tumor to require euthanasia. C) Breakdown of the cause of death for all animals treated over the course of the three individual experiments. Mice that were sacrificed due to either primary tumor burden, secondary tumor burden, or due to inflammation or dermatitis are indicated. Mice that were still alive at the conclusion of the experiment were labeled as disease-free if no palpable tumor was detectable. Mice that were still alive with tumors were considered, for this analysis, as dying from either the primary or secondary tumor, depending on which tumor was larger at the conclusion of the experiment. D) Average +/- SEM tumor volume from a representative experiment. Primary tumors are on the right side, and secondary tumors are on the left. Average growth curves terminate on the day post-treatment where the first member of that treatment cohort died. See Figure 3 for individual tumor growth curves corresponding to this experiment. E) Individual tumor volumes on treatment day 54 (when the first mouse in the RT/IC group was euthanized) for the experiment shown in Fig. 2D. Tumor volumes corresponding to 2 mice mice in the PBS group sacrificed prior to treatment day 54, with last value carried forward for analysis, are represented by an ‘X’. * = $p<0.05$, ** = $p<0.01$, *** = $p<0.001$, **** = $p<0.0001$, ns = not significant.

Figure 4.2

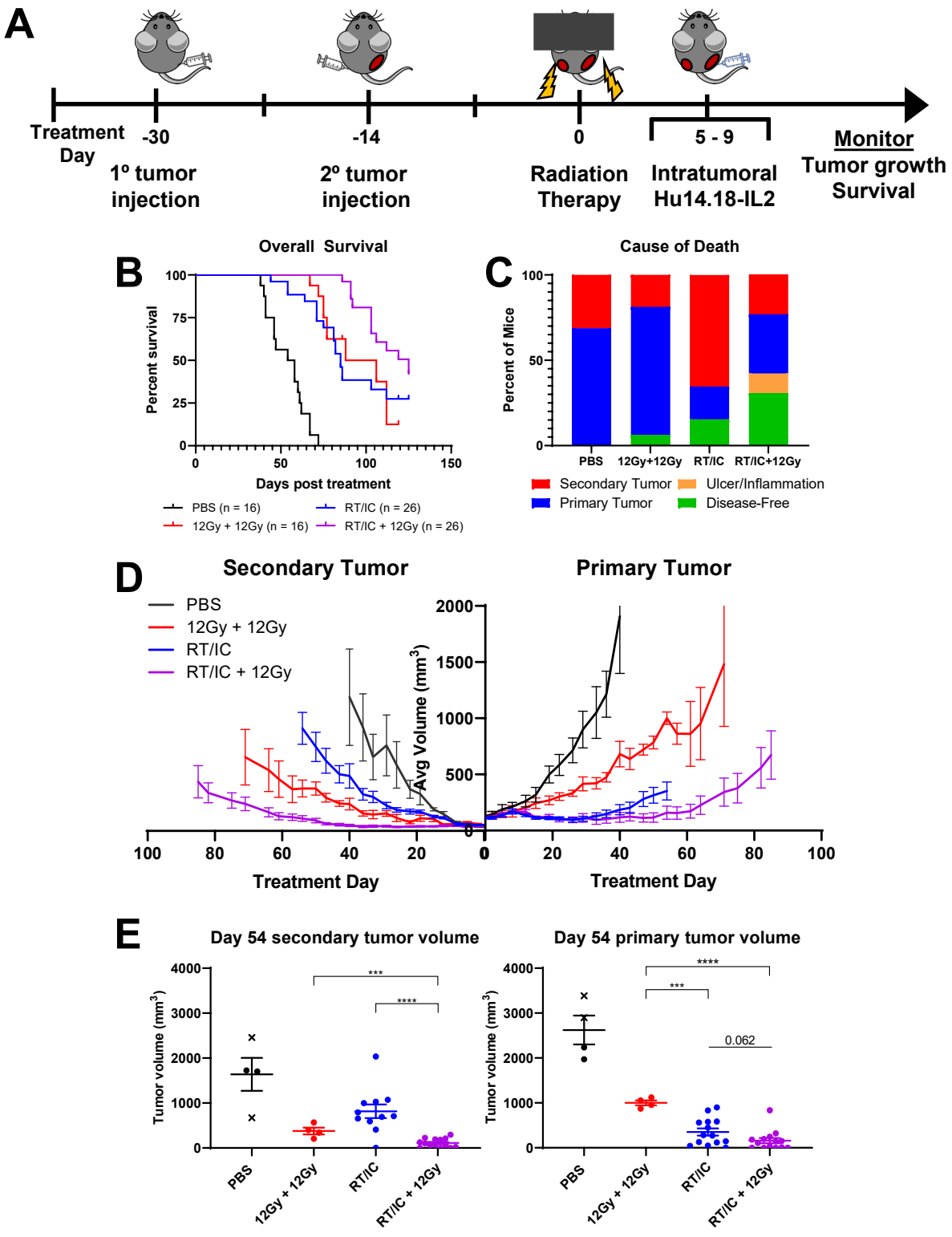
A
Treatment Day
-30
1º tumor injection
-14
2º tumor injection
0
Radiation Therapy
5 - 9
Intratumoral Hu14.18-IL2
Monitor
Tumor growth
Survival
B
Overall Survival
Percent survival
Days post treatment
PBS (n = 16)
12Gy + 12Gy (n = 16)
RT/IC (n = 26)
RT/IC + 12Gy (n = 26)
C
Cause of Death
Percent of Mice
PBS
12Gy+12Gy
RT/IC
RT/IC+12Gy
Secondary Tumor
Primary Tumor
Ulcer/Inflammation
Disease-Free
D
Secondary Tumor
Primary Tumor
PBS
12Gy + 12Gy
RT/IC
RT/IC + 12Gy
Avg Volume (mm3)
Treatment Day
E
Day 54 secondary tumor volume
Day 54 primary tumor volume
Tumor volume (mm3)
0.062

Figure 4.3: Individual tumor volumes corresponding to the experimental comparison in Figure 4.2D and 4.2E. A-D) Primary individual tumors are indicated on the right, and secondary individual tumors are indicated on the left of each combined graph. E) average +/- SEM primary and secondary tumor volume, graphed in a $\log_2$-transformed space. Linear mixed-effects modeling was conducted to estimate the slope and subsequent growth rate of tumors in each of these treatment groups.

Figure 4.3

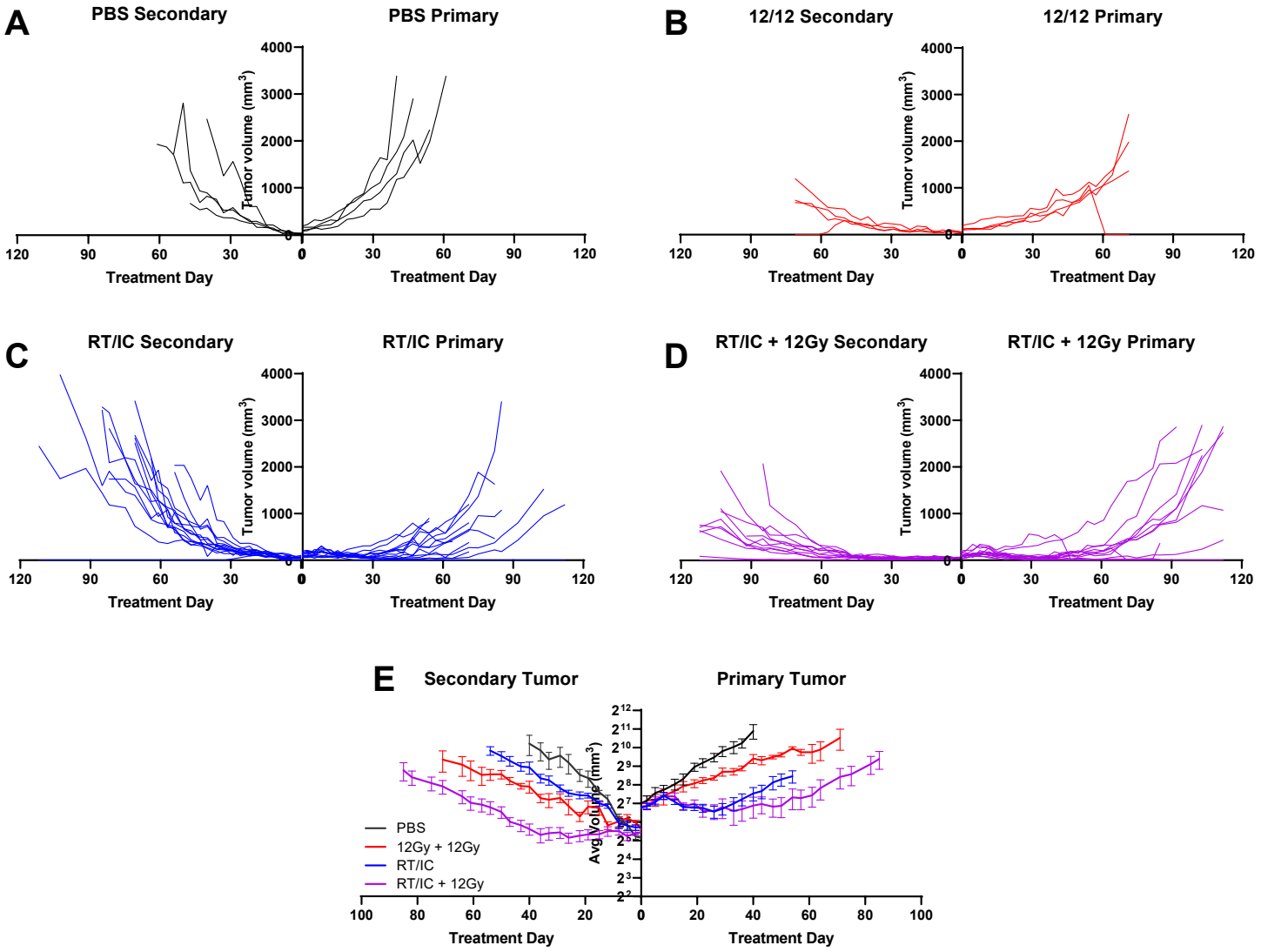
A
PBS Secondary
PBS Primary
B
12/12 Secondary
12/12 Primary
C
RT/IC Secondary
RT/IC Primary
D
RT/IC + 12Gy Secondary
RT/IC + 12Gy Primary
Tumor volume (mm3)
Treatment Day
E
Secondary Tumor
Primary Tumor
Avg. Volume (mm3)
PBS
12Gy + 12Gy
RT/IC
RT/IC + 12Gy

Figure 4.4: Injected activities of ^{90}Y-NM600 up to 100μCi do not interfere with the *in vivo* antitumor effect of RT+IC *in situ* vaccination. Female C57BL/6 mice were implanted with B78 murine melanoma cells as described in the materials and methods section to create a single flank tumor. Retrospective assessment of these studies are that these tumors were implanted SC. When tumors reached ~150mm^3, the mice were injected intravenously with either 0, 25, 50, or 100μCi of ^{90}Y-NM600 TRT via tail vein and radiated with 12Gy external beam radiation on treatment day 0. Intratumoral IC was given on treatment days 5-9. Depicted here are two independent replicate experiments. A) Tumor volume on treatment day 39, pooled for both experiments. Data points are individual tumors, with bars representing mean +/- SEM tumor volume. B) and C) depict average +/- SEM tumor volume for each treatment group over time in the 2 separate replicate experiments. Statistical analysis was conducted as a one-way ANOVA with multiple comparisons to the RT+100μCi radiation-only control using Tukey's method. * = $p<0.05$; ** = $p< 0.01$.

Figure 4.4

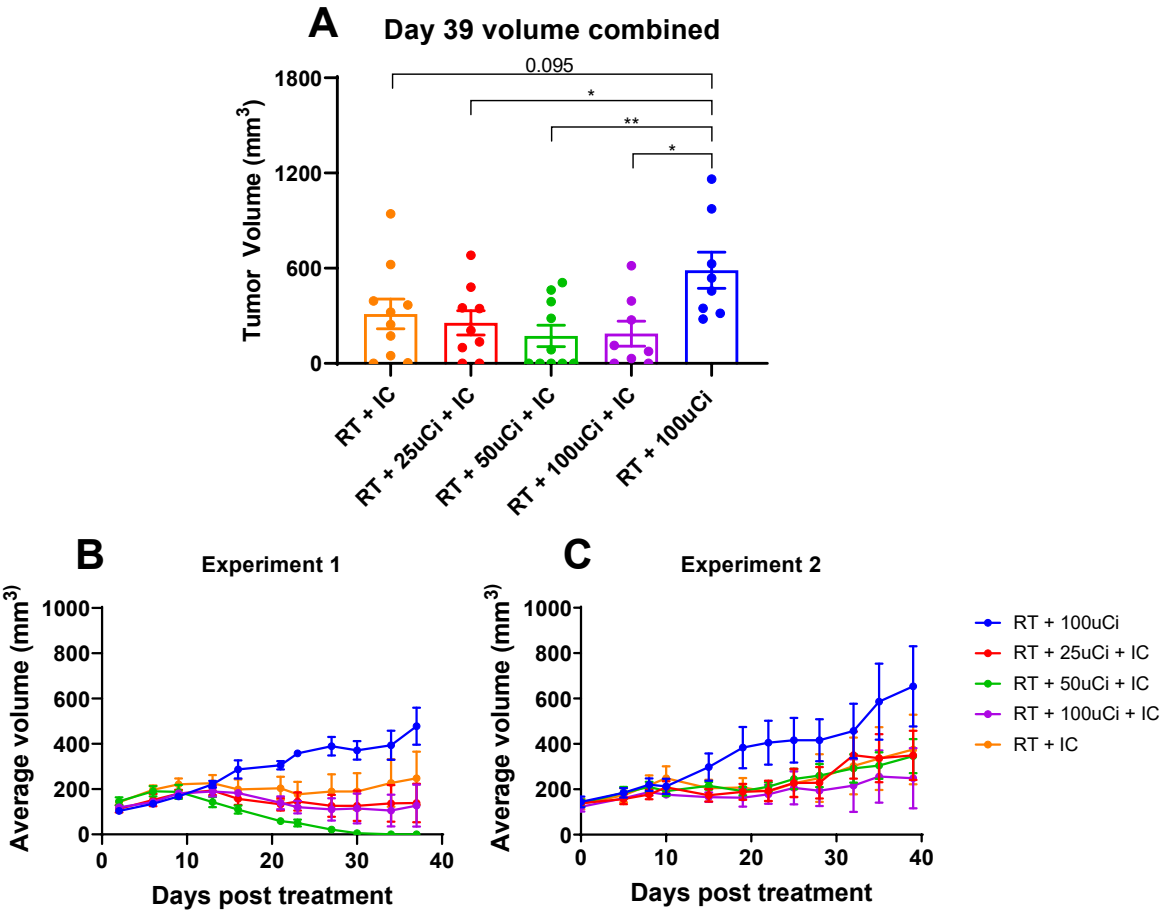
A
Day 39 volume combined
0.095
*
**
*
Tumor Volume (mm3)
1800
1200
600
0
RT + IC
RT + 25uCi + IC
RT + 50uCi + IC
RT + 100uCi + IC
RT + 100uCi
B
Experiment 1
Average volume (mm3)
1000
800
600
400
200
0
0
10
20
30
40
Days post treatment
C
Experiment 2
Average volume (mm3)
1000
800
600
400
200
0
0
10
20
30
40
Days post treatment
RT + 100uCi
RT + 25uCi + IC
RT + 50uCi + IC
RT + 100uCi + IC
RT + IC

Figure 4.5: Systemically delivered ^{90}Y-NM600 combined with local RT/IC in situ vaccination improves overall survival, and may allow for better tumor control compared to in situ vaccination alone.C57BL/6 mice were implanted ID with primary B78 syngeneic murine melanoma tumors in the right flank, followed by secondary tumors in the left flank 14 days later. Mice were randomized to receive either PBS control, 100μCi of ^{90}Y-NM600 TRT, RT/IC *in situ* vaccine to the primary tumor, or the combination of RT/IC + TRT. Of note, the PBS and RT/IC groups were shared with the experiment depicted in Figures 2 and 3. A) schema of this mouse multiple tumor model setup and subsequent in situ vaccination and radiation approach. B) overall survival of animals pooled over three separate experiments. Animals either died from their tumor burden or reached a predetermined size of tumor to require euthanasia. C) Mice that were sacrificed due to either primary tumor burden, secondary tumor burden, or due to inflammation or dermatitis are indicated. Mice that were still alive at the conclusion of the experiment were labeled as disease-free if no palpable tumor was detectable. Mice that were still alive with tumors were considered as dying from either the primary or secondary tumor, depending on which tumor was larger at the conclusion of the experiment. D) Average +/- SEM tumor volume from a representative experiment for each treatment group. Primary tumors are on the right side, and secondary tumors are on the left. Average growth curves terminate on the day post-treatment where the first member of that treatment cohort died. See Figure 6 for individual tumor growth curves corresponding to this experiment. E) Individual tumor volumes on treatment day 36 (when the first mouse in the TRT group was euthanized). Brackets indicate p values corresponding to students independent two-tailed t test between indicated groups. * = $p<0.05$, ** = $p<0.01$, ns = not significant.

Figure 4.5

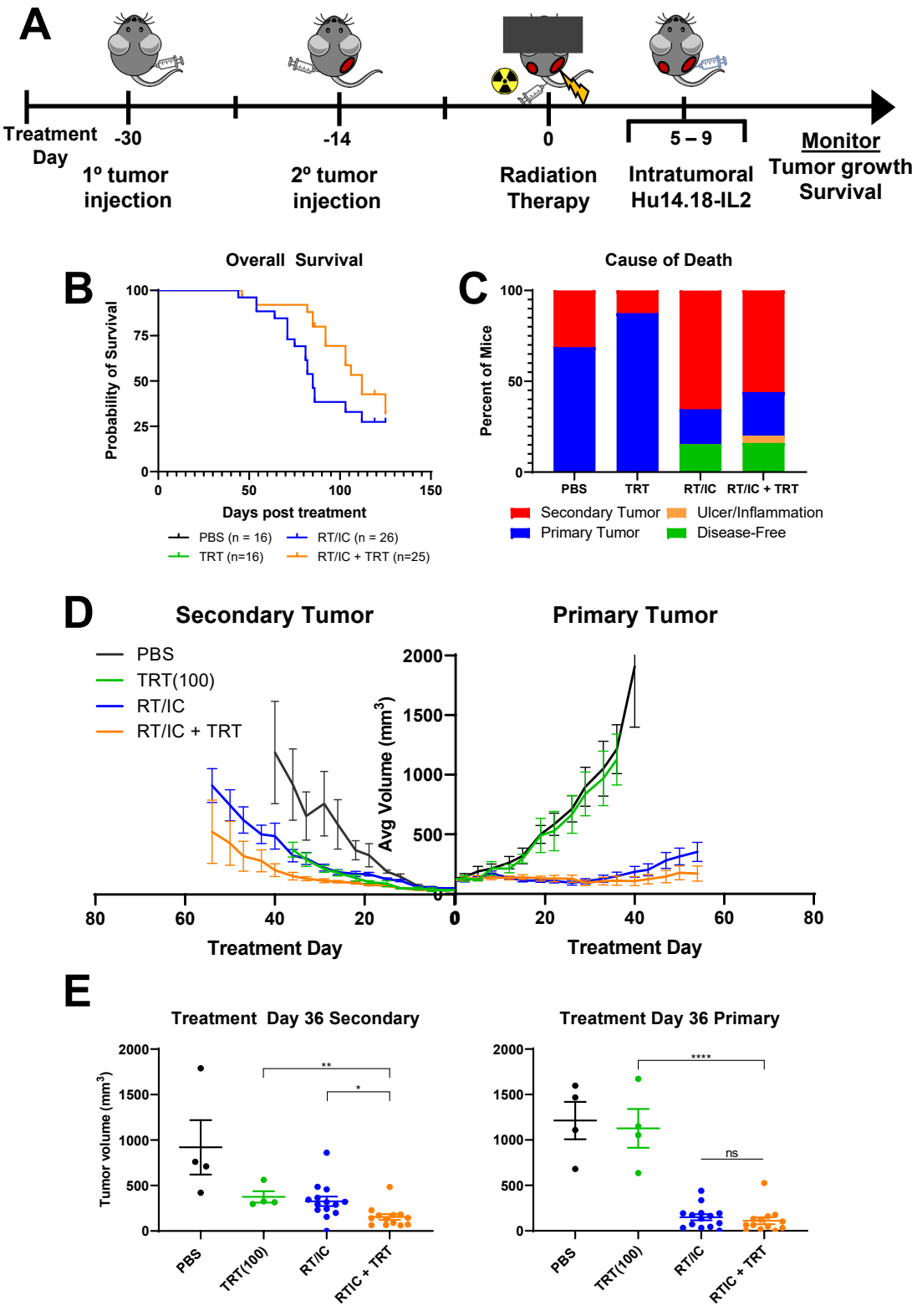
A
Treatment Day
-30
1º tumor injection
-14
2º tumor injection
0
Radiation Therapy
5 – 9
Intratumoral Hu14.18-IL2
Monitor
Tumor growth
Survival
B
Overall Survival
Probability of Survival
Days post treatment
PBS (n = 16)
RT/IC (n = 26)
TRT (n=16)
RT/IC + TRT (n=25)
C
Cause of Death
Percent of Mice
PBS
TRT
RT/IC
RT/IC + TRT
Secondary Tumor
Primary Tumor
Ulcer/Inflammation
Disease-Free
D
Secondary Tumor
Primary Tumor
PBS
TRT(100)
RT/IC
RT/IC + TRT
Avg Volume (mm3)
Treatment Day
Treatment Day
E
Treatment Day 36 Secondary
Treatment Day 36 Primary
Tumor volume (mm3)
PBS
TRT(100)
RT/IC
RTIC + TRT
ns

Figure 4.6: Individual tumor graphs corresponding to Figure 4.5. Note that the PBS (A) and RT/IC only (C) groups are represented here as shared comparator groups from Figures 2 and 3. A-D) Primary individual tumors are indicated on the right, and secondary individual tumors are indicated on the left of each combined graph. E) average +/- SEM primary and secondary tumor volume, graphed in a $\log_2$-transformed space. Linear mixed-effects modeling was conducted to estimate the slope and subsequent growth rate of tumors in each of these treatment group.

Figure 4.6

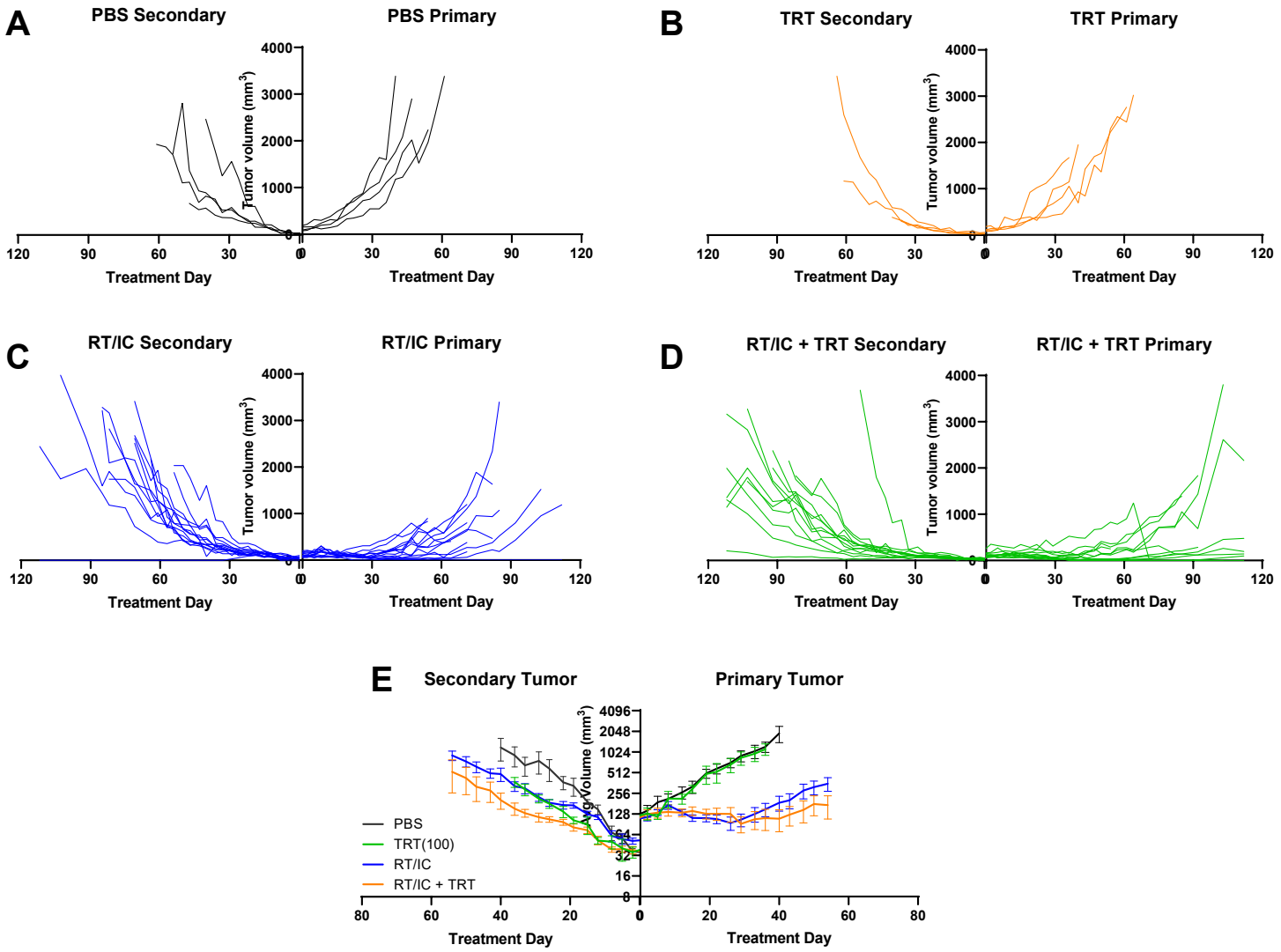
A
PBS Secondary
PBS Primary
B
TRT Secondary
TRT Primary
C
RT/IC Secondary
RT/IC Primary
D
RT/IC + TRT Secondary
RT/IC + TRT Primary
Tumor volume (mm3)
Treatment Day
E
Secondary Tumor
Primary Tumor
PBS
TRT(100)
RT/IC
RT/IC + TRT

Chapter 5

Summary and Future Directions

5.1 Overview

In this chapter I summarize the major conclusions from chapters 2-4. I will then discuss the major implications of these findings, and the important scientific questions that arise as a result. Finally, I will present some possible means of addressing these questions, including some preliminary results that I report in the Appendix.

5.2 Summary of Thesis Findings

5.2.1 *A novel method of sample preparation involving fixation and cryopreservation can be used to query immune populations in radioactive tissue*

The major goal of this thesis was to determine if the immune modulatory properties of low to moderate dose radiation could improve systemic response to *in situ* vaccination. This includes both external beam radiation and ^{90}Y-NM600 TRT as a means of delivering this immunomodulatory radiation. However, in order to interrogate immune changes in response to ^{90}Y-NM600, we required a means of analyzing radioactive tissue by flow cytometry. The flow cytometry core at our institution, like many others, does permit analysis of radioactive samples. To this end I developed a method of labeling and storing disaggregated tumor tissue for up to 30 days, until decay to radioactive background. I investigated introducing a cryopreservation step at three distinct points in the flow cytometry sample preparation workflow and evaluated differences in comprehensive immunophenotyping results compared to the same non-cryopreserved samples. I determined that cryopreservation can alter living, unfixed cells in their expression of the exhaustion marker PD-1 in a nonuniform manner (Figure 2.4). However, I found that in both tumor and splenic dissociate, cryopreservation *after* all sample preparation (including fixation and permeabilization for internal target staining) adequately preserves downstream fluorescent signal intensity, cell integrity, and relative population proportions to allow for analyses of experimental radioactive tissues (Figures 2.2 and 2.3).

I next evaluated the efficacy of our cryopreservation technique compared to the non-cryopreservation gold standard technique, in identifying immunologic changes that occur in a B78 tumor following treatment with 12Gy RT alone versus RT+IC *in situ* vaccine. First, we confirmed, using linear models, that there is no difference in sample outcome based on these 2 preparation techniques (Figure 2.5). Both methods identified several previously unreported alterations to the immune TME following the two experimental treatments, including increased NK cells, $CD4^+CD25^+FOXP3^+$ T_{reg} cells, and CD19+ B cells following radiation treatment. Furthermore, treatment with RT+IC additionally increased the number of $CD45^+$ cells, $CD4^+$ T cells, $CD8^+$ T cells, and the resulting $CD8/T_{reg}$ ratio. Lastly, we use our cryopreservation technique to demonstrate efficacy in flow cytometric evaluation of radioactive B78 melanoma tissue treated with ^{90}Y-NM600 (Figure 2.6). By studying two different ^{90}Y-NM600 dose levels, over four distinct time points, we uncovered significant time- and dose- effects on resulting immune populations. These included an influx of CD11b+ myeloid cells, increased $CD8+/T_{reg}$ ratio, decreased T_{reg} cells, and an increase in the fraction of NK cells expressing CD11b, most of which appeared to peak around 14 days post-injection. In summary, I developed a technique that permits the cryopreservation, storage, and later analysis by flow cytometry of radioactive tissue, that has been used throughout this thesis (Appendices A and B) and adopted successfully by other researchers in our working group to enable analyses of radioactive tumor tissue. In summary, this novel technique for cryopreservation and storage of samples for analysis by flow cytometry preserves the immune populations for analysis, which enables analysis of radioactive tissue where it was not possible previously.

5.2.2 *Depth of implantation in syngeneic murine tumor models impacts response to local in situ vaccine immunotherapy*

The core immunotherapy studied in this thesis is the combination of 12Gy local external beam RT on treatment day 0 and intratumoral injections of the hu14.18-IL2 immunocytokine on

treatment days 5-9 [65]. During the course of preparing mice for experimentation, I encountered inconsistencies between my treatment outcomes compared to other researchers. Despite a high level of scientific rigor in controlling outside factors, my mice were developing tumors at a much faster rate, and on average were not responding to RT+IC *in situ* vaccine as compared to mice with tumors injected concurrently by another researcher (Figure 3.1). After thorough physical examination, it was determined that different tumor cell implantation-injection techniques resulted in tumors that occupied different tissue planes within the mouse flank – one group had more superficial intradermal (ID) tumors, while another had deeper, subcutaneous (SC) tumors. Notably, these tumors had different physical properties. ID tumors were either attached or superficial to the panniculus carnosus, (a thin layer of striated muscle that separates the true skin compartment from the deeper tissue layers), and would therefore move with the skin structures when manipulated by physical exam ('mobile'). In contrast, SC tumors were deep to the panniculus carnosus, and would remain 'fixed' to the underlying flank musculature, allowing the cutaneous layers to slide over the tumor when manipulated by physical exam (Figure 3.1). In two independent experiments where we tightly controlled tumor size at the start of treatment by staggering treatment start into 'waves,' we clearly demonstrated that: 1) ID tumors develop slower than SC tumors; and 2) ID tumors are more likely to respond to RT+IC *in situ* vaccination compared to SC tumors, with both slower growth rate overall and significantly improved overall survival (Figure 3.2). Lastly, we demonstrated that, blind to the intended tumor injection depth, the simple physical exam status of 'fixed' or 'mobile' is very strongly associated with treatment outcome (Figure 3.5). This suggests that studies involving syngeneic implanted tumors would benefit from an extra 'inclusion criteria' of either all mobile or all fixed phenotypes to improve within-group variability and enable stronger comparisons between different treatment approaches. By outlining this difference in response as a function of tumor implantation technique, I added to our technical understanding of our mouse models, and introduced a

simple yet effective means of reducing the variability in response for future studies using flank-implanted B78 melanoma models.

5.2.3 *Radiation delivered to all sites of disease combined with* in situ *vaccination controls systemic disease burden better than either treatment alone*

Though previous models have demonstrated the significant effect of RT/IC *in situ* vaccination on outcomes in models of a single flank $GD2^+$ tumor, this effect is largely limited to the treated tumor in mice with multiple tumors. In some instances other tumors appear minimally affected, or even seem to inhibit response at the treated tumor itself [66]. My primary goal was to explore this phenomenon, specifically by exploring the utility of using additional radiation to augment systemic antitumor immunity. In our two-tumor model of ID-implanted B78 melanomas (one ~150mm^3 at the 'primary' right flank, and a smaller ~50mm^3 tumor at the 'secondary' left flank), I delivered RT+IC *in situ* vaccine to the primary tumor in combination with a range of 0,2,6, and 12 Gy additional RT to the secondary tumor. Here I demonstrated that 2,6, and 12Gy doses of secondary tumor radiation result in smaller secondary tumor volumes and slower secondary tumor growth rates compared to RT/IC to the primary site alone The magnitude of this secondary tumor response also appeared to be dose-dependent although statistical significance between doses was not achieved.. Importantly, the secondary tumor in the RT/IC + 12Gy secondary radiation grew slower than the radiation only control (12Gy to both tumors), which suggests a systemic antitumor effect is induced by the RT/IC to the primary, enabling a greater effect at the secondary tumor beyond the effect of radiation alone. I confirmed this finding in a larger study which demonstrated a significant improvement in overall survival in mice treated with RT/IC + 12Gy radiation to the secondary tumor compared to RT/IC alone or radiation alone controls. Further, RT/IC + 12Gy secondary tumor radiation increased the proportion of mice that cleared all initial disease burden and showed that they were then able to reject a subsequent B78 re-challenge. Linear mixed effects modeling of growth rate

demonstrated that **both** primary and secondary tumors in the RT/IC + 12Gy secondary radiation group grew slower than those receiving either RT/IC alone, or radiation alone. This has implications regarding the systemic nature of the antitumor immune response, as the *in situ* vaccine was capable of affecting the secondary tumor, but simultaneously radiation to the secondary tumor was **also** able to influence the efficacy of in situ vaccine at the primary tumor.

Lastly, I investigated the use of ^{90}Y-NM600 TRT as a means of delivering the additional radiation to supplement the *in situ* vaccine effect of RT+IC. I first titrated the level of injected activity of ^{90}Y-NM600 concurrent with RT/IC, and determined that injected activities up to 100μCi ^{90}Y-NM600 do not interfere with, or limit, the generation of an antitumor immune response in mice bearing a single B78 tumor. In larger studies on mice bearing multiple B78 tumors, mice treated with 100μCi of ^{90}Y-NM600 combined with RT/IC to the primary had significantly improved survival compared to RT/IC alone or TRT alone. There was also a trend towards reduced growth rates in both the primary and secondary tumors in the RT/IC + TRT group. Taken together these data suggest that low dose levels of radiation which are insufficient to eliminate a tumor on its own, are able to expand the antitumor effect of local *in situ* vaccination, by using external beam radiation to all sites of disease. These data also demonstrate a survival improvement when combining *in situ* vaccine with ^{90}Y-NM600 TRT in mice with multiple tumors.

5.3 Implications and Future Directions

5.3.1 *Expanding the use of post-staining cryopreservation and characterization of PD1 alterations following cryopreservation of live cells*

The new method I described in Chapter 2 expands the scope of what can reliably and reasonably be studied using shared resource flow cytometry facilities to include radioactive material. As interest in the effects of TRTs both on the immune system and on the tumor cells

themselves (evidence of DNA damage, IFN production within tumor cells, GH2Ax foci analyses of DNA breakage, Ki-67 based evaluation of proliferation, etc.) expand, this technique may prove useful for many other experimental questions [201,202]. Though purchase of dedicated cytometers for radioactive-only material is one means of avoiding the cryopreservation step, there would still be safety concerns and liquid waste concerns to consider. The use of this newly developed technique would obviate these considerations, and make it possible to safely leverage the expertise of shared resource cytometry equipment and staff.

Continuing work on this approach should focus on further understanding the impact of both fixation and cryopreservation on both the cells and antibody-fluorophore complexes, as well as expanding the generalizability of this technique. As I demonstrate in Chapter 2, the immune infiltrate of tumor tissue is substantially different than that of splenic tissue, both in relative proportion of certain populations and in activation state of cells such as $CD8^+$ T cells. This principle has been well documented in the literature as well [203,204]. To expand the applicable scope of this technique, future studies should evaluate the impact of our cryopreservation technique compared to non-cryopreserved standard technique in lymph nodes, skin, lung, brain, liver, and cardiac tissues, as each of these are known to have different tissue stromal properties [203]. This technique should be expanded to different tumor types as well, as these environments can vary in their degree of vascularity, extracellular matrix density, oxygen content, pH, and other variables that may influence the manner in which cells tolerate the stress of cryopreservation [205]. A similar study to what was used in Chapter 2 could be employed to evaluate these tissues by using pooled disaggregates of each of these tumor types, and preparing immune staining panels in each of these cryopreservation approaches. I would hypothesize that this approach will result in similar proportions of immune cells with the cryopreservation technique as with the ‘fresh’ analytes, however cell types that have very low frequencies (such as dendritic cells or gamma-delta T cells) may be more affected by this technique.

In the work presented here, antibodies directed against 20 different targets using 13 different fluorophore dyes were used and demonstrated relatively little change in integrity following fixation and cryopreservation. However there are hundreds, if not thousands, of molecules that can be targeted using fluorophore-conjugated antibodies and should be investigated prior to use in this type of approach. We additionally demonstrated that the fluorophore dyes remained largely intact for up to 30 days in storage at -80C. Future experiments should fully define the impact of cryopreservation duration on these signals, to understand how long cells can remain stored in this fashion as this will have implications regarding future experimental planning, or use with radionuclides with much longer decay half-lives. It stands to reason that fluorophores may eventually lose their fluorescence over time, but relative comparisons in staining intensity of a population of cells may still be possible. To confirm this trend, and characterize the “maximum” duration of cryopreservation to consider in such an approach, a staggered time study can be conducted, where a large population of pooled tumor and tissue samples can be stained en masse, separated into smaller aliquots, and frozen according to the protocol. Samples would then be thawed and analyzed at regular intervals over the course of several months and even years.

One other useful observation that resulted from this study was that the detected PD1 staining was substantially different depending on the preparation technique used. The ‘Before’ technique, which cryopreserves the sample before any staining or fixation, resulted in a near doubling of the PD1 intensity of CD4+ T cells, NK cells, and B cells in the spleen and tumor; however, the degree of PD1 intensity of CD8+ T cells, which is much higher at baseline in the tumor, remained largely the same. This means that this cryopreservation technique introduced a bias into the results – namely that low-PD1 expressing cells increased their PD1 expression due to this cryopreservation ‘Before’ approach. In contrast, this cryopreservation “Before” approach did not cause a detectible increase in the cells that already had high-PD1 expression. For example, if an experiment used the ‘Before’ cryopreservation technique to compare PD1 levels

between samples that did or did not receive immunotherapy treatment, the extra bias of augmenting PD1 expression on PD1-low cells, induced by the 'Before' cryopreservation technique may influence the analysis and result in a misleading conclusion. This observation may be consequential, as many multicenter clinical trials that take PBMC or tumor samples for analysis by flow typically cryopreserve cells for storage and shipping to a central lab prior to staining, similar to the 'Before' technique used here. If this bias does indeed translate into differences in results, this could have implications for future design and execution of clinical studies, particularly in cancer immunology. Future studies should clarify this differential effect and confirm if cryopreservation of living cells does result in altered expression of exhaustion markers. First, to account for potentially increased autofluorescence contributing to this enhanced PD1 signal detection, these findings should be confirmed using a different antibody-fluorophore combination. Simultaneously, other markers of T cell activation and exhaustion including CD69, LAG-3, Tim3 – and the transcription factor EOMES should be evaluated to confirm the observed phenotype [206]. These expression changes might also be evaluated using PCR-based analyses to see if overall levels of RNA for these markers are affected by cryopreservation, as appears to be the case for their protein expression.

5.3.2 *Mechanistic characterization of difference in response* to in situ *vaccination based on tumor depth – opportunity to model clinical heterogeneity in response.*

The results detailed in Chapter 3 emphasize how a small difference in tumor implantation depth in a syngeneic tumor model can have a dramatic impact on the resulting response to immunotherapy. While maintaining a consistent injection depth and technique requires substantial expertise and practice, this chapter identified a simple 'fixed' vs 'mobile' physical exam finding that can help to ensure tumors selected for study are consistently the same depth. Despite demonstration of a substantial difference in *in vivo* outcome to treatment,

the mechanism behind such a difference remains elusive, and requires future study. Based on the *in vivo* effect, we can clearly see that *something* is contributing to a greater antitumor effect in ID tumors than in SC tumors. However, when comparing SC treated tumors to SC untreated tumors, there is still a reduction in tumor growth rate and a greater median survival. This shows that there is some effect of RT+IC *in situ* vaccination in SC tumors as well, just not sustained or activated enough to prevent the growth of the tumor. Based on my observations, I hypothesize that the difference in response to RT+IC between ID and SC tumors might be explained by either of these 2 processes: 1) treatment generates a stronger **antitumor response** in ID vs SC tumors, 2) SC tumors have a stronger **immunosuppressive environment** compared to ID tumors.

To test options 1 and 2, a combination of flow cytometry and immunohistochemistry can be used to phenotype the amount and activation state of both effector and suppressor immune populations. To query the immunosuppressive capacity of the tumor microenvironment, $CD4^+CD25^+FOXP3^+$ T_{regs}, $CD11b^+Ly6G^+TGF\text{-}B^+$ Myeloid-derived suppressor cells (MDSCs), and $F4/80^+CD206^+$ M2 macrophages can be quantified using flow cytometry staining [138]. Staining targets on histological frozen sections can be used to confirm these findings. To query the degree of immune activation following treatment in both ID and SC tumors, populations of $CD8^+$ and $CD4^+$ T cells, as well as NK cells can be quantified along with their expression of activation markers such as CD25, CD69, CD44, CD62L, CD103, CD107a, and others [207]. Finally, doppler ultrasound can be used to measure blood flow to the tumor stroma prior to harvesting the tumor [208]. After harvest, intensity of Ki-67 staining can estimate the rate of proliferation and cell division within the tumor which, combined with information about the degree of blood flow to the tumor, can provide a strong estimate of the rate of cell division within these $GD2^+$ tumors [209]. The results of these three experimental approaches together should

provide mechanistic insight into how ID tumors are more susceptible to RT+IC *in situ* vaccination.

The B78 syngeneic murine melanoma model is a unique tumor model in that it rarely metastasizes or invades nearby tissue structures in our hands (data not shown). As a result it can model the “ideal” tumor microenvironment for a purely ID or a purely SC tumor very effectively. However it is not known how the difference in tumor depth can affect response to treatment in a tumor that has **both** ID and SC components, as is the case in invasive tumor models, or tumors seeded along the needle injection tract. To study both this effect, and the generalizability of our findings, future experiments could consider testing other tumor models that express the GD2 immunocytokine target and are known to have varying degrees of immunogenicity, such as GD2-transfected B16 melanoma, GD2-transfected panc02 pancreatic adenocarcinoma, NSX2 neuroblastoma, and 9464D neuroblastoma . Finally, influence of tumor depth on response should be studied in models of multiple tumors. In the case of clinical metastatic melanoma, various loci of disease can be found throughout the body, including both the intradermal and subcutaneous compartments (although it is harder to clearly delineate ID or SC in humans, which lack the panniculus carnosus muscle). In a clinical study of intratumoral IL-2 (which is a component of the immunocytokine used in this thesis), deeper subcutaneous tumors responded less strongly than more superficial tumors [25]. This does suggest that differential immune reactivity can persist in the setting of multiple disease sites, and should be studied in models of two ID, two SC, and one ID tumor / one SC tumor settings.

The difference in response to RT+IC immunotherapy based on tissue depth presents an intriguing opportunity for modeling a cancer immunotherapeutic phenomenon in clinic. Part of the distinction in describing immune “hot” tumors vs. immune “cold” tumors both clinically and preclinically is based on their ability to respond to immunotherapy – “hot” tumors are more likely to respond to checkpoint blockade, while “cold” tumors are not [7]. Substantial resources have

been devoted to trying to predict the “hot” responders and the “cold” non-responders in patients, in an attempt: 1) to identify immune biomarkers of response; and 2) to identify patients and mechanisms that may benefit from combinatorial approaches to treatment. Murine models of this phenomenon have been difficult to reliably produce, and involve either patient-derived xenografts and biopsies from responders or nonresponders, or retrospectively assigning mice as being “responder” or “nonresponder” after determining if the mouse did in fact respond [210]. The experiments described in this thesis have unintentionally recreated this same observation; a population of genetically identical mice, with (mostly) genetically identical tumors of the same size, treated with the same treatment conditions, produced a subset of “responders” and a subset of “nonresponders” *in a predictable manner*. Though some ID treated mice end up “nonresponders” and some SC treated mice experience partial response, on a *population* level ID implanted B78 tumors appear to be more immunologically “hot” responders, and SC implanted B78 tumors appear to be more immunologically “cold” nonresponders. Using these two different implantation techniques, this model would allow for study of different immunotherapies and immunotherapy combinations in the setting of known responding or nonresponding mice, while still controlling for the type of tumor, and type of immune response mounted against the tumor.

5.3.3 *Mechanistic characterization of the means by which irradiated tumors are more susceptible to response from a distant in situ vaccine*

The results described in chapter 4 imply a role for immunotherapy in combination with radiation delivered to all sites of disease in improving overall survival and response to multiple tumors. Using external beam radiation to treat all identifiable disease sites in the setting of oligometastatic cancer is becoming more popular among radiation oncologists. In this setting, local delivery of *in situ* vaccine immunotherapy may significantly improve overall response.

Future experimentation for this project could focus on two main questions; 1) What immunologic effector mechanisms are being engaged at the primary and secondary tumor in the setting of *in situ* vaccination with and without secondary tumor radiation? And 2) What additional treatment approaches can be used to further augment antitumor effect and expand the efficacy of this approach?

To further define the immunologic mechanisms being activated by RT+IC, future experiments will utilize several cellular and molecular assays to explore the cells which are functionally active, in both the primary and secondary tumors. In a previously published study, Morris and colleagues have demonstrated that depletion of T cells eliminates the antitumor effect of RT+IC in a model of single B78 tumors [65]. Further, characterization of tumors treated with RT+IC in Chapter two by flow cytometry demonstrated enhanced CD45+ cells, CD4+ T cells, NK cells, CD8+ T cells, T_{regs}, and CD11b+ cells in tumors 14 days after treatment with RT+IC compared to PBS alone. This implies that enhanced effector cells including CD4+ helper T cells and CD8+ cytotoxic T lymphocytes are recruited to the tumor. We will continue this phenotypic characterization of the tumor infiltrating cells in tumors responding to this immunotherapy by expanding the number of phenotypic targets interrogated using combination comprehensive innate and adaptive panels, which can identify neutrophils / MDSCs, macrophages, subtypes of classical and monocyte-derived dendritic cells, NKT cells, as well as tissue-resident memory lymphocytes. These panels have already been used to generate preliminary data in primary and secondary tumors treated with RT+IC, with and without 12Gy radiation to the secondary tumor these preliminary results are summarized in Appendix A.

After identifying the major immune cell types that are altered in response to treatment, particularly those changes identified in the secondary tumor, antibody-based depletion studies can confirm the necessity of these cell types for treatment effect. Our recent preliminary data, not presented in this thesis, suggest that B78 has minimal expression of the classic CD8+ T cell

receptor target MHCI, and instead has substantial expression of the CD4+ T cell target MHCII. Elucidating the exact degree of contribution between CD8+ and CD4+ T cells may shed further light on the mechanism of tumor destruction in this system. While $CD8^+$ T cells affect tumor killing via direct cytolysis and release of perforin and granzyme B, CD4+ T cells can kill directly via MHCII recognition and also via recruitment of other effector cell types including macrophages, neutrophils, and B cells to mediate phagocytosis. Using bead-based assay kits and a tissue homogenization system, direct measurement of cytokine proteins in primary tumors, secondary tumors, and tumor draining lymph nodes is possible, and may aid in characterizing changes in the immune landscape in response to treatment [211]. For example, a tumor rich in Granulocyte Colony Stimulating Factor (G-CSF), Granulocyte-Macrophage Colony Stimulating Factor (GM-CSF), and Macrophage Inflammatory Protein (MIP1α and MIP1β), combined with flow cytometric evidence of increased CD4+ helper T cells, macrophages, and monocytes would support an overall immune TME driven by CD4+ recognition of tumor MHCII, and recruitment of innate phagocytes to affect tumor killing [212]. In contrast, a tumor rich in IL2, IFNγ, RANTES, TNFα, IL-12, and IL-33 combined with flow cytometric evidence of increased $CD8^+$ T cells, increased $CD8^+/T_{reg}$ ratio, and increased expression of the high-affinity IL-2 receptor CD25 and granule release marker CD107a on the surface of $CD8^+$ T cells and NK cells supports an immune TME dominated by recruitment of directly cytotoxic T lymphocytes and NK cells [213].

In reality, one or both of these mechanisms may be engaged in response to treatment, and both may be required for effective antitumor response. To further characterize the nature of the T cell response in this system, T Cell Receptor sequencing (TCRseq) can also be used. By sequencing the variety and copy number of each unique TCR mRNA sequence that arises as a result of VDJ recombination, one can reasonably estimate the number of T cell clones, and the size of each clonal population [211]. In addition, by comparing pre- and post-treatment samples

one can determine if the clones arising as a result of treatment were pre-existing (a dormant memory population) or if they arose *de novo* as a result of enhanced antigen processing and presentation. In the setting of two treated tumors, one can also determine which clones that dominate in the primary treated tumor are also found in the distant, secondary tumor and if those clones are enriched following additional secondary tumor radiation.

One of the interesting observations in these data is that in the model of two B78 tumors where RT+IC *in situ* vaccine is delivered to the primary with no treatment to the secondary, the secondary tumors grow *slower* than the 'no treatment' control tumors. This implies that the *in situ* vaccine, delivered at the distant primary site, is able to generate a systemic antitumor immune response that *does* infiltrate the secondary tumor, but is for some reason unable to induce substantial shrinkage. This suggests that either 1) the immune response is not strong enough to destroy a sufficient number of tumor cells at the secondary site, or 2) the microenvironment at the secondary tumor is largely immunosuppressive such that any activated immune cells entering the TME would be inhibited. It may be that radiating the secondary tumor is a means of altering the TME to be less suppressive and more accessible to the systemic antitumor effectors generated by the *in situ* vaccine. However, combination treatments with other immunotherapies could also be considered to strengthen the magnitude of the immune response. Dual checkpoint blockade using monoclonal antibodies against CTLA-4 and PD-1 have been used successfully in both preclinical and clinical settings to enhance pre-existing antitumor immune responses [84]. Morris and colleagues have demonstrated that intraperitoneal (IP) injections of anti-CTLA4 combined with RT+IC *in situ* vaccine have shown enhanced efficacy against larger B78 primary tumors (~500m^3), which *in situ* vaccine alone was unable to control [65]. In addition, manuscripts published by Morris, Sondel, and colleagues have demonstrated that RT+IC combined with anti-CTLA4 has improved immunologic effect against distant flank tumors, implanted brain tumors, and involves generation of humoral

memory immune responses (Appendix B). Adding anti-CTLA4 to the regimen consisting of RT+IC *in situ* vaccine at a primary tumor and 12Gy RT at a secondary tumor is expected to improve response rates even further, including rates of complete response.

5.3.4 *Expanding our understanding of immunomodulatory TRT in combination with immunotherapy*

Our results in chapter 4 demonstrating a survival improvement in mice bearing two B78 tumors treated with RT+IC and ^{90}Y-NM600 TRT compared to RT/IC alone suggest a benefit in combining low dose TRT with RT+IC immunotherapy. As is also the case with additional external beam radiation augmenting immune response, future studies will focus on describing the specific immunologic effects of TRT on the TME, and how they combine with RT+IC systemic effects. To this end the flow cytometry preparation technique outlined in Chapter 2 will be helpful in characterizing the radioactive TME. The data presented in Figure 2.6 outlining the changes to the TME over time following injection with ^{90}Y-NM600 already suggest some immune-favorable effects, including a decrease in suppressive T_{reg} content with subsequent increase in the CD8/T_{reg} ratio, and an influx of CD11b^{+} myeloid cells. However there are also changes to the TME that may not be as helpful, such as a decrease in CD8^{+} T cell and NK cell content at the higher injected activity level of 250μCi. Further characterization of the immune content, as described above in section 5.3.2, will also be helpful in characterizing the nature of the immune response triggered by TRT. This includes expanded innate and adaptive flow cytometry staining panels, measurement of cytokine content in the tumor, and TCRseq-based analysis of clonal T cell populations. Some of these studies are currently underway as of the time of this writing, and some interesting, yet preliminary, findings are presented in Appendix A. Importantly, conducting an evaluation of the immune changes occurring due to external beam radiation or TRT to the secondary will allow for comparison of the effects of different radiation

modalities on the immune system. One example already identified in chapter 2, is that in one set of experiments, external beam RT alone appeared to increase the T_{reg} content at 14 days post treatment (Figure 2.5), but 50μCi of ^{90}Y-NM600 did not raise the T_{reg} level, and 250μCi of ^{90}Y-NM600 decreased the T_{reg} level substantially compared to the untreated control (Figure 2.6). Repeating this study in a two tumor model, specifically controlling for dose and tumor size, is required to confidently characterize these differences. However these and other findings may shed light on different mechanisms of immune modulation between high dose rate, short treatment-duration external beam radiation and low dose rate, high treatment duration TRT. An understanding of these differences, and how these differences may change over time, is critical in designing optimal combination radioimmunotherapy treatments.

The potential benefit of using TRT over external beam RT is the potential to deliver targeted dose to sites that could not be irradiated using external beam RT, either due to risk to surrounding tissue, or an inability to locate the disease. This “micrometastatic” disease is a substantial cause of relapse and mortality in cancer patients [194]. To test the ability of TRT combined with RT/IC to improve response against such micrometastatic disease, mouse models seeding disseminated metastases could be used. Future studies could use tail vein injections of luciferase-transfected B78 melanoma cells in addition to a primary flank tumor. These cells, once in the bloodstream, will settle in end-organ tissues such as the lungs, and develop into metastatic disease. By injecting luciferin substrate into the mouse, the luciferase-expressing disease would then luminesce, which can be detected by sensitive *in vivo* imaging systems [214]. Thus, distant metastatic disease burden could be monitored, and relative treatment response to RT+IC *in situ* vaccine vs. RT+IC plus TRT could be compared. Similar approaches could be taken with spontaneously metastasizing models such as NSX2 neuroblastoma, which would avoid systemic injection and more accurately model physiologic

disease spread. Modeling this disease condition would expand the use of low dose radiation to all disease sites into scenarios where external beam RT is not possible.

Of note, there are several logistic and dosimetry challenges that must be addressed to better understand combination TRT immunotherapy approaches. These include determining best practices for radiation safety, measurement of dose using combination PET/CT detectable and therapeutic isotopes and measuring pharmacodynamic and pharmacokinetic changes in the TRT vehicle as a function of tumor type, and tumor burden. In addition, physically larger animal studies are required to more accurately assess the ratio of dose delivered to the target tissue to dose delivered to adjacent structures. For example, the path length of a ^{90}Y beta particle emission is approximately 1cm. This distance encompasses a large fraction of a mouse body, yet only a small fraction of the human body. Because path length is fixed and cannot scale with the size of the model animal, larger animal models should be studied to more accurately represent potential off target effects. These studies and several others are currently underway as part of a collaborative effort among the Sondel, Morris, Weichert, Bednarz, and Vail laboratories.

References

1 Emens LA, Ascierto PA, Darcy PK, *et al.* Cancer immunotherapy: Opportunities and challenges in the rapidly evolving clinical landscape. *Eur J Cancer* 2017;**81**:116–29. doi:10.1016/j.ejca.2017.01.035

2 Seelige R, Searles S, Jack ·, *et al.* Mechanisms regulating immune surveillance of cellular stress in cancer. *Cell Mol Life Sci* 2018;**75**:225–40. doi:10.1007/s00018-017-2597-7

3 Bates JP, Derakhshandeh R, Jones L, *et al.* Mechanisms of immune evasion in breast cancer. doi:10.1186/s12885-018-4441-3

4 Dunn GP, Old LJ, Schreiber RD. The Three Es of Cancer Immunoediting. *Annu Rev Immunol* 2004;**22**:329–60. doi:10.1146/annurev.immunol.22.012703.104803

5 Escors D. Tumour Immunogenicity, Antigen Presentation, and Immunological Barriers in Cancer Immunotherapy. *New J Sci* 2014;**2014**:1–25. doi:10.1155/2014/734515

6 Galon J, Bruni D. Approaches to treat immune hot, altered and cold tumours with combination immunotherapies. Nat. Rev. Drug Discov. 2019;**18**:197–218. doi:10.1038/s41573-018-0007-y

7 Vareki SM. High and low mutational burden tumors versus immunologically hot and cold tumors and response to immune checkpoint inhibitors. doi:10.1186/s40425-018-0479-7

8 Hammerich L, Binder A, Brody JD. In situ vaccination: Cancer immunotherapy both personalized and off-the-shelf. *Mol Oncol* 2015;**9**:1966–81. doi:10.1016/j.molonc.2015.10.016

9 Gan C, Mostafid H, Khan MS, *et al.* BCG immunotherapy for bladder cancer - The effects of substrain differences. Nat. Rev. Urol. 2013. doi:10.1038/nrurol.2013.194

10 Mostafid AH, Palou Redorta J, Sylvester R, *et al.* Therapeutic options in high-risk non-muscle-invasive bladder cancer during the current worldwide shortage of bacille calmette-guérin. Eur. Urol. 2015. doi:10.1016/j.eururo.2014.11.031

11 Agrawal N, Bettegowda C, Cheong I, *et al.* Bacteriolytic therapy can generate a potent immune response against experimental tumors. *Proc Natl Acad Sci U S A* Published Online First: 2004. doi:10.1073/pnas.0406242101

12 Kaufman HL, Kohlhapp FJ, Zloza A. Oncolytic viruses: A new class of immunotherapy drugs. Nat. Rev. Drug Discov. 2015. doi:10.1038/nrd4663

13 Johnson DB, Puzanov I, Kelley MC. Talimogene laherparepvec (T-VEC) for the treatment of advanced melanoma. *Immunotherapy* Published Online First: 2015. doi:10.2217/imt.15.35

14 Green DS, Dalgleish AG, Belonwu N, *et al.* Topical imiquimod and intralesional interleukin-2 increase activated lymphocytes and restore the Th1/Th2 balance in patients with metastatic melanoma. *Br J Dermatol* Published Online First: 2008. doi:10.1111/j.1365-2133.2008.08709.x

15 Latz E, Schoenemeyer A, Visintin A, *et al.* TLR9 signals after translocating from the ER to CpG DNA in the lysosome. *Nat Immunol* Published Online First: 2004. doi:10.1038/ni1028

16 Houot R, Levy R. T-cell modulation combined with intratumoral CpG cures lymphoma in a mouse model without the need for chemotherapy. *Blood* Published Online First: 2009. doi:10.1182/blood-2008-07-170274

17 Rakhmilevich AL, Felder M, Lever L, *et al.* Effective Combination of Innate and Adaptive Immunotherapeutic Approaches in a Mouse Melanoma Model. *J Immunol* 2017;**198**:1575–84. doi:10.4049/jimmunol.1601255

18 Gitlin L, Barchet W, Gilfillan S, *et al.* Essential role of mda-5 in type I IFN responses to polyriboinosinic: polyribocytidylic acid and encephalomyocarditis picornavirus. *Proc Natl Acad Sci U S A* Published Online First: 2006. doi:10.1073/pnas.0603082103

19 Lu YC, Yeh WC, Ohashi PS. LPS/TLR4 signal transduction pathway. Cytokine. 2008. doi:10.1016/j.cyto.2008.01.006

20 Colombo MP, Trinchieri G. Interleukin-12 in anti-tumor immunity and immunotherapy. Cytokine Growth Factor Rev. 2002. doi:10.1016/S1359-6101(01)00032-6

21 Brunda MJ, Luistro L, Warrier RR, *et al.* Antitumor and Antimetastatic Activity of Interleukin 12 against Murine Tumors. *J Exp Med* Published Online First: 1993. doi:10.1084/jem.178.4.1223

22 Leonard JP, Sherman ML, Fisher GL, *et al.* Effects of single-dose interleukin-12 exposure on interleukin-12 associated toxicity and interferon-γ production. *Blood* Published Online First: 1997. doi:10.1182/blood.V90.7.2541

23 Atkins MB, Lotze MT, Dutcher JP, *et al.* High-dose recombinant interleukin 2 therapy for patients with metastatic melanoma: Analysis of 270 patients treated between 1985 and 1993. *J Clin Oncol* Published Online First: 1999. doi:10.1200/jco.1999.17.7.2105

24 Mahvi DM, Henry MB, Albertini MR, *et al.* Intratumoral injection of IL-12 plasmid DNA - Results of a phase I/IB clinical trial. *Cancer Gene Ther* Published Online First: 2007. doi:10.1038/sj.cgt.7701064

25 Weide B, Derhovanessian E, Pflugfelder A, *et al.* High response rate after intratumoral treatment with interleukin-2: Results from a phase 2 study in 51 patients with metastasized melanoma. *Cancer* 2010;**116**:4139–46. doi:10.1002/cncr.25156

26 Clarke JM, George DJ, Lisi S, *et al.* Immune Checkpoint Blockade: The New Frontier in Cancer Treatment. *Target Oncol* 2018;**13**:1–20. doi:10.1007/s11523-017-0549-7

27 Murphy JB, Hussey RG, Nakahara W, *et al.* Studies on x-ray effects: VI. effect of the cellular reaction induced by x-rays on cancer grains. *J Exp Med* 1921;**33**:299–313. doi:10.1084/jem.33.3.299

28 Slone HB, Peters LJ, Milas L. Effect of host immune capability on radiocurability and subsequent transplantability of a murine fibrosarcoma. *J Natl Cancer Inst* 1979;**63**:1229–35. doi:10.1093/jnci/63.5.1229

29 Abuodeh Y, Venkat P, Kim S. Systematic review of case reports on the abscopal effect. *Curr Probl Cancer* Published Online First: 2016. doi:10.1016/j.currproblcancer.2015.10.001

30 Law AW, Mole RH. Direct and Abscopal Effects of X-radiation on the Thymus of the Weanling Rat. *Int J Radiat Biol Relat Stud Physics, Chem Med* 1961;**3**:233–48. doi:10.1080/09553006114551161

31 Brody JD, Ai WZ, Czerwinski DK, *et al.* In situ vaccination with a TLR9 agonist induces systemic lymphoma regression: A phase I/II study. *J Clin Oncol* Published Online First: 2010. doi:10.1200/JCO.2010.28.9793

32 Marabelle A, Tselikas L, de Baere T, *et al.* Intratumoral immunotherapy: Using the tumor as the remedy. Ann. Oncol. 2017. doi:10.1093/annonc/mdx683

33 Kinner A, Wu W, Staudt C, *et al.* Gamma-H2AX in recognition and signaling of DNA double-strand breaks in the context of chromatin. Nucleic Acids Res. 2008. doi:10.1093/nar/gkn550

34 Krysko D V., Garg AD, Kaczmarek A, *et al.* Immunogenic cell death and DAMPs in cancer therapy. Nat. Rev. Cancer. 2012. doi:10.1038/nrc3380

35 Golden EB, Apetoh L. Radiotherapy and Immunogenic Cell Death. Semin. Radiat. Oncol. 2015. doi:10.1016/j.semradonc.2014.07.005

36 Green DR, Ferguson T, Zitvogel L, *et al.* Immunogenic and tolerogenic cell death. Nat. Rev. Immunol. 2009. doi:10.1038/nri2545

37 Panaretakis T, Kepp O, Brockmeier U, *et al.* Mechanisms of pre-apoptotic calreticulin exposure in immunogenic cell death. *EMBO J* 2009;**28**:578–90. doi:10.1038/emboj.2009.1

38 Golden EB, Frances D, Pellicciotta I, *et al.* Radiation fosters dose-dependent and chemotherapy-induced immunogenic cell death. *Oncoimmunology* 2014;**3**:e28518. doi:10.4161/onci.28518

39 Apetoh L, Ghiringhelli F, Tesniere A, *et al.* Toll-like receptor 4-dependent contribution of the immune system to anticancer chemotherapy and radiotherapy. *Nat Med* 2007;**13**:1050–9. doi:10.1038/nm1622

40 Lotze MT, Tracey KJ. High-mobility group box 1 protein (HMGB1): Nuclear weapon in the immune arsenal. Nat. Rev. Immunol. 2005;**5**:331–42. doi:10.1038/nri1594

41 Ohshima Y, Tsukimoto M, Takenouchi T, *et al.* γ-Irradiation induces P2X7 receptor-dependent ATP release from B16 melanoma cells. *Biochim Biophys Acta - Gen Subj* 2010;**1800**:40–6. doi:10.1016/j.bbagen.2009.10.008

42 Ghiringhelli F, Apetoh L, Tesniere A, *et al.* Activation of the NLRP3 inflammasome in dendritic cells induces IL-1B-dependent adaptive immunity against tumors. *Nat Med* 2009;**15**:1170–8. doi:10.1038/nm.2028

43 Newcomb EW, Demaria S, Lukyanov Y, *et al.* The combination of ionizing radiation and peripheral vaccination produces long-term survival of mice bearing established invasive GL261 gliomas. *Clin Cancer Res* 2006;**12**:4730–7. doi:10.1158/1078-0432.CCR-06-0593

44 Son CH, Lee HR, Koh EK, *et al.* Combination treatment with decitabine and ionizing radiation enhances tumor cells susceptibility of T cells. *Sci Rep* Published Online First: 2016. doi:10.1038/srep32470

45 Malamas AS, Gameiro SR, Knudson KM, *et al.* Sublethal exposure to alpha radiation (223Ra dichloride) enhances various carcinomas' sensitivity to lysis by antigenspecific cytotoxic T lymphocytes through calreticulin-mediated immunogenic modulation. *Oncotarget* 2016;**7**:86937–47. doi:10.18632/oncotarget.13520

46 Chakraborty M, Abrams SI, Camphausen K, *et al.* Irradiation of Tumor Cells Up-Regulates Fas and Enhances CTL Lytic Activity and CTL Adoptive Immunotherapy. *J Immunol* Published Online First: 2003. doi:10.4049/jimmunol.170.12.6338

47 Fu J, Kanne DB, Leong M, *et al.* STING agonist formulated cancer vaccines can cure established tumors resistant to PD-1 blockade. *Sci Transl Med* 2015;**7**:283ra52. doi:10.1126/scitranslmed.aaa4306

48 Ager CR, Reilley MJ, Nicholas C, *et al.* Intratumoral STING activation with T-cell checkpoint modulation generates systemic antitumor immunity. *Cancer Immunol Res* 2017;**5**:676–84. doi:10.1158/2326-6066.CIR-17-0049

49 Benci JL, Xu B, Qiu Y, *et al.* Tumor Interferon Signaling Regulates a Multigenic Resistance Program to Immune Checkpoint Blockade HHS Public Access. *Cell* 2016;**167**:1540–54. doi:10.1016/j.cell.2016.11.022

50 Vanpouille-Box C, Alard A, Aryankalayil MJ, *et al.* DNA exonuclease Trex1 regulates radiotherapy-induced tumour immunogenicity. *Nat Commun* 2017;**8**:15618. doi:10.1038/ncomms15618

51 Di Maggio FM, Minafra L, Forte GI, *et al.* Portrait of inflammatory response to ionizing radiation treatment. J. Inflamm. (United Kingdom). 2015. doi:10.1186/s12950-015-0058-3

52 Nakamura N, Kusunoki Y, Akiyama M. Radiosensitivity of CD4 or CD8 Positive Human T-Lymphocytes by an in Vitro Colony Formation Assay. *Radiat Res* Published Online First: 1990. doi:10.2307/3577549

53 Balogh A, Persa E, Bogdándi EN, *et al.* The effect of ionizing radiation on the homeostasis and functional integrity of murine splenic regulatory T cells. *Inflamm Res* Published Online First: 2013. doi:10.1007/s00011-012-0567-y

54 Liu R, Xiong S, Zhang L, *et al.* Enhancement of antitumor immunity by low-dose total body irradiationis associated with selectively decreasing the proportion and number of T regulatorycells. *Cell Mol Immunol* Published Online First: 2010. doi:10.1038/cmi.2009.117

55 Liu S-Z. Nonlinear Dose-Response Relationship in the Immune System following Exposure to Ionizing Radiation: Mechanisms and Implications. *Nonlinearity Biol Toxicol Med* Published Online First: 2003. doi:10.1080/15401420390844483

56 Xu J, Escamilla J, Mok S, *et al.* CSF1R signaling blockade stanches tumor-infiltrating myeloid cells and improves the efficacy of radiotherapy in prostate cancer. *Cancer Res* Published Online First: 2013. doi:10.1158/0008-5472.CAN-12-3981

57 Chiang CS, Fu SY, Wang SC, *et al.* Irradiation promotes an M2 macrophage phenotype in tumor hypoxia. *Front Oncol* Published Online First: 2012. doi:10.3389/fonc.2012.00089

58 Schaue D, Ratikan JA, Iwamoto KS, *et al.* Maximizing tumor immunity with fractionated radiation. *Int J Radiat Oncol Biol Phys* Published Online First: 2012. doi:10.1016/j.ijrobp.2011.09.049

59 Lin AJ, Gang M, Rao YJ, *et al.* Association of Posttreatment Lymphopenia and Elevated Neutrophil-to-Lymphocyte Ratio with Poor Clinical Outcomes in Patients with Human Papillomavirus-Negative Oropharyngeal Cancers. *JAMA Otolaryngol - Head Neck Surg* 2019;**145**:413–21. doi:10.1001/jamaoto.2019.0034

60 Kim DY, Kim IS, Park SG, *et al.* Prognostic value of posttreatment neutrophil-lymphocyte

ratio in head and neck squamous cell carcinoma treated by chemoradiotherapy. doi:10.1016/j.anl.2016.05.013

61 Rader C, Bishop MR. Monoclonal antibodies in cancer therapy. In: *General Principles of Tumor Immunotherapy: Basic and Clinical Applications of Tumor Immunology*. 2008. doi:10.1007/978-1-4020-6087-8_20

62 Honsik CJ, Jung G, Reisfeld RA. Lymphokine-activated killer cells targeted by monoclonal antibodies to the disialogangliosides GD2 and GD3 specifically lyse human tumor cells of neuroectodermal origin. *Proc Natl Acad Sci U S A* Published Online First: 1986. doi:10.1073/pnas.83.20.7893

63 Yu AL, Gilman AL, Ozkaynak MF, *et al.* Anti-GD2 Antibody with GM-CSF, Interleukin-2, and Isotretinoin for Neuroblastoma. *N Engl J Med* 2010;**363**:1324–34. doi:10.1056/NEJMoa0911123

64 Yang RK, Kalogriopoulos NA, Rakhmilevich AL, *et al.* Intratumoral treatment of smaller mouse neuroblastoma tumors with a recombinant protein consisting of IL-2 linked to the hu14.18 antibody increases intratumoral CD8+ T and NK cells and improves survival. *Cancer Immunol Immunother* 2013;**62**:1303–13. doi:10.1007/s00262-013-1430-x

65 Morris ZS, Guy EI, Francis DM, *et al.* In situ tumor vaccination by combining local radiation and tumor-specific antibody or immunocytokine treatments. *Cancer Res* 2016;**76**:3929–41. doi:10.1158/0008-5472.CAN-15-2644

66 Morris ZS, Guy EI, Werner LR, *et al.* Tumor-Specific Inhibition of *In Situ* Vaccination by Distant Untreated Tumor Sites. *Cancer Immunol Res* 2018;**6**:825–34. doi:10.1158/2326-6066.CIR-17-0353

67 Gomez DR, Blumenschein GR, Lee JJ, *et al.* Local consolidative therapy versus maintenance therapy or observation for patients with oligometastatic non-small-cell lung cancer without progression after first-line systemic therapy: a multicentre, randomised, controlled, phase 2 study. *Lancet Oncol* 2016;**17**:1672–82. doi:10.1016/S1470-2045(16)30532-0

68 Gill MR, Falzone N, Du Y, *et al.* Review Targeted radionuclide therapy in combined-modality regimens. *Lancet Oncol* 2019;**18**:e414–23. doi:10.1016/S1470-2045(17)30379-0

69 Divgi C. The Current State of Radiopharmaceutical Therapy. 2018;**59**:2018–20. doi:10.2967/jnumed.118.214122

70 Dolgin E. Radioactive drugs emerge from the shadows to storm the market. Nat. Biotechnol. 2018. doi:10.1038/nbt1218-1125

71 Czernin J. Molecular Imaging and Therapy with a Purpose : A Renaissance of Nuclear Medicine. ;:21–3.

72 Zukotynski K, Jadvar H, Capala J, *et al.* Targeted Radionuclide Therapy: Practical Applications and Future Prospects Supplementary Issue: Biomarkers and their Essential Role in the Development of Personalised Therapies (A). *Biomark Cancer*;**2016**. doi:10.4137/BiC.s31804

73 LaFleur MW, Muroyama Y, Drake CG, *et al.* Inhibitors of the PD-1 Pathway in Tumor Therapy. *J Immunol* 2018;**200**:375–83. doi:10.4049/jimmunol.1701044

74 Hino R, Kabashima K, Kato Y, *et al.* Tumor cell expression of programmed cell death-1

ligand 1 is a prognostic factor for malignant melanoma. *Cancer* 2010;**116**:1757–66. doi:10.1002/cncr.24899

75 Weichert JP, Clark P a, Kandela IK, *et al.* Alkylphosphocholine analogs for broad-spectrum cancer imaging and therapy. *Sci Transl Med* 2014;**6**:240ra75. doi:10.1126/scitranslmed.3007646

76 R. H, R. P, J. G, *et al.* Combination of targeted radionuclide therapy and checkpoint blockade augments therapeutic response in a syngeneic murine model of melanoma. *J Nucl Med* 2018.

77 Chen H, Zhao L, Fu K, *et al.* Integrin αvβ3-targeted radionuclide therapy combined with immune checkpoint blockade immunotherapy synergistically enhances anti-tumor efficacy. *Theranostics* 2019;**9**:7948–60. doi:10.7150/thno.39203

78 Choi J, Beaino W, Fecek RJ, *et al.* Combined VLA-4–targeted radionuclide therapy and immunotherapy in a mouse model of melanoma. *J Nucl Med* 2018;**59**:1843–9. doi:10.2967/jnumed.118.209510

79 ClinicalTrials.gov. Phase I Study of Investigational Medicinal Products in Children with Relapsed/Refractory Neruoblastoma. https://clinicaltrials.gov/ct2/show/NCT02914405

80 Kratochwil C, Haberkorn U, Giesel FL. Radionuclide Therapy of Metastatic Prostate Cancer. *Semin Nucl Med* 2019;**49**:313–25. doi:10.1053/j.semnuclmed.2019.02.003

81 ClinicalTrials.gov. Study evaluating the addition of pembrolizumab to Radium-223 in mCRPC. https://clinicaltrials.gov/ct2/show/NCT03093428

82 ClinicaTrials.gov. Safety and tolerability of Atezolizumab in combination with Radium-223 Dichloride in metastatic castrate resistant prostate cancer progressed following treatment with an androgen pathway inhibitor. https://clinicaltrials.gov/ct2/show/NCT02814669

83 ClinicalTrials.gov. PRINCE (PSMA-lutetium Radionuclide Therapy and ImmuNotherapy in Prostate CancEr). https://clinicaltrials.gov/ct2/show/NCT03658447

84 Victor CT-S, Rech AJ, Maity A, *et al.* Radiation and dual checkpoint blockade activate non-redundant immune mechanisms in cancer. *Nature* 2015;**520**:373–7. doi:10.1038/nature14292

85 Formenti SC, Rudqvist N, Golden E, *et al.* Radiotherapy induces responses of lung cancer to CTLA-4 blockade. *Nat Med* 2018;**24**:1845–51. doi:10.1038/s41591-018-0232-2

86 Dietrich A, Koi L, Zöphel K, *et al.* Improving external beam radiotherapy by combination with internal irradiation. *Br J Radiol* 2015;**88**. doi:10.1259/bjr.20150042

87 Dietrich A, Koi L, Sihver W, *et al.* Improving external beam radiotherapy by combination with internal irradiation. *J Radiol* 2015;**88**. doi:10.1259/bjr.20150042

88 Kaufman HL, Kohlhapp FJ, Zloza A. Oncolytic viruses: A new class of immunotherapy drugs. Nat. Rev. Drug Discov. 2015. doi:10.1038/nrd4663

89 Sorensen A, Mairs RJ, Braidwood L, *et al.* In vivo evaluation of a cancer therapy strategy combining HSV1716-mediated oncolysis with gene transfer and targeted radiotherapy. *J Nucl Med* 2012;**53**:647–54. doi:10.2967/jnumed.111.090886

90 Peerlinck I, Merron A, Baril P, *et al.* Targeted radionuclide therapy using a wnt-targeted replicating adenovirus encoding the Na/I symporter. *Clin Cancer Res* 2009;**15**:6595–601.

doi:10.1158/1078-0432.CCR-09-0262

91 Rekoske BT, Smith HA, Olson BM, *et al.* PD-1 or PD-L1 blockade restores antitumor efficacy following SSX2 epitope-modified DNA vaccine immunization. *Cancer Immunol Res* Published Online First: 2015. doi:10.1158/2326-6066.CIR-14-0206

92 Olson BM, Johnson LE, McNeel DG. The androgen receptor: A biologically relevant vaccine target for the treatment of prostate cancer. *Cancer Immunol Immunother* Published Online First: 2013. doi:10.1007/s00262-012-1363-9

93 Olson BM, McNeel DG. CD8+ T cells specific for the androgen receptor are common in patients with prostate cancer and are able to lyse prostate tumor cells. *Cancer Immunol Immunother* Published Online First: 2011. doi:10.1007/s00262-011-0987-5

94 Hemanth Potluri, Reinier Hernandez, Christopher Zahm, Joseph Grudzinski, Christopher Massey, Jamey Weichert DM. Molecularly targeted radionuclide therapy modulates the composition of the murine prostate cancer microenvironment. *J Immunother Cancer* 2019;**7**.https://jitc.biomedcentral.com/articles/10.1186/s40425-019-0764-0

95 Kantoff PW, Higano CS, Shore ND, *et al.* Sipuleucel-T immunotherapy for castration-resistant prostate cancer. *N Engl J Med* Published Online First: 2010. doi:10.1056/NEJMoa1001294

96 Small EJ, Schellhammer PF, Higano CS, *et al.* Placebo-controlled phase III trial of immunologic therapy with Sipuleucel-T (APC8015) in patients with metastatic, asymptomatic hormone refractory prostate cancer. *J Clin Oncol* Published Online First: 2006. doi:10.1200/JCO.2005.04.5252

97 ClinicalTrials.gov. Study of Sipuleucel-T with or without Radium-223 in men with asymptommatic or minimally symptomatic MCRPC. https://clinicaltrials.gov/ct2/show/NCT02463799

98 Bendall SC, Nolan GP, Roederer M, *et al.* A deep profiler's guide to cytometry. *Trends Immunol* 2012;**33**:323–32. doi:10.1016/j.it.2012.02.010

99 Wilson GD, Marples B. Flow cytometry in radiation research: past, present and future. *Radiat Res* 2007;**168**:391–403. doi:10.1667/RR1042.1

100 Verschoor CP, Kohli V, Balion C. A comprehensive assessment of immunophenotyping performed in cryopreserved peripheral whole blood. *Cytom Part B - Clin Cytom* 2018;**94**:662–70. doi:10.1002/cyto.b.21526

101 Gianchecchi E, Delfino DV, Fierabracci A. Recent insights into the role of the PD-1/PD-L1 pathway in immunological tolerance and autoimmunity. *Autoimmun Rev* 2013;**12**:1091–100. doi:10.1016/j.autrev.2013.05.003

102 Olson B, Li Y, Lin Y, *et al.* Mouse models for cancer immunotherapy research. *Cancer Discov* 2018;**8**:1358–65. doi:10.1158/2159-8290.CD-18-0044

103 Zitvogel L, Pitt JM, Daillère R, *et al.* Mouse models in oncoimmunology. *Nat Rev Cancer* 2016;**16**:759–73. doi:10.1038/nrc.2016.91

104 Malissen B, Tamoutounour S, Henri S. The origins and functions of dendritic cells and macrophages in the skin. *Nat Rev Immunol* 2014;**14**:417–28. doi:10.1038/nri3683

105 Tong PL, Roediger B, Kolesnikoff N, *et al.* The Skin Immune Atlas: Three-Dimensional

Analysis of Cutaneous Leukocyte Subsets by Multiphoton Microscopy. *J Invest Dermatol* 2015;**135**:84–93. doi:10.1038/jid.2014.289

106 Saitoh A, Aizawa Y. Intradermal vaccination for infants and children. *Hum Vaccines Immunother* 2016;**12**:2447–55. doi:10.1080/21645515.2016.1176652

107 Joncker NT, Bettini S, Boulet D, *et al.* The site of tumor development determines immunogenicity via temporal mobilization of antigen-laden dendritic cells in draining lymph nodes. *Eur J Immunol* 2016;**46**:609–18. doi:10.1002/eji.201545797

108 Mallone R, Mannering SI, Brooks-Worrell BM, *et al.* Isolation And Preservation Of Peripheral Blood Mononuclear cells for analysis of islet antigen-reactive T cell responses: Position statement of the T-Cell Workshop Committee of the Immunology of Diabetes Society. *Clin Exp Immunol* 2011;**163**:33–49. doi:10.1111/j.1365-2249.2010.04272.x

109 Sacchi A, Tumino N, Grassi G, *et al.* A new procedure to analyze polymorphonuclear myeloid derived suppressor cells in cryopreserved samples cells by flow cytometry. *PLoS One* 2018;**13**:1–11. doi:10.1371/journal.pone.0202920

110 Costantini A, Mancini S, Giuliodoro S, *et al.* Effects of cryopreservation on lymphocyte immunophenotype and function. *J Immunol Methods* 2003;**278**:145–55. doi:10.1016/S0022-1759(03)00202-3

111 Gerrits JH, Athanassopoulos P, Vaessen LMB, *et al.* Peripheral blood manipulation significantly affects the result of dendritic cell monitoring. *Transpl Immunol* 2007;**17**:169–77. doi:10.1016/j.trim.2006.11.006

112 Liu K, Yang Y, Mansbridge J. Comparison of the Stress Response to Cryopreservation in Monolayer and Three-Dimensional Human Fibroblast Cultures: Stress Proteins, MAP Kinases, and Growth Factor Gene Expression. *Tissue Eng* 2000;**6**:539–54. doi:10.1089/107632700750022189

113 BD Biosciences. BB515 Rat Anti-Mouse CD25 Technical Data Sheet. 2017.https://www.bdbiosciences.com/ds/pm/tds/564424.pdf

114 BD Biosciences. PE-CF594 Mouse Anti-Mouse NK1.1. 2011.https://www.bdbiosciences.com/us/reagents/research/antibodies-buffers/immunology-reagents/anti-mouse-antibodies/cell-surface-antigens/pe-cf594-mouse-anti-mouse-nk-11-pk136/p/562864

115 BioLegend. Brilliant Violet 785(TM) anti-mouse CD4 Antibody Technical Data Sheet. 2013.https://www.biolegend.com/en-us/global-elements/pdf-popup/brilliant-violet-785-anti-mouse-cd4-antibody-7954?filename=Brilliant Violet 785trade anti-mouse CD4 Antibody.pdf&pdfgen=true

116 Abay A, Simionato G, Chachanidze R, *et al.* Glutaraldehyde - A subtle tool in the investigation of healthy and pathologic red blood cells. *Front Physiol* 2019;**10**:1–14. doi:10.3389/fphys.2019.00514

117 van Pul KM, Vuylsteke RJCLM, Bril H, *et al.* Feasibility of flowcytometric quantitation of immune effector cell subsets in the sentinel lymph node of the breast after cryopreservation. *J Immunol Methods* 2012;**375**:189–95. doi:10.1016/j.jim.2011.10.011

118 Weinberg A, Song LY, Wilkening C, *et al.* Optimization and limitations of use of cryopreserved peripheral blood mononuclear cells for functional and phenotypic T-cell characterization. *Clin Vaccine Immunol* 2009;**16**:1176–86. doi:10.1128/CVI.00342-08

119 Pinto LA, Trivett MT, Wallace D, *et al.* Fixation and cryopreservation of whole blood and isolated mononuclear cells: Influence of different procedures on lymphocyte subset analysis by flow cytometry. *Cytom Part B - Clin Cytom* 2005;**63**:47–55. doi:10.1002/cyto.b.20038

120 Brenner DJ. The Linear-Quadratic Model Is an Appropriate Methodology for Determining Isoeffective Doses at Large Doses Per Fraction. *Semin Radiat Oncol* 2008;**18**:234–9. doi:10.1016/j.semradonc.2008.04.004

121 Rodríguez-Ruiz ME, Vanpouille-Box C, Melero I, *et al.* Immunological Mechanisms Responsible for Radiation-Induced Abscopal Effect. *Trends Immunol* 2018;**39**:644–55. doi:10.1016/j.it.2018.06.001

122 Barker HE, Paget JTE, Khan AA, *et al.* The tumour microenvironment after radiotherapy: Mechanisms of resistance and recurrence. *Nat Rev Cancer* 2015;**15**:409–25. doi:10.1038/nrc3958

123 Wennerberg E, Vanpouille-Box C, Bornstein S, *et al.* Immune recognition of irradiated cancer cells. *Immunol Rev* 2017;**280**:220–30. doi:10.1111/imr.12568

124 Liu S, Sun X, Luo J, *et al.* Effects of radiation on T regulatory cells in normal states and cancer: Mechanisms and clinical implications. Am. J. Cancer Res. 2015.

125 Wennerberg E, Lhuillier C, Vanpouille-Box C, *et al.* Barriers to radiation-induced in situ tumor vaccination. *Front Immunol* 2017;**8**. doi:10.3389/fimmu.2017.00229

126 Patel, Ravi; Hernandez, Reinier; Carlson, Peter; Grudzinski, Joseph; Bates, Amber; Jagodinski, Justin; Erbe Amy, Marsh, Ian; Alucio-Sarduy, Eduardo; Rakhmilevich, Alexander; Vail, DAvid; Engle, Jonathan; Kim, KyungMann; Bednarz, Bryan; Sondel, Paul; Weich JMZ. Low-dose targeted radionuclide therapy renders immunologically 'cold' tumors responsive to immune checkpoint blockade. *Submitted* 2020.

127 Grudzinski JJ, Hernandez R, Marsh I, *et al.* Preclinical Characterization of $^{86/90}$ Y-NM600 in a Variety of Murine and Human Cancer Tumor Models. *J Nucl Med* 2019;**60**:1622–8. doi:10.2967/jnumed.118.224808

128 Haraguchi M, Yamashiro S, Yamamoto A, *et al.* Isolation of G(D3) synthase gene by expression cloning of G(M3) α-2,8- sialyltransferase cDNA using anti-G(D2) monoclonal antibody. *Proc Natl Acad Sci U S A* Published Online First: 1994. doi:10.1073/pnas.91.22.10455

129 Haraguchi M, Yamashiro S, Yamamoto A, *et al.* Isolation of GD3 synthase gene by expression cloning of GM3 alpha-2,8-sialyltransferase cDNA using anti-GD2 monoclonal antibody. *Proc Natl Acad Sci U S A* 1994;**91**:10455–9. doi:10.1073/pnas.91.22.10455

130 Ruf P, Schäfer B, Eissler N, *et al.* Ganglioside GD2-specific trifunctional surrogate antibody Surek demonstrates therapeutic activity in a mouse melanoma model. *J Transl Med* 2012;**10**:1–10. doi:10.1186/1479-5876-10-219

131 Hernandez R, Walker KL, Grudzinski JJ, *et al.* 90Y-NM600 targeted radionuclide therapy induces immunologic memory in syngeneic models of T-cell Non-Hodgkin's Lymphoma. *Commun Biol* 2019;**2**. doi:10.1038/s42003-019-0327-4

132 Fontenot JD, Gavin MA, Alexander RY. Pillars Article : Foxp3 Programs the Development and Function of CD4 + CD25 +. *J Immunol* 2017;:986–92.

133 Nettenstrom L, Alderson K, Raschke EE, *et al.* An optimized multi-parameter flow cytometry protocol for human T regulatory cell analysis on fresh and viably frozen cells, correlation with epigenetic analysis, and comparison of cord and adult blood. *J Immunol Methods* 2013;**387**:81–8. doi:10.1016/j.jim.2012.09.014

134 Qin W, Hu L, Zhang X, *et al.* The Diverse Function of PD-1/PD-L Pathway Beyond Cancer. *Front Immunol* 2019;**10**:2298. doi:10.3389/fimmu.2019.02298

135 MacKay LK, Rahimpour A, Ma JZ, *et al.* The developmental pathway for CD103+ CD8+ tissue-resident memory T cells of skin. *Nat Immunol* 2013;**14**:1294–301. doi:10.1038/ni.2744

136 Djenidi F, Adam J, Goubar A, *et al.* CD8+CD103+ tumor-infiltrating lymphocytes are tumor-specific tissue-resident memory T cells and a prognostic factor for survival in lung cancer patients. *J Immunol* 2015;**194**:3475–86. doi:10.4049/jimmunol.1402711

137 Gautier EL, Shay T, Miller J, *et al.* Gene-expression profiles and transcriptional regulatory pathways that underlie the identity and diversity of mouse tissue macrophages. *Nat Immunol* 2012;**13**:1118–28. doi:10.1038/ni.2419

138 Guilliams M, Dutertre C-A, Scott CL, *et al.* Unsupervised High-Dimensional Analysis Aligns Dendritic Cells across Tissues and Species. *Immunity* 2016;**45**:669–84. doi:10.1016/j.immuni.2016.08.015

139 Bain CC, Scott CL, Uronen-Hansson H, *et al.* Resident and pro-inflammatory macrophages in the colon represent alternative context-dependent fates of the same Ly6Chi monocyte precursors. *Mucosal Immunol* 2013;**6**:498–510. doi:10.1038/mi.2012.89

140 Veremeyko T, Yung AWY, Anthony DC, *et al.* Early Growth Response Gene-2 Is Essential for M1 and M2 Macrophage Activation and Plasticity by Modulation of the Transcription Factor CEBPβ. *Front Immunol* 2018;**9**:2515. doi:10.3389/FIMMU.2018.02515

141 Merad M, Sathe P, Helft J, *et al.* The dendritic cell lineage: ontogeny and function of dendritic cells and their subsets in the steady state and the inflamed setting. *Annu Rev Immunol* 2013;**31**:563–604. doi:10.1146/annurev-immunol-020711-074950

142 Tamoutounour S, Guilliams M, MontananaSanchis F, *et al.* Origins and functional specialization of macrophages and of conventional and monocyte-derived dendritic cells in mouse skin. *Immunity* 2013;**39**:925–38. doi:10.1016/j.immuni.2013.10.004

143 Guilliams M, Ginhoux F, Jakubzick C, *et al.* Dendritic cells, monocytes and macrophages: A unified nomenclature based on ontogeny. *Nat Rev Immunol* 2014;**14**:571–8. doi:10.1038/nri3712

144 DeLong JH, Hall AO, Konradt C, *et al.* Cytokine- and TCR-Mediated Regulation of T Cell Expression of Ly6C and Sca-1. *J Immunol* 2018;:ji1701154. doi:10.4049/jimmunol.1701154

145 Paredes RM, Tadaki DK, Sooter A, *et al.* Cryopreservation of human whole blood allows immunophenotyping by flow cytometry up to 30 days after cell isolation. *J Immunol Methods* 2018;**452**:32–8. doi:10.1016/j.jim.2017.08.013

146 Sattui S, De La Flor C, Sanchez C, *et al.* Cryopreservation modulates the detection of regulatory T cell markers. *Cytom Part B - Clin Cytom* 2012;**82 B**:54–8. doi:10.1002/cyto.b.20621

147 Wildenberg ME, Duijvestein M, Westera L, *et al.* Evaluation of the effect of storage condition on cell extraction and flow cytometric analysis from intestinal biopsies. *J Immunol Methods* 2018;**459**:50–4. doi:10.1016/j.jim.2018.05.004

148 Le Gallo M, De La Motte Rouge T, Poissonnier A, *et al.* Tumor analysis: Freeze-thawing cycle of triple-negative breast cancer cells alters tumor CD24/CD44 profiles and the percentage of tumor-infiltrating immune cells. *BMC Res Notes* 2018;**11**:1–20. doi:10.1186/s13104-018-3504-5

149 Wherry EJ, Kurachi M. Molecular and cellular insights into T cell exhaustion. *Nat Rev Immunol* 2015;**15**:486–99. doi:10.1038/nri3862

150 Heylmann D, Badura J, Becker H, *et al.* Sensitivity of CD3/CD28-stimulated versus non-stimulated lymphocytes to ionizing radiation and genotoxic anticancer drugs: key role of ATM in the differential radiation response. *Cell Death Dis* 2018;**9**:1053. doi:10.1038/s41419-018-1095-7

151 Bull M, Lee D, Stucky J, *et al.* Defining blood processing parameters for optimal detection of cryopreserved antigen-specific responses for HIV vaccine trials. *J Immunol Methods* 2007;**322**:57–69. doi:10.1016/j.jim.2007.02.003

152 Tompa A, Nilsson-Bowers A, Faresjö M. Subsets of CD4 + , CD8 + , and CD25 hi Lymphocytes Are in General Not Influenced by Isolation and Long-Term Cryopreservation . *J Immunol* 2018;**201**:1799–809. doi:10.4049/jimmunol.1701409

153 Draxler DF, Madondo MT, Hanafi G, *et al.* A flowcytometric analysis to efficiently quantify multiple innate immune cells and T Cell subsets in human blood. *Cytom Part A* 2017;**91**:336–50. doi:10.1002/cyto.a.23080

154 Lemieux J, Jobin C, Simard C, *et al.* A global look into human T cell subsets before and after cryopreservation using multiparametric flow cytometry and two-dimensional visualization analysis. *J Immunol Methods* 2016;**434**:73–82. doi:10.1016/j.jim.2016.04.010

155 Elkord E. Frequency of human T regulatory cells in peripheral blood is significantly reduced by cryopreservation. *J Immunol Methods* Published Online First: 2009. doi:10.1016/j.jim.2009.06.001

156 Zebertavage LK, Alice A, Crittenden MR, *et al.* Transcriptional Upregulation of NLRC5 by Radiation Drives STING- and Interferon-Independent MHC-I Expression on Cancer Cells and T Cell Cytotoxicity. *Sci Rep* 2020;**10**:1–14. doi:10.1038/s41598-020-64408-3

157 Alice AF, Kramer G, Bambina S, *et al.* Amplifying IFN-γ Signaling in Dendritic Cells by CD11c-Specific Loss of SOCS1 Increases Innate Immunity to Infection while Decreasing Adaptive Immunity. *J Immunol* 2018;**200**:177–85. doi:10.4049/jimmunol.1700909

158 Chiossone L, Chaix J, Fuseri N, *et al.* Maturation of mouse NK cells is a 4-stage developmental program. *Blood* 2009;**113**:5488–96. doi:10.1182/blood-2008-10-187179

159 Komiya T, Huang CH. Updates in the clinical development of Epacadostat and other indoleamine 2,3-dioxygenase 1 inhibitors (IDO1) for human cancers. *Front Oncol* 2018;**8**:1–7. doi:10.3389/fonc.2018.00423

160 Van Dang C. The half-Lives of facts, paradigm shifts, and reproducibility in cancer research. *Cancer Res* 2018;**78**:4105–6. doi:10.1158/0008-5472.CAN-18-1751

161 Health NI of. Rigor and Reproducibility. https://www.nih.gov/research-training/rigor-reproducibility

162 Sivan A, Corrales L, Hubert N, *et al.* Commensal Bifidobacterium promotes antitumor immunity and facilitates anti-PD-L1 efficacy. *Science (80-)* 2015;**350**:1084–9. doi:10.1126/science.aac4255

163 Messmer MN, Kokolus KM, Eng JW-L, *et al.* Mild cold-stress depresses immune responses: Implications for cancer models involving laboratory mice. *Bioessays* 2014;**36**:884–91. doi:10.1002/bies.201400066

164 Bucsek MJ, Qiao G, MacDonald CR, *et al.* β-Adrenergic signaling in mice housed at standard temperatures suppresses an effector phenotype in CD8+T cells and undermines checkpoint inhibitor therapy. *Cancer Res* 2017;**77**:5639–51. doi:10.1158/0008-5472.CAN-17-0546

165 Moreno-Smith M, Lutgendorf SK, Sood AK. Impact of stress on cancer metastasis. *Future Oncol* 2010;**6**:1863. doi:10.2217/FON.10.142

166 Gouveia K, Hurst JL. Reducing Mouse Anxiety during Handling: Effect of Experience with Handling Tunnels. *PLoS One* 2013;**8**. doi:10.1371/journal.pone.0066401

167 Haddad TC, Yee D. Of mice and (Wo)men: Is this any way to test a new drug? *J Clin Oncol* 2008;**26**:830–2. doi:10.1200/JCO.2007.14.9062

168 Romani N, Flacher V, Tripp CH, *et al.* Targeting skin dendritic cells to improve intradermal vaccination. *Curr Top Microbiol Immunol* 2012;**351**:113–38. doi:10.1007/82_2010_118

169 Bonnotte B, Gough M, Phan V, *et al.* Intradermal injection, as opposed to subcutaneous injection, enhances immunogenicity and suppresses tumorigenicity of tumor cells. *Cancer Res* 2003;**63**:2145–9.

170 Joncker NT, Bettini S, Boulet D, *et al.* The site of tumor development determines immunogenicity via temporal mobilization of antigen-laden dendritic cells in draining lymph nodes. 2016;:609–18. doi:10.1002/eji.201545797

171 Naldaiz-Gastesi N, Bahri OA, López de Munain A, *et al.* The panniculus carnosus muscle: an evolutionary enigma at the intersection of distinct research fields. *J Anat* 2018;**233**:275–88. doi:10.1111/joa.12840

172 Bahri OA, Naldaiz-Gastesi N, Kennedy DC, *et al.* The panniculus carnosus muscle: A novel model of striated muscle regeneration that exhibits sex differences in the mdx mouse. *Sci Rep* 2019;**9**:1–15. doi:10.1038/s41598-019-52071-2

173 Wang XN, McGovern N, Gunawan M, *et al.* A three-dimensional atlas of human dermal leukocytes, lymphatics, and blood vessels. *J Invest Dermatol* 2014;**134**:965–74. doi:10.1038/jid.2013.481

174 Gibney GT, Weiner LM, Atkins MB. Predictive biomarkers for checkpoint inhibitor-based immunotherapy. *Lancet Oncol* 2016;**17**:e542–51. doi:10.1016/S1470-2045(16)30406-5

175 Rios-Doria J, Stevens C, Maddage C, *et al.* Characterization of human cancer xenografts in humanized mice. *J Immunother Cancer* 2020;**8**:1–8. doi:10.1136/jitc-2019-000416

176 Stroup DF, Smith CK, Truman BI. Reporting the methods used in public health research

and practice. *J Public Heal Emerg* 2017;**1**:89–89. doi:10.21037/jphe.2017.12.01

177 Abès R, Héritier S, Dutertre CA, *et al.* Immune control of tumors: Host immune response and antibody-based immunotherapy. *Intern Med Clin Lab* Published Online First: 2007. doi:10.1016/j.biopha.2008.07.066

178 Marabelle A, Kohrt H, Caux C, *et al.* Intratumoral immunization: A new paradigm for cancer therapy. *Clin Cancer Res* 2014;**20**:1747–56. doi:10.1158/1078-0432.CCR-13-2116

179 Cavallo F, De Giovanni C, Nanni P, *et al.* 2011: the immune hallmarks of cancer. *Cancer Immunol Immunother* 2011;**60**:319–26.

180 Demaria S, Bhardwaj N, McBride WH, *et al.* Combining radiotherapy and immunotherapy: A revived partnership. *Int J Radiat Oncol Biol Phys* 2005;**63**:655–66. doi:10.1016/j.ijrobp.2005.06.032

181 Kroemer G, Galluzzi L, Kepp O, *et al.* Immunogenic Cell Death in Cancer Therapy. *Annu Rev Immunol* Published Online First: 2013. doi:10.1146/annurev-immunol-032712-100008

182 Hlavata Z, Solinas C, De Silva P, *et al.* The Abscopal Effect in the Era of Cancer Immunotherapy: a Spontaneous Synergism Boosting Anti-tumor Immunity? *Target Oncol* 2018;**13**:113–23. doi:10.1007/s11523-018-0556-3

183 Siva S, Macmanus MP, Martin RF, *et al.* Abscopal effects of radiation therapy: A clinical review for the radiobiologist. *Cancer Lett* 2015;**356**:82–90. doi:10.1016/j.canlet.2013.09.018

184 Demaria S, Formenti SC. Role of T lymphocytes in tumor response to radiotherapy. *Front Oncol* 2012;**2 AUG**:1–7. doi:10.3389/fonc.2012.00095

185 Palma DA, Salama JK, Lo SS, *et al.* The oligometastatic state-separating truth from wishful thinking. Nat. Rev. Clin. Oncol. 2014. doi:10.1038/nrclinonc.2014.96

186 Reyes DK, Pienta KJ. The biology and treatment of oligometastatic cancer. *Oncotarget* Published Online First: 2015. doi:10.18632/oncotarget.3455

187 Ersahin D, Doddamane I, Cheng D. Targeted radionuclide therapy. *Cancers (Basel)* 2011;**3**:3838–55. doi:10.3390/cancers3043838

188 Pinchuk AN, Rampy MA, Longino MA, *et al.* Synthesis and structure-activity relationship effects on the tumor avidity of radioiodinated phospholipid ether analogues. *J Med Chem* 2006;**49**:2155–65. doi:10.1021/jm050252g

189 Weekes SL, Barker B, Bober S, *et al.* A multicompartment mathematical model of cancer stem cell-driven tumor growth dynamics. *Bull Math Biol* 2014;**76**:1762–82. doi:10.1007/s11538-014-9976-0

190 Retsky MW, Swartzendruber DE, Wardwell RH, *et al.* Is Gompertzian or exponential kinetics a valid description of individual human cancer growth? *Med Hypotheses* 1990;**33**:95–106. doi:10.1016/0306-9877(90)90186-I

191 Laajala TD, Corander J, Saarinen NM, *et al.* Improved statistical modeling of tumor growth and treatment effect in preclinical animal studies with highly heterogeneous responses in vivo. *Clin Cancer Res* 2012;**18**:4385–96. doi:10.1158/1078-0432.CCR-11-

3215

192 Loizides C, Iacovides D, Hadjiandreou MM, *et al.* Model-based tumor growth dynamics and therapy response in a mouse model of de novo carcinogenesis. *PLoS One* 2015;**10**:1–18. doi:10.1371/journal.pone.0143840

193 Siegel RL, Miller KD, Jemal A. Cancer statistics. *CA Cancer J Clin* 2016;**66**:7–30. doi:10.3322/caac.21332.

194 Miller KD, Siegel RL, Lin CC, *et al.* Cancer treatment and survivorship statistics, 2016. *CA Cancer J Clin* 2016;**66**:271–89. doi:10.3322/caac.21349

195 Al-Helou G, Temesgen N, Gwizdala J, *et al.* Metastatic primary pulmonary melanoma successfully treated with checkpoint inhibitors. *BMJ Case Rep* 2018;**2018**. doi:10.1136/bcr-2017-223025

196 Palma DA, Olson R, Harrow S, *et al.* Stereotactic ablative radiotherapy versus standard of care palliative treatment in patients with oligometastatic cancers (SABR-COMET): a randomised, phase 2, open-label trial. *Lancet* 2019;**393**:2051–8. doi:10.1016/S0140-6736(18)32487-5

197 Ravi Patel, Reinier Hernandez, Peter Carlson, Ryan Brown, Luke Zangl, Amber Bates, Ian Arthur, Justin Jagodinsky, Joseph Grudinski, Amy Erbe, Jamey Weichert, Paul Sondel ZM. Mechanistic insights into combination low dose targeted radionuclide and checkpoint blockade treatment to turn a 'cold' tumor 'hot'. *J Immunother Cancer* 2019;**7**.https://jitc.biomedcentral.com/articles/10.1186/s40425-019-0764-0

198 Liu S, Cheung E, Ziegler MC, *et al.* 90 Y and 177 Lu Labeling of a DOTA-Conjugated Vitronectin Receptor Antagonist Useful for Tumor Therapy. Published Online First: 2001. doi:10.1021/bc000146n

199 Jadvar H. Targeted radionuclide therapy: An evolution toward precision cancer treatment. *Am J Roentgenol* 2017;**209**:277–88. doi:10.2214/AJR.17.18264

200 Bednarz B, Grudzinski J, Marsh I, *et al.* Murine-specific Internal Dosimetry for Preclinical Investigations of Imaging and Therapeutic Agents. *Health Phys* 2018;**114**:450–9. doi:10.1097/HP.0000000000000789

201 Golden EB, Apetoh L. Radiotherapy and Immunogenic Cell Death. *Semin Radiat Oncol* 2015;**25**:11–7. doi:10.1016/j.semradonc.2014.07.005

202 Schaue D. A century of radiation therapy and adaptive immunity. *Front Immunol* 2017;**8**:1–15. doi:10.3389/fimmu.2017.00431

203 Mueller SN, Gebhardt T, Carbone FR, *et al.* Memory T cell subsets, migration patterns, and tissue residence. Annu. Rev. Immunol. 2013. doi:10.1146/annurev-immunol-032712-095954

204 Yona S, Kim KW, Wolf Y, *et al.* Fate Mapping Reveals Origins and Dynamics of Monocytes and Tissue Macrophages under Homeostasis. *Immunity* Published Online First: 2013. doi:10.1016/j.immuni.2012.12.001

205 Ensley JF, Maciorowski Z, Pietraszkiewicz H, *et al.* Solid tumor preparation for flow cytometry using a standard murine model. *Cytometry* 1987;**8**:479–87. doi:10.1002/cyto.990080508

206 Naidoo J, Page DB, Wolchok JD. Immune Checkpoint Blockade. Hematol. Oncol. Clin. North Am. 2014. doi:10.1016/j.hoc.2014.02.002

207 Jackson SS, Schmitz JE, Kuroda MJ, *et al.* Evaluation of CD62L expression as a marker for vaccine-elicited memory cytotoxic T lymphocytes. *Immunology* 2005;**116**:443–53. doi:10.1111/j.1365-2567.2005.02243.x

208 Krzykawska-Serda M, Ho JCS, Ware MJ, *et al.* Ultrasound Doppler as an Imaging Modality for Selection of Murine 4T1 Breast Tumors for Combination Radiofrequency Hyperthermia and Chemotherapy. *Transl Oncol* Published Online First: 2018. doi:10.1016/j.tranon.2018.04.010

209 Kadić E, Moniz RJ, Huo Y, *et al.* Effect of cryopreservation on delineation of immune cell subpopulations in tumor specimens as determinated by multiparametric single cell mass cytometry analysis. *BMC Immunol* 2017;**18**:1–15. doi:10.1186/s12865-017-0192-1

210 Lechner MG, Karimi SS, Barry-Holson K, *et al.* Immunogenicity of murine solid tumor models as a defining feature of in vivo behavior and response to immunotherapy. *J Immunother* Published Online First: 2013. doi:10.1097/01.cji.0000436722.46675.4a

211 Crittenden MR, Zebertavage L, Kramer G, *et al.* Tumor cure by radiation therapy and checkpoint inhibitors depends on pre-existing immunity. *Sci Rep* 2018;**8**:1–15. doi:10.1038/s41598-018-25482-w

212 Knutson KL, Disis ML. Tumor antigen-specific T helper cells in cancer immunity and immunotherapy. Cancer Immunol. Immunother. 2005. doi:10.1007/s00262-004-0653-2

213 Balkhi MY, Ma Q, Ahmad S, *et al.* T cell exhaustion and Interleukin 2 downregulation. *Cytokine* 2015;**71**:339–47. doi:10.1016/j.cyto.2014.11.024

214 Abdelwahab MG, Sankar T, Preul MC, *et al.* Intracranial implantation with subsequent 3D in vivo bioluminescent imaging of Murine gliomas. *J Vis Exp* Published Online First: 2011. doi:10.3791/3403

215 Besemer AE, Yang YM, Grudzinski JJ, *et al.* Development and Validation of RAPID: A Patient-Specific Monte Carlo Three-Dimensional Internal Dosimetry Platform. *Cancer Biother Radiopharm* 2018;**33**:155–65. doi:10.1089/cbr.2018.2451

216 Sprangers S, Vries TJD, Everts V. Monocyte Heterogeneity: Consequences for Monocyte-Derived Immune Cells. *J Immunol Res* 2016;**2016**. doi:10.1155/2016/1475435

217 Gebhardt T, Palendira U, Tscharke DC, *et al.* Tissue-resident memory T cells in tissue homeostasis, persistent infection, and cancer surveillance. *Immunol Rev* 2018;**283**:54–76. doi:10.1111/imr.12650

218 Gilkes DM, Wirtz D. Hypoxia and extracelluar matrix:drivers of tumor metastasis. *Nat Rev Cancer* 2014;**14**:430–9. doi:10.1038/nrc3726.Hypoxia

Appendix A

Cellular and molecular characterization of tumors treated with RT + IC *in situ* vaccine with and without additional radiation

A.1 Overview

This appendix contains additional work in progress that is relevant to the work presented in Chapter 4 of this thesis. As described in Chapter 4, RT+IC *in situ* vaccine plus 12Gy external beam RT resulted in slower growth rates at both the primary and secondary tumors compared to either treatment alone. In addition, ^{90}Y-NM600 given along with RT+IC *in situ* vaccine extended survival, but did not substantially impact tumor growth rates, compared to either treatment alone. As mentioned in Chapter 5 of this thesis, additional studies are required to determine the extent and nature of the immune response in these settings, both at the treated primary and the radiated secondary tumors. In this appendix, data acquired by flow cytometry will be presented that characterizes changes to the immune tumor microenvironment (TME). Data will also be presented quantifying the cytokine content in tumor homogenates. In addition, data will be presented quantifying the relationship between tumor volume or tumor number and uptake of the ^{90}Y-NM600 TRT agent, which was used to confirm previous dosimetry findings. It should be noted that these data are preliminary and are under further investigation in preparation for inclusion in a manuscript along with data presented in Chapter 4 of this thesis.

A.2 Materials and Methods

Study Design

This appendix contains data and analyses derived from two experiments:

1) In one experiment, mice bearing multiple equally sized B78 tumors, and mice bearing a single B78 tumor with a range of volumes were injected with ^{90}Y-NM600, and tissues were harvested to measure *ex vivo* drug uptake and distribution. Some of the mice injected in that study were instead injected with ^{86}Y-NM600, and serially imaged using PET/CT for dosimetry studies. The purpose of the study was to characterize how uptake of the TRT agent changed as a function of tumor burden.

2) In the second experiment, mice bearing a ~150mm^3 B78 primary tumor in the right flank and a ~150mm^3 tumor in the left flank were generated. N=10 mice each were assigned to receive PBS, 12Gy RT to both tumors, 100μCi of ^{90}Y-NM600, RT/IC to the primary tumor, RT/IC to the primary plus 100μCi of ^{90}Y-NM600, or RT/IC to the primary plus 12Gy RT to the secondary tumor. 14 days after treatment, N=5 mice per group were randomly selected for analysis by flow cytometry, and the other 5 mice per group were used for cytokine analysis. The purpose of the study was to characterize changes to the TME in response to RT/IC at the primary and secondary tumors, and characterize how those changes are affected by 1) additional external beam RT and 2) additional TRT. The analysis of these groups is divided into two parts, one focusing on the effect of external beam RT combined with RT/IC, and one focusing on the effect of TRT combined with RT/IC.

These studies will be described in further detail below. Some of the methods presented in this appendix are sourced from the manuscript “Low-dose targeted radionuclide therapy renders immunologically “cold” tumors responsive to immune checkpoint blockade” by R. Patel et al, found in Appendix B of this thesis. Other components of these methods are sourced from chapters 2-4 of this thesis.

Syngeneic tumor cell line

B78-D14 (B78) murine melanoma is a cell line derived from B16-F10 melanoma, as previously described. This cell line was generously provided by Ralph Reisfeld at the Scripps Research Institute. Cells were cultured in RPMI 1640 (Mediatech, Inc, Manassas, VA)

supplemented with 10% fetal bovine serum, 100U/mL penicillin, 100µg/mL streptomycin, and 2mM L-glutamine as described this thesis.

Animal studies and tumor models

Animals used in this study were housed and cared for using an approved protocol reviewed by the University of Wisconsin-Madison Institutional Animal Care and Use Committee (IACUC). Female, 6-8 week old C57BL/6 mice were ordered from Taconic Biosciences (Rensselaer, NY) and allowed to acclimate in our animal facility for at least one week following arrival. Tumors were engrafted by injecting $2x10^6$ B78 cells in 100µL intradermally in the flank using a 26g needle. Mice bearing two tumors had a second tumor implanted in the left flank. Mice bearing four tumors had a right and left flank ,and a right and left shoulder injection. To generate tumors with a range of volumes, tumors were implanted 6, 4, and 2 weeks before the initiation of treatment. Tumor volume for all experiments was measured using calipers and approximated as $(width^2 \times length)/2$.

External beam radiation and molecularly targeted radiation preparation and administration

External beam radiation was delivered using an X-RAD 320 system (Precision X-Ray Inc, North Branford, CT). Mice were immobilized using custom lead jigs and surgical tape such that only the dorsal right flank is exposed, with the rest of the mouse (including the contralateral flank and spleen) shielded. To deliver external beam radiation dose to the secondary tumor on the left flank, at the same time that the primary (right flank) tumor is irradiated, lead shields were left off of the mouse's left flank during the radiation.

$^{90}YCl_3$ was purchased from Perkin Elmer (Waltham, MA). The alkylphosphocholine molecule used for molecular targeted radionuclide therapy, NM600, was kindly provided by Archeus Technologies (Madison, WI). ^{90}Y-NM600 and its counterpart, ^{86}Y-NM600 were prepared as previously described (see appendix B2 for detailed methodology and [127]). Mice

receiving EBRT were radiated on treatment day 0, and mice receiving TRT were injected with 100μCi of ^{90}Y-NM600 preparation by tail vein injection on treatment day 0. Mice receiving ^{86}Y-NM600 for imaging studies were given 250μCi by tail vein injection.

Immunotherapy preparation and administration

Immunocytokine (IC, hu14.18-IL2) was provided in lyophilized form (4mg/vial) by Apeiron Biologics (Vienna, Austria). It was reconstituted by adding 8mL of sterile PBS for a working concentration of 0.5mg/mL. For mice being treated with RT+IC, 100μL of the 0.5mg/mL IC solution was injected intratumorally (IT) daily on treatment days 6 through 10, for a total dose of 250μg per mouse, as described in Chapters 2-4.

Imaging and bio-distribution.

Mice bearing B78 tumors for imaging were scanned using serial CT (80 kVp; 1000 mAs; 220 angles) and 80 million coincidence events static PET scans (time window: 3.432 ns; energy window: 350-650 keV) were acquired with an Inveon microPET/microCT scanner (Siemens Medical Solutions, Knoxville, TN) at 3, 24, 48, and 72 hours post injection of ^{86}Y-NM600. Static PET scans were reconstructed using a three-dimensional ordered subset expectation maximization (OSEM3D) algorithm. CT images were employed for attenuation correction, anatomical referencing, and to generate density maps for the dosimetry estimations. Region-of-interest analysis of the PET images was performed to determine the magnitude and kinetics of ^{86}Y-NM600 uptake in the tumor and normal tissues of interest. Quantitative data were expressed as percent injected activity per gram of tissue (%IA/g; mean ± SD). For mice harvested for *ex* vivo biodistribution, mice were euthanized by CO_2 asphyxiation. Tumors and normal tissue specimens were collected, wet-weighed, radioactivity counted in an automated β-

counter, and the %IA/g (mean ± SD) corresponding to each tissue was calculated with decay correction.

Tumor Dosimetry Calculations.

Subject-specific tumor dosimetry for ^{90}Y-NM600 TRT was estimated using the Radiopharmaceutical Assessment Platform for Internal Dosimetry (RAPID) [215]. The theranostic dosimetry approach in this work utilized serial ^{86}Y-NM600 microPET/CT imaging to estimate the biodistribution of ^{90}Y-NM600 over time, correcting for the different rates of radioactive decay. PET and CT volumes at each time point were used to define the source and geometry distributions, respectively, in Monte Carlo (Geant4 v9.6) simulations. Contours for tumor and organs of interest were delineated on the anatomic CT images and used to quantify the *in vivo* pharmacokinetics of NM600 as well as characterize the spatial distribution of absorbed dose imparted by ^{90}Y-NM600 TRT. The cumulative absorbed dose in each region of interest was calculated by integrating the mean absorbed dose rate at each timepoint using a hybrid trapezoidal-exponential model of the time-dose-rate curves. The processing of PET/CT image volumes and generation of 3D cumulative absorbed dose distributions (0.42 x 0.42 x 0.42 mm) in the RAPID (Radiopharmaceutical Assessment Platform for Internal Dosimetry) software package were previously described in detail [200].

Flow Cytometry

At the time of harvest, mice were euthanized by CO_2 asphyxiation, and the tumor was dissected out. The tumor was cut into ~5mm fragments, and added to gentleMACS C tubes (Miltenyi Biotec, Bergish Gladbach, Germany) containing 2.5 mL of RPMI 1640 with 5μg/mL brefeldin A (Biolegend, cat 420601). 100μL of DNAse I solution in RPMI 1640 (2.5mg/mL,

Sigma-Aldrich, St. Louis, MO) and 100µL collagenase IV solution in RPMI 1640 (25mg/mL, Gibco, Life Technologies, Grand Island, NY) were then added, and the samples were disaggregated using a GentleMACS octodissocator (Miltenyi Biotec, Bergish Gladbach, Germany) using the preset dissociation protocol “37C_m_TDK1” for mouse tumor dissociations. Sample dissociate was filtered through a 70µm cell strainer, washed with 10mL of cold PBS, and stained according to the novel flow cytometry protocol described in Chapter 2 of this thesis. Staining was conducted in two panels; the antibodies for each panel are detailed in Table A.1 of this appendix. Samples remained in -80°C storage behind radioactive shielding until 30 days past treatment injection.

Samples were acquired on an Attune™ NxT flow cytometer (Thermo Fischer, Waltham, MA) with manufacturer provided acquisition software. This cytometer was equipped with the following excitation lasers: 488nm (BL), 561nm (YL), 405m (VL), and 633nm (RL). The cytometer was equipped with the following channel/bandpass filter combinations: BL1 (530/30), BL2 (590/40), BL3 (695/40), YL1 (585/16), YL2 (620/15), YL3 (695/40), YL4 (780/60), VL1 (440/50), VL2 (512/25), VL3 (603/48), VL4 (710/50), RL1 (670/14), RL2 (720/30), and RL3 (780/60). Of note, staining panels that used BV711 used the 710/50 filter on VL4, and staining panels that used BV785 required substituting the 710/50 filter on VL4 with a 780/60 filter. All flow cytometry experiments included Fluorescence Minus One controls used for setting gates. Data were analyzed using the FCS Express 7 software (De Novo Software, Pasadena, CA) platform.

Cytokine Multiplex Immunoassay.

Tumors were harvested, weighed, and 5 µl/mg of Cell Lysis Buffer with PMSF (Cell Signaling Technology) and Halt™ Phosphatase Inhibitor Cocktail (Thermo Scientific) was added to the tumor lysate. Tumors were frozen at -80°C until decay to background

(30 days post-injection). The tumors were homogenized using a Bead Mill Homogenizer (Bead Ruptor Elite, Omni International Cat # 19-040E). A multiplex immunoassay was used to determine the concentration of 32 cytokines and chemokines in the tumor lysates (MILLIPLEX MAP Mouse Cytokine/Chemokine Magnetic Bead Panel, Millipore) following the manufacturer's instructions. The multiplex plate was read on the MAGPIX System (Millipore) and the protein concentrations were interpolated from curves constructed from the protein standards and their respective median fluorescence intensity (MFI) readings (Milliplex Analyst, Millipore).

A.3 Results

Immunophenotyping changes in tumors treated by combination RT/IC and external beam RT

To characterize the changes to the TME following treatment with RT/IC and additional RT to a secondary tumor in models of two-tumor mice, a comprehensive pair of immunophenotyping panels was conducted on mice bearing two equally sized B78 tumors treated with PBS, 12Gy RT to both tumors, RT/IC to the primary tumor only, and RT/IC to the primary plus 12Gy RT to the secondary tumor. Tumors were harvested on treatment day 14 for analysis. Results demonstrate increased infiltration of $CD45^+$ haematopoietically-derived immune cells in both the primary and secondary tumors following treatment with either RT/IC or RT/IC + 12Gy RT (Figure A.1A). CD45+ infiltration was also trending higher in secondary tumors receiving RT/IC + 12Gy RT compared to RT/IC secondaries, and was statistically higher than the RT alone group. $CD8^+$ cytotoxic T lymphocytes and CD4+ non-T_{reg} cells were higher in the primary tumor in the RT/IC + 12Gy group compared to PBS (Figure A.1B and A1.C). Secondary tumors treated with RT/IC + 12Gy had higher CD8+ infiltration compared to all three other groups, but no significant change was detected for $CD4^+$ non-T_{reg} cells in secondary tumors. T_{reg} content was substantially affected by both radiation and *in situ* vaccination (Figure

A1.D). Both primary and secondary tumors treated with 12Gy RT only had increased T_{reg} content compared to PBS. Primary Tumors treated with RT/IC (regardless of RT dose to the secondary tumor) had a substantially lower T_{reg} content compared to The RT alone group (12Gy + 12Gy). RT delivered to the secondary tumor in the setting of RT/IC delivered to the primary tumor resulted in increased T_{reg} content (compared to PBS), but not as increased as the RT alone group. The increase in CD8+ and CD4+ T cell content combined with the decrease in T_{reg} content resulted in substantially increased CD8:T_{reg} (Figure A.1E) and CD4 effector : CD4 T_{reg} (Figure A1.F) ratios in the RT/IC and the RT/IC + 12Gy groups in the primary and secondary tumors compared to RT only and PBS control groups, though the treated primary tumors experienced a substantially greater increase in these ratios compared to secondary tumors. No difference in NK cell content was detected among primary tumors, though secondary tumors in mice treated with RT/IC had a substantially greater NK cell content compared to all other groups (Figure A1.H). NKT cells were increased in the primary and secondary tumors of mice treated with RT/IC + 12Gy compared to RT alone or PBS controls (Figure A1.I). This increase was also detected in the secondary tumors of mice treated with RT/IC alone.

Changes in innate immune cells were also detected in the TME following treatment. Neutrophil/MDSC content was increased in the primary tumors of mice treated with RT/IC, though only secondary tumors in mice treated with RT/IC alone had greater neutrophil/MDSC content (Figure A2.A). The primary and secondary tumors in mice treated with RT/IC + 12Gy had increased macrophage content compared to the RT/IC group (Figure A.2B). After excluding neutrophils and macrophages, cells can be divided into $CD11b^{+}Ly6C^{+}$ “classical” monocytes and DC precursors, and $CD11b^{+}Ly6C^{-}$ “nonclassical” monocytes and DC precursors [216]. Infiltration of the $CD11b^{+}Ly6C^{+}$ classical monocyte family of innate cells was increased in primary tumors treated with RT/IC + 12Gy compared to the PBS, RT only, and RT/IC only groups. Infiltration in the secondary tumors was increased in the RT/IC only group, and to a

lesser extent the RT/IC + 12Gy group when compared to the PBS group (Figure A.2C). The $CD11b^{+}Ly6C^{-}$ nonclassical monocyte family was decreased compared to the PBS group in primary tumors in the RT/IC only and RT/IC + 12Gy groups. No substantial change in the secondary tumors was noted save for a slight (but statistically significant) decreased infiltration in the RT/IC +12Gy group compared to RT only, but not compared to PBS (Figure A.2D). Both classical type 1 and 2 dendritic cells had no apparent change in primary tumors, and treatment may slightly decrease infiltration in secondary tumors for mice treated with RT/IC or RT/IC+12Gy (Figure A.2E and A.2F). Infiltration of monocyte derived DCs is lower in primary tumors treated with RT/IC or RT/IC +12Gy compared to PBS, and lower in secondary tumors treated with RT/IC or RT/IC +12Gy compared to RT alone (Figure A2.G).

Activation of lymphocytes and NK cells in tumors treated by combination RT/IC and external beam RT

Expression of the high affinity IL2 receptor CD25, the exhaustion marker PD1, and the effector cytokine IFNγ were measured as part of the adaptive flow cytometry panel (Figure A.3). Among $CD8^{+}$ T cells, primary tumors treated with both RT/IC and RT/IC + 12Gy had higher expression of CD25 compared to either PBS or RT alone, and no differences were detected among secondary tumors (Figure A.3A). Higher expression of CD25 in primary tumors, but not in secondary tumors, was also observed in NK cells, (Figure A.3G) and NKT cells (Figure A3.I) for the RT/IC + 12Gy group vs. the PBS and RT alone groups. $CD4^{+}$ non-T_{reg} cells had a slightly larger expression of CD25 in primary tumors treated with RT/IC + 12Gy compared to PBS, and no detectable difference compared to PBS in secondary tumors (Figure A3.D). $CD8^{+}$ T cells also had higher expression of IFNγ in primary tumors treated with RT/IC + 12Gy compared to PBS and RT alone. No change in IFNγ expression among $CD8^{+}$ T cells in secondary tumors was detected compared to PBS alone (Figure A3.C). This pattern was also

observed in NK cells (Figure A3.H) and NKT cells (Figure A3.J). In $CD4^+$ non-T_{reg} cells, primary tumors treated with RT/IC and RT/IC + 12Gy had greater expression of IFNγ compared to either PBS or RT only controls, and no difference was detected among secondary tumors (Figure A.3F). Among $CD8^+$ T cells in the primary and secondary tumor, all conditions had lower PD1 expression compared to PBS. Primary tumors in mice treated with RT/IC and RT/IC + 12Gy had even lower PD1 expression that RT alone (Figure A.3B). Secondary tumors in mice treated with RT/IC only had the lowest PD1 expression, and secondary tumors in mice treated with RT/IC + 12Gy had no change in PD1 expression compared to RT alone, though still lower than the PBS control. Among $CD4^+$ T_{regs} PD1 expression was lower in all 3 groups of treated primary tumors compared to PBS control, and was lower than PBS in secondary tumors in the groups receiving RT/IC and RT/IC + 12Gy (Figure A3.E).

To characterize the degree of maturity among lymphocytes in both primary and secondary tumors, the fraction of lymphocytes expressing PD1 and CD103 were determined. PD1 is increased on exhausted T cells in response to chronic antigen exposure [134]. CD103 is expressed on tissue resident memory lymphocytes, which differentiate from activated effector lymphocytes over time in the target tissue [217]. Among $CD4^+$ non-T_{reg} lymphocytes, distribution of PD1+ and CD103+ cells shifted in response to treatment (Figure A.4). The fraction of $CD4^+$ non-T_{reg} cells expressing both CD103 and PD1 in the RT/IC and in the RT/IC + 12Gy groups was substantially decreased in both the primary and secondary tumors compared to PBS, and also decreased in the primary group compared to RT alone (Figure A4.D). Secondary tumors treated with RT/IC + 12Gy did not experience as large of a decrease in proportion of PD1+/CD103+ cells compared to RT/IC alone. This decrease for the RT/IC and RT/IC + 12Gy groups in Figure A4.D was accompanied by a subsequent increase in the PD1 negative, CD103 negative population in both primary and secondary tumors (Figure A4.E). Again, secondary

tumors treated with RT/IC + 12Gy did not experience as large of an increase in proportion compared to RT/IC alone.

Detection of cytokines in tumors treated by combination RT/IC and external beam RT

To more fully characterize the nature of the immune response following treatment, primary tumors treated with PBS, RT only, RT/IC to the primary, and RT/IC to the primary plus 12Gy to the secondary were harvested, homogenized, and analyzed by a multiplex bead kit for expression of 32 different cytokines and chemokines (Figure A.5). Any cytokines or chemokines for which the coefficient of variance (CV) in concentration for all samples was less than 10% were excluded from analysis, resulting in 19 different parameters for which there was substantial change in response to treatment effect. Figure A.5 presents these cytokines for both primary and secondary tumors in detail. These results are presented in 4 separate panels separated by the broad function of the cytokines or chemokines in the panels: 1)Pan-Activating, 2) NK cell and $CD8^+$ T cell focused, 3) IFNγ, T helper cell focused, and 4) Macrophage/Monocyte/Neutrophil focused. Cytokines of note include IFNγ, which is increased in primary and secondary tumors in the RT/IC and RT/IC + 12Gy groups compared to PBS and RT only controls. Other cytokines including IL-5 and IL-4 also seem to follow this pattern, although the differences were less significant for IL-4. Expression of the pan-activating cytokines IL-1β and TNFα were increased in primary, but not secondary, tumors in the RT/IC and RT/IC + 12Gy groups. Some cytokines that activate innate phagocytes and monocytes, including G-CSF, GM-CSF, and M-CSF, all demonstrated increased expression in primary tumors in the RT/IC and RT/IC + 12Gy groups. In many of the innate-focused cytokines including GM-CSF, KC, MIP1α, and MIP1β, RT alone increased expression as well as RT/IC and RT/IC + 12Gy.

Taken together, these flow cytometry and cytokine data suggest that treatment with RT/IC *in situ* vaccine, with and without additional RT to the secondary tumor, results in substantial alterations to the tumor immune microenvironment, both in adaptive and innate effector arms. These changes broadly include increased lymphocyte content, increased lymphocyte effector : T_{reg} suppressor ratios, increased NKT cell content, increased neutrophils, and increased monocyte precursors in primary tumors treated with both RT/IC and RT/IC + 12Gy. These increases in primary tumors also translate somewhat to secondary tumors, but to a much lower degree. These tumor infiltrating lymphocytes tend to have higher CD25 expression, higher IFNγ expression, and lower PD1 expression in primary tumors treated with both RT/IC and RT/IC + 12Gy, but only decreased PD1 expression in the secondary tumors. T cells appeared to shift from a PD1+CD103+ to a PD1-CD103- phenotype in both primary and secondary tumors treated with both RT/IC and RT/IC + 12Gy. These changes are accompanied by substantially increased cytokine and chemokine expression across several cell types, including cytokines known to be pan-activating, as well as having predominant effects on NK cells, $CD8^+$ T cells, CD4+ T cells, and macrophages/monocytes/neutrophils.

^{90}Y-NM600 TRT uptake is consistent regardless of tumor volume or number, and can deliver immunomodulatory doses to all tumor environments

In order to be used to modulate the *collective* TME and improve response to immunotherapy, the TRT agent under consideration in this thesis, NM600, must be able to distribute comparable doses of radiation to all sites of disease. Because the agent is retained by tumor cells preferentially over non-tumor tissue, it stands to reason that larger tumors, with more tumor cells, can retain and concentrate more TRT agent. If the tumor had one large tumor and several smaller tumors, the large tumor may act as a “sink” and absorb TRT agent such that much less is available to the smaller distant tumors. Therefore, we used ^{86}Y-NM600 serial

PET/CT scans and ^{90}Y-NM600 *ex vivo* dosimetry to investigate whether uptake of TRT agent changed as a function of 1) tumor volume and 2) tumor number. Mice bearing either one, two, or four ~100mm^3 B78 tumors (5 mice per group) were generated, as described in the materials and methods section. Concurrently, using a staggered injection approach, mice bearing a single B78 tumor with target volumes of 50, 100, 300, and 500mm^3 (5 mice per group) were generated. All mice were injected with 100μCI of ^{90}Y-NM600 by tail vein injection. After 48 hours, tumors and tissue were harvested, weighed, and residual radioactivity was counted using a beta counter. After correcting for decay, the uptake of TRT agent was calculated as the percent of the injected dose per gram of tissue (%ID/g). Results demonstrated that there was no change in NM600 uptake at 48 hours between the individual tumors in one-tumor, two-tumor, and four-tumor bearing mice (Figure A.6H). Results also indicated that uptake was relatively consistent as a function of tumor volume, at approximately 6% ID/g with the exception of the smallest tumors (~50mm^3) which did appear to have an increased uptake at around 12% ID/g (Figure A.6I). Regardless of tumor volume, there was no relationship between tumor uptake and uptake in non-tumor tissues including the blood and the spleen (Figure A.6J and A.6K) this suggests that drug was not being diverted from other pool sources, and that there is adequate distribution of drug to achieve similar uptake regardless of disease burden (and perhaps even higher uptake in very small tumors, potentially reflecting greater blood perfusion in all tumor tissue for smaller tumors).

To measure the kinetics of drug uptake and dose distribution over time, serial PET/CT scans were obtained after injection of 250μCI ^{86}Y-NM600 into five mice with ~150mm^3 primary and ~50mm^3 secondary tumor volumes as described in the materials and methods section. Using monte carlo based simulations, the uptake of drug and absorbed dose delivered to each tumor was calculated at 3, 24, 48, and 72 hours post-injection. Results demonstrate that uptake in both the primary and secondary tumor peaks around 24-48 hours post injection, and that the

smaller secondary tumor had a slightly higher uptake than the primary, though not statistically significant (Figure A.6G). Estimation of dose delivered to the tumor as a function of injected activity also demonstrate no difference between the ~150mm^3 primary tumors and the ~50mm^3 secondary tumors (Figure A.6F). Taken together, this experiment suggests that it is possible to use NM600 to deliver TRT to mice bearing multiple tumors, and that the degree of tumor burden does not substantially alter the uptake or dosimetry of NM600.

Immunophenotyping changes in tumors treated by combination RT/IC and ^{90}Y-NM600 TRT

To characterize the changes to the TME following treatment with RT/IC and TRT to a secondary tumor in models of two tumor mice, a comprehensive pair of immunophenotyping panels was conducted (Figures A.7 and A.8). Concurrent with the previously described experiment, mice treated with 100μCi of ^{90}Y-NM600 only, and mice treated with RT/IC to the primary tumor and 100μCi of ^{90}Y-NM600 were included in the experiment, with the PBS and RT/IC only groups shared between these two analyses. As such, the results corresponding to the RT/IC group will not be repeated here, except for in comparison to the RT/IC + TRT group. Results from this initial analysis suggest higher CD45+ immune cells in the TRT, RT/IC, and RT/IC + TRT groups compared to PBS control in both primary and secondary tumors, though only the RT/IC treated tumors among the primary tumors reached statistical significance (Figure A.7A) and only the RT/IC and RT/IC +TRT groups were significant in the secondary tumors. There was a slight increase in CD8+ T cells in the secondary tumors treated with RT/IC plus TRT (Figure A.7B). Primary tumors treated with RT/IC + TRT had the same decrease in T_{reg} infiltration compared to PBS as RT/IC, and no changes were detected in T_{reg} content among secondary tumors, including the TRT only control (Figure A.7D). The CD8+ T cell : T_{reg} cell ratio was increased in both primary and secondary tumors in the RT/IC + TRT group compared to the PBS and TRT only groups, and was no different than the RT/IC alone group (Figure A.7E). This

same pattern (in Figure A.7E) was observed in the primary tumors for the CD4+ effector T cell : T_{reg} cell ratio; this CD4+ effector T cell : T_{reg} cell ratio in secondary tumors is elevated only for the RT/IC alone group compared to PBS and TRT alone (Figure A7.F). Like the RT/IC alone group, NK cells were increased in the secondary tumor of mice treated with RT/IC + TRT compared to PBS or TRT alone while no difference was detected among primary tumors for NK cells (Figure A.7H). Both primary and secondary tumors had increased infiltration of NKT cells in mice treated with RT/IC + TRT, when compared to PBS or TRT alone (Figure A.7I).

Changes in innate immune cells were also detected in the TME following treatment. Neutrophil/MDSC content was increased in the primary tumors of mice treated with RT/IC + TRT, though only secondary tumors in mice treated with RT/IC alone had greater neutrophil/MDSC content (Figure A8.A). Primary tumors treated with TRT only had significantly greater macrophage infiltration compared to all other groups at the primary tumor (Figure A.8B). Primary tumors treated with RT/IC + TRT had greater infiltration of $CD11b^{+}Ly6C^{+}$ classical monocyte family cells compared to either PBS or TRT alone, and had greater infiltration compared to PBS alone in the secondary tumors (Figure A.8C). Primary tumors treated with RT/IC + TRT had lower infiltration of $CD11b^{+}Ly6C^{-}$ nonclassical monocyte family cells compared to TRT alone, and had no difference in infiltration compared to other groups at the secondary tumor (Figure A.8D). Both primary and secondary tumors had decreased infiltrate of type 1 classical dendritic cells in the RT/IC + TRT group compared to PBS or TRT alone (Figure A.8E). No substantial changes were detected in infiltration levels of type 2 classical dendritic cells (Figure A8/F). Infiltration of monocyte derived DCs was lower in primary tumors treated with RT/IC or RT/IC +TRT compared to PBS alone, and no changes were detected among secondary tumors (Figure A8.G).

Activation of lymphocytes and NK cells in tumors treated by combination RT/IC and external beam RT

Expression of the high affinity IL2 receptor CD25, the exhaustion marker PD1, and the effector cytokine IFNγ was measured as part of the adaptive flow cytometry panel (Figure A.9). Among $CD8^+$ T cells, primary tumors treated with both RT/IC and RT/IC + TRT had higher expression of CD25 compared to either PBS or TRT alone, and secondary tumors from mice treated with RT/IC + TRT had slightly increased CD25 expression compared to PBS and TRT alone (Figure A.9A). This pattern was also observed for NK cells in primary tumors (Figure A.9G) and for NKT cells in primary tumors (Figure A9.I), but no changes were detected for CD25 expression in either cell population among secondary tumors. $CD4^+$ non-T_{reg} cells had greater expression of CD25 in primary tumors treated with RT/IC + TRT compared to all treatment groups including RT/IC alone, and had increased expression in secondary tumors in the RT/IC + TRT group compared to RT/IC alone (Figure A.9D). $CD8^+$ T cells also had higher expression of IFNγ in primary tumors treated with RT/IC + TRT compared to PBS and RT alone and RT/IC alone. No change in IFNγ expression among $CD8^+$ T cells in secondary tumors was detected for any treatment group (Figure A9.C). This pattern was also observed in NK cells (Figure A3.H) and NKT cells (Figure A9.J). In $CD4^+$ non-T_{reg} cells, primary tumors treated with RT/IC and RT/IC + 12Gy had greater expression of IFNγ compared to either PBS or TRT only controls, secondary tumors treated with RT/IC + TRT had greater expression compared to PBS controls (Figure A9.F). Among $CD8^+$ T cells in the primary and secondary tumor, all 3 treatment groups had lower PD1 expression compared to PBS only. Primary and secondary tumors in the RT/IC and RT/IC + TRT group had lower PD1 expression still compared to TRT alone (Figure A.9B). Among $CD4^+$ non-T_{regs} PD1 expression was lower in all primary and secondary tumors compared to PBS control, but no difference was detected between RT/IC alone, TRT alone, or RT/IC + TRT groups (Figure A3.E).

To characterize the degree of maturity among lymphocytes in both primary and secondary tumors, the fraction of lymphocytes expressing PD1 and CD103 were determined, as described for Figure A.4 (Figure A.10). The fraction of $CD4^+$ non-T_{reg} cells expressing both CD103 and PD1 was substantially decreased for primary tumors in the RT/IC + TRT group compared to PBS and TRT alone, and for the secondary tumors compared to PBS (Figure A10.D). The fraction of $CD4^+$ non-T_{reg} cells expressing CD103 but not PD1 was substantially decreased for primary and secondary tumors in the RT/IC + TRT group compared to PBS and TRT alone compared to PBS (Figure A10.F).

Detection of cytokines in tumors treated by combination RT/IC and external beam RT

To more fully characterize the nature of the immune response following treatment, primary tumors treated with PBS, TRT only, RT/IC to the primary, and RT/IC to the primary plus TRT were analyzed for expression of 32 different cytokines and chemokines as in Figure A.5 Figure A.10 presents these cytokine data for both primary and secondary tumors in detail, separated by broad function of the cytokine or chemokine: 1) Pan-Activating, 2) NK cell and $CD8^+$ T cell focused, 3) IFNγ and T helper cell focused, and 4) Macrophage/Monocyte/Neutrophil focused). Cytokines of note include IL-5 and IL-4, which are increased in primary and secondary tumors in the RT/IC and RT/IC + TRT groups compared to PBS and TRT only controls. Expression of the pan-activating cytokine TNFα was increased in primary and secondary tumors in the RT/IC + TRT group. A fair number of cytokines that activate innate phagocytes and monocytes including G-CSF, GM-CSF, and M-CSF all demonstrated increased expression in primary tumors in the RT/IC and RT/IC + TRT groups. No change was detected among any measured cytokine levels in response to TRT alone compared to PBS control.

A.4 Discussion, Hypotheses, and future directions

The data presented in this appendix will be incorporated with the findings presented in Chapter 4 of this thesis for submission following additional studies. It should be emphasized that these data are preliminary and warrant repeating before proceeding to additional study. However this appendix does demonstrate the potential utility of flow cytometry and multiplex cytokine quantification in gaining insight into many different immune populations within the tumor, even those which are radioactive. The studies presented here measure a large number of immune parameters, both by flow cytometry and by cytokine multiplex analyses. As such, a unifying and consistent simple hypothesis or theory behind mechanism of action of combination RT/IC *in situ* vaccine and radiation to distant tumors is unlikely. Further planned analyses of these data, including tSNE analyses of pooled data in flow cytometry and clustering analyses of the cytokine data, are currently being investigated. As changes in individual immune populations or cytokines are detailed in the results and figures sections, they will not be restated here; rather patterns in general will be outlined, including potential hypotheses and future directions to explore these concepts.

RT/IC in situ vaccination alters the immune TME to favor antitumor effector responses

The data presented here suggest profound alterations in the tumor microenvironment at day 14 after treatment with RT/IC *in situ* vaccine. Some of these changes including the increased infiltration of $CD45^+$ cells, $CD8^+$ T cells, $CD4^+$ T cells, and CD8 : T_{reg} ratio compared to PBS controls has been demonstrated in prior work, including Chapter 2 of this thesis [65]. These data are repeated here in this study, and expand on those findings by further describing enhanced CD4 effector : T_{reg} ratio, trends toward increased NKT cell infiltration, as well as increased neutrophils and decreased monocyte-derived DCs in primary tumors treated with RT/IC. These data additionally expand on known quantitative changes in T cell subsets by

characterizing their activation status, noting increased CD25 and IFNγ expression in all T cell subpopulations evaluated, as well as in both NK and NKT cells. Further, increased levels of the cytokines IFNγ, RANTES (CCL5), TNFα and IL-6 all support a general program of lymphocyte activation in tumors treated with RT/IC *in situ* vaccine.

Recently, the B78 melanoma cell line has been demonstrated to express the $CD4^+$ T cell – recognized ligand MHCII (preliminary data not shown). In addition to activation of directly cytotoxic NK, NKT, and $CD8^+$ T cells, the data presented here also suggest activation of $CD4^+$ helper T cells, as evidenced by increased number, activation state, and $CD4^+$ effector : T_{reg} ratio. Importantly, there is also evidence of increased effector cytokine activity deriving from these T helper cells. This includes increased neutrophil and macrophage infiltrate, and increased detection of numerous cytokines directed towards macrophages and other phagocytes. Taken together, this characterization suggests that in addition to driving increased direct cytotoxic activity, CD4+ T helper cells may be recruiting phagocytes and other innate effectors to the TME to aid in tumor elimination. Future studies should include direct depletion of each of these effector immune cell lineages during treatment, to establish the degree of contribution of these components to the RT/IC *in situ* vaccine response.

This study additionally characterizes the degree to which these immune changes initiated at the *in situ* vaccine site (the primary tumor) circulate systemically to affect the secondary tumor, which in the case of the RT/IC only group, is not directly treated or altered (other than the low level of IC that may reach distant sites after a primary tumor receives IT-IC. One of the patterns noted across these data are that changes induced by RT/IC in the primary tumor can also be seen (or trends to be seen) in the secondary tumor, but to a much attenuated degree. This is especially true in the CD8 : T_{reg} and CD4 : T_{reg} ratios, the decrease in PD1 expression on CD8 and CD4 T lymphocytes, neutrophil recruitment, as well as in measured content of some (but not all) cytokines. This suggests that the *in situ* vaccine does generate a systemic response that is capable of circulating to other tumor environments, yet is not as

effective in those environments. This could be due to the activating activity of the IL-2 component of the immunocytokine in the RT/IC treated primary tumors, or could be due to persistent immunosuppressive mechanisms in the distant secondary tumors. Further experimentation will be needed to better delineate this mechanism of action.

Additional RT delivered to the secondary tumor combined with RT/IC to the primary tumor results in some favorable immune changes, but largely results in similar changes to those induced by RT/IC itself

Comparison of the RT/IC alone group to the RT/IC plus 12Gy to the secondary group results in very few detected differences. For the most part, changes in both the primary and secondary tumor when 12Gy to the secondary are added to the RT/IC are the same as seen in the RT/IC alone group. Notable exceptions include $CD8^+$ T cells, which had the same degree of infiltrate in the primary tumor, but much greater infiltration in the secondary tumor, in the RT/IC + 12Gy group compared to RT/IC alone. This may be due to the known effect of RT to induce MHCI upregulation in irradiated tissue [184]. Though the RT/IC *in situ* vaccine generated antitumor $CD8^+$ T cells, the lack of MHCI expression in the secondary tumor may have prevented the tumor-specific $CD8^+$ T cells from binding and remaining in the secondary TME. Increased MHCI expression following the 12Gy RT to the secondary may have then permitted the RT/IC generated $CD8^+$ T cells at the primary tumor to accumulate in the secondary tumor and affect tissue destruction. Future experiments will explore this hypothesis by directly measuring MHCI expression in the tumor by flow cytometry and by qRT-PCR. Another exception is the greater infiltrate of macrophages in both the primary and secondary tumors from mice treated with RT/IC + 12Gy compared to mice treated with RT/IC alone. These could be in response to increased tumor inflammatory cell death and subsequent recruitment to clear cell debris, or perhaps due to increased functional secretion of cytokines including G-CSF, GM-CSF, and M-CSF, all of which were detected in primary tumors treated with RT/IC + 12Gy.

Infiltrating lymphocytes may be derived from distant, clonally expanded subsets, as opposed to tissue – resident populations

In a typical antitumor immune response involving lymphocyte populations, effector cells can be derived from several locations, including lymph nodes, splenic germinal centers, and tissue resident memory populations [217]. Understanding the source of the effector cells can help determine the type of antigen that is driving response to treatment. For example, a response largely derived from a lymph node following treatment may suggest that novel tumor-specific antigens are being recognized *after* treatment, driven by increased antigen processing and presentation. Conversely, detection of increased numbers cells derived from tumor-resident immune populations (like tissue-resident memory T cells) may point to reactivation and expansion of lymphocyte clones that were *already* antigen-sensitized, and were for some reason dormant or exhausted prior to treatment. Distinguishing between these two types of response can aid in characterizing the mechanism of action of the RT/IC *in situ* vaccine; namely increased release and recognition of tumor antigens, or reactivation / expansion of preexisting clones. These data demonstrate that both the $CD8^+$ and $CD4^+$ T cell populations in the tumor following treatment have decreased expression of the exhaustion marker PD1, which is known to be elevated among lymphocytes resident in a tumor for a long period of time [213]. In addition, the $CD4^+$ T helper population shifted away from a PD1+ CD103+ population that may represent tissue resident memory cells, towards a PD1-CD103- population, which may represent recent infiltrates into the tissue. These data suggest that the lymphocyte populations within the tumor favor an origin from distant circulation, as they do not have the resident memory marker CD103+ [217]. To more completely characterize this distinction, TCRseq could be used to enumerate the specific clonal populations before and after treatment in the primary and secondary tumors. Initial efforts towards this are being pursued.

^{90}Y-NM600 combined with RT/IC has many of the same changes as RT/IC alone, yet may favor increased lymphocyte activation

The addition of TRT to the RT/IC *in situ* vaccine again produced largely the same changes to the immune TME and detected cytokines as RT/IC alone, and many of the same changes discussed above for 12Gy external beam RT to the secondary. Though there was not as profound of an increase in lymphocyte infiltrate in the RT/IC + TRT group, both the CD8:T_{reg} and CD4 effector : T_{reg} ratios were increased in the primary tumor, and the CD8:T_{reg} was also increased in the secondary tumors, although still to a lesser degree. Unlike in the case with external beam radiation, TRT did not increase the infiltrate of CD8+ T cells or macrophages in either the primary or secondary tumors beyond that of RT/IC alone. However unlike with external beam RT, the primary tumors in mice treated with RT/IC + TRT had greater CD25 MFI and IFNγ expression in CD8+ T cells, and greater CD25 expression in CD4+ effector T cells compared to primary tumors treated with RT/IC alone. This may indicate a greater degree of immune activation in these lymphocytes, possibly as a result of the combined radiation effect of external beam and TRT within the primary tumor. However this may be counterbalanced by the fewer number of lymphocytes in general detected as a result of RT/IC + TRT treatment. Further studies will be needed to fully determine the degree of activation of these cells, and the functional significance of these expression changes.

It should be noted that direct comparisons of the effect of ^{90}Y-NM600 and external beam RT are difficult to make in this experimental design, and warrants further study. Not only is the dose rate different between these two modalities, but the total dose delivered (12Gy for RT and 4-6 Gy for a 100μCi injection of ^{90}Y-NM600) to the tumors are different as well. It is however promising that *in vivo* antitumor effect does not appear hindered by the use of TRT (as discussed in Chapter 4), and the tumor immune changes induced by RT/IC as examined in this appendix also do not appear to be substantially hindered by the addition of TRT. Future studies

comparing the different immune effects of RT and TRT are underway, with some such comparisons noted in the manuscript authored by Patel et al in Appendix B.

The findings of the *ex vivo* biodistribution and PET/CT dosimetry experiment support previous findings that NM600 uptake can be estimated for B78 melanoma to be approximately 3-6 %ID/g [127]. The lack of change in uptake as a function of tumor burden is also promising, as it indicates that the TRT agent can behave in a predictable manner in settings of multiple tumors, and tumors with different sizes. The trend for increased uptake with the very small tumors (less than $50mm^3$) is very promising, and may be explained by differences in blood flow between smaller and larger tumors. The ischemic, hypoxic core of a larger tumor is less vascularized, and may be less able to take up TRT agent [218]. Therefore, the smaller tumors may be able to absorb more agent per unit volume, because they have less ischemic, dead tissue in their core. However the path length of ^{90}Y beta emissions is fixed to a maximum range of 1cm, meaning that the distribution of dose from a point source like a small tumor is a fixed sphere extending out to a radius of 1cm. The relative proportion of that sphere that is tumor vs. non tumor surrounding tissue decreases as the size of the tumor decreases, meaning a larger fraction of the radiation is deposited outside of the tumor itself [127]. Thus, despite reduced efficiency in delivering dose to smaller tumors, the increased uptake may at least partially compensate for this effect, and may explain why the estimated absorbed dose per injected activity is relatively similar between larger ~$150mm^3$ tumors and smaller ~$50mm^3$ tumors in these data. Future experiments are planned to confirm this observation using other tumor models, including tail vein-injected tumors that can seed multiple lung metastases. In addition, investigations using particle emissions of smaller path length such as ^{177}Lu or even the alpha-emitting ^{225}Ac could further increase efficiency in delivering radiation to smaller tumors.

Table A.1: Antibodies used for flow cytometric analyses depicted in this appendix. Note that these antibodies are clustered into a lymphoid panel and a myeloid panel due to channel limitations of the cytometry instruments.

	Target	Fluorophore	Company (Cat.)	Clone	Volume per Test (µL)
Lymphoid Panel	CD25	BB515	BD Biosciences (564424)	PC61	1.5
	IFNγ	PE	BioLegend (505808)	XMG1.2	1.2
	NK1.1	PE-CF594	BD Biosciences (562864)	PK136	1.2
	CD103	BV605	BioLegend (121433)	2E7	1.2
	FOXP3	PE-Cy7	Invitrogen (25-5773-82)	FJK-16s	1.4
	PD-1	V450	Tonbo (75-9981-U100)	RMP1-30	1.2
	CD45	BV510	BioLegend (103137)	30-F11	1
	CD3	PE-Cy5	BioLegend (100310)	145-2C11	1
	CD4	BV785	BioLegend (100453)	GK1.5	1
	CD19	APC	BioLegend (115512)	6D5	0.5
	CD8	APC-R700	BD Biosciences (564983)	53-6.7	1
	Live/Dead	GhostRed 780	Tonbo (13-0865-T100)	-	0.5µL
Myeloid Panel	CD45	FITC	Tonbo (35-0451-U500)	30-F11	1
	CD103	PE	BioLegend (121406)	2E7	1.5
	MHCII	PE-Dazzle594	BioLegend (107648)	M5/114.15.2	1.2
	F4/80	PE-Cy5	Invitrogen (15-4801-82)	BM8	1
	CD64	PE-Cy7	BioLegend (139314)	X54-5/7.1	1.2
	CD11b	V450	BD Biosciences (560455)	M1/70	1.5
	XCR1	BV510	BioLegend (148218)	ZET	3
	Ly6C	BV605	BD Biosciences (563011)	AL-21	2
	CD24	BV711	BD Biosciences (563450)	M1/69	1.2
	CD11c	APC	BioLegend (117310)	N418	1.2
	Ly6G	AF700	BD Biosciences (561236)	1A8	1.2
	Live/Dead	GhostRed 780	Tonbo (13-0865-T100)	-	0.5µL

Table A.2: Gating phenotypes used in defining immune populations in this appendix. All phenotypes are first gated on cells, single cells, and live cells as depicted in Figures A.1 and A.2.

	Population	Gating Phenotype (after Cells/Single/Live)
Lymphoid Panel	CD45+	CD45+
	NKT Cells	CD45+/CD3+/NK1.1+
	CD8+ T Cells	CD45+/CD3+/NK1.1-/CD8+
	CD4+ T Cells	CD45+/CD3+/NK1.1-/CD4+
	Treg Cells	CD45+/CD3+/NK1.1-/CD4+/CD25+/foxp3+
	B Cells	CD45+/CD3-/CD19+
	NK Cells	CD45+/CD3-/NK1.1+
Myeloid Panel	Neutrophils	CD45+/CD11b+/Ly6G+
	Macrophages	CD45+/Ly6G-/F4/80+CD64+
	Classical monocyte family and precursors	CD45+/Ly6G-/F4/80-CD64-/CD11b+/Ly6C+
	Nonclassical monocyte family and precursors	CD45+/Ly6G-/F4/80-CD64-/CD11b+Ly6C-
	Classical type 1 DCs	CD45+/Ly6G-/F4/80-CD64-/CD11b-/Ly6C-/CD11c+/MHCII+/CD103+/XCR1+
	Classical type 2 DCs	CD45+/Ly6G-/F4/80-CD64-/CD11b+/Ly6C+/CD11c+/MHCII+/CD103-/XCR1-
	Monocyte-derived DCs	CD45+/Ly6G-/F4/80-CD64-/CD11b+/Ly6C-/CD11c+/MHCII+/F4/80+/CD103-

Figure A.1: Adaptive immunophenotyping of primary and secondary tumors in mice treated with *in situ* vaccine combined with radiation to distant tumors. Female C57BL/6 mice were implanted ID with B78 tumors on the right and left flanks simultaneously. After 4 weeks, mice were treated with either PBS (black), 12Gy external beam radiation (RT, red) to both primary and secondary tumors, 12Gy RT and intratumoral immunocytokine (IC) to the primary tumor only (blue), or RT+IC to the primary tumor and 12Gy RT to the secondary tumor (purple). RT was given on treatment day 0, and IC was given on treatment days 5-9. On treatment day 14, tumors were harvested and dissociated as described in the materials and methods section. Aliquots of tumors were stained using the adaptive and innate antibody panels outlined in Table A.1, according to the novel cryopreservation protocol described in Chapter 2 of this thesis. Cells were gated according to expression of the markers outlined in Table A.2. Immune populations are expressed as a percentage of all live, single cells, except where otherwise noted. In each population pair of graphs depicted, results corresponding to the right flank primary tumor are on the right, and results corresponding to the left flank secondary tumor are on the left. Statistical analyses were conducted using one-way ANOVA, with multiple comparisons using Fischer's least significant difference tests. No corrections were made to account for multiple comparisons. * = $p<0.05$, ** = $p<0.01$, *** = $p<0.001$, **** = $p<0.0001$, ns = not significant.

Figure A.1

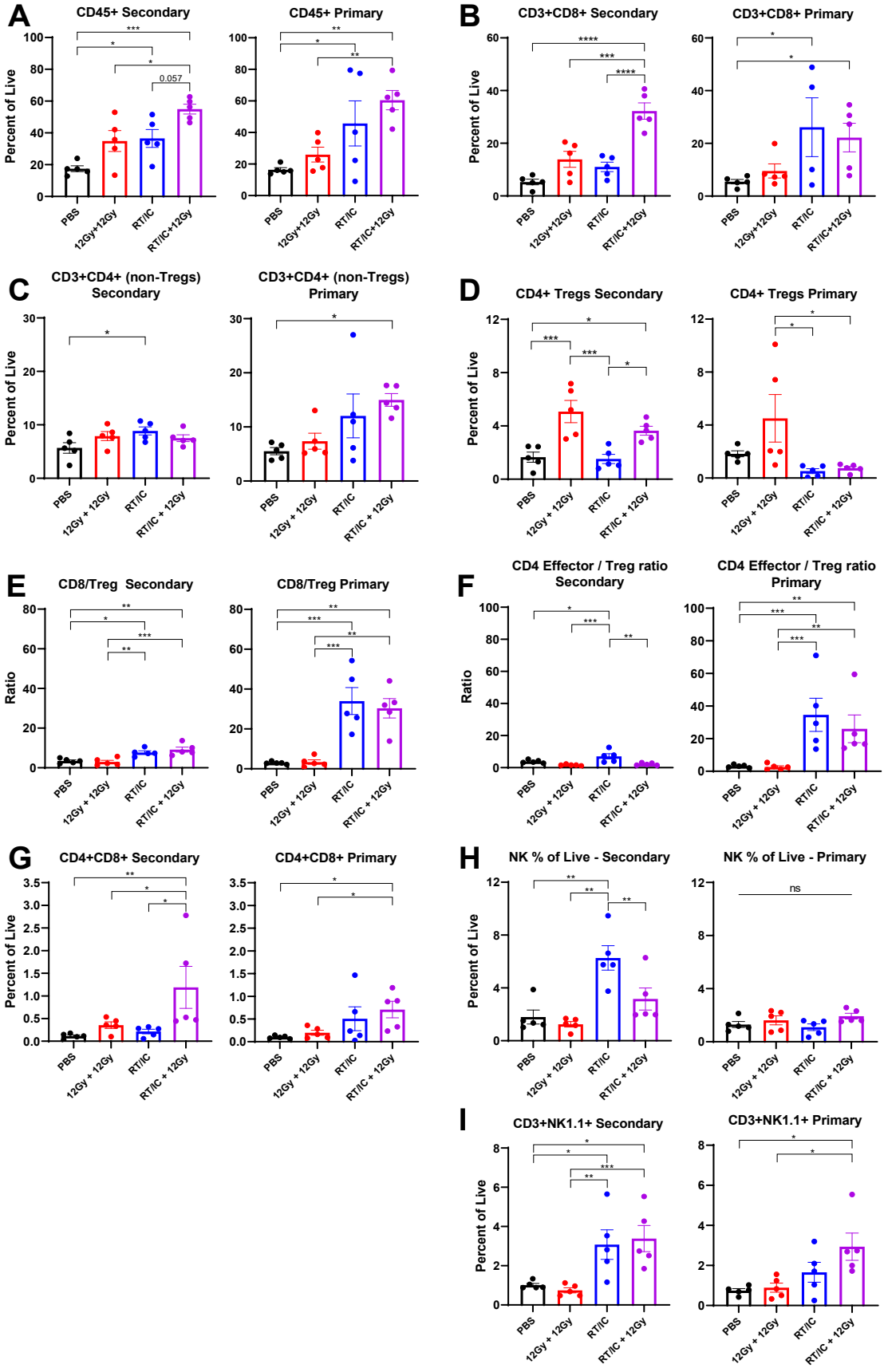
A
CD45+ Secondary
CD45+ Primary
B
CD3+CD8+ Secondary
CD3+CD8+ Primary
C
CD3+CD4+ (non-Tregs) Secondary
CD3+CD4+ (non-Tregs) Primary
D
CD4+ Tregs Secondary
CD4+ Tregs Primary
E
CD8/Treg Secondary
CD8/Treg Primary
F
CD4 Effector / Treg ratio Secondary
CD4 Effector / Treg ratio Primary
G
CD4+CD8+ Secondary
CD4+CD8+ Primary
H
NK % of Live - Secondary
NK % of Live - Primary
I
CD3+NK1.1+ Secondary
CD3+NK1.1+ Primary
Percent of Live
Ratio
PBS
12Gy+12Gy
12Gy + 12Gy
RT/IC
RT/IC+12Gy
RT/IC + 12Gy
0.057
ns

Figure A.2: Innate immunophenotyping of primary and secondary tumors in mice treated with *in situ* vaccine combined with radiation to distant tumors. Female C57BL/6 mice were implanted ID with B78 tumors on the right and left flanks simultaneously. After 4 weeks, mice were treated with either PBS (black), 12Gy external beam radiation (RT, red) to both primary and secondary tumors, 12Gy RT and intratumoral immunocytokine (IC) to the primary tumor only (blue), or RT+IC to the primary tumor and 12Gy RT to the secondary tumor (purple). RT was given on treatment day 0, and IC was given on treatment days 5-9. On treatment day 14, tumors were harvested and dissociated as described in the materials and methods section. Aliquots of tumors were stained using the adaptive and innate antibody panels outlined in Table A.1, according to the novel cryopreservation protocol described in Chapter 2 of this thesis. Cells were gated according to expression of the markers outlined in Table A.2. Immune populations are expressed as a percentage of all live, single cells, except where otherwise noted. In each population pair of graphs depicted, results corresponding to the right flank primary tumor are on the right, and results corresponding to the left flank secondary tumor are on the left. Statistical analyses were conducted using one-way ANOVA, with multiple comparisons using Fischer's least significant difference tests. No corrections were made to account for multiple comparisons. * = $p<0.05$, ** = $p<0.01$, *** = $p<0.001$, **** = $p<0.0001$, ns = not significant.

Figure A.2

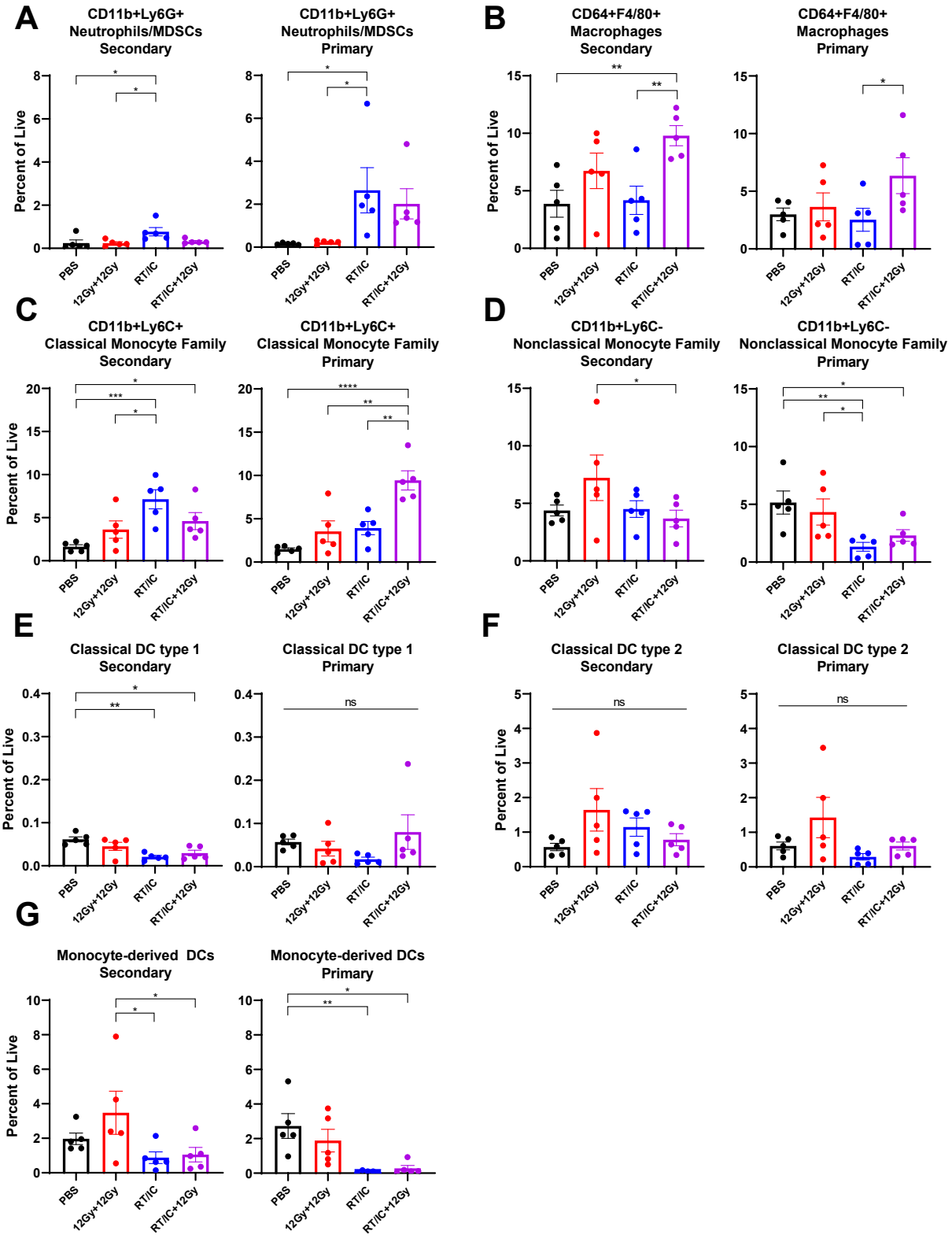
A
CD11b+Ly6G+ Neutrophils/MDSCs Secondary
CD11b+Ly6G+ Neutrophils/MDSCs Primary
B
CD64+F4/80+ Macrophages Secondary
CD64+F4/80+ Macrophages Primary
C
CD11b+Ly6C+ Classical Monocyte Family Secondary
CD11b+Ly6C+ Classical Monocyte Family Primary
D
CD11b+Ly6C- Nonclassical Monocyte Family Secondary
CD11b+Ly6C- Nonclassical Monocyte Family Primary
E
Classical DC type 1 Secondary
Classical DC type 1 Primary
F
Classical DC type 2 Secondary
Classical DC type 2 Primary
G
Monocyte-derived DCs Secondary
Monocyte-derived DCs Primary
Percent of Live
PBS
12Gy+12Gy
RT/IC
RT/IC+12Gy
ns

Figure A.3: Expression of activation markers on T cells and NK cells in tumors isolated from mice treated with *in situ* vaccine combined with radiation to distant tumors. Female C57BL/6 mice were implanted ID with B78 tumors on the right and left flanks simultaneously. After 4 weeks, mice were treated with either PBS (black), 12Gy external beam radiation (RT, red) to both primary and secondary tumors, 12Gy RT and intratumoral immunocytokine (IC) to the primary tumor only (blue), or RT+IC to the primary tumor and 12Gy RT to the secondary tumor (purple). RT was given on treatment day 0, and IC was given on treatment days 5-9. On treatment day 14, tumors were harvested and dissociated as described in the materials and methods section. Aliquots of tumors were stained using the adaptive and innate antibody panels outlined in Table A.1, according to the novel cryopreservation protocol described in Chapter 2 of this thesis. Cells were gated according to expression of the markers outlined in Table A.2. Expression of activation markers CD25, the activation / exhaustion marker PD1, and the effector cytokine IFNγ on T cells, NK cells, and NKT cells are shown here. Data are expressed as median fluorescence intensity (MFI) unless otherwise noted. In each population pair of graphs depicted, results corresponding to the right flank primary tumor are on the right, and results corresponding to the left flank secondary tumor are on the left. Statistical analyses were conducted using one-way ANOVA, with multiple comparisons using Fischer's least significant difference tests. No corrections were made to account for multiple comparisons. * = $p<0.05$, ** = $p<0.01$, *** = $p<0.001$, **** = $p<0.0001$, ns = not significant.

Figure A.3

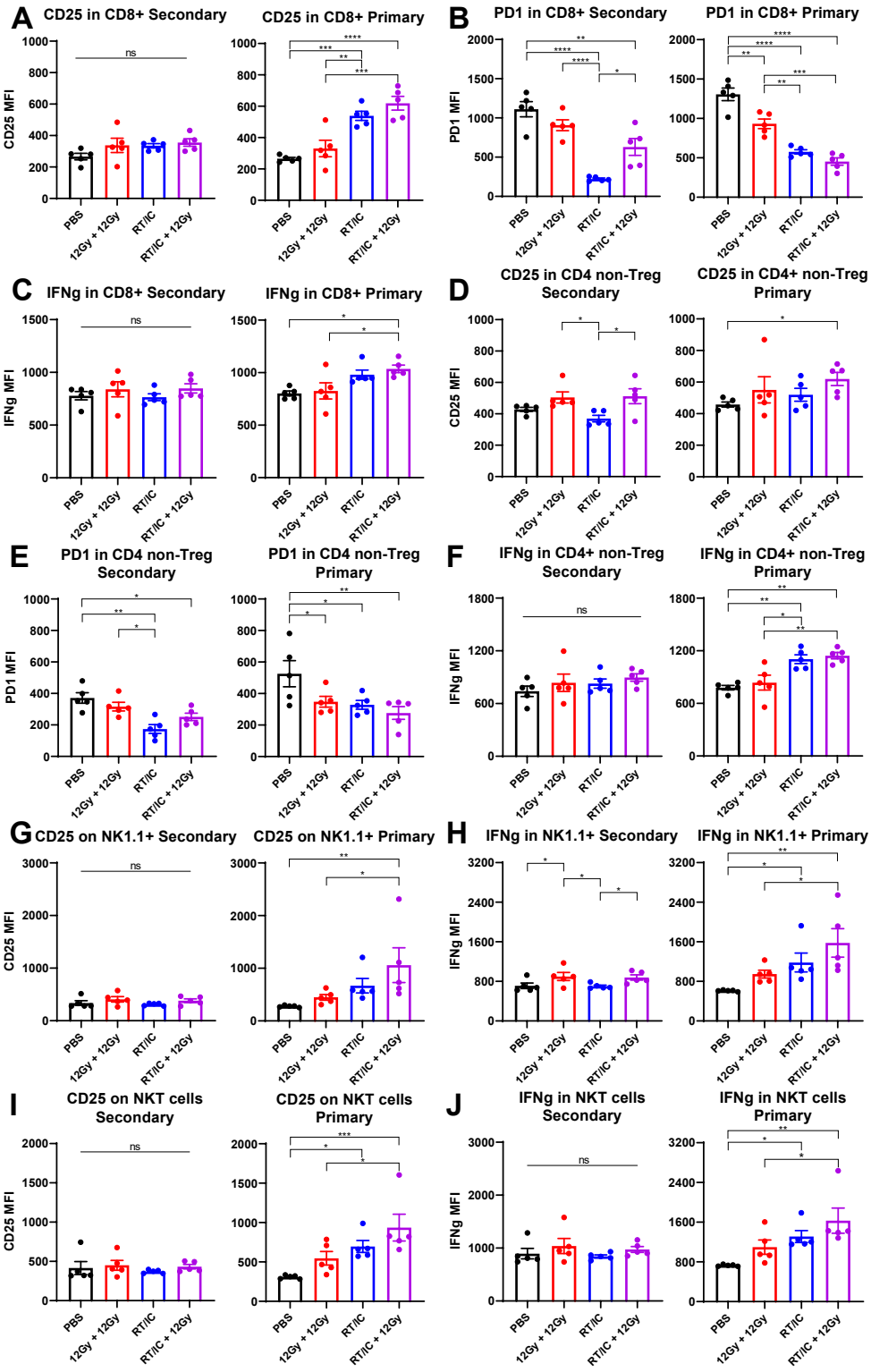
A
CD25 in CD8+ Secondary
CD25 in CD8+ Primary
CD25 MFI
B
PD1 in CD8+ Secondary
PD1 in CD8+ Primary
PD1 MFI
C
IFNg in CD8+ Secondary
IFNg in CD8+ Primary
IFNg MFI
D
CD25 in CD4 non-Treg Secondary
CD25 in CD4+ non-Treg Primary
CD25 MFI
E
PD1 in CD4 non-Treg Secondary
PD1 in CD4 non-Treg Primary
PD1 MFI
F
IFNg in CD4+ non-Treg Secondary
IFNg in CD4+ non-Treg Primary
IFNg MFI
G
CD25 on NK1.1+ Secondary
CD25 on NK1.1+ Primary
CD25 MFI
H
IFNg in NK1.1+ Secondary
IFNg in NK1.1+ Primary
IFNg MFI
I
CD25 on NKT cells Secondary
CD25 on NKT cells Primary
CD25 MFI
J
IFNg in NKT cells Secondary
IFNg in NKT cells Primary
IFNg MFI
PBS
12Gy + 12Gy
RT/IC
RT/IC + 12Gy
ns

Figure A.4: PD1 and CD103 status in CD4+ non-T_{regs} among tumors treated with RT/IC with or without 12Gy RT to the secondary tumor. Female C57BL/6 mice were implanted ID with B78 tumors on the right and left flanks simultaneously. After 4 weeks, mice were treated with either PBS (black), 12Gy external beam radiation (RT, red) to both primary and secondary tumors, 12Gy RT and intratumoral immunocytokine (IC) to the primary tumor only (blue), or RT+IC to the primary tumor and 12Gy RT to the secondary tumor (purple). RT was given on treatment day 0, and IC was given on treatment days 5-9. On treatment day 14, tumors were harvested and dissociated as described in the materials and methods section. Aliquots of tumors were stained using the adaptive and innate antibody panels outlined in Table A.1, according to the novel cryopreservation protocol described in Chapter 2 of this thesis. Cells were gated according to expression of the markers outlined in Table A.2. Depicted here is PD1 and CD103 expression on CD4+ T cells, after gating out CD25+FOXP3+ T_{reg} cells. A-B) representative dot plots outlining the four quadrants of expression status for PD1 and CD103 in PBS control (A) and RT/IC + 12Gy (B) primary tumors. C-F) Percentage of CD4+ non-T_{regs} in each of the four quadrants depicted in A and B. Statistical analyses were conducted using one-way ANOVA, with multiple comparisons using. Fischer's least significant difference tests. No corrections were made to account for multiple comparisons. * = $p<0.05$, ** = $p<0.01$, *** = $p<0.001$, **** = $p<0.0001$, ns = not significant.

Figure A.4

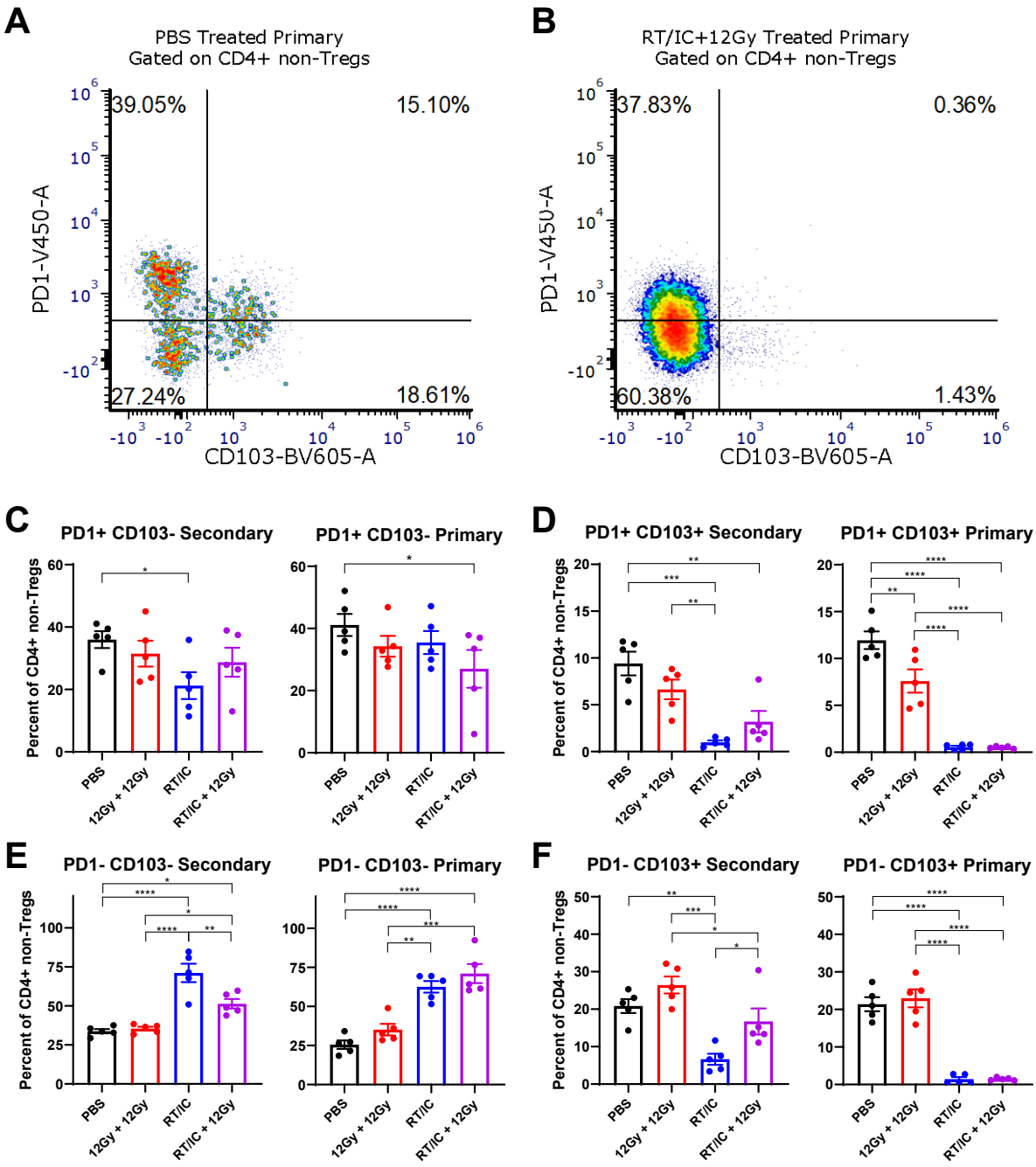
A
PBS Treated Primary
Gated on CD4+ non-Tregs
39.05%
15.10%
27.24%
18.61%
PD1-V450-A
CD103-BV605-A
B
RT/IC+12Gy Treated Primary
Gated on CD4+ non-Tregs
37.83%
0.36%
60.38%
1.43%
PD1-V450-A
CD103-BV605-A
C
PD1+ CD103- Secondary
PD1+ CD103- Primary
D
PD1+ CD103+ Secondary
PD1+ CD103+ Primary
E
PD1- CD103- Secondary
PD1- CD103- Primary
F
PD1- CD103+ Secondary
PD1- CD103+ Primary
Percent of CD4+ non-Tregs
PBS
12Gy + 12Gy
RT/IC
RT/IC + 12Gy

Figure A.5:Cytokine profile in primary and secondary tumors treated with RT+IC and external beam radiation. Female C57BL/6 mice were implanted ID with B78 tumors on the right and left flanks simultaneously. After 4 weeks, mice were treated with either PBS (black), 12Gy external beam radiation (RT, red) to both primary and secondary tumors, 12Gy RT and intratumoral immunocytokine (IC) to the primary tumor only (blue), or RT+IC to the primary tumor and 12Gy RT to the secondary tumor (purple). RT was given on treatment day 0, and IC was given on treatment days 5-9. On treatment day 14, tumors were harvested and flash frozen in liquid nitrogen. After storage for 30 days, tissues were homogenized and analyzed using the MILLIPLEX MAP Mouse Cytokine/Chemokine Magnetic Bead Panel as described in the materials and methods section. Cytokine content is presented in pg/mL unless otherwise noted. Statistical analyses were conducted using one-way ANOVA, with multiple comparisons using Fischer's least significant difference tests. No corrections were made to account for multiple comparisons. * = $p<0.05$, ** = $p<0.01$, *** = $p<0.001$, **** = $p<0.0001$, ns = not significant.

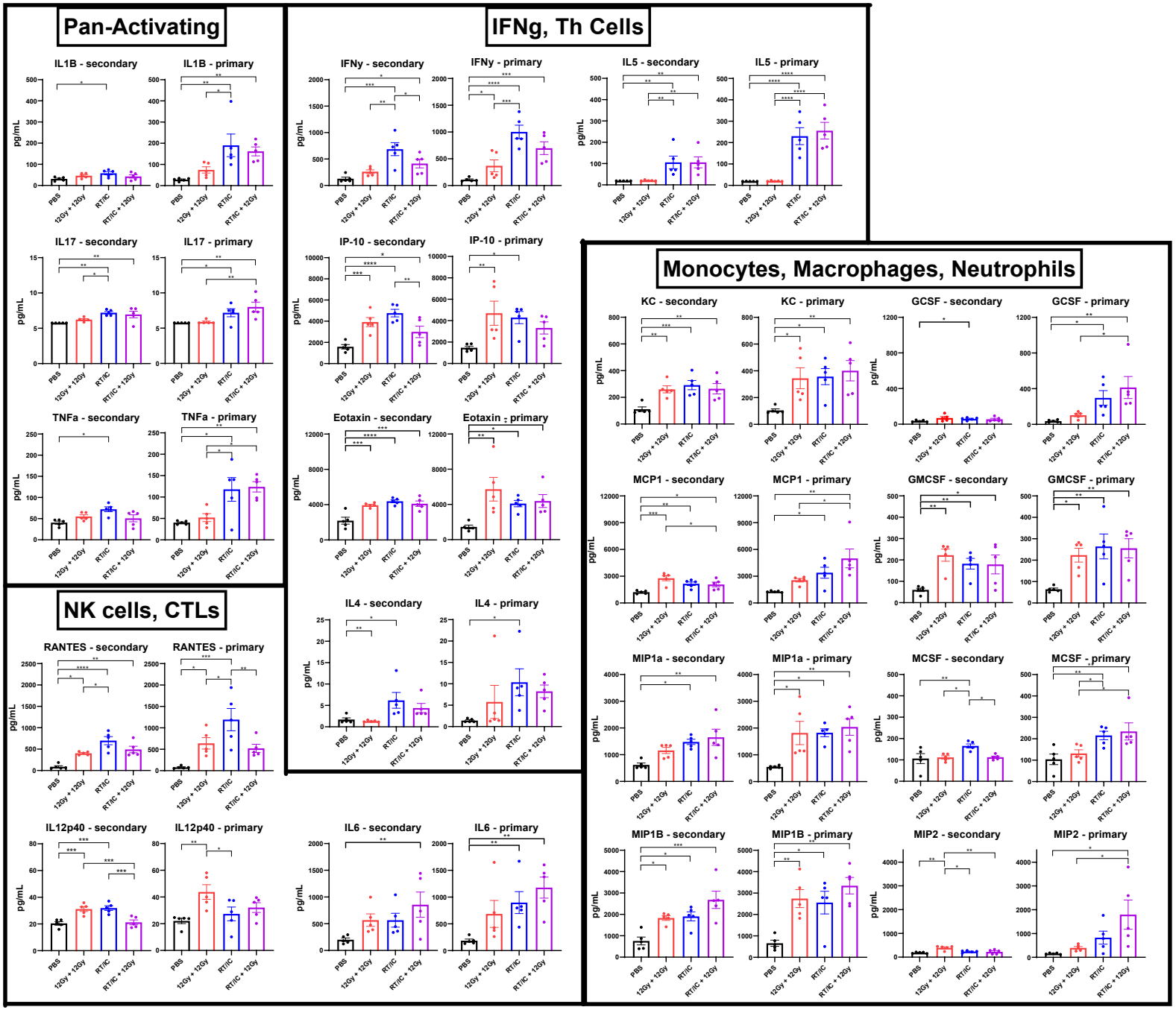
Pan-Activating
IL1B - secondary
IL1B - primary
IL17 - secondary
IL17 - primary
TNFa - secondary
TNFa - primary
IFNg, Th Cells
IFNy - secondary
IFNy - primary
IL5 - secondary
IL5 - primary
IP-10 - secondary
IP-10 - primary
Eotaxin - secondary
Eotaxin - primary
IL4 - secondary
IL4 - primary
NK cells, CTLs
RANTES - secondary
RANTES - primary
IL12p40 - secondary
IL12p40 - primary
IL6 - secondary
IL6 - primary
Monocytes, Macrophages, Neutrophils
KC - secondary
KC - primary
GCSF - secondary
GCSF - primary
MCP1 - secondary
MCP1 - primary
GMCSF - secondary
GMCSF - primary
MIP1a - secondary
MIP1a - primary
MCSF - secondary
MCSF - primary
MIP1B - secondary
MIP1B - primary
MIP2 - secondary
MIP2 - primary
pg/mL
PBS
12Gy + 12Gy
RT/IC
RT/IC + 12Gy

Figure A.6: Pharmacokinetic and dosimetry characterization of ^{86}Y/^{90}Y-NM600 in B78 melanoma. A) molecular structure of ^{90}Y-NM600. **B**) whole body isosurface reconstruction of representative C57Bl/6 mice bearing a ~150mm^3 primary and a ~50mm^3 secondary B78 melanoma tumors 48h after injection of 250μCi of ^{86}Y-NM600. Maximum intensity projections of detected PET signal superimposed on CT images are presented in the coronal (**C**) and axial (**D and E**) planes in representative slices. **F**) Using a monte carlo based simulation of contoured tissue volumes, the estimated dose (in Gy) delivered to the primary and secondary tumor was calculated and integrated over infinite time, and expressed as a function of injected activity (in Megabecquerel, MBq) of ^{90}Y-NM600. **G**) Estimated uptake of NM600 drug, expressed as percent injected dose (ID) per gram of tissue, depicted for both primary and secondary tumors over time. **H**) In a second parallel group, n=5 mice each were implanted with one, two, or four B78 tumors and allowed to develop over 4 weeks. They were injected with 200μCi ^{90}Y-NM600, and 48 hours later the tumors were harvested and radioactivity was counted using a beta counter. After decay-correction, the uptake of drug at 48 hours (expressed %ID/g) was calculated for each of the tumor conditions. Individual tumor data points are shown, with the bar representing mean uptake. **I-K**) Mice bearing a single B78 tumor with a range of volumes from 50 to 600mm^3 were all injected on the same day with 200μCi ^{90}Y-NM600. 48 hours after injection, animals were euthanized and tumor, spleen, and blood was harvested and residual activity counted on a beta counter. After decay-correction, the uptake of drug at 48 hours (expressed %ID/g) was calculated for each tissue type. Colors correspond to the intended tumor volume at the time of injection (either 50, 100, 300, or 500mm^3). (**I**) depicts the relationship between harvest tumor volume and uptake of ^{90}Y-NM600 for each tumor measured. (**J**) and (**K**) depict the relationship between calculated uptake of ^{90}Y-NM600 in the tumor vs uptake in the blood (**J**) and spleen (**K**) of the same mouse from which the tumor was harvested.

Figure A.6

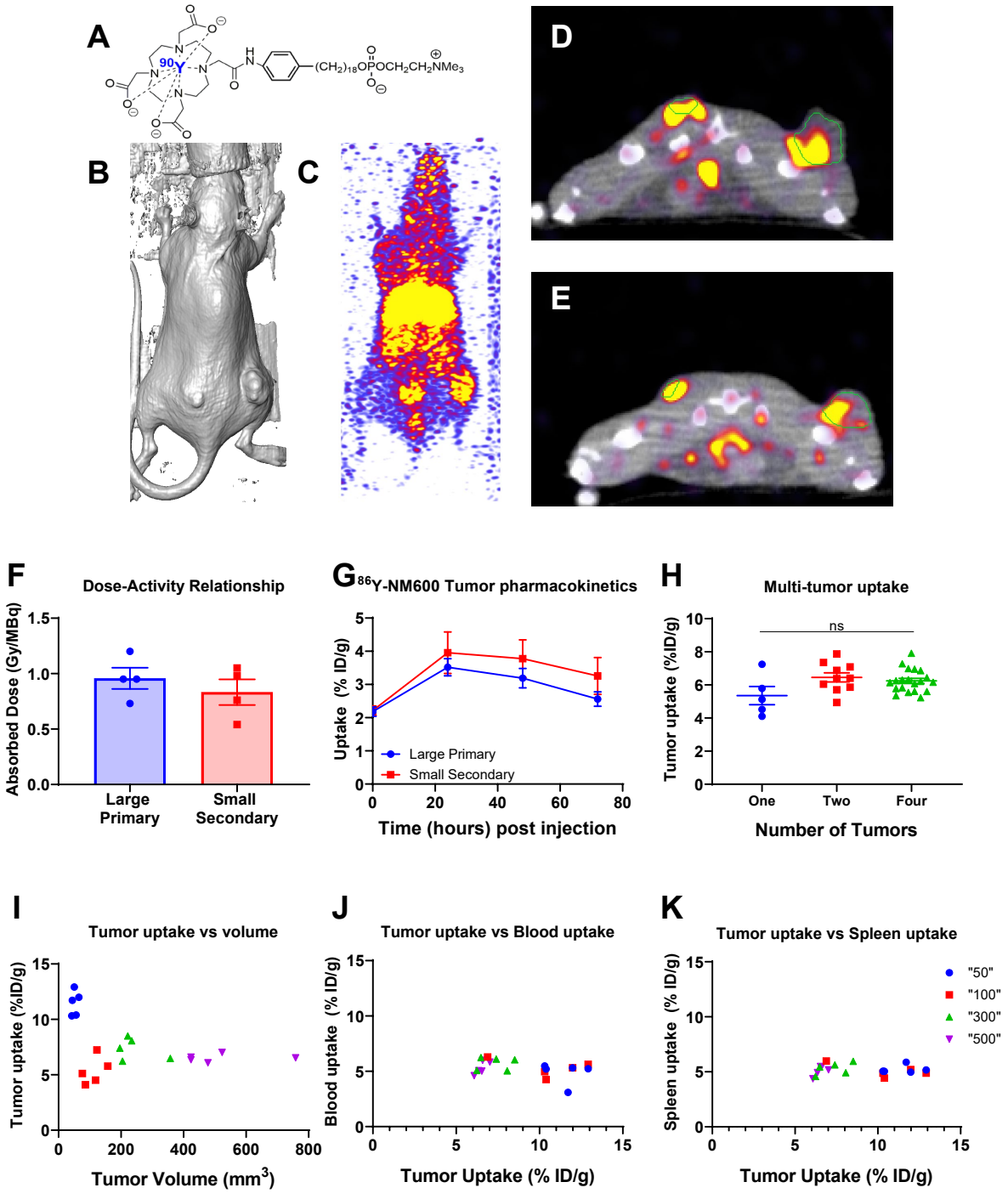
A
B
C
D
E
F
Dose-Activity Relationship
Absorbed Dose (Gy/MBq)
Large Primary
Small Secondary
G
86Y-NM600 Tumor pharmacokinetics
Uptake (% ID/g)
Large Primary
Small Secondary
Time (hours) post injection
H
Multi-tumor uptake
ns
Tumor uptake (%ID/g)
One
Two
Four
Number of Tumors
I
Tumor uptake vs volume
Tumor uptake (%ID/g)
Tumor Volume (mm3)
J
Tumor uptake vs Blood uptake
Blood uptake (% ID/g)
Tumor Uptake (% ID/g)
K
Tumor uptake vs Spleen uptake
Spleen uptake (% ID/g)
"50"
"100"
"300"
"500"
Tumor Uptake (% ID/g)

Figure A.7: **Adaptive immunophenotyping of primary and secondary tumors in mice treated with *in situ* vaccine combined with ^{90}Y-NM600 TRT**. Female C57BL/6 mice were implanted ID with B78 tumors on the right and left flanks simultaneously. After 4 weeks, mice were treated with either PBS (black), 100μCi of ^{90}Y-NM600 by tail vein injection (green), 12Gy RT and intratumoral immunocytokine (IC) to the primary tumor only (blue), or RT+IC to the primary tumor and 100μCi of ^{90}Y-NM600 (orange). RT and TRT was given on treatment day 0, and IC was given on treatment days 5-9. On treatment day 14, tumors were harvested and dissociated as described in the materials and methods section. Aliquots of tumors were stained using the adaptive and innate antibody panels outlined in Table A.1, according to the novel cryopreservation protocol described in Chapter 2 of this thesis. Cells were gated according to expression of the markers outlined in Table A.2. Immune populations are expressed as a percentage of all live, single cells, except where otherwise noted. In each population pair of graphs depicted, results corresponding to the right flank primary tumor are on the right, and results corresponding to the left flank secondary tumor are on the left. Statistical analyses were conducted using one-way ANOVA, with multiple comparisons using Fischer's least significant difference tests. No corrections were made to account for multiple comparisons. Note that these data were collected as part of the same experiment outlined in Figures A.1-A.5, and share common PBS and RT/IC groups, which are presented again here.

Figure A.7

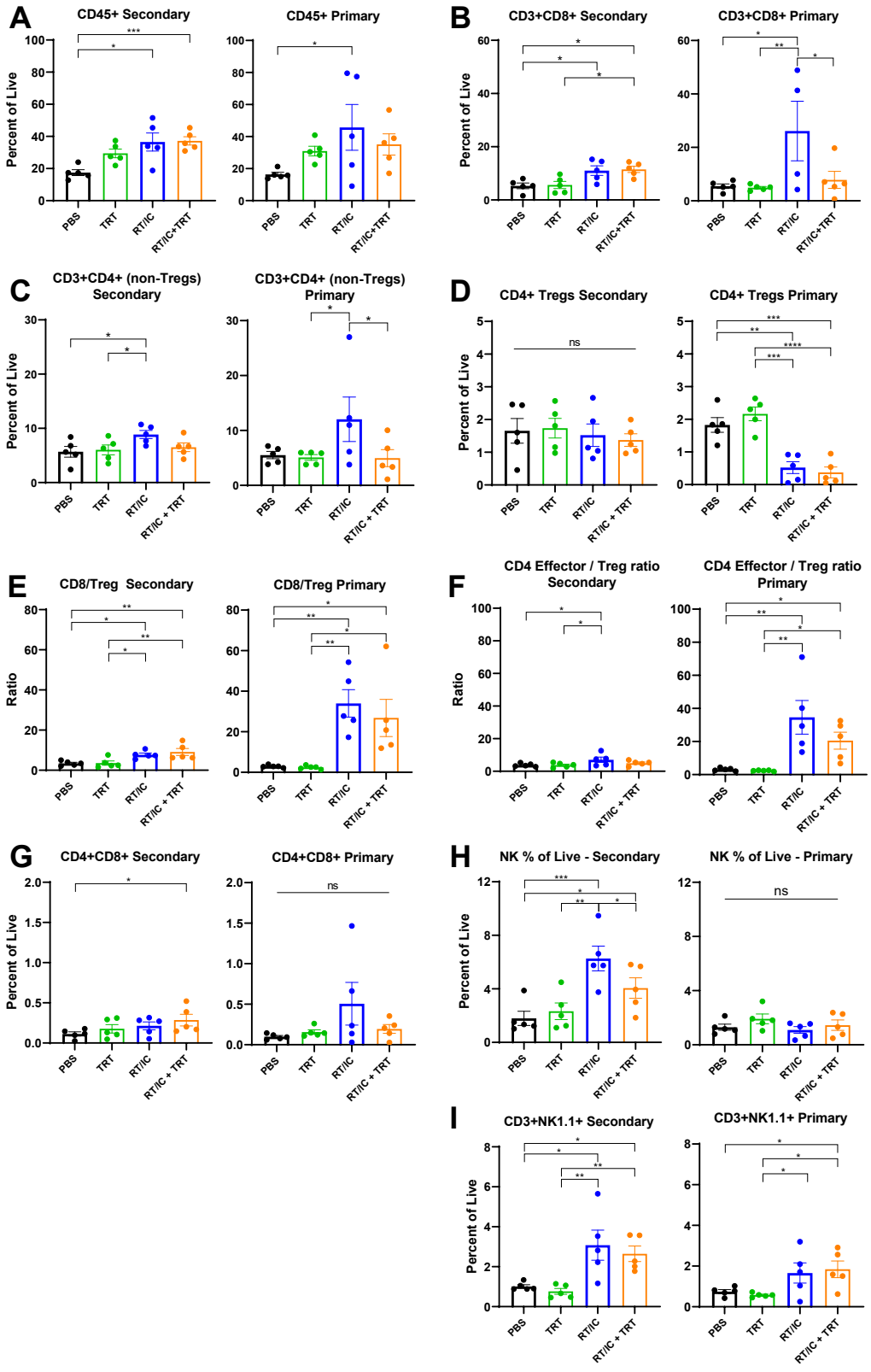
A
CD45+ Secondary
CD45+ Primary
B
CD3+CD8+ Secondary
CD3+CD8+ Primary
C
CD3+CD4+ (non-Tregs) Secondary
CD3+CD4+ (non-Tregs) Primary
D
CD4+ Tregs Secondary
CD4+ Tregs Primary
E
CD8/Treg Secondary
CD8/Treg Primary
F
CD4 Effector / Treg ratio Secondary
CD4 Effector / Treg ratio Primary
G
CD4+CD8+ Secondary
CD4+CD8+ Primary
H
NK % of Live - Secondary
NK % of Live - Primary
I
CD3+NK1.1+ Secondary
CD3+NK1.1+ Primary
Percent of Live
Ratio
PBS
TRT
RT/IC
RT/IC+TRT
RT/IC + TRT
ns

Figure A.8: Innate immunophenotyping of primary and secondary tumors in mice treated with *in situ* vaccine combined with ^{90}Y-NM600 TRT. Female C57BL/6 mice were implanted ID with B78 tumors on the right and left flanks simultaneously. After 4 weeks, mice were treated with either PBS (black), 100μCi of ^{90}Y-NM600 by tail vein injection (green), 12Gy RT and intratumoral immunocytokine (IC) to the primary tumor only (blue), or RT+IC to the primary tumor and 100μCi of ^{90}Y-NM600 (orange). RT and TRT was given on treatment day 0, and IC was given on treatment days 5-9. On treatment day 14, tumors were harvested and dissociated as described in the materials and methods section. Aliquots of tumors were stained using the adaptive and innate antibody panels outlined in Table A.1, according to the novel cryopreservation protocol described in Chapter 2 of this thesis. Cells were gated according to expression of the markers outlined in Table A.2. Immune populations are expressed as a percentage of all live, single cells, except where otherwise noted. In each population pair of graphs depicted, results corresponding to the right flank primary tumor are on the right, and results corresponding to the left flank secondary tumor are on the left. Statistical analyses were conducted using one-way ANOVA, with multiple comparisons using Fischer's least significant difference tests. No corrections were made to account for multiple comparisons. Note that these data were collected as part of the same experiment outlined in Figures A.1-A.5, and share common PBS and RT/IC groups, which are presented again here. * = $p<0.05$, ** = $p<0.01$, *** = $p<0.001$, **** = $p<0.0001$, ns = not significant.

Figure A.8

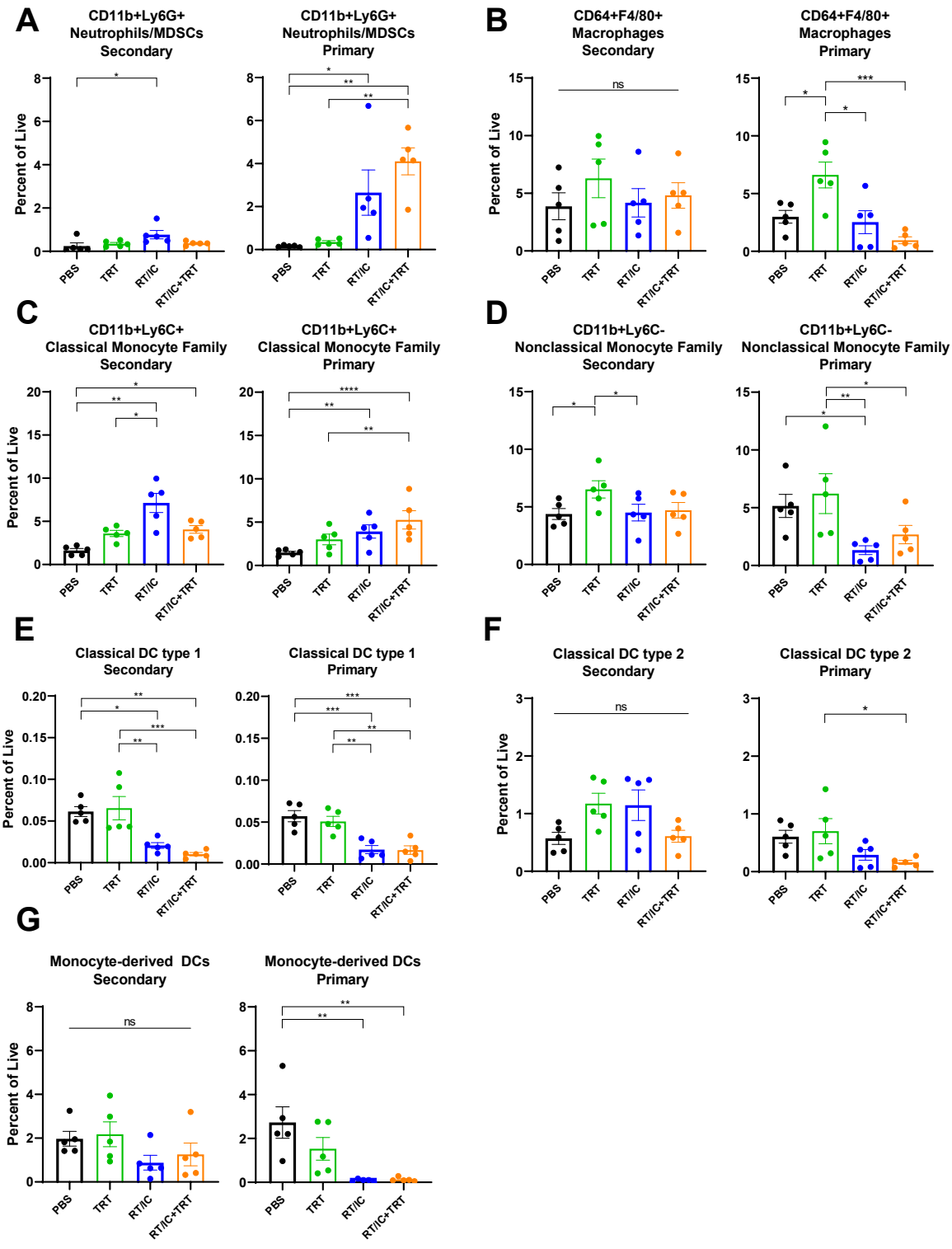
A
CD11b+Ly6G+ Neutrophils/MDSCs Secondary
CD11b+Ly6G+ Neutrophils/MDSCs Primary
B
CD64+F4/80+ Macrophages Secondary
CD64+F4/80+ Macrophages Primary
C
CD11b+Ly6C+ Classical Monocyte Family Secondary
CD11b+Ly6C+ Classical Monocyte Family Primary
D
CD11b+Ly6C- Nonclassical Monocyte Family Secondary
CD11b+Ly6C- Nonclassical Monocyte Family Primary
E
Classical DC type 1 Secondary
Classical DC type 1 Primary
F
Classical DC type 2 Secondary
Classical DC type 2 Primary
G
Monocyte-derived DCs Secondary
Monocyte-derived DCs Primary
Percent of Live
PBS
TRT
RT/IC
RT/IC+TRT
ns

Figure A.9: Expression of activation markers on T cells and NK cells in tumors isolated from mice treated with RT/IC *in situ* vaccine and ^{90}Y-NM600 TRT. Female C57BL/6 mice were implanted ID with B78 tumors on the right and left flanks simultaneously. After 4 weeks, mice were treated with either PBS (black), 100μCi of ^{90}Y-NM600 by tail vein injection (green), 12Gy RT and intratumoral immunocytokine (IC) to the primary tumor only (blue), or RT+IC to the primary tumor and 100μCi of ^{90}Y-NM600 (orange). RT and TRT was given on treatment day 0, and IC was given on treatment days 5-9. On treatment day 14, tumors were harvested and dissociated as described in the materials and methods section. Aliquots of tumors were stained using the adaptive and innate antibody panels outlined in Table A.1, according to the novel cryopreservation protocol described in Chapter 2 of this thesis. Cells were gated according to expression of the markers outlined in Table A.2. Expression of activation markers CD25, the activation / exhaustion marker PD1, and the effector cytokine IFNγ. Within the adaptive immune populations previously identified are outline here. Data is expressed as median fluorescence intensity (MFI) unless otherwise noted. In each population pair of graphs depicted, results corresponding to the right flank primary tumor are on the right, and results corresponding to the left flank secondary tumor are on the left. Statistical analyses were conducted using one-way ANOVA, with multiple comparisons using Fischer's least significant difference tests. No corrections were made to account for multiple comparisons. Note that these data were collected as part of the same experiment outlined in Figures A.1-A.5, and share common PBS and RT/IC groups, which are presented again here. * = $p<0.05$, ** = $p<0.01$, *** = $p<0.001$, **** = $p<0.0001$, ns = not significant.

Figure A.9

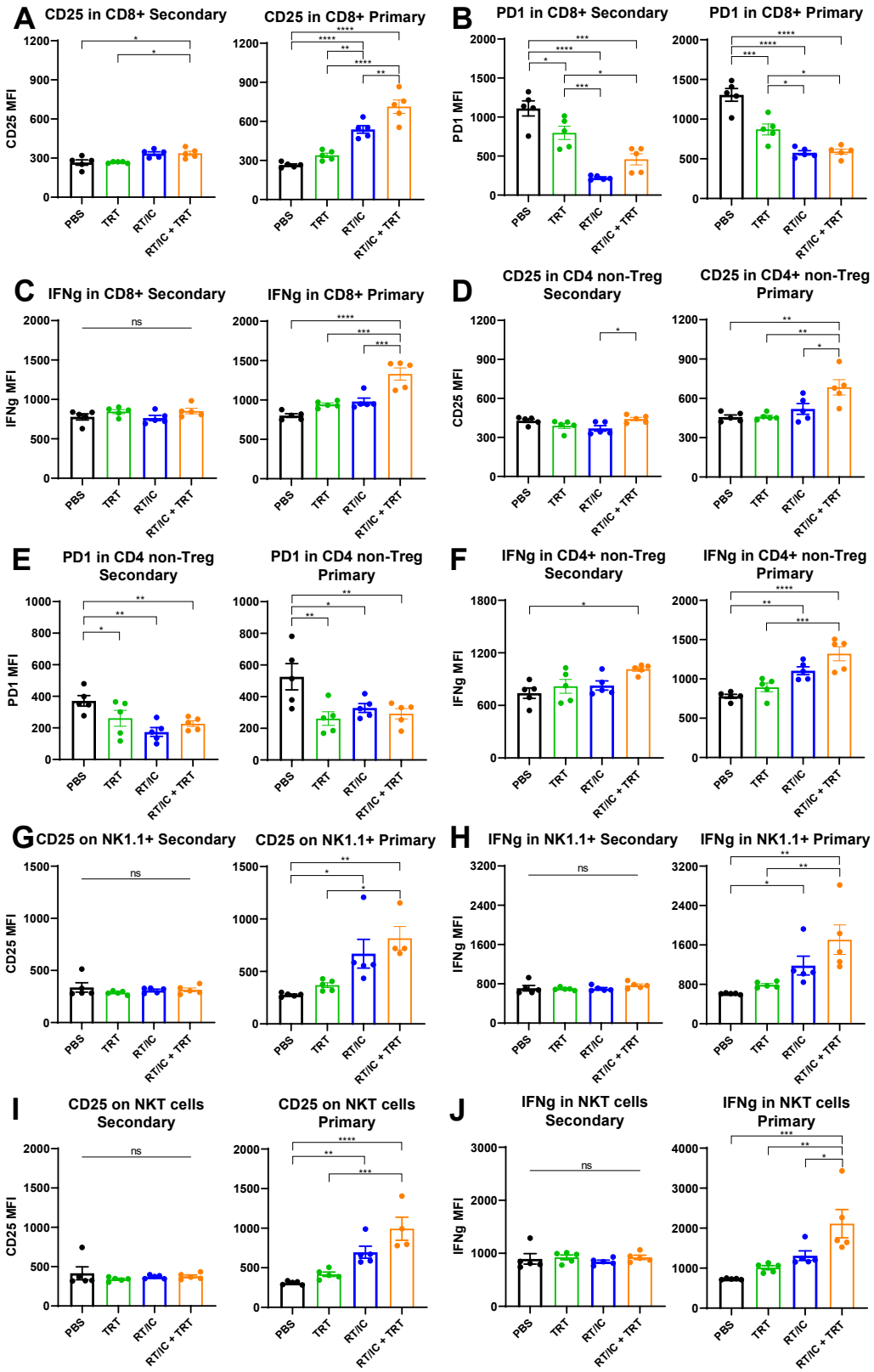
A
CD25 in CD8+ Secondary
CD25 in CD8+ Primary
CD25 MFI
B
PD1 in CD8+ Secondary
PD1 in CD8+ Primary
PD1 MFI
C
IFNg in CD8+ Secondary
IFNg in CD8+ Primary
IFNg MFI
D
CD25 in CD4 non-Treg Secondary
CD25 in CD4+ non-Treg Primary
CD25 MFI
E
PD1 in CD4 non-Treg Secondary
PD1 in CD4 non-Treg Primary
PD1 MFI
F
IFNg in CD4+ non-Treg Secondary
IFNg in CD4+ non-Treg Primary
IFNg MFI
G
CD25 on NK1.1+ Secondary
CD25 on NK1.1+ Primary
CD25 MFI
H
IFNg in NK1.1+ Secondary
IFNg in NK1.1+ Primary
IFNg MFI
I
CD25 on NKT cells Secondary
CD25 on NKT cells Primary
CD25 MFI
J
IFNg in NKT cells Secondary
IFNg in NKT cells Primary
IFNg MFI
PBS
TRT
RT/IC
RT/IC + TRT
ns

Figure A.10: PD1 and CD103 status in CD4+ non-T_{regs} in tumors isolated from mice treated with RT/IC *in situ* vaccine and ^{90}Y-NM600 TRT. Female C57BL/6 mice were implanted ID with B78 tumors on the right and left flanks simultaneously. After 4 weeks, mice were treated with either PBS (black), 100μCi of ^{90}Y-NM600 by tail vein injection (green), 12Gy RT and intratumoral immunocytokine (IC) to the primary tumor only (blue), or RT+IC to the primary tumor and 100μCi of ^{90}Y-NM600 (orange). RT and TRT was given on treatment day 0, and IC was given on treatment days 5-9. On treatment day 14, tumors were harvested and dissociated as described in the materials and methods section. Aliquots of tumors were stained using the adaptive and innate antibody panels outlined in Table A.1, according to the novel cryopreservation protocol described in Chapter 2 of this thesis. Cells were gated according to expression of the markers outlined in Table A.2. Depicted here is PD1 and CD103 expression on CD4+ T cells, after gating out CD25+FOXP3+ T_{reg} cells. A-B) representative dot plots outlining the four quadrants of expression status for PD1 and CD103 in PBS control (A) and RT/IC + 12Gy (B) primary tumors. C-F) Percentage of CD4+ non-T_{regs} in each of the four quadrants depicted in A and B Statistical analyses were conducted using one-way ANOVA, with multiple comparisons using. Fischer's least significant difference tests. No corrections were made to account for multiple comparisons. Note that these data were collected as part of the same experiment outlined in Figures A.1-A.5, and share common PBS and RT/IC groups, which are presented again here. * = $p<0.05$, ** = $p<0.01$, *** = $p<0.001$, **** = $p<0.0001$, ns = not significant.

Figure A.10

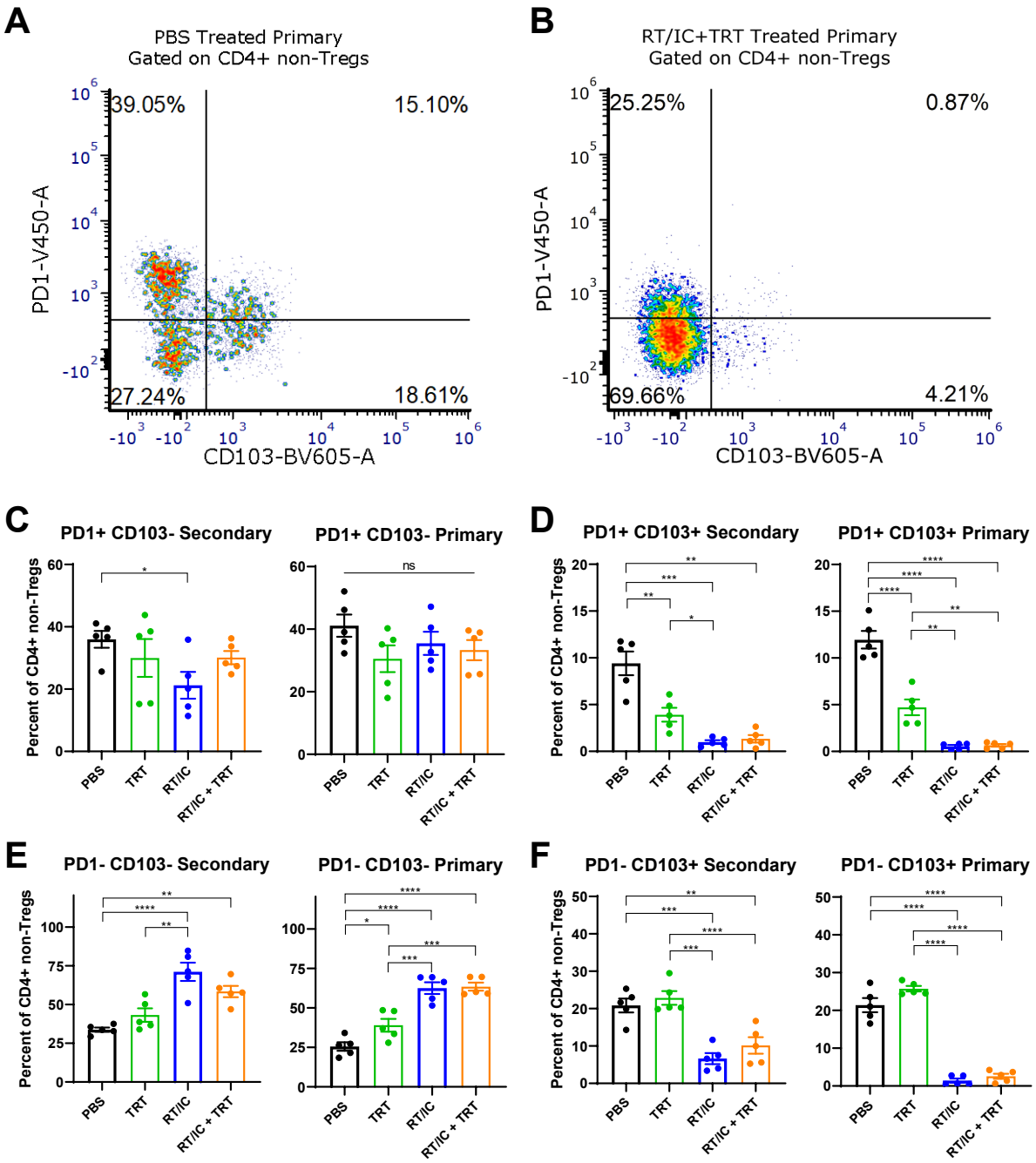
A
PBS Treated Primary
Gated on CD4+ non-Tregs
39.05%
15.10%
27.24%
18.61%
PD1-V450-A
CD103-BV605-A
B
RT/IC+TRT Treated Primary
Gated on CD4+ non-Tregs
25.25%
0.87%
69.66%
4.21%
PD1-V450-A
CD103-BV605-A
C
PD1+ CD103- Secondary
PD1+ CD103- Primary
D
PD1+ CD103+ Secondary
PD1+ CD103+ Primary
E
PD1- CD103- Secondary
PD1- CD103- Primary
F
PD1- CD103+ Secondary
PD1- CD103+ Primary
Percent of CD4+ non-Tregs
PBS
TRT
RT/IC
RT/IC + TRT
ns

Figure A.11: Cytokine profile in primary and secondary tumors treated with RT/IC *in situ* vaccine and ^{90}Y-NM600 TRT. Female C57BL/6 mice were implanted ID with B78 tumors on the right and left flanks simultaneously. After 4 weeks, mice were treated with either PBS (black), 100μCi of ^{90}Y-NM600 by tail vein injection (green), 12Gy RT and intratumoral immunocytokine (IC) to the primary tumor only (blue), or RT+IC to the primary tumor and 100μCi of ^{90}Y-NM600 (orange). RT and TRT was given on treatment day 0, and IC was given on treatment days 5-9. On treatment day 14, tumors were harvested and flash frozen in liquid nitrogen. After storage for 30 days, tissues were homogenized and analyzed using the MILLIPLEX MAP Mouse Cytokine/Chemokine Magnetic Bead Panel as described in the materials and methods section. Cytokine content is presented in pg/mL unless otherwise noted. Statistical analyses were conducted using one-way ANOVA, with multiple comparisons using Fischer's least significant difference tests. No corrections were made to account for multiple comparisons. Note that these data were collected as part of the same experiment outlined in Figures A.1-A.5, and share common PBS and RT/IC groups, which are presented again here. * = $p<0.05$, ** = $p<0.01$, *** = $p<0.001$, **** = $p<0.0001$, ns = not significant.

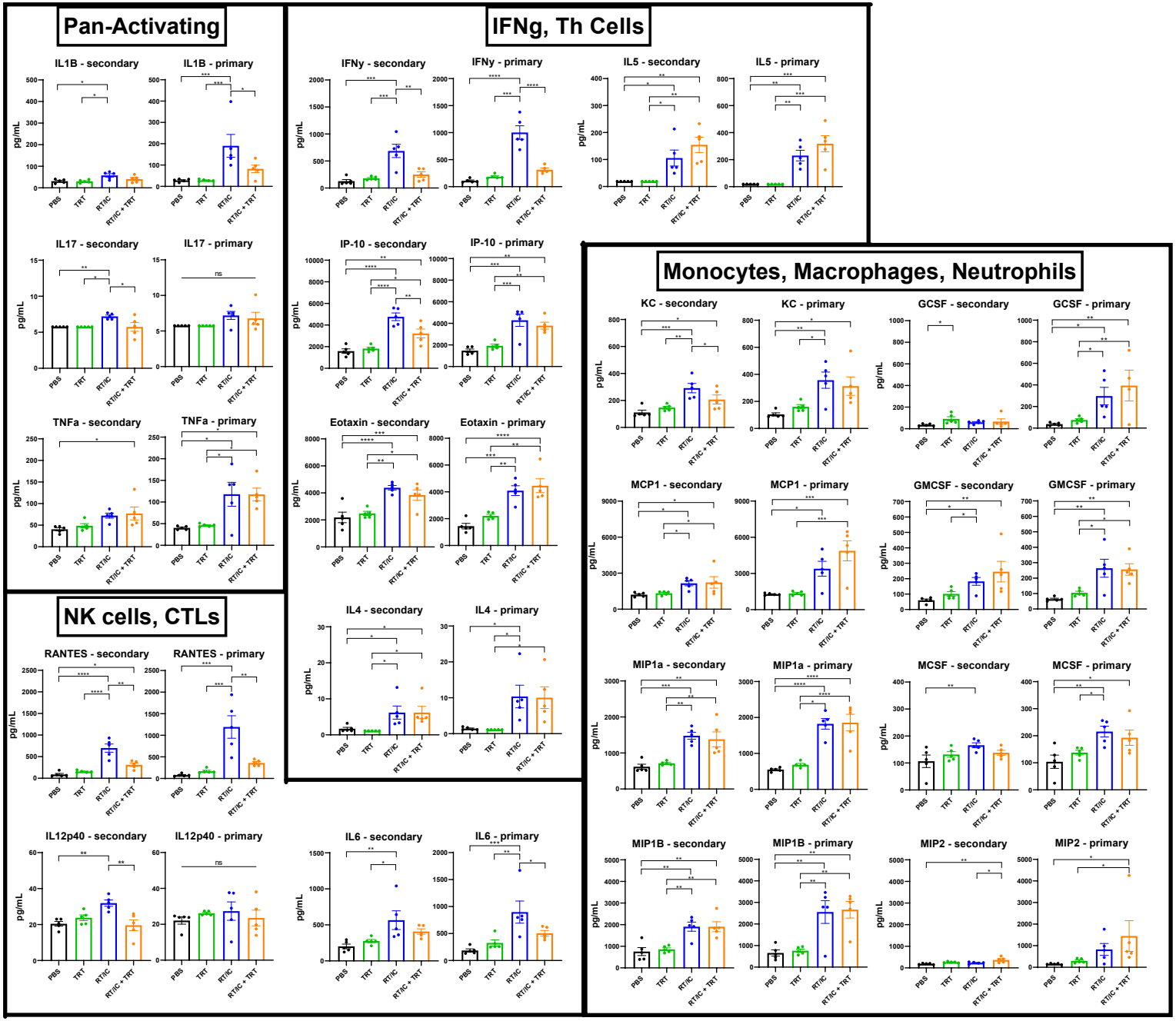
Pan-Activating
IL1B - secondary
IL1B - primary
IL17 - secondary
IL17 - primary
TNFa - secondary
TNFa - primary
NK cells, CTLs
RANTES - secondary
RANTES - primary
IL12p40 - secondary
IL12p40 - primary
IFNg, Th Cells
IFNy - secondary
IFNy - primary
IL5 - secondary
IL5 - primary
IP-10 - secondary
IP-10 - primary
Eotaxin - secondary
Eotaxin - primary
IL4 - secondary
IL4 - primary
IL6 - secondary
IL6 - primary
Monocytes, Macrophages, Neutrophils
KC - secondary
KC - primary
GCSF - secondary
GCSF - primary
MCP1 - secondary
MCP1 - primary
GMCSF - secondary
GMCSF - primary
MIP1a - secondary
MIP1a - primary
MCSF - secondary
MCSF - primary
MIP1B - secondary
MIP1B - primary
MIP2 - secondary
MIP2 - primary
pg/mL
PBS
TRT
RT/IC
RT/IC + TRT

Appendix B

Collaborative work resulting in co-authorship conducted during PhD work

Overview

This thesis appendix outlines the work submitted by other members of the Sondel and Morris research groups to which I was a contributing author. This effort resulted in five manuscripts published in various journals, and one manuscript that has been submitted for review. Each subsection of this appendix will begin with a brief introduction to the main findings of the paper, as well as a description of my specific contributions to the work. For all published papers, the published PDF version of the manuscript has been provided for referral and reading. The following papers will be discussed individually in the respective sections below:

B.1 Zachary S. Morris, Emily I. Guy, Lauryn R. Werner, Peter M. Carlson, Clinton M. Heinze, Jasdeep S. Kler, Sara M. Busche, Abigail A. Jaquish, Raghava N. Sriramaneni, Lakeesha L. Carmchael, Hans Loibner, Stephen D. Gilles, Alan K. Korman, Amy K. Erbe, Jacquelyn A. Hank, Alexander L. Rakhmilevich, Paul M. Harari, Paul M. Sondel. "Tumor-Specific Inhibition of *In Situ* Vaccination by Distant Untreated Tumor Sites" Cancer Immunol Res July 1 2018 (6) (7) 825-834; DOI**:** 10.1158/2326-6066.CIR-17-0353

B.2 Ravi B. Patel, Reinier Hernandez, Peter Carlson, Joe Grudinski, Amber M. Bates, Justin C. Jagodinsky, Amy Erbe, Ian R. Marsh, Ian Arthur, Eduardo Aluicio-Sarduy, Alexander L. Rakhmilevich, David Vail, Johnathan W. Engle, Trang Le, KyungMann Kim, Bryan Bednarz, Paul M. Sondel, Jamey Weichert, Zachary S. Morris. "Low-dose targeted radionuclide therapy renders immunologically "cold" tumors responsive to immune checkpoint blockade" Science Translational Medicine, submitted.

B.3 Ravi B. Patel, Mingzhou Ye, Peter M. Carlson, Abigail Jaquish, Luke Zangl, Ben Ma, Yuyuan Wang, Ian Arthur, Ruosen Xie, Ryan J. Brown, Xing Wang, Raghava Sriramaneni, KyungMann Kim, Shaogin Gong, Zachary S. Morris. "Development of an In Situ Cancer Vaccine via Combinational Radiation and Bacterial-Membrane-Coated Nanoparticles" *Adv Mater*. 2019;31(43):e1902626. doi:10.1002/adma.201902626

B.4 Julie Voeller, Amy K. Erbe, Jacob Slowinski, Kayla Rasmussen, Peter M. Carlson, Anna Hoefges, Sabrina VandenHeuvel, Ashley Stuckwisch, Xing Wang, Stephen D. Gilles, Ravi B. Patel, Alvin Farrel, Jo Lynne Rokita, John Maris, Jacquelyn A. Hank, Zachary S. Morris, Alexander L Rakhmilevich, and Paul M. Sondel. "Combined innate and adaptive immunotherapy overcomes resistance of immunologically cold syngeneic murine neuroblastoma to checkpoint inhibition". *J Immunother Cancer*. 2019;7(1):344. doi:10.1186/s40425-019-0823-6

B.5 Claire C. Baniel, Clinton M. Heinze, Anna Hoefges, Elizabeth G. Sumiec, Jacquelyn A. Hank, Peter M. Carlson, Won Jong Jin, Ravi B. Patel, Raghava N. Sriramaneni, Stephen D. Gillies, Amy K. Erbe, Ciara N. Schwarz, Alexander A. Pieper, Alexander L. Rakhmilevich, Paul M. Sondel, Zachary S. Morris. "Combination In Situ Vaccine Plus Checkpoint Blockade Induces Memory Humoral Response". *Int J Radiat Oncol* 2019;**105**:S127. doi:10.1016/j.ijrobp.2019.06.107

B.6 Paul A. Clark, Raghava N. Sriramaneni, Wonjong Jin, Justin C. Jagodinsky, Abigail Jauish, Bryce Anderson, Johnathan A. Lubin, Amber M. Bates, Clinton Heinze, Emily I. Guy, Jasdeep Kler, Kelsey A. Klar, Peter Carlson, John S. Kuo, Zachary S. Morris. “In situ vaccination at a peripheral tumor site augments response against melanoma brain metastases”. *J Immunother cancer* 2020;**8**:1–15. doi:10.1136/jitc-2020-000809

B.1 – Impact of distant, untreated tumors on the generation of *in situ* vaccines

This manuscript, authored by thesis committee member and co-mentor Dr. Zachary Morris et al, is an evaluation of RT+IC *in situ* vaccine in the setting of multiple tumors. Here we investigate a specific phenomenon that appeared using models of B78 melanoma and GD2-transfected panoc02 pancreatic adenocarcinoma in which mice with one such tumor would respond to RT+IC immunotherapy, but the response would be antagonized by the presence of a distant, untreated tumor. The effect was shown to be tumor specific, meaning that if both tumors were identical, this antagonistic effect was observed, but response at the treated primary remained intact if the second tumor was not related to the first. Using 12Gy RT delivered to the secondary, we demonstrated restoration of RT+IC effect at the primary tumor. We also demonstrated that systemic depletion of T_{regs} using either the transgenic DEREG platform (in which every FOXP3 expressing cell is killed following administration of diptheria toxin) or administration the T_{reg} depleting anti-CTLA4 antibody also restored antitumor effect of RT+IC *in situ* vaccination, which supports a tumor-antigen specific phenomenon we eventually termed "Concomitant Immune Tolerance." My role in this work was in the execution and analysis of the mouse *in vivo* experiments, including the depletion of T_{regs} in the DEREG model and the harvest and analysis of tissue samples by histology for $foxp3^{+}$ staining. This paper was published in the journal *Cancer Immunology Research*.

B.2 – The use of ^{90}Y-NM600 to augment response to systemic checkpoint blockade

This manuscript, lead by Dr. Ravi Patel, studies a related use of the ^{90}Y-NM600 TRT agent in B78 models. Instead of utilizing RT+IC *in situ* vaccine, this work demonstrates synergy between TRT and systemically administered anti-CTLA4 checkpoint blockade. We used the ^{86}Y-NM600 PET detectable isotope variant of NM600 to model TRT update over time in the B78 tumor compared to other organs, and used Monte Carlo simulation algorithms to predict the dose that would be delivered to the tumor over time as a function of injected ^{90}Y-NM600 activity. This manuscript demonstrates that ^{90}Y-NM600 synergizes with systemic checkpoint blockade to render over half of treated mice disease-free, with minimal toxicity and sustained tumor-specific memory, in B78 melanoma, 4T1 breast cancer, and NSX2 neuroblastoma tumor models. We then examined the mechanism of immune activation in response to this low dose TRT. Using the novel tumor preparation and cryopreservation method outlined in Chapter 2 of this thesis, we conducted a time course experiment using tumors harvested from mice receiving either external beam RT or a 50μCi dose of TRT; the flow cytometry data demonstrated modest increases in CD11b+ myeloid cells, NK cells, and the CD8/T_{reg} ratio following both external beam RT and TRT. Using the same cryopreservation and flow cytometry technique, we also demonstrated strong immune responses following treatment with combined TRT and anti-CTLA4 checkpoint blockade including increased CD3+ T cells, CD8+ cytotoxic T lymphocytes, and gamma delta T cells. The CD8+ cytotoxic T lymphocytes that were in the tumor also had higher expression of the tissue resident memory marker CD103, and lower expression of the exhaustion marker PD1. Cytokine analysis also demonstrated greater production of a panel of immune activating cytokines, and TCR sequencing indicated a sustained clonal expansion of T cells following the combination of TRT and checkpoint blockade compared to either alone. This paper also demonstrates feasibility of using TRT in combination with local immunotherapeutic effects, by combining systemic TRT, systemic anti-CTLA4, and locally delivered external beam RT to one tumor in a model of two B78 tumors and demonstrates antitumor effect at both

locations. Lastly, the manuscript demonstrates feasibility of using this TRT agent in larger animal models by presenting representative images and dosimetry for use in a canine model.

I contributed to this work by helping the lead author generate mouse models, including treatment and measurement of treatment effect. I also harvested and conducted the flow cytometry experiments presented here using the novel preparation/cryopreservation technique I developed, including the data analysis and some figure generation. The results of this study have implications for combining TRT, immune checkpoint blockade, and RT+IC *in situ* vaccination. As of the time of this writing, this manuscript is under review at the journal *Science, Translational Medicine*.

B.3 – The use of bioengineered nanoparticles to deliver immune adjuvant components for *in situ* vaccination

This manuscript, written by co-first authors Drs. Ravi Patel and Mingzhou Ye, is the result of a collaboration between Dr. Shaoqin Gong and co-mentor and Thesis Committee member Dr. Zachary Morris. In this work, we use an engineering nanoparticle as a vehicle for enhancing dendritic cell (DC) activation within the tumor microenvironment following local radiation treatment. The nanoparticle consisted of a PC7A core which was loaded to contain the TLR agonist CpG, as well as an outer coating of bacterial membrane and imide groups. Together, this complex was injected into a B78 tumor following radiation, and was hypothesized to increase uptake of neoantigens and tumor fragments, and directly simulate DCs to then process those antigens and drive *in situ* vaccine generation. Using flow cytometry, we demonstrated increased uptake of tumor antigens onto the particles themselves, which in turn led to upregulation of DC activation markers CD80, CD86, and CD40 on dendritic cells. Additional flow cytometry demonstrated that the combination of bacterial membrane-coated nanoparticle (BNP) and 12Gy RT increased expression of T cell activation markers including CD25 and 41BB in both CD4+ and CD8+ T cells. Lastly, we demonstrate *in vivo* efficacy of combination RT and BNP in B78 melanoma and NSX2 neuroblastoma models with improved overall survival and disease-free mice in the BNP+RT group compared to either alone. Importantly, over 50% of mice rendered disease-free by the BNP+RT treatment rejected a subsequent tumor rechallenge, which supports the hypothesis that this combination treatment can indeed generate an *in situ* vaccine. My work on this project consisted of harvesting, staining, and acquiring the flow cytometry components of this manuscript. This included assisting in data analysis and figure generation. This manuscript was published in 2019 in the journal *Advanced Materials*.

B.4 – Using both innate and adaptive activating agents to generate *in situ* vaccines in a model of immunologically cold neuroblastoma

This manuscript, written by Dr. Julie Voeller, describes attempts to expand the efficacy of RT+IC *in situ* vaccination in a syngeneic mouse models of neuroblastoma. She demonstrated that the GD2-transfected 9464D-GD2 line had a very low tumor mutation burden, and was not responsive to RT+IC *in situ* vaccination, while the NSX2 line had higher tumor mutation burden and was responsive to RT+IC *in situ* vaccination. Next, she demonstrated that addition of anti-CTLA4 checkpoint blockade still did not affect response to RT+IC in 9464D-GD2 tumors, which strongly suggested that this could be used to model high-risk clinical neuroblastoma. In this highly resistant line, it was demonstrated that the addition of the TLR agonist CpG and CD40 agonist antibody to the RT+IC + checkpoint blockade regimen was sufficient to generate antitumor immune response and render mice disease-free. Subsequent rechallenges did result in outgrowth of tumor, but at a slower rate compared to naïve control mice, which suggests immune memory response consistent with an *in situ* vaccine effect. Using flow cytometry it was demonstrated that tumors from mice treated with RT+IC, checkpoint blockade, CpG, and CD40 agonist antibody had substantially greater CD4+ and CD8+ T cells, Macrophages, and monocytes, and much lower T_{reg} cells compared to untreated controls. My role in this work was in assisting in the design of the flow cytometry panels, as well as assisting in the harvest, acquisition, analysis, and subsequent figure generation of these flow cytometry data. This work was published in 2019 in the *Journal for Immunotherapy of Cancer*.

B.5 – Measuring the humoral immune response to RT+IC *in situ* vaccination

This manuscript, written by Dr. Claire Baniel, focuses on expanding our understanding of the immune mechanisms of response to *in situ* vaccination. The magnitude of B cell response, specifically the generation of antitumor antibodies, was characterized in mice bearing a B78 tumor treated with RT+IC and systemic anti-CTLA4 checkpoint blockade. Serum was collected at various time points to monitor for the generation of antitumor antibodies, which was quantified by using flow cytometry. The parent B78 cells were incubated in harvested serum, and stained with a fluorescent secondary antibody specific to mouse IgG. Using this approach, we demonstrated that tumor-specific IgG could be detected in mice rendered disease free by treatment. Comparing the kinetics of antibody generation to the tumor volume in response to treatment revealed that serum antibody levels peaked at approximately the same time that tumors would respond to treatment and undergo their greatest degree of shrinkage. Pre-incubating tumor cells in the serum from disease-free mice did not affect engraftment rates in naïve mice, which suggests that the antibodies may not have a strong antitumor effect, but could be used as a biomarker for response. In this work I helped establish the mouse models which we monitored for serum response, including conducting the facial vein bleeds and isolating the sera for storage. I was also involved in the experimental designs for this study, and assisted authors Claire Baniel and Clinton Heinze in conducting the flow cytometry studies. This work was published in 2020 in the journal *Frontiers in Immunology*.

B.6 – Measuring propagation of *in situ* vaccine to brain metastases

This manuscript, written by Dr. Paul Clark, studies the effect of local *in situ* vaccine directed at a flank tumor to control implanted brain metastases in the B78 melanoma model. Using mice rendered disease-free by RT+IC *in situ* vaccine and systemic anti-CTLA4 checkpoint blockade, they challenged mice with additional B78 cells in both the left flank and in the brain. They showed that 11 of 12 mice rejected rechallenge in the brain, which does suggest that systemic immune responses to the *in situ* vaccine were capable of attacking the inoculum of tumor cells in the brain. They next used a model of pre-existing implanted B78 metastases, and treated a primary tumor with the same immunotherapy, and demonstrated increased survival compared to mice receiving checkpoint blockade alone. When comparing the magnitude of immune response at a flank 'distant' tumor and a brain 'distant' tumor following *in situ* vaccination plus checkpoint blockade, similar levels of checkpoint receptor expression, MHCI expression, and cytokine production were found. However treatment was able to clear the flank 'distant' tumor, but did not clear (albeit it slowed) the brain tumor. Using both flow cytometry and immunohistochemical staining, it was demonstrated that the flank 'distant' tumor had a higher degree of $CD8^+$ T cell infiltrate and a higher CD8 / T_{reg} ratio compared to the brain 'distant' tumor. The work presented in this paper demonstrated that some degree of immune response does propagate to intracranial metastases, but additional immunotherapies beyond what is needed to control extracranial metastases may be needed. My role in this work was in helping with the design of the flow cytometry panel, and in helping with tissue harvest, sample preparation, acquisition, and data analysis for the flow cytometry experiments. This work was published in 2019 in the *Journal for Immunotherapy of Cancer*.